

G9061

**STRUCTURAL AND SPECTRAL INVESTIGATIONS  
OF TRANSITION METAL COMPLEXES OF  
DI-2-PYRIDYL KETONE N(4),N(4)-DISUBSTITUTED  
THIOSEMICARBAZONES**

*Thesis submitted to*

**COCHIN UNIVERSITY OF SCIENCE AND TECHNOLOGY**

*in partial fulfillment of the requirements  
for the degree of*

**DOCTOR OF PHILOSOPHY**

*in*

**CHEMISTRY**

*by*

**VARUGHESE PHILIP**



**DEPARTMENT OF APPLIED CHEMISTRY  
COCHIN UNIVERSITY OF SCIENCE AND TECHNOLOGY**

**KOCHI 682022**

**JULY 2004**

Phone Off. 0484-2575804  
Phone Res. 0484-2576904  
Telex: 885-5019 CUIN  
Fax: 0484-2577595  
Email: [mrp@cusat.ac.in](mailto:mrp@cusat.ac.in)  
[mrp\\_k@yahoo.com](mailto:mrp_k@yahoo.com)

**DEPARTMENT OF APPLIED CHEMISTRY**  
**COCHIN UNIVERSITY OF SCIENCE AND TECHNOLOGY**  
KOCHI - 682 022, INDIA

---

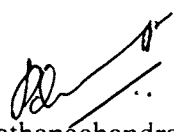
M. R. PRATHAPACHANDRA KURUP  
Professor of Inorganic Chemistry

5<sup>th</sup> July 2004

---

**CERTIFICATE**

This is to certify that the thesis entitled “**STRUCTURAL AND SPECTRAL INVESTIGATIONS OF TRANSITION METAL COMPLEXES OF DI-2-PYRIDYLKETONE *N*(4),*N*(4)-DISUBSTITUTED THIOSEMICARBAZONES**” submitted by **Mr. VARUGHESE PHILIP**, in partial fulfillment of the requirements of the degree of Doctor of Philosophy, to the Cochin University of Science and Technology, Kochi is an authentic and bonafide record of the original research work carried out by him under my guidance and supervision. Further, the results embodied in this thesis in full or part, have not been submitted for any award of degree.

  
Dr. M. R. Prathapachandra Kurup  
(Supervisor)

# CONTENTS

## CHAPTER 1

### THIOSEMICARBAZONES AND THEIR TRANSITION METAL COMPLEXES - A BRIEF INTRODUCTION

1.1	Introduction	1
1.2	Stereochemistry and oxidation states	2
1.3	Structural characterization techniques	7
	<i>1.3.1 Analytical Estimations</i>	7
	<i>1.3.2 Magnetic measurements</i>	7
	<i>1.3.3 Electronic spectroscopy</i>	10
	<i>1.3.4 Infrared spectroscopy</i>	10
	<i>1.3.5 Electron paramagnetic resonance spectroscopy</i>	11
	<i>1.3.6 X-ray crystallography</i>	11
1.4	Biological significance	12
1.5	Objective and scope of the present work	14

CHAPTER 2  
SYNTHESES, SPECTRAL AND STRUCTURAL  
CHARACTERIZATION OF  
THIOSEMICARBAZONES

2.1	<b>Introduction</b>	15
2.2	<b>Experimental</b>	15
	2.2.1 <i>Materials and methods</i>	15
	2.2.2 <i>Synthesis of thiosemicarbazones</i>	16
	2.2.3 <i>X- ray crystal analysis of HL<sup>1</sup></i>	19
	2.2.4 <i>X- ray crystal analysis of HL<sup>2</sup></i>	20
2.3	<b>Results and discussion</b>	21
	2.3.1 <i>Molecular and crystal structure of HL<sup>1</sup></i>	21
	2.3.2 <i>Molecular and crystal structure of HL<sup>2</sup></i>	23
	2.3.3 <i>Infrared spectra</i>	27
	2.3.4 <i><sup>1</sup>H NMR spectra</i>	29
	2.3.5 <i>Electronic spectra</i>	31
2.4	<b>Concluding remarks</b>	31

CHAPTER 3  
 SYNTHESSES, STRUCTURAL AND SPECTRAL  
 CHARACTERIZATION OF COPPER(II) COMPLEXES DERIVED  
 FROM LIGANDS, DI-2-PYRIDYL KETONE 3-  
 TETRAMETHYLENEIMINYLTHTIOSEMICARBAZONE AND DI-2-  
 PYRIDYL KETONE N(4)-METHYL N(4)-  
 PHENYLTHIOSEMICARBAZONE

3.1	Introduction	32
3.2	Experimental	33
	3.2.1 <i>Materials and methods.</i>	33
	3.2.2 <i>Physical measurements</i>	34
	3.2.3 <i>Syntheses of complexes</i>	34
	3.2.4 <i>X-ray crystallography</i>	35
3.3	Results and discussion	37
	3.3.1 <i>Molecular and crystal structure of</i> <i><math>[Cu_2L_2^1(SO_4)]_2 \cdot 6H_2O</math></i>	38
	3.3.2 <i>Molecular and crystal structure of <math>[CuL^2Br]_2</math></i>	42
	3.3.3 <i>Molecular and crystal structure of <math>[CuL^{2(N_3)}]_2</math></i>	46
	3.3.4 <i>Molecular and crystal structure of</i> <i><math>[CuL^2(SH)]_2 \cdot 2H_2O</math></i>	50
	3.3.5 <i>Magnetic susceptibility</i>	54
	3.3.6 <i>Infrared spectra</i>	57
	3.3.7 <i>Electronic spectra</i>	60
	3.3.8 <i>EPR spectral investigations</i>	64
3.4	Concluding remarks	76

CHAPTER 4  
 SYNTHESIS, STRUCTURAL AND SPECTRAL  
 CHARACTERIZATIONS OF NICKEL(II) COMPLEXES OF DI-2-  
 PYRIDYL KETONE 3-  
 TETRAMETHYLENEIMINYLTHTIOSEMICARBAZONE

4.1	Introduction	77
4.2	Experimental	78
	4.2.1 <i>Materials and methods</i>	78
	4.2.2 <i>Physical measurements</i>	78
	4.2.3 <i>Syntheses of complexes</i>	78
	4.2.3.1 <i>Synthesis of <math>[\text{NiL}^1\text{Cl}] \cdot \frac{1}{2} \text{H}_2\text{O}</math></i>	78
	4.2.3.2 <i>Synthesis of <math>[\text{NiL}^1\text{N}_3] \cdot \frac{1}{2} \text{H}_2\text{O}</math></i>	78
	4.2.3.3 <i>Synthesis of <math>[\text{NiL}^1(\text{SCN})]</math></i>	79
	4.2.4 <i>X-ray crystallography</i>	79
4.3	Results and discussion	80
	4.3.1 <i>Analytical data</i>	80
	4.3.2 <i>Molecular and Crystal structures of <math>[\text{NiL}^1\text{Cl}]</math> and <math>[\text{NiL}^1\text{N}_3]</math></i>	81
	4.3.3 <i>Infrared spectra</i>	85
	4.3.4 <i>Electronic spectra</i>	87
	4.3.5 <i><math>^1\text{H}</math> NMR spectra</i>	89
4.4	Concluding Remarks	89

CHAPTER 5  
 SYNTHESSES, STRUCTURAL AND SPECTRAL  
 CHARACTERIZATIONS OF MANGANESE(II) COMPLEXES OF DI-2-  
 PYRIDYL KETONE 3-  
 TETRAMETHYLENEIMINYLTHTIOSEMICARBAZONE AND DI-2-  
 PYRIDYLKETONE *N*(4)-METHYL, *N*(4)-  
 PHENYLTHIOSEMICARBAZONE

5.1	Introduction	91
5.2	Experimental	92
	<i>5.2.1 Materials and Methods</i>	92
	<i>5.2.2 Physical Measurements</i>	92
	<i>5.2.3 Synthesis of complexes</i>	92
	<i>5.2.4 X-Ray crystallography</i>	93
5.3	Results and discussion	93
	<i>5.3.1 Magnetic susceptibility</i>	94
	<i>5.3.2 Molecular and crystal structure of [MnL<sup>1</sup><sub>2</sub>]</i>	94
	<i>5.3.3 Infrared spectra</i>	97
	<i>5.3.4 Electronic spectra</i>	99
	<i>5.3.5 Electron spin resonance spectra</i>	100
5.4	Concluding remarks	104

**CHAPTER 6**  
**SYNTHESIS, STRUCTURAL AND IR SPECTRAL**  
**CHARACTERIZATION OF VANADATE(V) COMPLEX OF DI-2-**  
**PYRIDYL KETONE 3-**  
**TETRAMETHYLENEIMINYLTHTIOSEMICARBAZONE**

6.1	Introduction	105
6.2	Experimental	106
	6.2.1 <i>Materials and methods</i>	106
	6.2.2 <i>Physical measurements</i>	106
	6.2.3 <i>Synthesis of the complex [VO<sub>2</sub>L<sup>1</sup>]</i>	106
	6.2.4 <i>X-ray crystallography</i>	107
6.3	Results and Discussion	108
	6.3.1 <i>Molecular and crystal structure of [VO<sub>2</sub>L<sup>1</sup>]</i>	108
	6.3.2 <i>Infrared Spectra</i>	111
6.4	Concluding Remarks	113



CHAPTER 7  
SYNTHESES, STRUCTURAL AND SPECTRAL  
CHARACTERIZATIONS OF COBALT(III) COMPLEXES OF DI-2-  
PYRIDYL KETONE 3-  
TETRAMETHYLENEIMINYLTHTIOSEMICARBAZONE

7.1	Introduction	114
7.2	Experimental	115
	7.2.1 <i>Materials and methods</i>	115
	7.2.2 <i>Physical measurements</i>	115
	7.2.3 <i>Preparation of the complexes</i>	116
	7.2.3.1 <i>Preparation of <math>[\text{CoL}^1_2]\text{Cl}\cdot 2\frac{1}{2}\text{H}_2\text{O}</math></i>	116
	7.2.3.2 <i>Preparation of <math>[\text{CoL}^1_2]\text{NO}_3\cdot 2\frac{1}{2}\text{H}_2\text{O}</math></i>	116
7.3	Results and discussion	116
	7.3.1 <i>Infrared spectra</i>	117
	7.3.2 <i>Electronic spectra</i>	118
	7.3.3 <i><math>^1\text{H}</math> NMR Spectra</i>	119
7.4	Concluding remarks	122

## CHAPTER 8

### SYNTHESIS, AND SPECTRAL CHARACTERIZATIONS OF ZINC(II) AND CADMIUM(II) COMPLEXES OF DI-2-PYRIDYL KETONE.3- TETRAMETHYLENEIMINYLTHTIOSEMICARBAZONE

8.1	<b>Introduction</b>	123
8.2	<b>Experimental</b>	124
	8.2.1 <i>Materials and methods</i>	124
	8.2.2 <i>Physical measurements</i>	124
	8.2.3 <i>Synthesis of complexes</i>	124
	8.2.3.1 <i>Synntthesis of zinc(II) complexes</i>	124
	8.2.3.2 <i>Synthesis of cadmium(II) complex</i>	125
8.3	<b>Results and discussion</b>	125
	8.3.1 <i>Infrared spectra</i>	126
	8.3.2 <i>Electronic spectra</i>	129
	8.3.3 <i><sup>1</sup>H NMR spectra</i>	129
8.4	<b>Structure and concluding remarks</b>	131
	<b>REFERENCES</b>	132

## THIOSEMICARBAZONES AND THEIR TRANSITION METAL COMPLEXES - A BRIEF INTRODUCTION

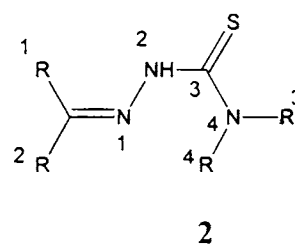
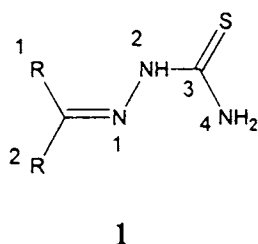
---

### 1.1. Introduction

Coordination compounds are now widely used as potential drugs, in the field of catalysis [1, 2] and in biological fields. The development of instrumental techniques provides methods of investigating thermal, spectral and magnetic properties of metal complexes. Recent reports from journals regarding researches in inorganic chemistry are widely centered on complexes.

Thiosemicarbazones are a group of highly reactive compounds that forms chelate complexes with metal ions. Livingstone [3] has reviewed complexes with chelates of sulphur and nitrogen as donor atoms. Another review published in 1974 [4] gives detailed account of thiosemicarbazides and thiosemicarbazones. There are reports regarding therapeutic use of metal complexes of thiosemicarbazones and are now widely used as potential antimalarial [5], antitumour [6] and antibacterial [7] and antifungal agents [8].

Thiosemicarbazones are obtained by condensation of thiosemicarbazide or a substituted thiosemicarbazide at the *N*(4) position with a suitable aldehyde or ketone. Thiosemicarbazones are represented by the general formula 1, where



$R^1$  is generally an alkyl group or aryl group and  $R^2$  is alkyl, aryl or hydrogen atom. When *N*(4) is substituted it can be represented by the general formula 2. In the formula 2,  $R^3$  and  $R^4$  can be alkyl or aryl groups or a part of a cyclic

system. In solution thiosemicarbazones exist as an equilibrium mixture of thione (**1a**) and thiol (**1b**) forms



Recent researches in coordination chemistry are centered on thiosemicarbazones of heterocyclic ketones as they have considerable biological activity. Thiosemicarbazones of  $\alpha$ -N heterocyclic carbaldehydes act as tridentate ligands. The biological activity of thiosemicarbazone depends on the parent aldehyde and ketone [9, 10]. Among thousands of screened compounds, 2-acetylpyridine thiosemicarbazones were the first compounds reported as potent antimalarial agents [5]. Acetylaminobenzaldehyde thiosemicarbazone, called contiban is found to be effective against tuberculosis.

## 1.2. Stereochemistry and oxidation states

Stereochemistry of metal complexes of thiosemicarbazone depends on (i) charge on the ligand and (ii) additional coordination site on the ligand moiety. The charge on the ligand depends on thione  $\leftrightarrow$  thiol equilibrium. Thiosemicarbazone may generally exist in the *E* form (trans) and in such a situation thiosemicarbazones act as a unidentate ligand by bonding through sulfur [11]. (Figure 1.1)



Figure 1.1

Thiosemicarbazones can act as neutral bidentate ligands, as in benzaldehyde thiosemicarbazone yielding complexes of the type  $[ML_2X_2]$  where ligand is in the thione form and X is the monoanionic ligand and metal  $M = Co(II), Ni(II), Cu(II),$  or  $Fe(II)$ . In such metal complexes, coordination takes place through azomethine nitrogen and thione/thiol sulfur [12, 13]. If an additional coordinating functionality is present, tridentate coordination will be preferred. For example, cobalt(II) complexes of diacetylmonoxime thiosemicarbazone [14] are reported to be octahedral. Coordination occurs *via* azomethine nitrogen, thione sulfur and oxime nitrogen, where oxime nitrogen is an additional coordinating functionality.

Thiosemicarbazones can also act as multidentate ligands, if donor atoms are present in parent aldehyde or ketone moiety. Heterocyclic thiosemicarbazones can coordinate to the metal ion through more than two coordination sites where one of the sites is a hetero atom such as nitrogen or oxygen. For example, nickel(II) complex of 2-acetylpyridine thiosemicarbazone [15] have one of the coordinating sites occupied by pyridyl nitrogen. In addition nickel(II) complex of di-2-pyridyl ketone *N*(4), *N*(4)-dimethyl thiosemicarbazone [16] is found to be square planar and one of its coordinating site is pyridyl nitrogen as shown below. (Figure 1.2)

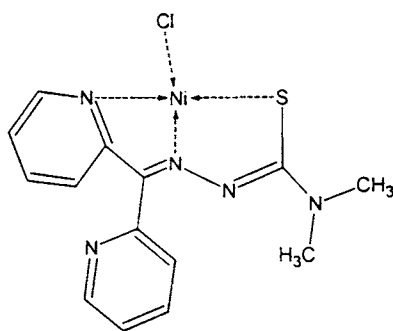


Figure 1.2

Thiosemicarbazones can also coordinate to metal centers as tetra dentate ligands. Ligands having SNON [17] and NNSS [18] donor sites have been reported. In copper(II) complexes of di-2-pyridyl ketone thiosemicarbazone,

each copper atom is found to be five coordinate with nitrogen atoms of the each pyridyl rings coordinate to two copper centers [19]. Pentadentate ligands of thiosemicarbazones are also reported. For example, 2,6-diacetylpyridine bis(thiosemicarbazone) [20] is pentadentate, coordinate to the metal as SNNNS donors as shown in Figure 1.3.

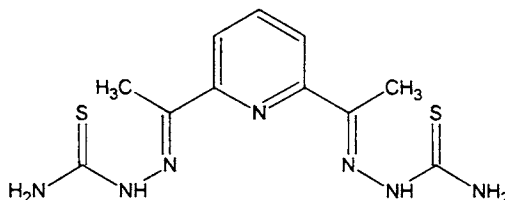


Figure 1.3

Stereochemistry of metal complexes of thiosemicarbazones depends very much on the oxidation state of the metal [2]. The oxidation state of the metal determines the degree of “softness” character. This effect is found to be stronger in transition metals. Thus degree of softness and hardness plays an important part in determining the stability of a thiosemicarbazone metal complex. Thus low spin  $d^8$  and  $d^{10}$  metal ions such as Pd(II), Pt(II) and Hg(II) may form stable complexes with thiosemicarbazone ligands. The increased stability is due to the formation of strong  $\sigma$  bonds as well as  $d\pi-d\pi$  bonds by donation of a pair of electrons to ligands.

Stereochemistries of thiosemicarbazones are decided by steric effect of substituents attached to thiosemicarbazone moiety [21]. This phenomenon is known as ‘chelate’ effect where the increased stability is due to electron delocalisation with the chelated ring system (Figure 1.4).

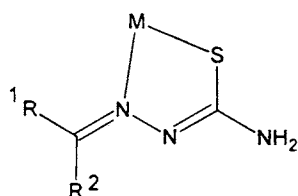


Figure 1.4 Chelate effect

Intramolecular hydrogen bonding is another factor that further that enhances the stability of thiosemicarbazones and the confirmation is *E* (trans). This mode of hydrogen bonding and confirmation is the same as reported for 2-formylpyridine thiosemicarbazones [22] and found for many heterocyclic mono-substituted thiosemicarbazones [23].

Metal complexes of thiosemicarbazones are usually octahedral and square planar in geometry. Octahedral stereochemistry is common to thiosemicarbazones and are generally seen in complexes of Fe(III), Mn(II), Co(III) having the general formula  $[ML_2]^{n+}$  where M is the metal ion [24-26]. Tetrahedral complexes of di-2-pyridyl ketone *N*(4), *N*(4)-dimethyl thiosemicarbazone are also reported [16]. Copper(II) complexes are usually square planar in geometry. Five coordinate mononuclear copper(II) complexes 2-hydroxyacetophenone 3-hexamethyleneiminylthiosemicarbazone of square pyramidal geometry are also reported [27]. X-ray crystal studies of copper(II) complexes of 2-benzoylpyridine Schiff's bases of S-benzylthiocarbamate revealed that stereochemistry around copper atom in the complex is intermediate between square-pyramidal and trigonal-bipyramidal geometries [28]. Complexes of the type  $[Fe(NNS)_2X]$ , (where NNS is the monoanion of 2-acetylpyridine thiosemicarbazone and X = Cl, Br, NO<sub>3</sub>, SCN etc) have been described [29]. This complex is believed to have a pentagonal bipyramidal configuration around Fe atom with rhombic distortion. Stereochemistry of iron atom in Fe(III) complexes of 2-acetylpyridine 4-phenyl 3-thiosemicarbazone of general formula  $[FeLX_2]$  where X= Cl, Br, NO<sub>3</sub>, SCN etc is square pyramidal with  $A_{2g}$  ground state [30].

First row of transition metals are unique in their ability to form complexes in which octahedral, tetrahedral, square-coplanar and other stereochemistries predominate. The copper(II) ion is a typical transition metal ion which forms coordination complexes of different stereochemistries, but it is reluctant to take up regular octahedral or tetrahedral stereochemistries. The  $3d^9$  outer electronic configuration of copper(II) ion lacks cubic symmetry and hence

it yields other distorted forms of the basic stereochemistries. The copper(II) ion forms coordination complexes in which coordination numbers four, five or six predominates. Due to large distortion in bond lengths, the splitting of electronic energy levels in copper(II) ions tends to be larger than other first row transition metals. Thus the electronic properties of copper(II) complexes are relatively sensitive to stereochemistry. There are many factors that affect stereochemistries of copper(II) ion in coordination complexes. Jahn- Teller theorem removes the degeneracy of the ground state (the single unpaired electron is in  $d_{x^2-y^2}$  or  $d_z^2$ ) which is degenerate in a regular octahedral ligand field. This type of distortion can be shown to be any of the non-totally symmetric normal vibrations and the extrema of these vibrations are the static distortions found in six coordinate octahedral complexes. Elongated structures such as elongated tetragonally distorted octahedron, rhombically distorted octahedron are more energetically favorable than compressed structures. In these stereochemistries, the odd electron is in the  $d_{x^2-y^2}$  orbital, which minimizes the columbic repulsion between the copper electrons and the negatively charged ligands in the  $xy$ -plane than along the  $z$ -axis. Four coordinate square planar stereochemistries are not common in  $\sigma$ -bonded complexes, but it does occur with  $\pi$  bonding ligands like pyridyl thiosemicarbazones. Distorted tetragonal octahedron stereochemistry is preferable for  $\sigma$ -bonded complexes where bonding effects of ligands in the axial positions are not ignored. This situation can be described by the concept of semicoordination, which suggests that the axial fifth and sixth ligands are bonded at a definite distance, the copper ion is considered as ellipsoidal, not spherical. The in-plane covalent radius of the copper(II) ion is estimated to be  $ca.1.30 \text{ \AA}$  and out-of-plane radius would be  $ca.1.90 \text{ \AA}$ . In copper(II) complexes tetragonal distortion ( $T$ ) may be measured by the ratio  $R_s/R_l$  where  $R_s$  and  $R_l$  are short and long copper ligand bond lengths. The value is unity for an octahedral complex and 0.56-0.66 for a square coplanar structure. Decrease in  $T$  is a decrease of the short copper-ligand



bond distances, suggesting that lowest values of  $R_s$  occur for a square planar geometry [31].

### 1.3. Structural characterization techniques

Many new methods are recently available for elucidating the structure of coordination compounds. Elemental, magnetic, IR, UV-Vis, and NMR spectral techniques were used for structural analysis. X-ray crystallographic analysis is the most reliable and accurate physical method recently used for structural analysis. Some of the common physico chemical methods adopted during the present investigation are discussed below.

#### 1.3.1. Analytical estimations

##### (i) Analysis of carbon, hydrogen and nitrogen

Elemental analyses were carried out on a Heraeus elemental analyzer or on a Perkin Elmer model elemental analyzer. Instrumentation for C H N analyzer is based upon two general procedures. One involves the separation of carbon dioxide, nitrogen and water by a gas chromatographic column. The other involves separation by means of specific absorbents for water and carbon dioxide with the resulting change in composition of the gas mixture being measured. Thermal conductivity is the detection method in both techniques. Results are calculated by analyzing standard and occasional blank.

##### (ii) Estimation of metals

The complexes have been decomposed with conc. nitric acid and the solution was made up to a known volume. Atomic Absorption Spectroscopy is used to determine metal content of the solution.

#### 1.3.2. Magnetic measurements

The complex metal ion may contain unpaired electrons. Such complexes are found to be paramagnetic. Paramagnetic compounds will be attracted in a magnetic field, while diamagnetic compounds are repelled. The magnetic moment value corresponds to the spin only value and it varies with

spin orbit coupling and nature of coordination and delocalisation. The magnetic susceptibility may increase or decrease from the spin only value for a complex having more than one metal center. This is because the magnetic fields may align in the opposite direction. For example the paramagnetic susceptibility for a copper(II) complex is found to be 1.73 B.M. and the value may increase or decrease for a complex in the dimeric state. Thus measurement of magnetic moment gives some insight into the stereochemistry and oxidation state of the metal.

The magnetic moment is calculated using the relation

$$\mu_{eff} = 2.828\sqrt{\chi_M T} \text{ B.M}$$

where  $\chi_M$  is the molar susceptibility

The susceptibility value calculated from magnetic measurements is the sum of paramagnetic and diamagnetic susceptibilities. To calculate the exact paramagnetic susceptibility ( $\mu_{eff}$ ), the value of diamagnetic susceptibility is subtracted from the susceptibility calculated from observed results. When the structural formula of the complexes is correctly known, diamagnetic correction can be calculated from Pascal's constants.

Paramagnetic susceptibilities varies inversely with temperature (Curie's law), follow the equation

$$\chi_M = C / T,$$

where T is the temperature on Kelvin scale and 'C' is a constant. A plot of  $\chi_M$  versus 1/T yields a straight line passing through the origin and 'C' is the slope.

For many systems, this behavior is not obtained experimentally. Modifying the Curie's law as

$$\chi_M = C / T - \theta,$$

represents such systems where  $\theta$  is the temperature at which the line cuts the T-axis.

This equation is known as Curie-Weiss law and  $\theta$  is known as Weiss constant.

Then the magnetic moment is given by

$$\mu_{eff} = 2.828\sqrt{\chi_M(T - \theta)} \text{ B.M.}$$

In most of the complexes the values are very close to the spin only formula

$$\mu_s = \mu_{eff} = g\sqrt{S(S+1)} \text{ B.M.}$$

But the value may vary due to (i) orbital angular momentum contribution (ii) spin orbit coupling (iii) intermolecular effects (iv) high spin-low spin equilibria.

For transition metal ions possessing orbital angular momentum  $\mu_{eff}$  is given by

$$\mu_{S+L} = [4S(S+1) + L(L+1)]^{1/2} \text{ B.M.}$$

But in many complexes the magnetic moment values are greater than  $\mu_s$  but less than  $\mu_{S+L}$ . This is because electric field of other atoms, ion and molecules surrounding the metal ion in the complex restrict the orbital motion of electrons where the orbital moments are wholly or partly quenched. Orbital contribution is strongly quenched by the crystal field. Many complexes with  $A_{2g}$  and  $E_g$  ground state, magnetic moments differ from the spin only value due to

(i) mixing of the excited state that has some contributions from spin orbit coupling.

(ii) temperature Independent Para magnetism (TIP)

$$\mu_{eff}(A_{2g}) = \mu_s(1 - 4\lambda/10Dq) + \text{TIP},$$

where  $4\lambda/10Dq$  term arises from the mixing of excited state *via* spin orbit coupling. For the  $E_g$  state mixing in an excited state is given by

$$\mu_{eff}(E_g) = \mu_s(1 - 2\lambda/10Dq) + \text{TIP}$$

Thus the mixing of ground state and excited state depends on  $10Dq$ . Thus magnetic moments of complexes of transition metal ions are characteristic of electronic ground state and its structure [32].

Magnetic moment measurements are carried out in the polycrystalline state on a Vibrating Sample Magnetometer (VSM) at 5000 Gauss field strength. The system is calibrated using 8/32" and 3/32" cylindrical sample of high purity nickel supplied with the system. The sample has a saturation moment of 55 emu/g with a saturation flux of about 8000 Gauss.

### 1.3.3. Electronic spectroscopy

Electronic spectroscopy is a very important tool for the structural identification of thiosemicarbazones and its complexes. It is usually measured in the range 250 -900 nm. Organic ligands absorb in the region 250-350 nm and the bands are mainly due to  $\pi^* \leftarrow \pi$  and  $\pi^* \leftarrow n$  transitions. On complexation these bands may suffer a blue or red shift. Charge transfer bands may appear on complexation are of two types:  $M \leftarrow L$  or  $L \leftarrow M$  [33]. Electronic spectra also involve  $d \leftarrow d$  transitions, and are of two types (i) high intensity spin allowed and (ii) low intensity spin forbidden transitions, which appear as shoulders on spin allowed transitions. This information gives us some insight into the structure and geometry of transition metal complexes. Electronic spectral studies with EPR spectra have been used to find out bonding parameters  $\alpha^2$ ,  $\beta^2$ ,  $\gamma^2$  [31].

### 1.3.4. Infrared spectroscopy

Infrared spectroscopy is a widely used technique for the characterization of metal complexes. The basic theory is that the stretching modes of ligands changes upon complexation resulting in the subsequent change in position of the bands appearing in the IR spectrum. The shift may be to higher or lower wavelengths. Nakamoto discusses at length the characterization of metal complexes with the help of IR spectroscopy. The bands due to metal-ligand vibrations are observed mainly in the far IR region i.e., 50 - 500  $\text{cm}^{-1}$  [34]

### 1.3.5. Electron paramagnetic resonance spectroscopy

EPR spectroscopy is another important tool for the characterization of paramagnetic metal complexes. The  $g_{\parallel}$  and  $g_{\perp}$  values are calculated from the EPR spectra give some information regarding the stereochemistry of metal complexes. Hathaway and coworkers studied single crystal EPR spectra of different copper(II) complexes and correlated the observations with crystal structure and also combined electronic  $d-d$  transitions and magnetic measurements with EPR. These studies gave much insight into the structural characterization [31].

### 1.3.6. X-ray crystallography

Atoms in a single crystal of compounds diffract X-rays and this technique is used in the elucidation of structure and geometry of metal complexes.

## 1.4. Biological significance

Thiosemicarbazones possess a wide range of biological applications. Dogmak had reported the antitubercular activities of thiosemicarbazone in 1946 [35]. The applications of thiosemicarbazones include antitumour, antiviral [36], antibacterial [7], antimalarial and antifungal activities [37]. A thiosemicarbazone possessing antitumour activity against leukemia in mice was first reported by Brockman et al [38]. Blanz and French studied formyl thiosemicarbazone of different heterocyclic systems and showed that thiosemicarbazone side chain adjacent to the heterocyclic nitrogen and a conjugated NNS tridentate ligand system is necessary for anticancer activity [39]. Metal complexes of thiosemicarbazones are found to possess antifungal activity, which is effected by a substituent group at  $N(1)$  and  $N(4)$  positions of thiosemicarbazone moiety [10]. Because of promising the biological activity, 2-formyl, 2-benzoylpyridine and 2-acetylpyridine  $N(4)$ -substituted thiosemicarbazones have been extensively studied [40-43]. Heterocyclic thiosemicarbazones exercise therapeutic properties in cells by

inhibiting ribonucleotide reductase, a key enzyme in the synthesis of DNA [39]. Thiosemicarbazones inactivate the non-heme subunit and this inhibitory action is due to the coordination of iron *via* their tridentate ligating system, either by a preformed iron complex binding to the enzyme [44]. Studies have shown that iron and copper complexes are more active in cell destruction as well as in the inhibition DNA synthesis than the uncomplexed thiosemicarbazone [45]. 5-Hydroxy 2-formyl thiosemicarbazone has shown to cause lesions in DNA [46]. Therefore there may be a second site of action in addition to inhibition of ribonucleotide reductase. These observations provide an impetus to the synthesis of a large number of 2-heterocyclic thiosemicarbazones.

Copper(II) complexes of heterocyclic thiosemicarbazones have shown more fungal growth inhibition property. For example, copper(II) complexes of 2-acetylpyridine *N*(4)-substitutedthiosemicarbazones are found to be more active in the growth inhibition of the fungus *Paecilomyces variolii* at higher concentrations than nickel(II) complexes [47]. But increased activity is reported in nickel(II) complexes against *Aspergillus niger* with an increase in size of the substituent at the *N*(4) position [48]. Against *Aspergillus niger*, nickel(II) complexes of 2-acetylpyridine *N*(4)-substitutedthiosemicarbazones, the bulkiest the ligands, show modest activity of the thiosemicarbazone, while smaller complexes are inactive [49]. It is also observed that nickel(II) complex of 2-acetylpyridine *N*(4)-dimethylthiosemicarbazone where ligand is in the monoanionic form, showed an inhibitory zone of 27.7 mm at a concentration of 200  $\mu\text{g ml}^{-1}$  and 20.2 mm at 20  $\mu\text{g ml}^{-1}$  and was more active than nickel(II) complex of 2-acetylpyridine *N*(4)-dipropylthiosemicarbazone where ligand is in the monoanionic form. It is reported that the activity of nickel(II) complex of the larger pyrazine thiosemicarbazone is greater [49]. The considerably lower activity of the complex may be due to its lack of planarity based on magnetic moment. A non-planar complex may have greater difficulty in passing through the cell wall of the fungus or positioning itself once in the fungal cell.

Sarayan *et al.* [50] reported the antitumour activities of  $\alpha$ -N heterocyclic thiosemicarbazones. Brockman *et al* showed that 2-formylpyridine thiosemicarbazone is active against leukemic activity in mice [51]. It is also reported that 2-formyl 3-hydroxypyridine thiosemicarbazone [52], 2-formyl 5-hydroxypyridine thiosemicarbazone [53] are good anticancer agents. A thiosemicarbazone side chain and a conjugated NNS tridentate ligand system is essential for anticancer activity [39]. Further studies are done by modifying the sites such as aldehydic or ketonic carbon, thione group and the *N*(4) position along with the position of attachment to the pyridine/isoquinoline moiety in  $\alpha$ -N heterocyclic thiosemicarbazones. The structure activity relations of antitumour compounds were studied in detail, and can be found in reviews by Satorelli [54] and Petering [55].

Hamre *et al* [56, 57] in 1950 studied the antiviral properties of thiosemicarbazones such as *p*-aminobenzaldehyde 3-thiosemicarbazone. They reported that the compound is found to be very effective against vaccina virus in mice. Bauer and co-workers studied activity against virus and structure–activity relations of a series of compounds [58, 59]. It was found that by substitution of thiosemicarbazone moiety with aromatic ring lowered the activity against virus. The most active against vaccina virus were found to be 2-acetylpyridine *N*(4)-methyl and *N*(4)-ethyl thiosemicarbazones. The compound, 2-acetylpyridine *N*(4)-methylthiosemicarbazone, known as ‘methisazone’ is used against smallpox [60, 61, 62]. Thiosemicarbazones have also been tested against a series of other viral infections including herpes, virus, adenovirus, rhinovirus, and RNA tumor virus with mixed results [63]. Heterocyclic thiosemicarbazones inhibit the replication of the virus to a greater extent than they inhibit cellular DNA or protein synthesis [64]

Thiosemicarbazones are good antimalarial chemotherapeutic agents [4]. The features essential for antimalarial activity were found to be due to 2-pyridyl ethylidene moiety, thione sulfur, and bulky substituents at the *N*(4) nitrogen atom of thiosemicarbazones. For example, 2-acetylpyridine *N*(4)-dialkyl

thiosemicarbazones was found to be most active against *Neisseria gonorrhoeae* [65]. It has been shown that 2-formylpyridine thiosemicarbazone inhibited adenosine uptake in rodent erythrocytes and reticulocytes parasitized with *Plasmodium Berghei* [66].

### 1.5. Objective and scope of the present work

Thiosemicarbazones are a group of highly reactive compounds that form chelate complexes with metal ions. These compounds are important for their significant biological activity. They also show interesting structural properties on complexation with metal ions. Generally metal complexes of thiosemicarbazones are good therapeutic agents and complexation with metal ions enhances its biological activity. The biological activity can be varied by (ii) varying the nature and size of carbonyl moiety (iii) changing the *N*(4)-substituent and modifying the sulfur center by alkylation (iv) replacing the sulfur of the thiocarbonyl group by oxygen, selenium, imine or oxime and, (v) shifting the point of coordination of the thiosemicarbazone moiety by heterocyclic ring.

In the light of above observations, we have decided to prepare some chelate metal complexes of the quadridentate NNNS donor ligand. di-2-pyridyl ketone *N*(4), *N*(4)-disubstituted thiosemicarbazones. We have chosen this ligand for study because (i) the ligands are prepared and characterized for the first time and (ii) since there are two pyridyl nitrogens, dimers and polymers of complexes result leading to interesting structural aspects

In the present work, we have prepared two ligands (i) di-2-pyridyl ketone 3-tetramethyleneiminylthiosemicarbazone (HL<sup>1</sup>) and (ii) di-2-pyridyl ketone *N*(4)-methyl, *N*(4)-phenylthiosemicarbazone. Their copper(II), manganese(II), nickel(II), zinc(II), cadmium(II) and vanadate(V) complexes are prepared. These complexes were characterized by spectral techniques. Structures of some of them are determined by single crystal X-ray diffraction.



## SYNTHESIS, SPECTRAL AND STRUCTURAL CHARACTERIZATION OF THIOSEMICARBAZONES

---

### 2.1. Introduction

Thiosemicarbazones are a group of organic derivatives whose biological activities are a function of parent aldehyde or ketone. Recent researches on thiosemicarbazones and its metal complexes are mainly centered on its therapeutic properties. In order to facilitate these investigations, an improved method of synthesizing thiosemicarbazones is desirable. Klayman *et al.* described the preparation of a variety of *N(4)*-mono and *N(4)*, *N(4)*-disubstituted thiosemicarbazones [67].

In this chapter we describe the synthesis of the following *N(4)*, *N(4)*-disubstituted thiosemicarbazones by a general procedure adopted by *Scovill* [68]

- (i) di-2-pyridyl ketone 3-tetramethyleneiminylthiosemicarbazone (HL<sup>1</sup>)
- (ii) di-2-pyridyl ketone *N(4)* methyl, *N(4)*-phenylthiosemicarbazone (HL<sup>2</sup>)

### 2.2. Experimental

#### 2.2.1. *Materials and methods*

Carbon disulfide (Glaxo), N-methylaniline (Aldrich), sodium chloroacetate (Merck), hydrazine hydrate 98% (Glaxo), di-2-pyridyl ketone (Aldrich), pyrrolidine (Aldrich) are used without prior purification.

## Solvents used

(i) Ethanol: Commercially supplied ethanol, distilled and dried using standard methods and procedures.

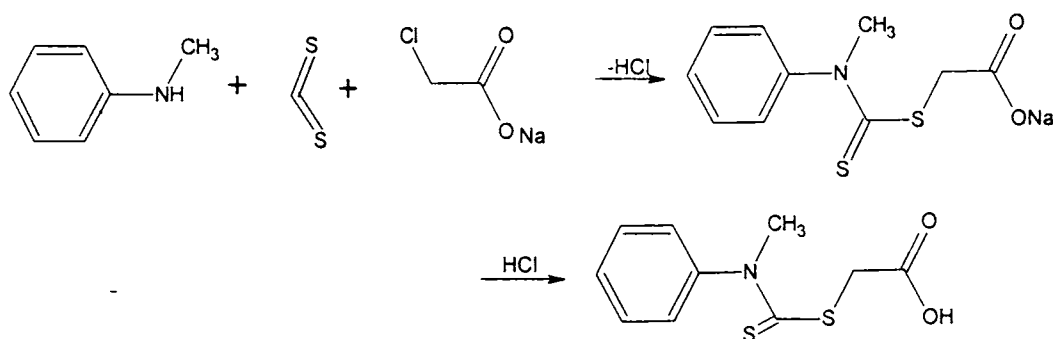
(ii) Methanol: Analar quality sample was used (Merck).

(iii) Acetonitrile: Analar quality sample (Merck) was used without any purification.

### 2.2.2. Synthesis of thiosemicarbazones

#### (i) Preparation of carboxy *N*-methyl, *N*-phenyl dithiocarbamate

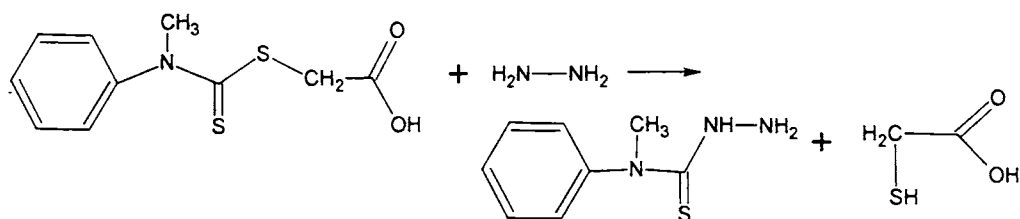
A mixture consisting of 12 ml (5.2 g, 0.2 mol) of carbon disulfide and 21.6 ml (21.2 g, 0.2 mol) of *N*-methylaniline was treated with a solution of sodium hydroxide (8.4 g, 0.21 mol) in 250 ml water. After stirring at room temperature for 4 hours, the organic layer had completely disappeared. At this point the straw colored solution was treated with 23.2 g (0.20 mol) of sodium chloroacetate and allowed to stand overnight (17 hours). The solution was acidified with 25 ml conc.HCl and the solid which separated was collected and dried. This afforded 39.7 g (82%) of pale buff colored carboxy *N*-methyl *N*-phenyl dithiocarbamate. (m.p.197-198 °C).



Carboxy *N*-methyl, *N*-phenyl dithiocarbamate

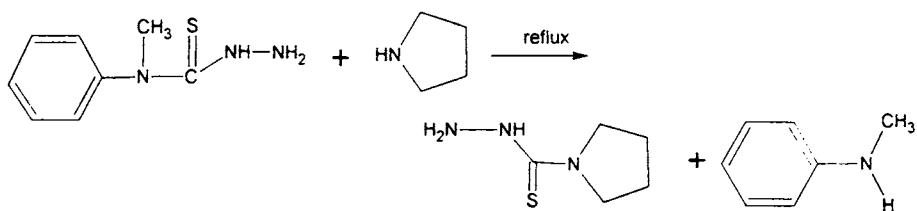
(ii) Preparation of *N*(4)-methyl, *N*(4)-phenyl 3-thiosemicarbazide (1a)

A solution of 17.7 g (0.0733 mol) of carboxy *N*-methyl *N*-phenyl dithiocarbamate in 20 ml 98% hydrazine hydrate and 10 ml water was heated in the rings of a steam bath at 85 °C. After 3 minutes crystals began to separate. Heating was continued for additional 22 minutes. The crystals were collected by filtration, washed well with water and dried. The crude product was recrystallised from a mixture of 50 ml ethanol and 25 ml water. This gave 10.8 g (81%) of stout crystals of 4-methyl, 4-phenyl 3-thiosemicarbazide. (m.p 124 °C).

*N*(4)-methyl, *N*(4)-phenyl 3-thiosemicarbazide (1a)

## (iii) Preparation of tetramethyleneimine 1-thiosemicarbazide

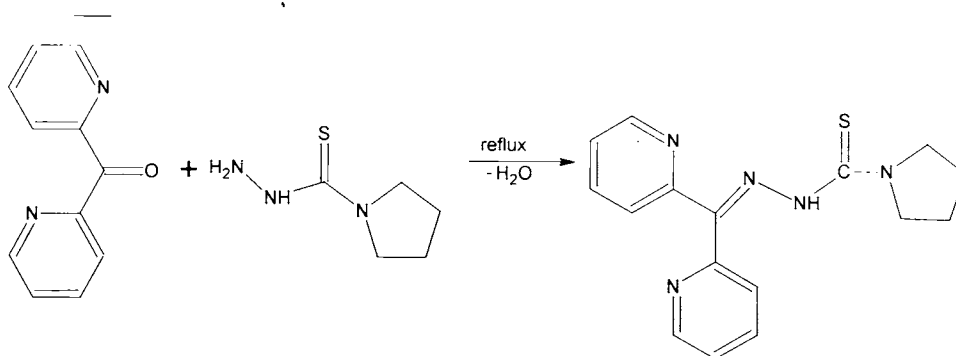
A solution of 1 g of 1a (5.52 mmol) in 5 ml acetonitrile was treated with 392 mg (5.52 mmol) of pyrrolidine and the resulting solution was heated under reflux for 15 minutes. The solution was chilled and the crystals, which separated were collected, washed well with acetonitrile. This afforded 574 mg (72%) of colorless needles of tetramethyleneimine 1-thiosemicarbazide. (m.p. 172-174 °C).



Tetramethyleneimine 1-thiosemicarbazide

(iv) *Synthesis of di-2-pyridyl ketone 3-tetramethyleneiminylthiosemicarbazone (HL<sup>1</sup>)*

The ligand was synthesized by adoption of an earlier reported method [68]. A solution of 10 mmol (1.84 g) of di-2-pyridyl ketone in 5 ml 99.5% ethanol was treated with 1.45 g (10 mmol) of tetramethyleneimine 1-thiosemicarbazide in 25 ml 99.5% ethanol and refluxed. Five drops of glacial acetic acid was added to the refluxing mixture and further refluxed for 2 hours. Yellow needle shaped crystals of di-2-pyridyl ketone 3-tetramethyleneiminyl thiosemicarbazone [69] were separated out on slow evaporation in air at room temperature. These crystals were collected, washed with little ethanol and dried over P<sub>4</sub>O<sub>10</sub> *in vacuo*. The compound was recrystallised from 99% methanol (m.p. 176 °C). Yield 1.2 g (50%). Crystals suitable for single crystal X-ray studies were obtained by a very slow evaporation of a very dilute solution of the compound in methanol.

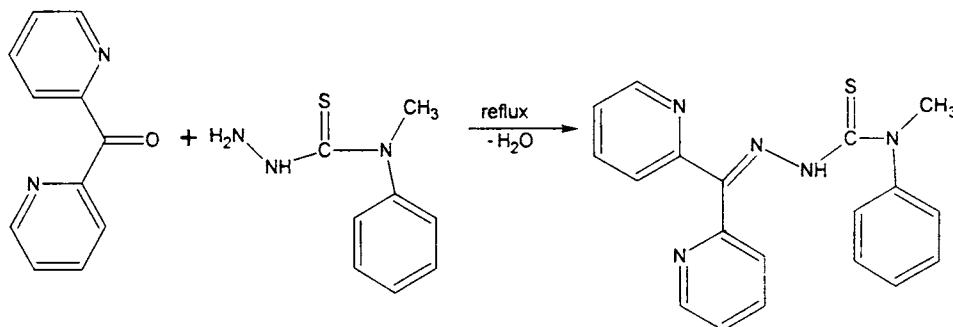


Di-2-pyridyl ketone 3-tetramethyleneiminylthiosemicarbazone (HL<sup>1</sup>)

(v) *Synthesis of di-2-pyridyl ketone N(4)-methyl, N(4)-phenylthiosemicarbazone (HL<sup>2</sup>)*

A solution of 10 mmol (1.84 g) of di-2-pyridyl ketone in 5 ml 99.5% methanol was treated with 1.81 g (10 mmol) of *N*(4)-methyl, *N*(4)-phenylthiosemicarbazide in 25 ml 99.5% methanol and refluxed. Five drops of glacial acetic acid was added to the mixture and further refluxed for 2 hours. On slow

evaporation at room temperature bright yellow plate shaped crystals of di-2-pyridyl ketone *N*(4)-methyl, *N*(4)-phenylthiosemicarbazone separated out. These crystals were collected, washed with little methanol and dried over  $P_4O_{10}$  *in vacuo*. m. p. 186 °C. Yield 1g (35%). Crystals suitable for single crystal X-ray studies were obtained by very slow evaporation of a very dilute solution of the compound in methanol.



Di-2-pyridyl ketone *N*(4)-methyl, *N*(4)-phenyl thiosemicarbazone (HL<sup>2</sup>)

### 2.2.3. X-ray crystallography of HL<sup>1</sup>

Dark orange crystals of the ligand were grown by slow evaporation of the compound in 99% methanol. Triclinic crystals of  $P\bar{1}$  space group symmetry were obtained on crystallization. A crystal of size 0.50 x 0.40 x 0.30 mm was mounted on a glass fiber with epoxy cement for X-ray crystallographic study. The pertinent crystallographic data are summarized in Table 2.2. X-ray crystal data were collected using a Siemens SMART CCD area detector diffractometer equipped with graphite-monochromatic Mo K $\alpha$  ( $\lambda = 0.71073 \text{ \AA}$ ). A total of 9492 reflections were collected. Out of these, 7124 were used in structural analysis. The data collection covered over a hemisphere of reciprocal space by a combination of three sets of exposures; each set had a different  $\phi$  angle (0, 88 and 180°) for the crystal and each exposure of 10 s covered 0.3° in  $\omega$ . The crystal-to-detector distance was 5 cm and the detector swing angle was -35°. Crystal scattering was monitored by repeating fifty initial frames at the end of data collection and analyzing the intensity of duplicate reflections, and was

found to be negligible. The intensity data were collected by  $\omega$ -scan mode within  $2.53^\circ < \theta < 28.26^\circ$  for  $hkl$  ( $-11 \leq h \leq 11$ ,  $-14 \leq k \leq 14$ ,  $-21 \leq l \leq 16$ ) in a triclinic system. The data collected were computed using SMART programme [70]. The collected data were reduced using SAINT program and the empirical absorption were carried out using the SADABS program [71]. The trial structures were obtained by direct methods using SHELXTL [72] and refined by full-matrix least squares on  $F^2$  [73] and the graphic tool was PLATON for windows [74]. Empirical absorption corrections were made on the intensity data [75]. Missing atoms were found by difference Fourier synthesis and all non-hydrogen atoms were refined with anisotropic thermal parameters. All the hydrogens were geometrically fixed and treated as riding on their parent carbon and nitrogen atoms. Scattering factors for the compound was taken from the international tables for X-ray crystallography (1974, Vol. IV). Absorption coefficients were employed using  $\psi$ -scan [ $T_{max}$  (0.9385) and  $T_{min}$  (0.9004)].

#### 2.2.4. X-ray crystallography of $HL^2$

Suitable crystals of the ligand were grown by slow evaporation of the compound in 99% methanol. Yellow triclinic crystals of  $P\bar{1}$  space group symmetry were obtained on crystallization. The crystals of size  $0.275 \times 0.225 \times 0.225$  mm were mounted on a glass fiber with epoxy cement for X-ray crystallographic study. The crystallographic data and structure refinement parameters obtained at 293 K are given in Table 2.2. X-ray crystal data were collected using an Enraf-Nonius CAD-4 diffractometer equipped with graphite-monochromatic Mo  $K\alpha$  ( $\lambda=0.71073$  Å) radiation. A total of 3316 reflections were collected. Out of these, 3311 were used in structural analysis. The intensity data were collected by  $\omega$ -scan mode within  $1.96^\circ < \theta < 24.97^\circ$  for  $hkl$  ( $-11 \leq h \leq 10$ ,  $0 \leq k \leq 11$ ,  $-12 \leq l \leq 12$ ) in a triclinic system. The data collected were computed using Argus (Nonius, MACH3 software). The collected data were reduced using Maxus (Nonius software) program. The trial structures were obtained by direct methods using SHELXS-97 [72] and refined by full-

matrix least squares  $F^2$  [73] and the graphic tool was PLATON for windows [74]. Empirical absorption corrections were made on the intensity data [75]. Missing atoms were found by difference Fourier synthesis and all non-hydrogen atoms were refined with anisotropic thermal parameters. All the hydrogens were geometrically fixed and treated as riding on their parent carbon and nitrogen atoms. Scattering factors for the compound was taken from the international tables for X-ray crystallography (1974, Vol.IV).

### 2.3. Results and discussion

The colors, elemental analytical data and melting points of both ligands are presented in Table 2.1. Both compounds are bright yellow with very sharp melting points.

#### 2.3.1. Molecular and crystal structure of HL<sup>1</sup>

Figure 2.1 shows the *ORTEP* plot with atomic numbering scheme. Bond lengths and bond angles are listed in Table 2.3. There are two crystallographically independent molecules **A** and **B**, in the asymmetric unit with bond lengths and bond angles agree with each other and are within normal ranges [76]. Molecules **A** and **B** are related by a pseudo-two fold rotation. Both molecules show an *E* configuration about C(6)–N(3) and C(12)–N(4) bonds relative to N(3)–N(4) bond [19]. The S and hydrazine N(3) atoms in both molecules are in the *Z* configuration with respect to the C(12)–N(4) bond. A similar configuration was observed in di-2-pyridyl ketone thiosemicarbazone [19], where the *N*(4) position is unsubstituted.

The C(12)–S(1) bond distances in both molecules are typical of a C=S double bond and indicate the existence of thione isomer in the solid state. The parent aldehyde or ketone has a strong influence on C–S bond distance. The electron withdrawing influence of the pyridyl rings decreases the C=S double bond distance from the standard value. Comparison of the N(3)–N(4) bond

**Table 2.1**  
**Elemental analyses data and colors of ligands HL<sup>1</sup> and HL<sup>2</sup>**

Compound	Empirical Formula	Color	Melting point (°C)	Yield (%)	Composition % (Found/Calcd)		
					Carbon	Hydrogen	Nitrogen
HL <sup>1</sup>	C <sub>16</sub> H <sub>17</sub> N <sub>5</sub> S	Yellow	176	50	62.10 (61.70)	5.56 (5.47)	22.43 (22.51)
HL <sup>2</sup>	C <sub>19</sub> H <sub>17</sub> N <sub>5</sub> S	Yellow	186	35	66.11(65.70)	4.98 (4.89)	19.94 (20.17)



**Table 2.2 Crystal data and structure refinements parameters for HL<sup>1</sup> and HL<sup>2</sup>**

Parameters	HL <sup>1</sup>	HL <sup>2</sup>
Empirical Formula	C <sub>16</sub> H <sub>17</sub> N <sub>5</sub> S	C <sub>19</sub> H <sub>1</sub> -N <sub>5</sub> S
Formula weight, M	311.41	347.44
Temperature, T (K)	293(2)	293(2)
Wavelength, Mo K $\alpha$ (Å)	0.71073	0.71073
Crystal system	Triclinic	Triclinic
Space group	$P\bar{1}$	$P\bar{1}$
Lattice constants $a$ (Å)	8.9191(2)	9.306
$b$ (Å)	11.2057(3)	9.497
$c$ (Å)	15.8582(4)	10.569
$\alpha$ (°)	103.480(1)	92.54
$\beta$ (°)	90.131(1)	99.26
$\gamma$ (°)	90.758(1)	104.92
Volume V (Å <sup>3</sup> )	1541.12(7)	887.2
Z	4	2
Calculated density, $\rho$ (Mg m <sup>-3</sup> )	1.351	1.301
Absorption coefficient, $\mu$ (mm <sup>-1</sup> )	0.214	0.194
$F(000)$	664	364
Crystal size (mm)	0.50 x 0.40 x 0.30 mm	0.275 x 0.225 x 0.225 mm
$\theta$ Range for data collection	2.53 to 28.26	1.96 to 24.97.
Limiting indices	-11 $\leq$ h $\leq$ 11, -14 $\leq$ k $\leq$ 14, -21 $\leq$ l $\leq$ 16	-11 $\leq$ h $\leq$ 10, 0 $\leq$ k $\leq$ 11, -12 $\leq$ l $\leq$ 12
Reflections collected	9492	3316
Unique Reflections	7124 [ $R(int)$ = 0.0826]	3311 [ $R(int)$ = 0.0111]
Completeness to $\theta$	28.26 93.7%	24.97 99.9%
Absorption correction	Empirical	None
Maximum and minimum transmission	0.9385 and 0.9004	0.7242 and 0.3596
Refinement method	Full-matrix least-squares on $F^2$	Full-matrix least-squares on $F^2$
Data/restraints/parameters	7124/ 0/ 398	3111 / 0 / 295
Goodness-of-fit on $F^2$	0.974	1.030
Final $R$ indices [ $I > 2\sigma(I)$ ]	$R_1 = 0.0958, wR_2 = 0.2401$	$R_1 = 0.0372, wR_2 = 0.0899$
$R$ indices (all data)	$R_1 = 0.1253, wR_2 = 0.2566$	$R_1 = 0.0712, wR_2 = 0.1012$
Extinction coefficient	0.002(2)	0.012(2)
Largest difference peak and hole (e Å <sup>-3</sup> )	0.967 and -1.272	0.235 and -0.160

distance 1.371(4) Å in molecule **A** and 1.360 (4) Å in molecule **B** with the corresponding distance in di-2-pyridyl ketone thiosemicarbazone (1.371 Å) [19] indicates that it is a single bond and weighted average of N(3)-N(4) bond distance in molecules **A** and **B** suggests the existence of thione form for HL<sup>1</sup>.

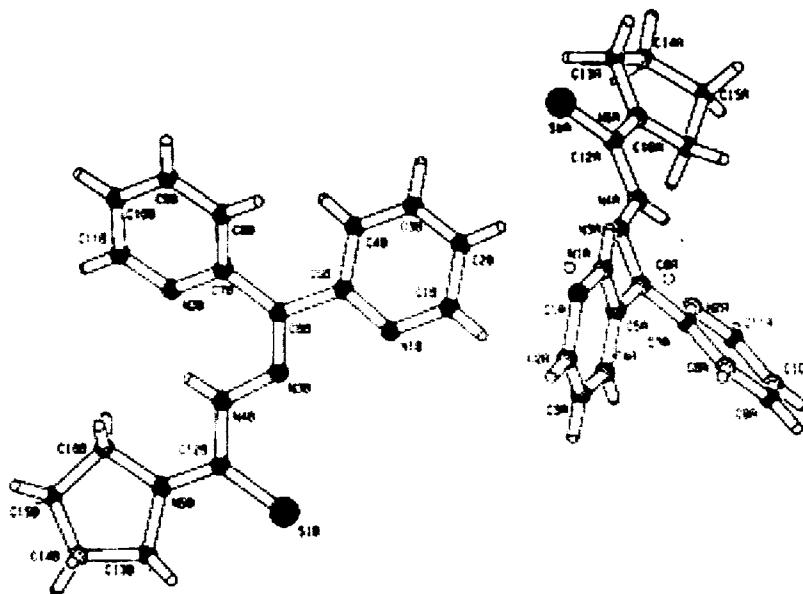


Figure 2.1. PLATON diagram of the compound HL<sup>1</sup>

The N(3)-N(4) bond length in HL<sup>1</sup> is shorter than N(1)-N(2) bond distance 1.404 Å reported in acetone thiosemicarbazone [77]. The explanation for the shortened N(3)-N(4) bond distance can be attributed to the interaction of a group on the C(6) atom. Thus aryl thiosemicarbazones can be treated as extensively delocalised systems. The C(6A)-N(3A) and C(6B)-N(3B) bond distances are found to be 1.299(4) and 1.308(4) Å respectively are greater than for a typical C-N double bond. The difference in bond length can be explained by the inclusion of resonance forms involving C(6)-N(3)-N(4) which lengthens C(6)-N(3) bond and shortens N(3)-N(4) bonds.

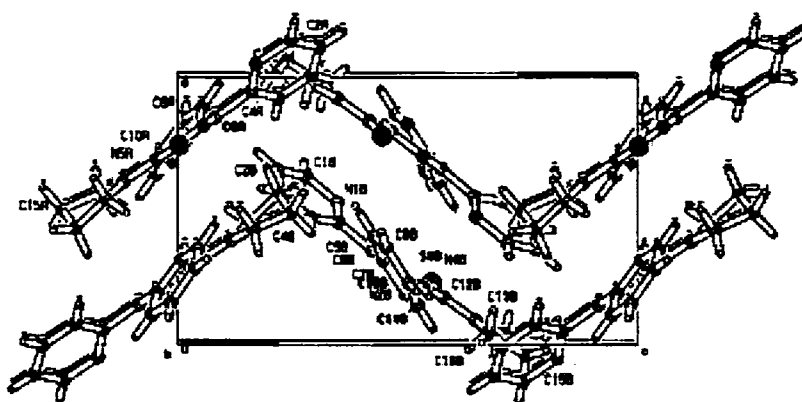


Figure 2.2. Unit cell packing diagram of HL<sup>1</sup> viewed down the b-axis.

In molecule **B**, this ring shows disorder, so that in the major and minor configurations, atoms C(14A) and C(14B) deviate in opposite directions by 0.382(2) and 0.543(2) Å respectively, from the N(5)/C(13)/C(15)/C(16) plane.

In both molecules of **A** and **B**, the relative conformations of two pyridyl rings with respect to the planar thiosemicarbazone (S(1)/N(3)/N(4)/C(6)/C(12) are conditioned by the sp<sup>2</sup> hybridized C(6) atom (the average bond angle subtended at C(6) is 120.0° in molecule **A** and 119.8° in molecule **B**). The dihedral angles between the thiosemicarbazone and the two pyridyl rings are relatively small, 35.8 (1)° and 22.7 (2)° in molecule **A**, and 21.7 (2)° and 22.7 (2)° in molecule **B**), due to a resonance effect between the π systems. An intramolecular N(4)–H(4)---N(2) hydrogen bond forms a six membered N(2)—C(7)—C(6)—N(3)—N(4)—H(4) ring in both molecules. In the packing, the molecules are stacked into molecular columns parallel to the *b* direction. (Figure 2.2, Table 2.4)

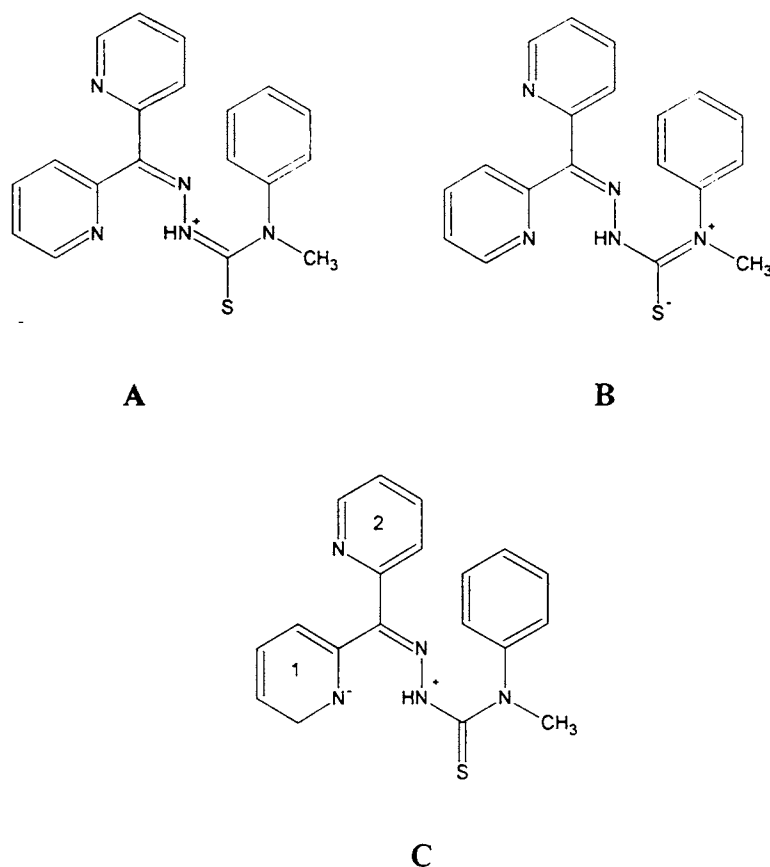
### 2.3.2. Molecular and crystal structure of HL<sup>2</sup>

Figure 2.3 shows the *PLATON* plot of HL<sup>2</sup> with atomic numbering scheme. Bond lengths and bond angles are listed in Table 2.3. The molecule is non-planar as a whole, consisting of three fragments, two planar pyridine rings

and the thiosemicarbazone moiety [19]. The structure adopts a *E* confirmation about C(6)—N(3) and C(12)—N(4) bonds relative to N(3)—N(4) bond as found in 2-acetylpyridine N(4)-methylthiosemicarbazone. The comparison of N(3)-N(4) bond distance of 1.362(2) Å with corresponding N-N bond distance of 1.44 Å for unsubstituted thiosemicarbazones [77], canonical form C might exist. The resonance form involving pyridine ring 1 would account for the shortening of N-N distance through extensive electron delocalisation. This is supported by shortening of bond distance C(6)-C(5) (1.487 Å) in pyridine ring 1 as compared to C(6)-C(7) (1.498 Å) in ring 2. The C(6)-N(3) bond distance of 1.295(2) Å might also be the indication of some single bond character in accordance with resonance form C in Scheme 1. The net result would be a small negative charge residing on pyridine nitrogen N(1) which is reported to be important in terms of biological activity [77-79].

The C(12)-S(1) bond distance 1.6686(12) Å is intermediate between 1.82 Å for a C-S single bond and 1.56 Å for a C=S double bond, respectively [80]. The corresponding C(12)-N(4) and C(12)-N(5) are found to be 1.377(2) Å and 1.349(2) Å are indicative of some double bond character is in agreement with resonance forms of A and B in Scheme 1 as shown below [81, 82].

The compound adopts a configuration in which the atom N(3) is *cis* to S(1). Rotation of the fragment by 180° about the C(12)-N(4) bond places the sulfur atom, imino nitrogen and the pyridine nitrogen N(2) on the same side, thus enabling the compound to function as a planar N<sub>2</sub>S tridentate anionic ligand as in most thiosemicarbazones such as 2-acetylpyridine [78] and 2-formylpyridine thiosemicarbazones [83].



Scheme 1

Unit cell packing diagram of the ligand  $HL^2$  viewed along the  $b$ -axis is shown in the Figure 2.4. The molecules in the unit cell are arranged with in such a way that the molecular units are geometrically opposite to each other giving centrosymmetry to the whole crystal. The assemblage of molecules are resulted by the diverse  $\pi$ - $\pi$  stacking,  $CH$ - $\pi$  and hydrogen bonding interactions are depicted in Table 2.5. The pyridyl ring Cg(1) is involved in  $\pi$ - $\pi$  interactions with the pyridyl ring (Cg(2) of the neighboring unit at a distance of 4.5843 Å. The crystal structure is further stabilized by four  $CH$ - $\pi$  interactions. The intramolecular hydrogen bonding interaction such as  $N(4)-H(104) \cdots N(2)$ ,  $C(8)-H(8) \cdots N(1)$  and  $C(19)-H(19A) \cdots S(1)$  at distances of 1.95, 2.52 and 2.63 Å respectively in the unit cell also adds to the stability of unit cell packing.

**Table 2.3****Comparison of selected bond lengths (Å) and bond angles (°) of HL<sup>1</sup> and HL<sup>2</sup>**

Bond length	HL <sup>1</sup>	HL <sup>2</sup>
S(1A)-(12A)	1.671(4)	
S(1B)-C(12B)	1.676(4)	
N(3A)-N(4A)	1.371(4)	
N(3B)-N(4B)	1.360(4)	
N(3A)-C(6A)	1.308(4)	
N(3B)-C(6B)	1.299(4)	
N(4A)-C(12A)	1.386(4)	
N(4B)-C(12B)	1.393(4)	
N(5A)-C(12A)	1.349(5)	
N(5B)-C(12B)	1.340(5)	
S(1)-C(12)		1.6686(12)
N(3)-N(4)		1.362(2)
N(4)-C(12)		1.377(2)
N(3)-C(6)		1.295(2)
N(5)-C(12)		1.349(2)
C(6A)-N(3A)-N(4A)	118.6(3)	
N(3A)-N(4A)-C(12A)	118.7(3)	
N(5A)-C(12A)-N(4A)	112.3(3)	
N(5A)-C(12A)-S(1A)	123.2(3)	
N(4A)-C(12A)-S(1A)	124.6(3)	
C(6B)-N(3B)-N(4B)	118.9(3)	
N(3B)-N(4B)-C(12B)	119.8(3)	
N(5B)-C(12B)-N(4B)	112.4(3)	
N(5B)-C(12B)-S(1B)	124.1(3)	
N(4B)-C(12B)-S(1B)	123.5(3)	
C(6)-N(3)-N(4)		120.94(16)
N(3)-N(4)-C(12)		118.67(16)
N(5)-C(12)-N(4)		113.73(16)
N(5)-C(12)-S(1)		123.48(14)
N(4)-C(12)-S(1)		122.79(14)

Table 2.4

H-bonding,  $\pi$ - $\pi$  and CH- $\pi$  interaction parameters of the compound HL<sup>1\*</sup>

<b>H-bonding</b>				
Donor---H...acceptor	D-H (Å)	H---A (Å)	D---A (Å)	D-H---A (°)
N(4A)-H(4AA)---N(2A)	0.86	1.99	2.6458	132
N(4B)-H(4BA)---N(2B)	0.86	1.94	2.6141	134
C10B-H(1B)---S(1B)	0.93	2.83	2.7057	158
C(2B)-H(2BB)---N(3A)	0.93	2.51	3.3561	151
<b><math>\pi</math>-<math>\pi</math> interactions</b>				
Cg(1)-Res(1)---Cg(J)	Cg-Cg (Å)	$\alpha^\circ$	$\beta^\circ$	
Cg(4) [2] -> Cg(6) <sup>a</sup>	4.3400	37.87	55.12	
Cg(6)[2] -> Cg(4) <sup>a</sup>	4.3400	37.87	17.58	
Equivalent position codes a = 1-x, -y, 1-z	Cg(4)=N(1B), C(1B), C(2B), C(3B), C(4B), C(5B) Cg(6)= N(2B), C(7B), C(8B), C(9B), C(10B), C(11B)			
<b>CH-<math>\pi</math> interactions</b>				
X-H(I)---Cg(J)	H--Cg (Å)	X-H--Cg (°)	X--Cg (Å)	
N(1A)-H(1AA)[1]-> Cg(5) <sup>c</sup>	2.7279	141.18	3.4404	
C(1A)-H(1AB)[1]->Cg(4) <sup>b</sup>	3.2198	156.58	4.0899	
N(1B)-H(1BA)[2]->Cg(6) <sup>a</sup>	2.8358	117.32	3.3197	
C(13B)-H(13C)[2]->Cg(6) <sup>c</sup>	3.3501	125.56	3.9929	
C(14A)-H(14B)[1]->Cg(5) <sup>d</sup>	3.2027	131.63	3.9148	
C(16A)-H(16A)[1]->Cg(3) <sup>e</sup>	3.1103	163.92	4.0512	
C(16B)-H(16C)[2]->Cg(4) <sup>a</sup>	3.0975	158.96	4.0180	
Equivalent position codes b = 1+x, y, z	Cg(3)=N(1A), C(1A), C(2A), C(3A), C(4A), C(5A)			
c = -x, 1-y, 1-z	Cg(4)=N(1B), C(1B), C(2B), C(3B), C(4B), C(5B)			
d = 1-x, -y, -z	Cg(5)=N(2A), C(7A), C(8A), C(9A), C(10A), C(11A)			
e = 2-x, -y, -z	Cg(6)= N(2B), C(7B), C(8B), C(9B), C(10B), C(11B)			

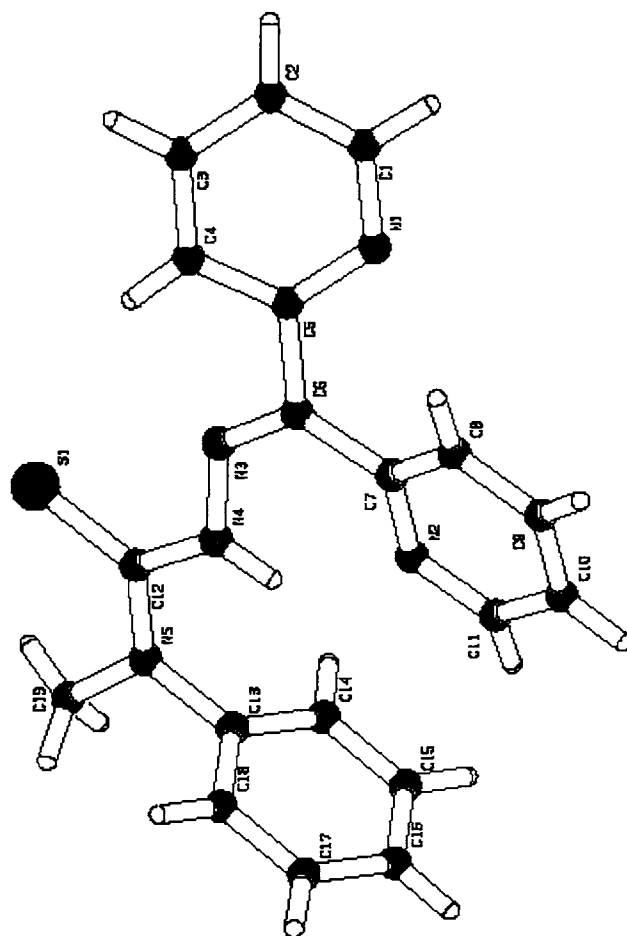
(D=Donor. A=acceptor. Cg=Centroid.  $\alpha$ =dihedral angles between planes I and J.  $\beta$ =angle Cg(1)-Cg(J))

**Table 2.5****H-bonding,  $\pi$ - $\pi$  and CH- $\pi$  interaction parameters of the compound HL<sup>2</sup>**

<b>H-bonding</b>				
Donor-H...acceptor	D-H (Å)	H...A (Å)	D...A (Å)	D-H...A (°)
N(4)—H(104)—N(2)	0.89	1.95	2.6424	134
C(8)—H(8)---N(1)	0.91	2.52	2.9503	109
C(19)—H(19A)---S(1)	0.94	2.63	3.0358	107
<b><math>\pi</math>-<math>\pi</math> interactions</b>				
Cg(I)-Res(I)---Cg(J)	Cg-Cg(Å)		$\alpha^\circ$	$\beta^\circ$
Cg(1)-[I]---Cg(2) <sup>c</sup>	4.5843		46.02	58.82
Cg(2)-(I)---Cg(1) <sup>c</sup>	4.5843		46.02	13.49
Equivalent position codes		Cg(1)=N(1), C(1), C(2), C(3),C(4),C(5)		
c = 1 - x, 1-y, -z		Cg(2)=N(2)C(7),C(8),C(9),C(10),C(11)		
<b>CH-<math>\pi</math> interactions</b>				
X-H(I)---Cg(J)	H..Cg(Å)	X-H--Cg (°)	X---.Cg(°)	
C(4)-H(4)[1]->Cg(2) <sup>c</sup>	2.8565	127.77	3.4861	
C(11)-H(11)[1]->Cg(3) <sup>a</sup>	3.3606	117.35	3.8694	
C(19)-H(19)[1]->Cg(3) <sup>b</sup>	3.1231	117.3	3.6058	
C(19)-H(19B)[1]->Cg(3) <sup>b</sup>	3.1657	112.83	3.6058	
Equivalent position codes a = x, y, z		Cg(2)=N(2)C(7),C(8),C(9),C(10),C(11)		
b = -x, 1-y, 1-z		Cg(3)=C(14), C(15), C(16),C(17),C(18)		
c = 1 - x, 1- $\bar{y}$ , -z				

(D=Donor, A=acceptor, Cg=Centroid,  $\alpha$ =dihedral angles between planes I & J,  $\beta$ =angle Cg(1)-Cg(J))



Figure 2.3. PLATON diagram of HL<sup>2</sup>

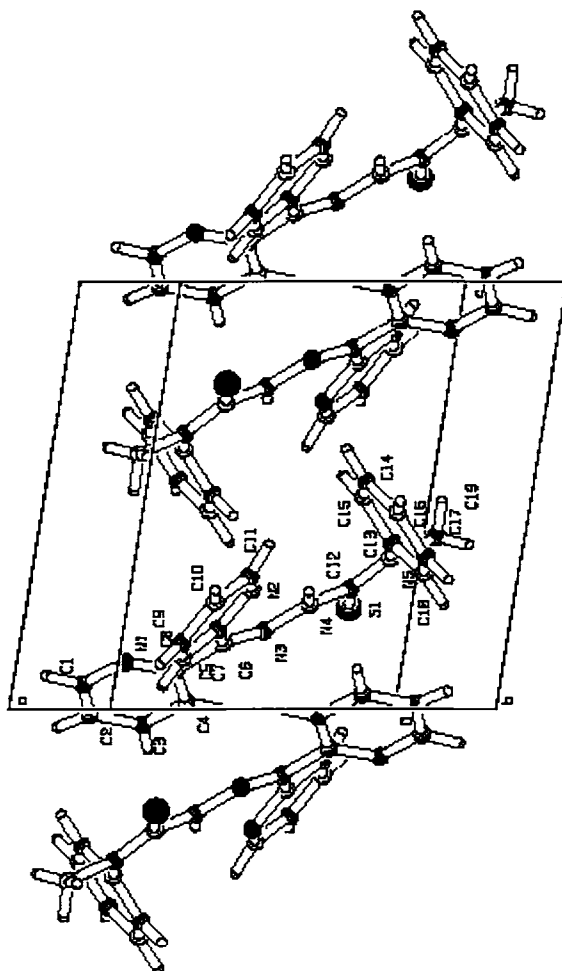


Figure 2.4. Unit cell packing diagram of HL<sup>2</sup> viewed along the *b*-axis

### 2.3.3. Infrared spectra

Table 2.6 lists the tentative assignments of selected IR bands of HL<sup>1</sup> and HL<sup>2</sup> in the 4000-400 cm<sup>-1</sup> region and their IR spectra are shown in the Figures 2.5 and 2.6 respectively. The infrared spectra of thiosemicarbazones HL<sup>1</sup> and HL<sup>2</sup> are similar, the  $\nu(\text{NH})$  region of their spectra feature broad shapeless bands, making meaningful assignments difficult. The highest frequency band at 3428 cm<sup>-1</sup> of HL<sup>1</sup> and HL<sup>2</sup> can be assigned to overlapping of  $\nu_a(\text{N-H})$  vibrations of imino group N(4)H with  $\nu(\text{O-H})$  vibrations of water impurity in the ligand. A weak band at 3049 cm<sup>-1</sup> also is indicative of  $\nu(\text{NH})$  stretching vibration. The

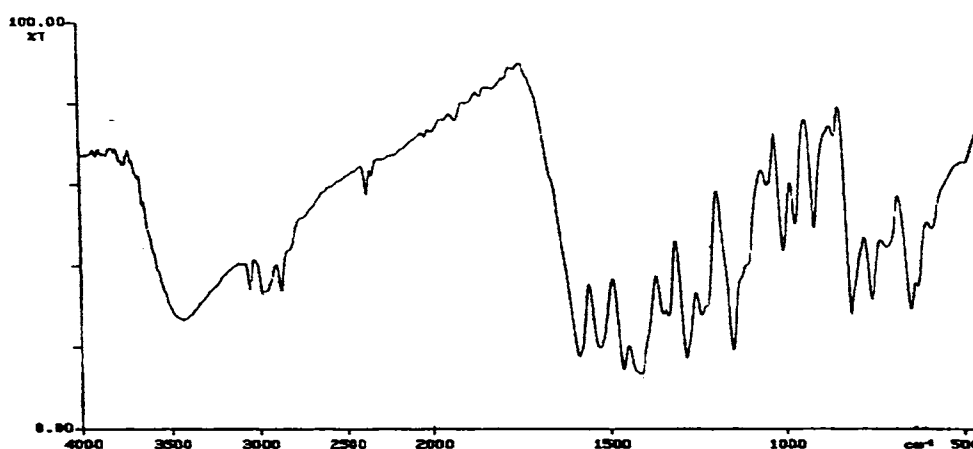


Figure 2.5. IR spectrum of HL<sup>1</sup>

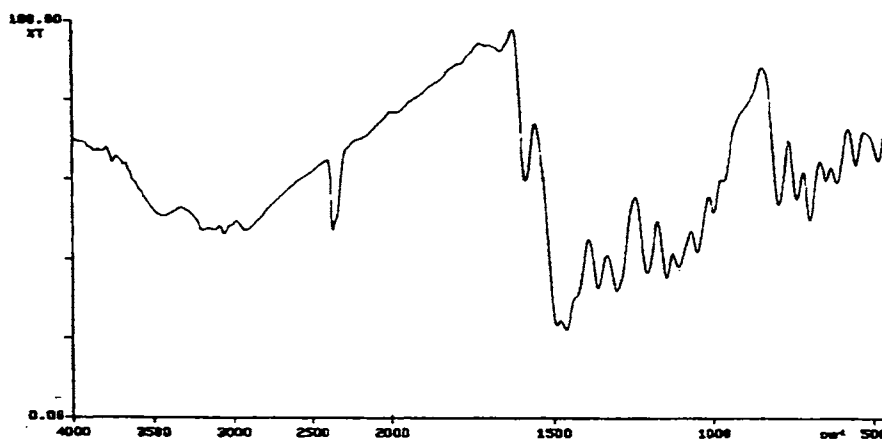


Figure 2.6. IR spectrum of HL<sup>2</sup>

downward shift of  $\nu_a(\text{N-H})$  bands confirms the strong hydrogen bonding with one of the pyridyl nitrogens. Strong bands at  $\sim 1580\text{ cm}^{-1}$  of both ligands suggest  $\nu(\text{C}(6)\text{-N}(3))$  stretching vibration in the thiosemicarbazone moiety. A band at  $2565\text{ cm}^{-1}$  due to  $\nu(\text{S-H})$  is absent indicating that both ligands exist predominantly in thione form in the solid state. This observation was further supported by the presence of a very broad band due to  $\nu(\text{N-H})$  at *ca.*  $3428\text{ cm}^{-1}$  [81].

A number of bands have contributions from  $\nu(\text{C}=\text{S})$ , but the many ring vibrations of these thiosemicarbazones contribute to the complexity of the spectra making thioamide bands difficult to assign. Higher bands appearing in the range  $1330\text{-}1360\text{ cm}^{-1}$  and lower bands *ca.*  $800\text{ cm}^{-1}$  have significant contributions from  $\text{C}=\text{S}$  stretching and  $\text{C}=\text{S}$  bending vibrations. Out of plane pyridyl ring vibration in thiosemicarbazone of both ligands are indicated by a medium band due to  $\rho(\text{py})$  found near  $640\text{ cm}^{-1}$ .

#### 2.3.4. $^1\text{H NMR}$ spectra

The  $^1\text{H NMR}$  spectra of ligands  $\text{HL}^1$  and  $\text{HL}^2$  are shown in Figures 2.7 and 2.8 respectively and their chemical shift values are listed in Table 2.7. The assignments of chemical shift are based on reported studies of  $N(4)$ -substituted thiosemicarbazones derived from 2-formyl [83], 2-acetyl [10], 2-benzoylpyridine [42] and 2-pyridineformamide [84]. The  $N(4)\text{H}$  resonance signals appear at a downfield value of 14.89 in  $\text{HL}^1$  and 14.68 in  $\text{HL}^2$  respectively indicates hydrogen bonding with one of the pyridyl nitrogens as shown by their crystal structure. Both ligands are found to be bright yellow indicating that a substantial amount of bifurcated amount of *E* isomer is present as in 2-acetylpyridine  $N(4)$ -dialkyl thiosemicarbazones [22]. The presence of this type of isomer has recently been found for di-2-pyridyl ketone  $N(4)$ ,  $N(4)$ -dimethylthiosemicarbazones [16]. This form of thiosemicarbazone has the hydrogen-bonding proton farthest downfield. The  $\text{C}(1)\text{H}$  resonance of the 2-acetyl, 2-formyl and 2-benzoyl pyridine  $N(4)$ -substituted thiosemicarbazone is



**Table 2.6**  
**Infrared spectral assignments (cm<sup>-1</sup>) for HL<sup>1</sup> and HL<sup>2</sup>**

Compound	$\nu(\text{N}(4)\text{-H})$	$\nu(\text{C}(6)\text{-N}(3))$	$\nu(\text{N}(3)\text{-N}(4))$	$\nu(\text{C}(12)\text{-S}(1))$	$\delta(\text{C}(12)\text{-S}(1))$	$\delta(\text{o.p})$
HL <sup>1</sup>	3048 w	1582 s	1000 m	1330 s	808 m	638 s
HL <sup>2</sup>	3057 w	1580 s	998 w	1361 s	793 m	644 m

s=strong, m= medium, w= weak, All values are reported in cm<sup>-1</sup>.

**Table 2.7**  
**<sup>1</sup>H NMR assignments of ligands. HL<sup>1</sup> and HL<sup>2</sup>**

Compound	N(4)H	C(1)H	C(2)H	C(3)H	C(4)H	C(8)H	C(9)H	C(10)H	C(11)H
HL <sup>1</sup>	14.68, 1H, s	8.71, 1H, d	7.34, 1H, t	7.78, 1H, t	8.07, 1H, d	7.67, 1H, d	7.78, 1H, t	7.28, H, q	860, 1H, d
HL <sup>2</sup>	14.84, 1H, s	8.51, 1H, d	7.34, 1H, q	7.77, 1H, t	8.04, 1H, d	7.64, 1H, d	7.85, 1H, t	7.26, 1H, t	8.51, 1H, d

(All chemical shift values are given in units of ppm), <sup>a</sup> = protons of tetrametyleneimine, <sup>b</sup> = protons of phenyl group.

**Table 2.8**  
**Electronic (Diffuse reflectance) spectral assignments (cm<sup>-1</sup>) for compounds HL<sup>1</sup> and HL<sup>2</sup>**

Compound	$\pi^* \leftarrow n$	$\pi^* \leftarrow \pi$
HL <sup>1</sup>	29155, 30864	36232, 35088
HL <sup>2</sup>	26882s, 30030 sh	37543s, 32787

### 2.3.5. Electronic spectra

Solid-state electronic spectra of the compounds are listed in Table 2.8. The ligands HL<sup>1</sup> and HL<sup>2</sup> show absorption maxima at 36232 and 37543 cm<sup>-1</sup> respectively, can be attributed to intraligand  $\pi^* \leftarrow \pi$  transitions of the pyridyl ring and imine function of the thiosemicarbazone moiety. The  $\pi^* \leftarrow n$  transitions are seen at 29155 and 26882 cm<sup>-1</sup> for HL<sup>1</sup> and HL<sup>2</sup> respectively. A shoulder at 22000 cm<sup>-1</sup> and 23810 cm<sup>-1</sup> of HL<sup>1</sup> and HL<sup>2</sup> respectively indicates  $\pi^* \leftarrow n$  transition of thioamide function. These  $\pi^* \leftarrow n$  bands shift to higher energy on complexation. (Figures 2.9 and 2.10).

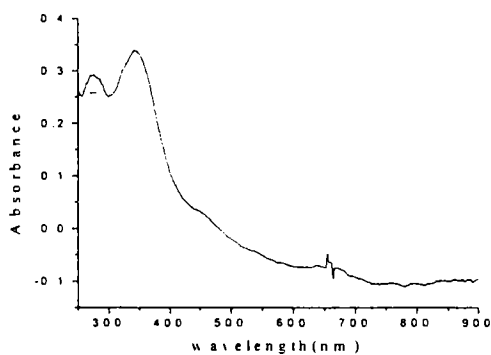


Figure 2.9. Electronic spectrum of HL<sup>1</sup>

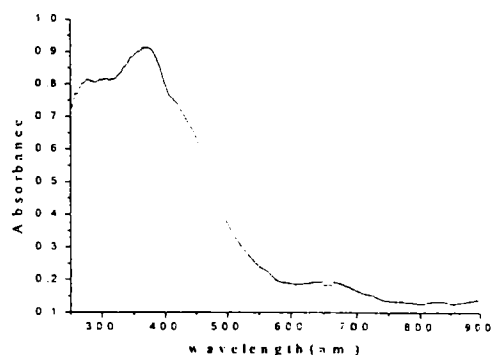


Figure 2.10. Electronic spectrum of HL<sup>2</sup>

### 2.4. Concluding remarks

We have synthesized two *N*(4), *N*(4)-disubstituted ligands of di-2-pyridyl ketone thiosemicarbazone abbreviated as HL<sup>1</sup> and HL<sup>2</sup>. Elemental analysis data is consistent with the empirical formula of ligands. The compounds are further characterized by IR, <sup>1</sup>H NMR and electronic spectral studies. The compounds were crystallized and further characterized by X-ray crystallographic analysis. The ligand HL<sup>1</sup> was stabilized by both inter and intraligand hydrogen bonding whereas HL<sup>2</sup> by intramolecular hydrogen bonding only. The results obtained from X-ray crystallographic analysis are found to be consistent with spectral studies.

**SYNTHESIS, STRUCTURAL AND SPECTRAL  
CHARACTERIZATION OF COPPER(II) COMPLEXES  
DERIVED FROM LIGANDS, DI-2-PYRIDYL KETONE 3-  
TETRAMETHYLENEIMINYLTIOSEMICARBAZONE  
AND DI-2-PYRIDYL KETONE *N*(4)-METHYL, *N*(4)-  
PHENYLTHIOSEMICARBAZONE**

---

### 3.1. Introduction

Thiosemicarbazones belong to a group of thiourea derivatives, the biological activities of which are a function of the parent aldehyde or ketone [9, 41, 89]. Their metal complexes, especially those containing copper(II) and iron(III) are more active than uncoordinated thiosemicarbazone [90] and this enhanced biological activity of metal thiosemicarbazones has been under investigation for some time [50]. They are more active in cell destruction, as well as in the inhibition of DNA synthesis [91-93]. The solution chemistry and crystal structure of pyridine 2-carbaldehyde thiosemicarbazone [94] and its precursor complex  $[\text{CuL}^1(\text{O}_2\text{CMe})]$  [95, 96] as well as many other  $\alpha$ -heterocyclic carbaldehyde thiosemicarbazones [97-101] and their metal complexes [102-105] have been studied. Biologically active copper(II) complexes of 2-acetylpyridine *N*(4)-substituted thiosemicarbazones were widely studied [21]. Copper catalyses redox reactions in biological systems primarily in the reduction of oxygen to water [106].



Copper and its complexes are widely used in catalytic, oxygenation [107] and organic reactions. Copper exists in two oxidation states, copper(I) and copper(II). The role of copper in organic reactions is related to its oxidation states. In this chapter we report spectral and structural studies of copper(II) complexes of a potentially NNNS donor ligand, di-2-pyridyl ketone thiosemicarbazones. The ligands chosen for the study are

- (i) di-2-pyridyl ketone 3-tetramethyleneiminylthiosemicarbazone (HL<sup>1</sup>)
- (ii) di-2-pyridyl ketone *N*(4)-methyl, *N*(4)-phenylthiosemicarbazone (HL<sup>2</sup>).

In this chapter we describe the preparation of thirteen copper(II) complexes of HL<sup>1</sup> and HL<sup>2</sup> and their characterization by various methods such as partial elemental analyses, molar conductivity, magnetic susceptibility at room temperature and IR, EPR and electronic spectra.. Four copper(II) complexes were analyzed meticulously by single crystal X-ray diffraction methods.

### 3.2. Experimental

#### 3.2.1. *Materials and methods*

Ligands HL<sup>1</sup> and HL<sup>2</sup> were synthesized by methods as described in Chapter 2. Following materials and solvents were used

Copper(II) acetate monohydrate (Merck), copper(II) sulfate pentahydrate (Merck), copper(II) nitrate hemipentahydrate (Merck), copper(II) chloride dihydrate (Merck), potassium thiocyanate (Merck), sodium azide (Merck), copper(II) bromide (Merck) were used as received.

Solvents used: Ethanol (99%), and methanol (99%) were purified before use by reported methods.

### 3.2.2. Physical measurements

Elemental analyses (C, H, N) were carried out using a Heraeus Elemental Analyzer at RSIC, CDRI, Lucknow, India. Molar conductance measurements of the complexes were carried out in DMF solvent at  $28 \pm 2$  °C on a Century CC-601 digital conductivity meter with dip type cell and platinum electrode. Approximately  $10^{-3}$  solutions were used. The magnetic susceptibility measurements were made using a Vibrating Sample Magnetometer (VSM) at IIT, Roorkee. IR spectra were recorded on a Shimadzu DR 8001 series FTIR instrument as KBr pellets for spectra run from 4000 to  $400\text{ cm}^{-1}$ , and far IR spectra of sample in polyethylene disc for the range  $500\text{-}100\text{ cm}^{-1}$  in a Nicolet Magna 550 FTIR instrument. Electronic spectra in the solid state were recorded on Ocean Optics SD 2000 Fibre Optic Spectrometer at our center. Single crystal XRD were done using a Bruker SMART APEX CCD diffractometer at IISc, Bangalore.

### 3.2.3. Syntheses of complexes

The general method of syntheses of copper complexes (1-8) of HL<sup>1</sup> is as described below.

Copper(II) complexes were prepared by refluxing an equimolar solution of the ligand HL<sup>1</sup> in 20 ml of hot ethanol and the appropriate copper(II) salt in the same solvent for two hours. The complex [Cu<sub>2</sub>L<sup>1</sup>Cl<sub>3</sub>] was prepared by refluxing ethanolic solutions of ligand HL<sup>1</sup> (1 mmol) and CuCl<sub>2</sub>·2H<sub>2</sub>O (2 mmol) for two hours. Azido and thiocyanato complexes were prepared by refluxing an equimolar mixture of ligand and copper(II) acetate in hot methanol and to the refluxing solution, sodium azide or potassium thiocyanate was added in portions in the same molar ratio. On slow evaporation at room temperature, dark blue crystals of complexes separated out, which were collected, washed with water, followed by ether and dried over P<sub>4</sub>O<sub>10</sub> *in vacuo*.

Copper(II) complexes of  $HL^2$  were prepared by similar methods as described above.

Out of eight copper(II) complexes of  $HL^1$ , five of them have the empirical formula  $[CuL^1X]$  where  $X = Cl$  (1), Br (2),  $NO_3$  (3),  $N_3$  (4), SCN (5). With copper perchlorate and  $HL^1$  yielded the complex  $[Cu_2L^1_2(OH)]ClO_4$  (6). With copper(II) chloride another complex was also yielded with empirical formula  $[Cu_2L^1Cl_3]$  (7). With copper(II) sulfate  $HL^1$  yielded the complex of the empirical formula  $[Cu_2L^1_2(SO_4)]$  (8).

Five copper(II) complexes were prepared using  $HL^2$  and they have the composition  $[CuL^2X]$  where  $X = Cl$  (9), Br (10),  $NO_3$  (11),  $N_3$  (12). With copper(II) sulfate  $HL^2$  yielded the complex having the empirical formula  $[CuL^2(SH)] \cdot H_2O$  (13)

#### 3.2.4. X-ray crystallography

Single crystal of compound **8** for X-ray analysis was grown by slow evaporation of the complexes in 1:1 mixture of methanol and chloroform. Dark blue triclinic crystals of the complex  $[Cu_2L^1_2(SO_4)]_2 \cdot 6H_2O$  having dimensions 0.40 x 0.35 x 0.30 mm with  $P\bar{1}$  symmetry were sealed in a glass capillary for X-ray crystallographic study. The intensity data was measured at room temperature on a SMART APEX CCD diffractometer equipped with graphite-monochromated Mo  $K\alpha$  ( $\lambda = 0.71073 \text{ \AA}$ ) radiation. Selected crystal data and data collection parameters are given in Table 3.2. The intensity data were collected by  $\Omega - \varphi$  mode within  $1.60^\circ < \theta < 27.46^\circ$  for  $hkl$  ( $-13 \leq h \leq 13$ ,  $-16 \leq k \leq 17$ ,  $-18 \leq l \leq 18$ ) in a triclinic system. Out of 19156 reflections collected, 7528 unique reflections were used for structural analysis. The collected data were reduced using SAINT program [70] and the empirical absorption was carried out using the SADABS program [71]. The trial structure was obtained by direct methods using SHELXTL [72], which revealed the position of all non-hydrogen atoms and refined by full-matrix least squares on  $F^2$  (SHELXL-97) [73] and

graphic tool was PLATON for windows [74]. The non-hydrogen atoms were refined with anisotropic thermal parameters. All the hydrogen atoms were geometrically fixed and allowed to refine using a riding model. Absorption corrections were employed using  $\phi$ -scan ( $T_{max}=0.6818$  and  $T_{min}=0.6078$ ).

Crystal structure of the compound **10** was analyzed by the same method as described above. Single crystals of the compound **10** suitable for X-ray analysis were grown by slow evaporation of the complex in 1:1 mixture of methanol and chloroform. Dark blue rectangular monoclinic crystal of  $[\text{CuL}^2\text{Br}]_2$  having dimensions 0.41 x 0.13 x 0.11 mm with  $P2_1/c$  symmetry was sealed in a glass capillary for X-ray crystallographic study. Selected crystal data and data collection parameters are given in Table 3.2. The intensity data are collected by  $\Omega - \phi$  mode within  $2.36^\circ < \theta < 27.98^\circ$  for  $hkl$  ( $-11 \leq h \leq 11$ ,  $-22 \leq k \leq 22$ ,  $-17 \leq l \leq 16$ ) in a monoclinic system. Out of 17855 reflections collected, 4877 unique reflections were used for structural analysis. Absorption corrections were employed using  $\phi$ -scan ( $T_{max}=0.3596$  and  $T_{min}=0.7242$ ).

Crystal structure of the compound **12** was analyzed by the same procedure as described above. Single crystals of the compound suitable for X-ray analysis were grown by slow evaporation of the complex in 1:1:1 mixture of methanol, chloroform and acetone. Dark blue rectangular monoclinic crystal of  $[\text{CuL}^2(\text{N}_3)]_2$  having dimensions 0.30 x 0.12 x 0.09 mm with  $P2_1/c$  symmetry was sealed in a glass capillary for X-ray crystallographic study. Selected crystal data and data collection parameters are given in Table 3.2. The intensity data were collected by  $\Omega - \phi$  mode within  $1.66^\circ < \theta < 28^\circ$  for  $hkl$  ( $-16 \leq h \leq 16$ ,  $-16 \leq k \leq 16$ ,  $-16 \leq l \leq 16$ ) in a monoclinic system. Out of 17083 reflections collected 4682 unique reflections were used for structural analysis. Absorption corrections were employed using  $\phi$ -scan ( $T_{max}=0.8978$  and  $T_{min}=0.7102$ ).

Crystal structure of the compound **13** was analyzed by the same method as described above. Single crystals of the compounds for X-ray analysis were

grown by slow evaporation of the complexes in 1:1:1 mixture of methanol and chloroform and acetone. Dark blue rectangular monoclinic crystal of  $[\text{CuL}^2(\text{SH})]_2 \cdot \text{H}_2\text{O}$  having dimensions 0.36 x 0.32 x 0.29 mm with  $P2_1/c$  symmetry were sealed in a glass capillary for X-ray crystallographic study. Selected crystal data and data collection parameters are given in Table 3.2. The intensity data were collected by  $\Omega - \varphi$  mode within  $1.95^\circ < \theta < 27.32^\circ$  for hkl ( $-11 \leq h \leq 11$ ,  $-21 \leq k \leq 21$ ,  $16 \leq l \leq 16$ ) in a monoclinic system. Out of 15767 reflections collected, 4223 unique reflections were used for structural analysis. Absorption corrections were employed using  $\varphi$ -scan ( $T_{max} = 0.7084$  and  $T_{min} = 0.6558$ ).

### 3.3. Results and discussion

Analytical data are summarized in Table 3.1. Thirteen copper(II) complexes are prepared and partial elemental analyses values agree good with the proposed empirical formulas  $[\text{Cu}(\text{L}^1)\text{X}]$  and  $[\text{Cu}(\text{L}^2)\text{X}]$  where  $\text{X} = \text{Cl}, \text{NO}_3, \text{Br}, \text{N}_3$ , and  $\text{SCN}$ ,  $[\text{Cu}_2(\text{L}^1)_2\text{X}]$  where  $\text{X} = \text{SO}_4$ . However  $\text{HL}^2$  yielded a compound of formula  $[\text{Cu}(\text{L}^2)\text{SH}]$  with copper(II) sulphate [26]. With  $\text{HL}^1$  and  $\text{CuCl}_2$  in 1:2 molar ratio, a complex of the composition  $[\text{Cu}_2\text{L}^1\text{Cl}_3]$  was also isolated. With copper perchlorate and  $\text{HL}^1$  in 1:1 molar ratio yielded the complex  $[\text{Cu}_2\text{L}^1_2(\text{OH})]\text{ClO}_4$ . All complexes are blue in color except perchlorate complex, which is greenish yellow. Color is common to the complexes involving thiosemicarbazone coordination, resulting from the sulfur to metal charge transfer bands [108, 109]. Conductivity measurements in DMF solution ( $10^{-3}$  M at 298 K) indicate that all complexes are essentially non-electrolytes suggesting that the ligand behaves as a uninegative ion, coordinates to copper(II) and the absence of gegenion outside the coordination sphere. Magnetic moment values calculated are found to be not in accordance with that for monomers.

**Table 3.1**  
**Colors, partial elemental analysis data, magnetic moments and molar conductivities of copper(II) complexes of ligands HL<sup>1</sup> and HL<sup>2</sup>**

Compound	Empirical formula	Color	Composition% (Found/Calcd)			$\lambda_M^a$	$\mu_{eff}^b$ (B.M.)
			Carbon	Hydrogen	Nitrogen		
HL <sup>1</sup>	C <sub>16</sub> H <sub>17</sub> N <sub>5</sub> S	Yellow	62.10 (62.70)	5.56 (5.46)	22.43 (22.53)		
[CuL <sup>1</sup> Cl] (1)	C <sub>16</sub> H <sub>16</sub> N <sub>5</sub> ClCuS	Blue	47.16 (46.94)	4.02 (3.91)	16.65 (17.11)	32	1.24
[CuL <sup>1</sup> Br] (2)	C <sub>16</sub> H <sub>16</sub> N <sub>5</sub> BrCuS	Blue	42.40 (42.34)	3.56 (3.53)	14.92 (15.44)	23	0.92
[CuL <sup>1</sup> (NO <sub>3</sub> )] (3)	C <sub>16</sub> H <sub>16</sub> N <sub>6</sub> CuO <sub>3</sub> S	Blue	43.48 (44.08)	3.77 (3.67)	18.88 (19.28)	22	1.61
[CuL <sup>1</sup> N <sub>3</sub> ] <sup>1/2</sup> H <sub>2</sub> O (4)	C <sub>16</sub> H <sub>17</sub> N <sub>8</sub> CuO <sub>0.5</sub> S	Blue	45.37 (45.23)	3.86 (4.00)	26.94 (26.38)	25	1.05
[CuL <sup>1</sup> (NCS)] (5)	C <sub>17</sub> H <sub>16</sub> N <sub>6</sub> CuS <sub>2</sub>	Greenish Yellow	46.94 (47.27)	3.81 (3.71)	19.42 (19.46)	30	1.27
[Cu <sub>2</sub> L <sup>2</sup> (OH)]ClO <sub>4</sub> ·H <sub>2</sub> O (6)	C <sub>32</sub> H <sub>36</sub> N <sub>10</sub> ClCu <sub>2</sub> O <sub>6</sub> S <sub>2</sub>	Blue	43.33 (43.46)	4.09 (4.18)	15.19 (15.84)	48	0.98
[Cu <sub>2</sub> L <sup>2</sup> Cl <sub>3</sub> ] (7)	C <sub>16</sub> H <sub>16</sub> N <sub>5</sub> Cl <sub>3</sub> Cu <sub>2</sub> S	Blue	35.75 (35.33)	3.07 (2.94)	12.27 (12.88)	27	2.86
[Cu <sub>2</sub> L <sup>2</sup> SO <sub>4</sub> ] <sub>2</sub> ·6H <sub>2</sub> O (8)	C <sub>32</sub> H <sub>35</sub> N <sub>10</sub> O <sub>7</sub> Cu <sub>2</sub> S <sub>4</sub>	Blue	42.80 (43.76)	4.30 (4.23)	15.60 (15.59)	15	2.07
HL <sup>2</sup>	C <sub>19</sub> H <sub>17</sub> N <sub>5</sub> S	Yellow	66.11 (65.70)	4.98 (4.89)	19.94 (20.17)		
[CuL <sup>2</sup> Cl]·1.5 H <sub>2</sub> O (9)	C <sub>19</sub> H <sub>19</sub> N <sub>5</sub> ClCuO <sub>1.5</sub> S	Blue	48.54 (48.31)	3.65 (4.03)	14.71 (14.83)	32	----
[CuL <sup>2</sup> Br] <sub>2</sub> (10)	C <sub>19</sub> H <sub>16</sub> N <sub>5</sub> BrCuS	Blue	46.63 (46.57)	3.32 (3.27)	14.35 (14.30)	27	2.24/Cu
[CuL <sup>2</sup> (NO <sub>3</sub> )] H <sub>2</sub> O (11)	C <sub>19</sub> H <sub>18</sub> N <sub>6</sub> CuO <sub>4</sub> S	Blue	46.67 (46.57)	3.45 (3.67)	17.98 (17.16)	24	2.56
[CuL <sup>2</sup> N <sub>3</sub> ] <sub>2</sub> (12)	C <sub>19</sub> H <sub>16</sub> N <sub>8</sub> CuS	Blue	50.53 (50.50)	3.62 (3.54)	24.82 (24.81)	27	1.98/Cu
[CuL <sup>2</sup> (SH)] <sub>2</sub> ·2H <sub>2</sub> O (13)	C <sub>19</sub> H <sub>19</sub> N <sub>5</sub> CuO <sub>2</sub> S <sub>2</sub>	Blue	49.89 (49.51)	3.90 (4.12)	15.50 (15.20)	18	1.69/Cu

<sup>a</sup> Molar conductivity ·10<sup>3</sup> M DMF at 298 K <sup>b</sup> Magnetic susceptibility

**Table 3.2**  
**Crystal data and structural refinement parameters for the complexes [Cu<sub>2</sub>L<sub>2</sub>(SO<sub>4</sub>)<sub>2</sub>·6H<sub>2</sub>O, [CuL<sup>2</sup>Br]<sub>2</sub>, [CuL<sup>2</sup>(N<sub>3</sub>)<sub>2</sub>], and [CuL<sup>2</sup>(SH)]<sub>2</sub>·2H<sub>2</sub>O**

Parameters	[Cu <sub>2</sub> L <sub>2</sub> (SO <sub>4</sub> ) <sub>2</sub> ·6H <sub>2</sub> O	[CuL <sup>2</sup> Br] <sub>2</sub>	[CuL <sup>2</sup> (N <sub>3</sub> ) <sub>2</sub> ]	[CuL <sup>2</sup> (SH)] <sub>2</sub> ·H <sub>2</sub> O
Empirical Formula	C <sub>64</sub> H <sub>76</sub> Cu <sub>4</sub> N <sub>20</sub> O <sub>14</sub> S <sub>6</sub>	C <sub>19</sub> H <sub>16</sub> BrCuN <sub>5</sub> S	C <sub>19</sub> H <sub>16</sub> CuN <sub>8</sub> S	C <sub>19</sub> H <sub>19</sub> CuN <sub>5</sub> OS <sub>2</sub>
Formula weight (M)	897.98	489.88	452.00	461.04
Temperature (T) K	293(2)	293(2)	293(2)	293(2)
Wavelength (Mo Kα) (Å)	0.71073	0.71073	0.71073	293(2)
Crystal system	Triclinic	Monoclinic	Monoclinic	Monoclinic
Space group	P1	P2 <sub>1</sub> /c	P2 <sub>1</sub> /c	P2 <sub>1</sub> /c
Lattice constants				
a (Å)	11.225(6)	9.029(4)	12.845(8)	8.966(5)
b (Å)	13.201(7)	17.279(8)	12.512(7)	17.338(10)
c (Å)	14.558(7)	13.217(6)	13.014(8)	13.195(8)
α (°)	68.112(7)	90.00	90	90.00
β (°)	67.786(7)	97.228(8)	107.753(10)	95.772(10)
γ (°)	78.048(8)	90.00	90.00	90.00
Volume V (Å <sup>3</sup> )	1847.6(16)	2045.6(16)	1992(2)	2041(2)
Z	2	4	4	4
Calculated density (ρ) (Mg m <sup>-3</sup> )	1.614	1.591	1.507	1.497
Absorption coefficient, μ (mm <sup>-1</sup> )	1.382	3.136	1.224	1.295
F(000)	924	980	924	944
Crystal size (mm)	0.40 x 0.35 x 0.30 mm	0.41 x 0.13 x 0.11 mm	0.30 x 0.12 x 0.09 mm	0.36 x 0.32 x 0.39 mm
θ Range for data collection	1.60 to 27.46	2.36 to 27.98	1.66 to 28.04	1.95 to 27.32
Limiting Indices	-13 ≤ h ≤ 13, -16 ≤ k ≤ 17, -18 ≤ l ≤ 18	-11 ≤ h ≤ 11, -22 ≤ k ≤ 22, -17 ≤ l ≤ 16	-16 ≤ h ≤ 16, -16 ≤ k ≤ 16, -16 ≤ l ≤ 16	-11 ≤ h ≤ 11, -21 ≤ k ≤ 21, -16 ≤ l ≤ 16
Reflections collected	19156	17855	17083	15767
Unique Reflections	7528 [R(int) = 0.0201]	4877 [R(int) = 0.0207]	4682 [R(int) = 0.0265]	4223 [R(int) = 0.0181]
Completeness to θ	27.46 89.2%	27.98 99.2%	28.04 97.1%	27.32%
Absorption correction	None	None	None	None
Max and min transmission	0.6818 and 0.6078	0.7242 and 0.3596	0.8978 and 0.7102	0.7084 and 0.6558
Refinement method	Full-matrix least-squares on F <sup>2</sup>	Full-matrix least-squares on F <sup>2</sup>	Full-matrix least-squares on F <sup>2</sup>	Full-matrix least-squares on F <sup>2</sup>
Data / restraints / parameters	7528/0/623	4877 / 0 / 296	4682 / 0 / 326	4223 / 0 / 317.
Goodness-of-fit on F <sup>2</sup>	1.079	1.025	1.074	1.049
Final R indices [I > 2σ (I)]	R <sub>f</sub> = 0.0335, wR <sub>s</sub> = 0.0897	R <sub>f</sub> = 0.0431, wR <sub>s</sub> = 0.1202	R <sub>f</sub> = 0.0375, wR <sub>s</sub> = 0.0859	R <sub>f</sub> = 0.0376, wR <sub>s</sub> = 0.1091
R indices (all data)	R <sub>f</sub> = 0.0407, wR <sub>s</sub> = 0.0944	R <sub>f</sub> = 0.0558, wR <sub>s</sub> = 0.1296	R <sub>f</sub> = 0.0490, wR <sub>s</sub> = 0.0908	R <sub>f</sub> = 0.0443, wR <sub>s</sub> = 0.1141
Largest difference peak and hole (e Å <sup>-3</sup> )	0.471 and -0.438 e Å <sup>-3</sup>	1.455 and -0.538 e Å <sup>-3</sup>	0.418 and -0.218 e Å <sup>-3</sup>	

### 3.3.1. Molecular and crystal structure of $[Cu_2L_2^1(SO_4)]_2 \cdot 6H_2O$ (8)

Figure 3.1 illustrates the structural features of the complex for which selected bond lengths and bond angles are listed in Tables 3.3 and 3.4. The structure contains four units comprising of two identical units of  $Cu(1)L^1$  (1 and 4) and two identical  $Cu(2)L^1$  (2 and 3) respectively. Each copper atom in (1 and 4) is coordinated to pyridyl nitrogen, azomethine nitrogen and thiolate sulfur of the thiosemicarbazone moiety and oxygen of the bridging sulfato group. Each copper atom in sub units 1 and 4 is tetracoordinate. The bond distances are  $Cu(1)-S(1)$  (2.2771(12) Å),  $Cu(1)-O(12)$  (1.9322(15) Å),  $Cu(1)-N(1)$  (2.0274(18) Å),  $Cu(1)-N(3)$  (1.9493(17) Å). The  $Cu-N_{pyridyl}$  bonds are 0.0781 Å greater than  $Cu-N_{imine}$  bonds that determines the strength of azomethine nitrogen coordination. The bond length and bond angle values suggest a square planar geometry about  $Cu(1)$  with some amount of distortion. The pyridine nitrogen  $N(1)$ , imino nitrogen  $N(3)$  and the thiolate sulfur  $S(1)$  together with  $O(12)$  of the sulfato group constitute the square plane around  $Cu(1)$ . The configuration of the thiosemicarbazone chain about  $C(6)-N(3)$  bond is *Z* which facilitate the coordination of thiolate sulphur to copper(II) in 1 and 4 sub units. The  $C(6)-N(3)$  bond length is 1.297(2) Å is slightly shorter than  $C(6)-N(3)$  bond distance of 1.308(4) Å of the free ligand. This indicates that there is no clear decrease in the double bond character of the C-N azomethine bond on chelation to the copper(II) ion. This can be attributed to the stabilization of the C-N azomethine bond in the copper(II) complexes due to the presence of an important metal-to-ligand  $\pi$ -back donation. The delocalisation of electron density in the thiosemicarbazone moiety gives rise to a reduction in the  $N(3)-N(4)$  bond length in the complex compared to the uncomplexed thiosemicarbazone. The loss of proton bound to  $N(4)$  in  $HL^1$  produces a negative charge, which is delocalised on the  $N(3)-N(4)-C(12)$  system. This is indicated by the lengthening of the bond  $S(1)-C(12)$  (1.7451(2) Å) compared to the bond length 1.671(4) Å in the free ligand. The decrease in the bond length of  $C(12)-N(4)$  to 1.329(2) from 1.386(4) Å of the free ligand also supports thiolate formation. The bond angles



S(1)-Cu(1)-O(12) ( $97.72(5)^\circ$ ), S(1)-Cu(1)-N(1) ( $164.20(4)^\circ$ ), S(1)-Cu(1)-N(3) ( $84.61(5)^\circ$ ), O(12)-Cu(1)-N(1) ( $96.22(6)^\circ$ ), O(12)-Cu(1)-N(3) ( $172.04(6)^\circ$ ), N(1)-Cu(1)-N(3) ( $80.60(6)^\circ$ ) are quite far from square planar geometry revealing the distortion of the square plane comprising of Cu(1), O(12), S(1), N(3) and N(1) atoms. The copper centers in 1 and 2 subunits are at a larger distance ( $3.578 \text{ \AA}$ ), indicating a weak or no copper-copper interaction. The dihedral angle between the planes Cu(1)/S(1)/C(12)/N(4)/N(3) and Cu(1)/N(2)/C(5)/C(6)/N(1) is  $5.71^\circ$  suggesting coplanarity of the metal chelate rings.

Each copper atom in units 2 and 3 is pentacoordinate with the bond distances Cu(2)-S(3) ( $2.2871(12) \text{ \AA}$ ), Cu(2)-O(11) ( $1.9386(13) \text{ \AA}$ ), Cu(2)-N(1A) ( $2.0255(17) \text{ \AA}$ ), Cu(2)-N(3A) ( $1.9534(15) \text{ \AA}$ ), Cu(2)-N(2A) ( $2.5958 \text{ \AA}$ ) adopting a square pyramidal geometry with N(2A) at the apical site. The bond angles S(3)-Cu(2)-N(2A) ( $99.06^\circ$ ), O(11)-Cu(2)-N(2A) ( $90.49^\circ$ ), N(1A)-Cu(2)-N(2A) ( $82.47^\circ$ ), N(2A)-Cu(2)-N(3A) ( $110.48^\circ$ ), N(1A)-Cu(2)-S(3) ( $164.61(4)^\circ$ ) indicates a distorted square pyramidal geometry around copper(II) with pyridyl nitrogen N(2A) is positioned at the apical site having the bond length Cu(2)-N(2A) ( $2.5958 \text{ \AA}$ ). The pyridyl nitrogen N(1A), the imino nitrogen N(3A), and the thiolate sulfur S(3) atom together with O(11) of the sulfato group constitute the basal plane. The dihedral angle between the planes Cu(1)/O(12)/S(2)/O(11)/Cu(2) and S(3)/C(12A)/N(4A)/N(3A)/Cu(2) is  $51.06^\circ$  and that of the planes S(3)/C(12A)/N(4A)/N(3A)/Cu(2) and N(1A)/C(5A)/C(6A)/N(3A)/Cu(2) is  $3.10^\circ$  suggesting that both newly formed metal chelate rings are coplanar. The bond lengths in basal plane agree with those found in copper(II) complexes containing thiosemicarbazones which act as uninegative tridentate ligands [110]. The electron withdrawing ability of the basal sulfato ligand weakens the axial N(2A)-Cu(2) bond leading to a less distorted square pyramidal geometry around copper(II). This is supported by observed bond angles for copper atom as given in Table 3.4. If we use the  $\tau$  parameter where  $\tau = (\alpha - \beta)/60$ , (where  $\tau = 0$  for a square pyramidal geometry and

$\tau = 1$  for a trigonal bipyramidal geometry) defined by Addison *et al.* to quantify geometry [111]. Cu(1)-N(2A) is selected as the axial site from the square plane and N(1A)-N(3A)-S(3)-O(11) constitutes the basal square plane around Cu(2). So  $\alpha = \text{S(3)-Cu(2)-N(1A)}$  ( $164.61(4)^\circ$ ) and  $\beta = \text{O(11)-Cu(2)-N(3A)}$  ( $156.94(6)^\circ$ ),  $\tau = 0.12$ . This means that coordination geometry around Cu(2) is very close to a square pyramidal arrangement. The distance between copper centers of 2 and 3 subunits is at  $5.563 \text{ \AA}$ , which exceeds the minimum required distance for Cu-Cu interaction suggesting no metal-metal interaction.

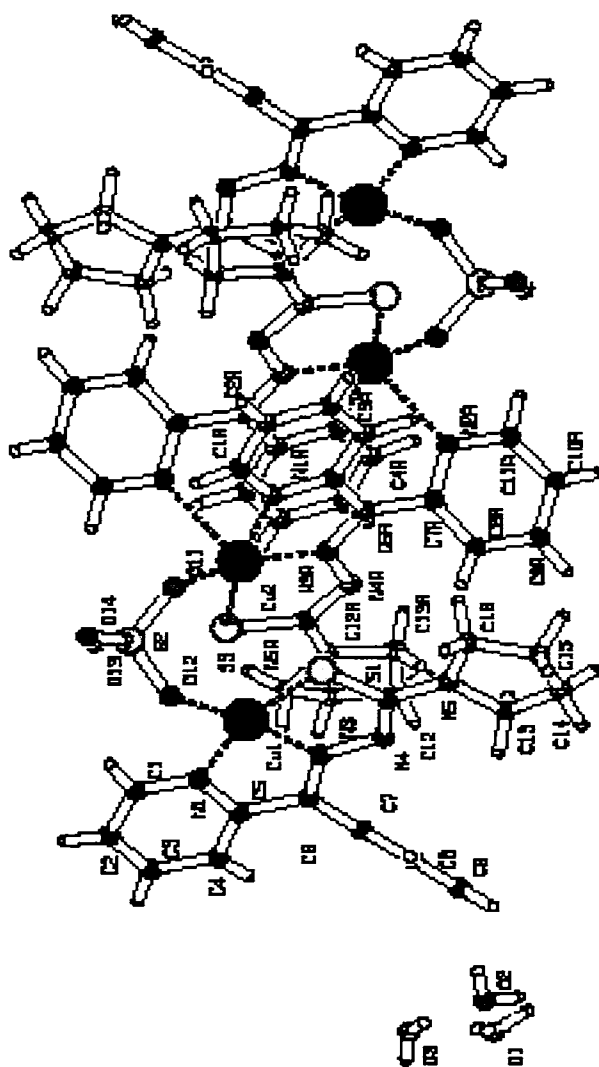


Figure 3.1. PLATON diagram of  $[\text{Cu}_2\text{L}^1_2(\text{SO}_4)]_2 \cdot 6\text{H}_2\text{O}$  (10)

**Table 3.3****Selected bond lengths (Å) of HL<sup>1</sup> and [Cu<sub>2</sub>L<sub>2</sub><sup>1</sup>(SO<sub>4</sub>)<sub>2</sub>·6H<sub>2</sub>O**

Bond length	HL <sup>1</sup>	[Cu <sub>2</sub> L <sub>2</sub> <sup>1</sup> (SO <sub>4</sub> ) <sub>2</sub> ·6H <sub>2</sub> O
Cu(1)-S(1)		2.2771(12)
Cu(1)-O(12)		1.9322(15)
Cu(1)-N(1)		2.0274(18)
Cu(1)-N(3)		1.9493(17)
Cu(2)-S(3)		2.2871(12)
Cu(2)-O(11)		1.9386(13)
Cu(2)-N(1A)		2.0225(17)
Cu(2)-N(2A)		2.5958
Cu(2)-N(3A)		1.9534(15)
S(1)-C(12)	1.671(4)	1.745(2)
S(2)-O(11)		1.4967(13)
S(2)-O(12)		1.4886(14)
S(2)-O(13)		1.4449(15)
S(3)-C(12A)		1.7423(18)
N(3)-C(6)	1.308(4)	1.297(2)
N(3A)-C(6A)	1.308(4)	1.304(2)
N(3)-N(4)	1.371(4)	1.349(2)
N(3A)-N(4A)	1.371(4)	1.349(2)
N(4)-C(12)	1.386(4)	1.329(2)
N(4A)-C(12A)	1.386(4)	1.330(2)
N(5)-C(12)	1.349(5)	1.336(2)
N(5A)-C(12A)	1.349(5)	1.337(2)

**Table 3.4****Selected bond angles (°) of HL<sup>1</sup> and [Cu<sub>2</sub>L<sub>2</sub><sup>1</sup>(SO<sub>4</sub>)<sub>2</sub>·6H<sub>2</sub>O**

	HL <sup>1</sup>	[Cu <sub>2</sub> L <sub>2</sub> <sup>1</sup> (SO <sub>4</sub> ) <sub>2</sub> ·6H <sub>2</sub> O
S(1)-Cu(1)-O(12)		97.72(5)
S(1)-Cu(1)-N(1)		164.20(4)
S(1)-Cu(1)-N(3)		84.61(5)
O(12)-Cu(1)-N(1)		96.22(6)
O(12)-Cu(1)-N(3)		172.04(6)
N(1)-Cu(1)-N(3)		80.60(6)
S(3)-Cu(2)-O(11)		101.66(4)
S(3)-Cu(2)-N(1A)		164.61(4)
S(3)-Cu(2)-N(2A)		99.06
S(3)-Cu(2)-N(3A)		84.89(5)
O(11)-Cu(2)-N(1A)		93.63(5)
O(11)-Cu(2)-N(2A)		90.49
O(11)-Cu(2)-N(3A)		156.94(6)
N(1A)-Cu(2)-N(2A)		82.47
N(1A)-Cu(2)-N(3A)		80.27(6)
N(2A)-Cu(2)-N(3A)		110.48
N(3A)-Cu(2)-S(3)		84.89(5)
N(1A)-Cu(2)-S(3)		164.61(4)
N(4)-N(3)-C(6)	118.6(3)	119.13(14)
N(4A)-N(3A)-C(6A)	118.6(3)	119.09(14)
N(3)-N(4)-C(12)	118.7(3)	112.23(14)
N(3A)-N(4A)-C(12A)	118.7(3)	112.50(13)
N(5)-C(12)-N(4)	112.3(3)	114.88(16)
N(5A)-C(12A)-N(4A)	112.3(3)	114.19(14)
N(5)-C(12)-S(1)	123.2(3)	119.75(14)
N(5A)-C(12A)-S(3)	123.2(3)	119.91(13)

Figure 3.2 shows the unit cell-packing diagram of the tetrameric complex is viewed down the *a*-axis. There are two 2 molecules in the unit cell arranged in a parallel fashion. The assemblage of molecules in the respective manner in the unit cell is resulted by the diverse  $\pi$  -  $\pi$  stacking, CH- $\pi$  and ring-metal interactions as shown in Tables 3.5 and 3.6. The metal chelate rings Cg(4) and Cg(7) of 2 and 3 units are involved in  $\pi$ - $\pi$  interactions with the pyridyl ring of the neighboring unit at average distances of 3.7415 and 3.6512 Å. In addition to the  $\pi$ - $\pi$  stacking, the CH- $\pi$  interactions between the pyridyl hydrogen and the metal chelate rings contribute to the stability of the unit cell packing. Short ring-metal interaction of the chelate ring Cg(3) with Cu(1) and Cu(2) of the neighboring unit is observed at distances of 3.666 and 3.844 Å respectively from the copper center. The interaction of chelate rings Cg(4) and Cg(5) of the unit 2 with Cu(1) of 1 and 4 units at a distance of 3.346 and 3.752 Å respectively adds to the stability of the unit cell..

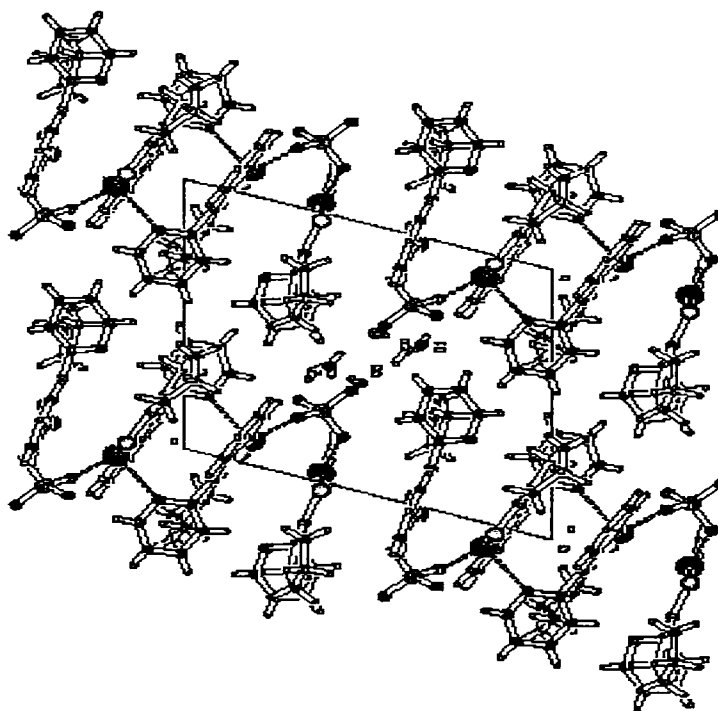


Figure 3.2. Unit cell packing diagram of [Cu<sub>2</sub>L<sup>1/2</sup>(SO<sub>4</sub>)]<sub>2</sub>·6H<sub>2</sub>O (10) viewed down the *a*- axis.

Table 3. 5

H-bonding and  $\pi$ --- $\pi$  interaction parameters for  $[\text{Cu}_4\text{L}_4^1(\text{SO}_4)]_2 \cdot 6\text{H}_2\text{O}$ 

<b>H-bonding</b>				
Donor---H...A	D-H (Å)	H---A (Å)	D---A (Å)	D-H---A (°)
O(1)---H(11)---O(13)	0.87	1.94	2.8073	175
O(1)---H(101)---O(3)	0.69	2.19	2.8715	171
O(2)---H(200)---O(14)	0.73	2.10	2.8048	163
O(2)---H(201)---O(14)	0.75	2.24	2.9570	161
O(3)---H(300)---O(2)	0.75	2.09	2.8287	168
O(3)---H(301)---O(1)	0.64	2.17	2.7979	170
C(1A)---H(1A)---O(2)	0.95	2.56	3.4637	160
C(2)---H(2)---O(3)	0.93	2.45	3.3389	159
C(4)---H(4)---N(2)	0.95	2.49	3.1139	123
C(8A)---H(8A)---N(5)	0.94	2.62	3.5360	164
C(11A)---H(11A)---O(11)	0.95	2.59	3.1619	118
C(11A)---H(11A)---O(13)	0.95	2.59	3.5120	164
<b><math>\pi</math>---<math>\pi</math> interactions</b>				
Cg(I)-R <sub>es</sub> (I)---Cg(J)	Cg-Cg(Å)	$\alpha$ (°)	$\beta$ (°)	
Cg(3)-[1]---Cg(4) <sup>a</sup>	3.3457	14.65	16.19	
Cg(3)-[1]---Cg(7) <sup>a</sup>	3.3703	15.37	13.24	
Cg(4)-[1]---Cg(3) <sup>a</sup>	3.3457	14.65	1.54	
Cg(4)-[1]---Cg(5) <sup>a</sup>	3.3637	14.37	5.31	
Cg(4)-[1]---Cg(14) <sup>b</sup>	3.7415	5.18	26.63	
Cg(5)-[1]---Cg(4) <sup>a</sup>	3.3637	14.37	16.16	
Cg(5)-[1]---Cg(7) <sup>a</sup>	3.4142	15.00	15.45	
Cg(7)-[1]---Cg(3) <sup>a</sup>	3.3703	15.37	05.64	
Cg(7)-[1]---Cg(5) <sup>a</sup>	3.4142	15.00	10.82	
Cg(7)-[1]---Cg(14) <sup>b</sup>	3.6512	04.10	24.76	
Cg(8)-[1]---Cg(8) <sup>b</sup>	3.5172	0.00	19.10	
Cg(14)-[1]---Cg(4) <sup>b</sup>	3.7415	05.18	29.40	
Cg(14)-[1]---Cg(7) <sup>b</sup>	3.6512	04.10	26.32	
Equivalent position codes:	Cg(3)=Cu(1), S(1), C(12), N(4)			
a = x, y, z	Cg(4)=Cu(2), S(3), C(12A), N(4A)			
b = -x, -y, -z	Cg(5)= Cu(1), S(1), C(12), N(4),N(3)			
	Cg(7)=Cu(2),S(3),C(12A),N(4A),N(3A)			
	Cg(8)=Cu(2),N(1A),C(5A),C(6A),N(3A)			
	Cg(14)=N(1A),C(1A),C(2A),C(3A),C(4A),C(5A)			

(D=Donor, A=acceptor, Cg=Centroid,  $\alpha$ =dihedral angles between planes I & J,  $\beta$ =angle Cg(I)-Cg(J))

Table 3. 6

CH— $\pi$ , and ring-metal interaction parameters of  $[\text{Cu}_4\text{L}_4(\text{SO}_4)_2]\cdot 6\text{H}_2\text{O}$ 

CH— $\pi$ interactions			
X-H(I)---Cg(J)	H..Cg(Å)	X-H..Cg (°)	X-H..Cg (°)
C(4A)-H(4A)----Cg(4) <sup>b</sup>	3.3153	80.05	3.2957
C(4A)-H(4A)----Cg(7) <sup>b</sup>	3.3660	76.58	3.2826
C(8A)-H(8A)----Cg(9) <sup>b</sup>	2.8918	140.20	3.6612
C(10A)-H(10A)----Cg(15) <sup>c</sup>	3.0467	151.69	3.8815
C(15A)-H(15B)----Cg(16) <sup>d</sup>	3.3162	159.61	4.1800
C(16A)-H(16A)----Cg(6) <sup>a</sup>	3.1225	136.23	3.8890
Equivalent position codes		Cg(4)=Cu(2), S(3), C(12A), N(4A)	
a = x, y, z		Cg(6)=Cu(1), N(1), C(5), C(6),N(3)	
b = -x -y, -z		Cg(7)= Cu(2), S(3), C(12A), N(4A),N(3A)	
c = x, -1+y, z		Cg(9)=N(5), C(13), C(14),C(15),C(16)	
d =1-x, -y, -z		Cg(15)=N(2), C(7), C(8),C(9),C(10),C(11)	
		Cg(16)=N(2A),C(7A),C(8A),C(9A),C(10A),C(11A)	
Ring- metal interaction			
Cg(I) Res(I) Me(J)		Cg(I)-Me(J) (Å)	Beta (°)
Cg(3) [ 1] -> Cu(1) <sup>e</sup>		3.666	18.84
Cg(3) [ 1] -> Cu(2) <sup>a</sup>		3.884	38.81
Cg(4) [ 1] -> Cu(1) <sup>3a</sup>		3.346	30.69
Cg(5) [ 1] -> Cu(1) <sup>e</sup>		3.752	21.75
Cg(5) [ 1] -> Cu(2) <sup>a</sup>		3.975	41.57
Cg(7) [ 1] -> Cu(1) <sup>a</sup>		3.498	35.14
Equivalent position codes		Cg(3)=Cu(1), S(1), C(12), N(4)	
a =x,y, z		Cg(4)=Cu(2), S(3), C(12A), N(4A)	
e = -x, -y, 1-z		Cg(5)= Cu(1), S(1), C(12), N(4),N(3)	
		Cg(7)= Cu(2), S(3), C(12A), N(4A),N(3A)	

(D=Donor, A=acceptor. Cg=Centroid,  $\alpha$ =dihedral angles between planes I & J.  $\beta$ =angle Cg(I)-Cg(J)

The crystal structure is further stabilized by six C–H– $\pi$  interactions. The intra and intermolecular hydrogen bonding forces are strong within the unit cell. The hydrogen bonding interactions such as C(11A)–H(11A)–O(11) and C(11A)–H(11A)–O(13) are intramolecular whereas the other hydrogen bonding interactions are intermolecular. Thus  $\pi$ – $\pi$ , C–H– $\pi$ , ring–metal and hydrogen bonding interactions stabilize the unit cell and point out the possibility for metalloaromaticity – a classic concept recently reviewed by Masui [112]. The intra and intermolecular hydrogen bonding interactions coexist with other interactions in the unit cell.

### 3.3.2. Molecular and crystal structure of $[\text{CuL}^2\text{Br}]_2$

The labeled asymmetric PLATON plot of the compound  $[\text{CuL}^2\text{Br}]_2$  (10) is shown in Figure 3.3. Selected bond lengths and bond angles for the compound are presented in Table 3.7. Crystal structure by X-ray diffraction reveals that the compound consists of a three-dimensional copper–thiosemicarbazone network. The structure consists of two units of  $[\text{CuL}^2]$ . Thus the three dimensional arrangement consists of two copper–thiosemicarbazone units where the apical position of copper(II) atom of each unit is occupied by the pyridine N(2) nitrogen of the second sub unit.. The structure contain two copper centers where each center is pentacoordinate with pyridyl nitrogen, azomethine nitrogen, thiolate sulfur, bromide ion and pyridyl nitrogen N(2) of second thiosemicarbazone moiety. If we use the  $\tau$  parameter where  $\tau = (\alpha - \beta)/60$ , (where  $\tau = 0$  for a square pyramidal geometry and  $\tau = 1$  for a trigonal bipyramidal geometry) defined by Addison *et al.* to quantify geometry [111]. Cu(1)–N(2) is selected as the axial site from the square plane and N(1)–N(3)–S(1)–Br(1) constitutes the basal square plane around Cu(1). So  $\alpha = \text{S}(1)\text{--Cu}(1)\text{--N}(1)$  ( $163.28^\circ$ ) and  $\beta = \text{Br}(1)\text{--Cu}(1)\text{--N}(3)$  ( $148.14^\circ$ ), then  $\tau = 0.25$ . This means that coordination geometry is very close to a distorted square pyramid. Copper atom in each of the sub unit is coordinated by bond distances Cu(1)–S(1) ( $2.2565(12)\text{Å}$ ), Cu(1)–Br(1) ( $2.4135(12)\text{Å}$ ), Cu(1)–N(1) ( $2.019(3)\text{Å}$ ), Cu(1)–



N(3) (1.9793(2) Å), Cu(1)-N(2) (2.352(4) Å). The loss of a N(4)-H in HL<sup>2</sup> produces a negative charge, which is delocalised on the N(3)-N(4)-C(12) system. This is indicated by the lengthening of the bond S(1)-C(12) to 1.721(3) Å compared to that of 1.6686(12) Å in the free ligand. The decrease in the bond length of C(12)-N(4) to 1.343(3) from 1.377(2) Å of the uncomplexed thiosemicarbazone also supports thiolate formation. The bond angles are quite far from perfect square pyramidal geometry with distortion of the basal square planes comprising of Br(1), S(1), N(3) and N(1) atoms. The Cu-N<sub>pyridyl</sub> bonds are 0.04 Å larger than Cu-N<sub>imine</sub> bonds shows the strength of azomethine nitrogen coordination. The configuration of the thiosemicarbazone chain about C(6)-N(3) bond is Z which facilitate the coordination of thiolate sulphur to copper(II) in the complex. The C(6)-N(3) bond distances in the complex is 1.295(3) Å in comparison to that of C(6)-N(3), 1.298(3) Å in the free ligand.. This indicates that there is no clear decrease in the double bond character of the C-N azomethine bond on chelation to the copper(II) ion. This can be attributed to the stabilization of the C-N<sub>azomethine</sub> bond in the copper(II) complexes due to the presence of an important metal-to-ligand  $\pi$ -back donation. The delocalisation of electron density in the thiosemicarbazone moiety gives rise to a reduction in the N(3)-N(4) bond length compared to the uncomplexed thiosemicarbazone. The bond angles Br(1)-Cu(1)-S(1) (95.22(3)°), Br(1)-Cu(1)-N(1) (96.81(8)°), Br(1)-Cu(1)-N(2) (97.60(7)°), Br(1)-Cu(1)-N(3) (148.14(7)°), S(1)-Cu(1)-N(1) (163.28(8)°), S(1)-Cu(1)-N(2) (100.88(7)°), S(1)-Cu(1)-N(3) (83.60(7)°), N(1)-Cu(1)-N(2) (89.00(10)°), N(1)-Cu(1)-N(3) (80.05(10)°), N(2)-Cu(1)-N(3) (113.93(10)°) are quite far from square pyramidal geometry with distortion of the basal square planes comprising of Cu(1), Br(1), S(1), N(3) and N(1) atoms. The dihedral angle constituted by the planes N(1)/C(1)/C(2)/C(3)/C(4)/C(5) and N(1)/C(5)/C(6)/N(3)/Cu(1) is 2.98° suggests that the pyridyl ring and the newly formed metal chelate ring are coplanar. Copper atom shows the maximum deviation of 0.0076° in the plane N(1)/C(5)/C(6)/N(3)/Cu(1). The dihedral angle between the planes

Cu(1)/N(1)/C(5)/C(6)/N3 and Cu(1)/N(3)/N(4)/C(12)/S(1) is  $3.10^\circ$  also suggests that the newly formed metal chelate rings are coplanar.

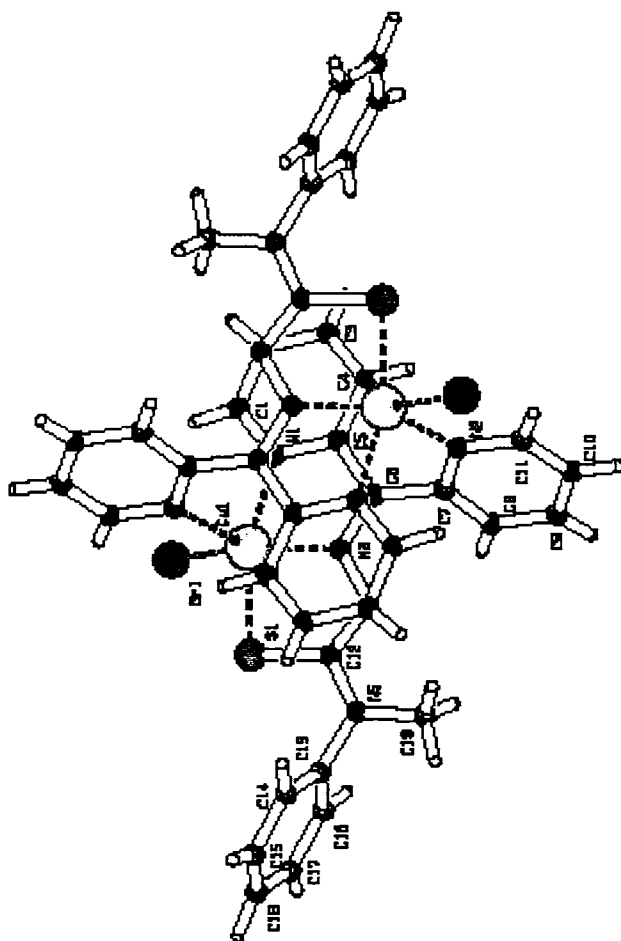


Figure 3.3. *PLATON* diagram of  $[\text{CuL}^2\text{Br}]_2$  (**10**)

Figure 3.4 shows the unit cell-packing diagram of the compound viewed down the *a*-axis. The molecules are arranged in such a manner that four molecules in the unit cell are placed at the four edges and one at the center of the unit cell giving centrosymmetry to the whole crystal. The molecule in the center is linked perfectly through hydrogen bonding interaction with four molecules placed at the edges of the unit cell. The molecules are also packed in

the unit volume cell through  $\pi$ - $\sigma$  interaction between the metal containing chelate rings and aromatic hydrogen atoms. The assemblage of molecules in the respective manner in the unit cell are resulted by the diverse  $\pi$ - $\pi$  stacking, CH- $\pi$  and ring-metal and hydrogen bonding interactions are depicted in Table 3.8. The metal chelate rings Cg(1) is involved in  $\pi$ - $\pi$  interactions with the pyridyl ring Cg(3) of the neighboring unit at a distance of 3.6581 Å. The metal chelate rings Cg(1) and Cg(2) are also involved in  $\pi$ - $\pi$  interaction with metal chelate rings of the neighboring molecule at a distance of 4.0193 Å.

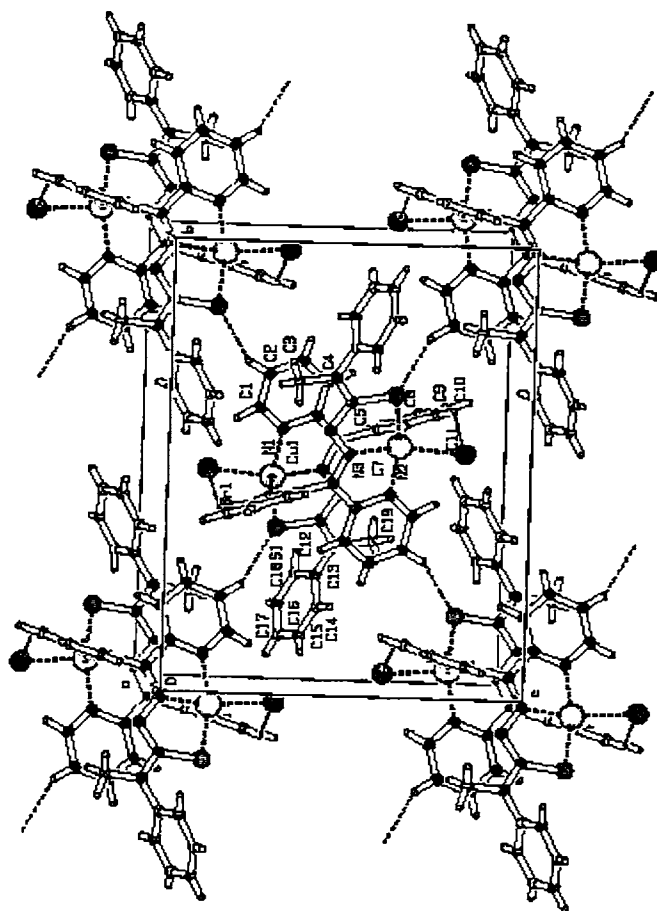


Figure 3.4. Unit cell packing diagram of [CuL<sup>1</sup>Br]<sub>2</sub> viewed down the *a*-axis

These interactions are more related to a  $\pi$  deficient -  $\pi$  deficient interaction leading to a stable structure. The crystal structure is further

**Table 3.7****Comparison of selected bond lengths (Å) and bond angles (°) of HL<sup>2</sup> and [CuL<sup>2</sup>Br]<sub>2</sub>**

	HL <sup>2</sup>	[CuL <sup>2</sup> Br] <sub>2</sub>
Br(1)-Cu(1)		2.4135(12)
Cu(1)-S(1)		2.2565(12)
Cu(1)-N(1)		2.019(3)
Cu(1)-N(3)		1.9793(2)
Cu(1)-N(2)		2.352(4)
S(1)-C(12)	1.6686(12)	1.721(3)
N(3)-N(4)	1.362(2)	1.354(3)
N(4)-C(12)	1.377(2)	1.343(3)
N(5)-C(12)	1.3489(2)	1.344(4)
N(3)-C(6)	1.295(2)	1.298(3)
Br(1)-Cu(1)-S(1)		95.22(3)
Br(1)-Cu(1)-N(1)		96.81(8)
Br(1)-Cu(1)-N(2)		97.60(7)
Br(1)-Cu(1)-N(3)		148.14(7)
S(1)-Cu(1)-N(1)		163.28(8)
S(1)-Cu(1)-N(2)		100.88(7)
S(1)-Cu(1)-N(3)		83.60(7)
N(1)-Cu(1)-N(2)		89.00(10)
N(1)-Cu(1)-N(3)		80.05(10)
N(2)-Cu(1)-N(3)		113.93(10)
C(6)-N(3)-N(4)	120.94(16)	
N(3)-N(4)-C(12)	118.67(16)	111.1(2)
N(5)-C(12)-N(4)	113.73(16)	115.6(3)
N(5)-C(12)-S(1)	123.48(14)	118.9(2)
N(4)-C(12)-S(1)	122.79(14)	125.4(2)

Table 3.8

H-bonding,  $\pi$ --- $\pi$  and CH--- $\pi$  interaction parameters of [Cu<sub>2</sub>L<sub>2</sub><sup>2</sup>Br<sub>2</sub>]

<b>H-bonding</b>				
Donor---H...acceptor	D-H (Å)	H---A (Å)	D---A (Å)	D-H---A (°)
C(2)---H(2)---S(1)	0.99	2.75	3.6581	153
C(11)---H(11)---Br(1)	0.85	2.92	3.4753	124
<b><math>\pi</math>---<math>\pi</math> interactions</b>				
Cg(I)-Res(I)---Cg(J)	Cg-Cg(Å)	$\alpha$ (°)	$\beta$ (°)	
Cg(1)-(I)---Cg(2) <sup>a</sup>	4.0193	3.10	38.78	
Cg(1)-(I)---Cg(3) <sup>a</sup>	3.6581	6.07	25.01	
Cg(2)-(I)---Cg(2) <sup>a</sup>	3.3630	0.00	18.44	
Cg(3)-(1)---Cg(1) <sup>a</sup>	3.6581	6.07	25.51	
Equivalent position codes	Cg(1)=Cu(1), S(1), C(12), N(4),N(3)			
a= 1-x, 1-y, 1-z	Cg(2)=Cu(1), N(1), C(5), C(6),N(3)			
	Cg(3)= N(1), C(1), C(2), C(3),C(4),C(5)			
<b>CH---<math>\pi</math> interactions</b>				
X-H(I)---Cg(J)	H..Cg(Å)	X-H..Cg (°)	X-H..Cg (°)	
C8-H(8)(I)---Cg(1) <sup>c</sup>	3.0810	146	3.8674	
C(10)-H(10)-(1)---Cg(5) <sup>d</sup>	2.6491	166.19	3.5908	
Equivalent position codes	Cg(5)=C(13), C(14),			
c=-1+x, y, z	C(15),C(16),C(17),C(18)			
d=-1+x, 1/2 -y, -1/2 +z	Cg(1)=Cu(1), S(1), C(12), N(4),N(3)			

(D=Donor, A=acceptor, Cg=Centroid,  $\alpha$ =dihedral angles between planes I & J,  $\beta$ =angle Cg(1)-Cg(J))

stabilized by two CH- $\pi$  interactions. The intermolecular hydrogen bonding interactions such as C(2)-H(2)---S(1) and C(11)-H(11)---Br(1) are at distances of 2.80 and 2.92 Å respectively adds to the stability of in the unit cell. Thus  $\pi$ - $\pi$  stacking, the CH- $\pi$  interactions contribute to its stability. These interactions lead to possibility for metalloaromaticity [112].

### 3.3.3. Molecular and crystal structure of $[\text{CuL}^2\text{N}_3]_2$

The asymmetric unit of compound  $[\text{CuL}^2\text{N}_3]_2$  (**12**) is shown in Figure 3.5 consists of two molecules characterized by a two fold axis perpendicular to the Cu(1)\N(6)\Cu(2)\N(6a) plane resulting in a centrosymmetric closely associated crystallographically equivalent molecules bridged *via* N(6) atoms of the azido group. Selected bond lengths and bond angles are presented in Table 3.9. Each copper atom in the dimeric unit is pentacoordinate with pyridyl nitrogen N(1), azomethine nitrogen N(3), thiolate sulfur S(1) and N(6) of the azido group [N(6)-N(7)-N(8)] and nitrogen atoms of the bridging azido group [N(6a)-N(7a)-N(8a)] adopting a distorted square pyramidal geometry with N(6a) at the apical position. The copper center of the second subunit has a similar type of coordination with another thiosemicarbazone unit, azido ligand N(6a)-N(7a)-N(8a) and bridges with N(6) nitrogen of the other azido ligand [N(6)-N(7)-N(8)] giving rise to a distorted square pyramidal geometry. Each copper atom is pentacoordinate with bond distances Cu(1)-S(1) (2.2603(11) Å), Cu(1)-N(6) (1.956(2) Å), Cu(1)-N(1) (2.0269 Å), Cu(1)-N(3) (1.964(2) Å), Cu(1)-N(6a) (2.5628 Å). The azido group acts as a bridging ligand that bridges the two copper centers. The Cu-N<sub>pyridyl</sub> bond length is 0.0629 Å greater than Cu-N<sub>imine</sub> bond that suggesting the strength of azomethine nitrogen coordination. The coordination geometry about Cu(1) is square pyramidal with N(6a) at the apex of the square pyramid with some amount of distortion where pyridine nitrogen N(1), imine nitrogen N(3), thiolate sulfur S(1) and N(6) of bridging azido group together forms the basal square plane around Cu(1). The configuration of the thiosemicarbazone chain about C(6)-N(3) bond is *Z* which

facilitate the coordination of thiolate sulphur to copper(II) in the complex.. The C(6)-N(3) bond distances in the complex is observed at 1.299(3) Å in comparison to the C(6)-N(3) bond distance of 1.295(2) Å in the free ligand. This indicates that there is no clear decrease in the double bond character of the C-N azomethine bond on chelation to the copper(II) ion. This can be attributed to the stabilization of the C-N<sub>azomethine</sub> bond in the copper(II) complexes due to the presence of an important metal-to-ligand  $\pi$ -back donation. The delocalisation of electron density in the thiosemicarbazone moiety gives rise to a reduction in the N(3)-N(4) (1.370(2) Å) compared to the uncomplexed thiosemicarbazone. The loss of N(4)-H proton in HL<sup>2</sup> produces a negative charge, which is delocalised on the N(3)-N(4)-C(12) system. This is indicated by the lengthening of the bond S(1)-C(12) (1.744(2) Å) compared to the value of 1.6686(12) Å in the free ligand. The decrease in the bond length of C(12)-N(4) (1.326(3) Å) in the complex from that of the free ligand also supports thiolate formation. The Cu(1)-N(6a) bond length is greater than Cu(1)-N(6) bond length by 0.6068 Å suggesting that N(6a) is at the apical position of the square pyramidal structure. Thus Cu(1), N(6), Cu(1a), N(6a) constitutes a rectangular arrangement. The bond angles S(1)-Cu(1)-N(6) (100.81(6)°), S(1)-Cu(1)-N(3) (84.95(6)°), N(1)-Cu(1)-N(6) (94.28(7)°), N(1)-Cu(1)-N(3) (80.56(7)°), S(1)-Cu(1)-N(1) (160.88(5)°), N(3)-Cu(1)-N(6) (173.80(7)°) further suggests that pyridyl nitrogen N(1), thiolate sulfur S(1), azomethine nitrogen N(3) and N(6) of monoligated azido group constitutes the basal plane. The bond angles S(1)-Cu(1)-N(6a) (104.53°), N(1)-Cu(1)-N(6a) (87.77°), N(3)-Cu(1)-N(6a) (89.29°), N(6)-Cu(1)-N(6a) (87.06°) also suggest that N(6a) is positioned geometrically at the apex of the square pyramidal structure. The comparison of bond distances Cu(1)-N(6) (1.956(2) Å) and Cu(1)-N(6a) (2.5628 Å) confirms the possibility of a bridging binuclear structure with a moderate Cu-Cu distance 3.303 Å. The  $\tau$  parameter  $(\alpha-\beta)/60$  where  $\alpha = \text{N(3)-Cu(1)-N(6)}$  (173.80(7)°) and  $\beta = \text{S(1)-Cu(1)-N(1)} = 160.88(5)^\circ$ , then  $\tau = 0.2159$  [111]. This means that coordination geometry around each copper(II) ion is

very close to a distorted square pyramidal structure. In the complex, azide ion acts as a bridging bidentate ligand, whereas N(6) coordinates to Cu(1) and bridges Cu(1a) as indicated by the bond angle Cu(1)-N(6)-Cu(1a) ( $92.94^\circ$ ) and bond length Cu(1)-N(6a) ( $2.5628 \text{ \AA}$ ). The dihedral angle constituted by the planes N(1)/C(1)/C(2)/C(3)/C(4)/C(5) and N(1)/C(5)/C(6)/N(3)/Cu(1) is  $6.97^\circ$  shows that the pyridyl ring and the newly formed metal chelate ring are coplanar. The dihedral angle between the planes N(1)/C(1)/Cu(1)/Cu(1a) and Cu(1)/N(6)/Cu(1a)/N(6A) is  $70.77^\circ$  shows that the bridging plane is almost perpendicular to the plane containing pyridyl nitrogen N(1) coordinated to Cu(1) confirming that N(6a) is at the apex of the square pyramid.

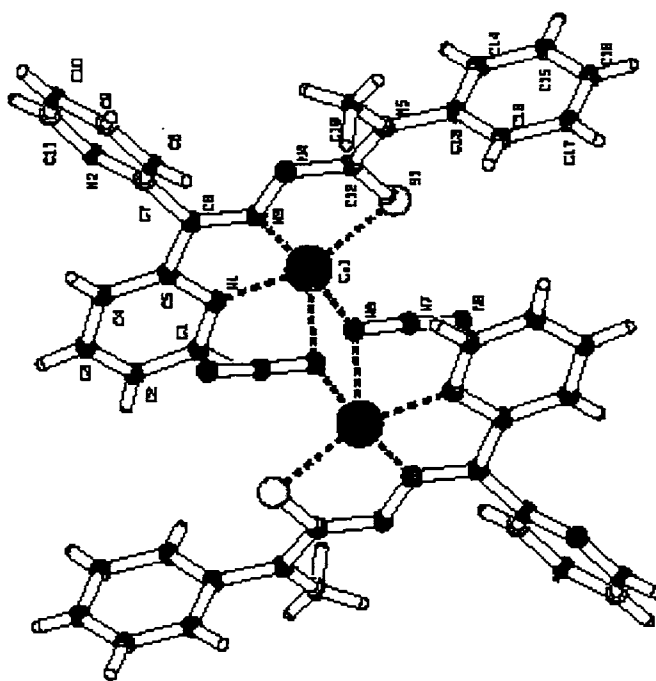


Figure 3.5. PLATON diagram of the compound  $[\text{CuL}^2(\text{N}_3)]_2$  (12).

Figure 3.6 shows the unit cell-packing diagram of the compound viewed along down the *b*-axis. In the unit cell, molecules are arranged in a parallel fashion through interaction with neighboring molecules due to  $\pi$ - $\sigma$  interaction between the metal containing chelate rings and aromatic hydrogen atoms. The unit cell contains four molecules in which two molecules are stacked by H-



bonding interaction. Each unit containing two molecules are stacked with another unit through, CH- $\pi$  interactions. Thus assemblage of molecules in the respective manner in the unit cell is resulted by the diverse  $\pi$ - $\pi$  stacking, CH- $\pi$ , ring-metal and hydrogen bonding interactions are depicted in Table 3.10. The pyridyl rings Cg(1) and Cg(2) are involved in  $\pi$ - $\pi$  interactions

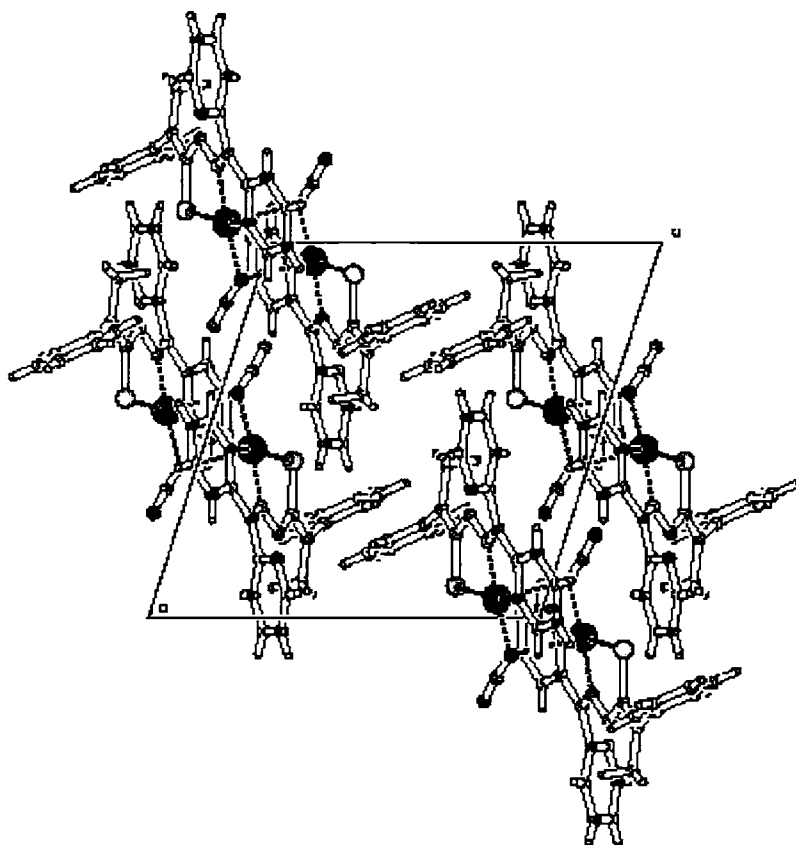


Figure 3.6 Unit cell packing diagram of  $[\text{CuL}^2(\text{N}_3)]_2$  viewed down  $b$ - axis

with the pyridyl ring of the neighboring unit at a distance of 4.3282 Å indicating weak interaction. The CH- $\pi$  interactions are comparatively stronger than  $\pi$ - $\pi$  interactions. The CH- $\pi$  interactions between the pyridyl hydrogen and the phenyl rings such as C(10)-H(7)(1)-----Cg(3) and C(15)-H(5)(1)----Cg(2) of the neighboring molecules at a distances of 2.9888 and 2.9357 Å contribute to the stability of the unit cell packing. An intermolecular hydrogen bonding interaction between pyridyl and N (2), N (4) and N (6) nitrogens of the

**Table 3.9****Selected bond lengths (Å) and bond angles (°) of HL<sup>2</sup> and [CuL<sup>2</sup>(N<sub>3</sub>)<sub>2</sub>]**

	HL <sup>2</sup>	[CuL <sup>2</sup> (N <sub>3</sub> ) <sub>2</sub> ]
Cu(1)-S(1)		2.2603(11)
Cu(1)-N(1)		2.027(2)
Cu(1)-N(3)		1.964(2)
Cu(1)-N(6)		1.956(2)
Cu(1)-N(6)a		2.5628
S(1)-C(12)	1.6686(12)	1.744(2)
N(3)-N(4)	1.362(2)	1.370(2)
N(3)-C(6)	1.295(2)	1.299(3)
N(4)-C(12)	1.377(2)	1.326(3)
N(5)-C(12)	1.3489(2)	1.354(3)
S(1)-Cu(1)-N(1)		160.88(5)
S(1)-Cu(1)-N(3)		84.95(6)
S(1)-Cu(1)-N(6)		100.81(6)
S(1)-Cu(1)-N(6)a		104.53
N(1)-Cu(1)-N(3)		80.56(7)
N(1)-Cu(1)-N(6)		94.28(7)
N(1)-Cu(1)-N(6)a		87.77
N(3)-Cu(1)-N(6)		173.80(7)
N(3)-Cu(1)-N(6)a		89.29
N(6)-Cu(1)-N(6)a		87.06
Cu(1)-N(6)-Cu(1)a		92.94
N(3)-N(4)-C(12)	118.67(16)	
C(6)-N(3)-N(4)	120.94(16)	120.37
N(3)-N(4)-C(12)	118.67(16)	111.68
N(5)-C(12)-N(4)	113.73(16)	115.02
N(5)-C(12)-S(1)	123.48(14)	119.09
N(4)-C(12)-S(1)	122.79(14)	125.89

Table 3.10

H-bonding,  $\pi$ --- $\pi$ , CH--- $\pi$  and ring-metal interaction parameters of,  $\text{Cu}_2\text{L}_2^2(\text{N}_3)_2$ 

<b>H-bonding</b>				
Donor---H---A	D-H (Å)	H---A (Å)	D---A (Å)	D-H---A (°)
C(1)---H(1)---N(6)	0.93	2.59	3.1209	117
C(4)---H(4)---N(2)	0.88	2.57	3.0226	113
C(8)---H(8)---N(4)	0.84	2.61	2.9410	105
C(18)---H(18)---N(8)	0.84	2.61	3.3416	146
<b><math>\pi</math>---<math>\pi</math> interactions</b>				
Cg(I)-Res(I)---Cg(J)	Cg-Cg(Å)	$\alpha$ (°)	$\beta$ (°)	
Cg(I)-(I)---Cg(2) <sup>a</sup>	4.3282	10.81	38.80	
Cg(2)-(I)---Cg(1) <sup>b</sup>	4.3282	10.81	38.28	
Equivalent position codes		Cg(1)=N(1), C(1), C(2), C(3),C(4),C(5)		
a= x, 1/2-y, -1/2+z		Cg(2)=N(2), C(7), C(8),C(9),C(10),C(11)		
b= x, 1/2-y, 1/2+z				
<b>CH---<math>\pi</math> interactions</b>				
X-H(I)---Cg(J)	H..Cg(Å)	X-H..Cg (°)	X-H..Cg (°)	
C(10)-H(7)(I)---Cg(3) <sup>c</sup>	2.9888	144.71	3.7696	
C(15)-H(15)-(1)---Cg(2) <sup>d</sup>	2.9357	152.35	3.7774	
Equivalent position codes		Cg(2)=N(2), C(7), C(8),C(9),C(10),C(11)		
c=-1-x,-y, -z		Cg(3)=C(13), C(14), C(15), C(16),C(17),C(18)		
d=1-x,-1/2+y,1/2-z				
<b>Ring-metal interactions</b>				
Cg(I) Res(I) Me(J)	Cg(I)-Me(J) (Å)			
Cg(2) [ 1 ] -> Cu(1) <sup>b</sup>	3.774			
Equivalent position codes		Cg(2)=N(2), C(7),(8),C(9),C(10),C(11)		
b= x, 1/2-y, 1/2+z				

(D=Donor, A=acceptor, Cg=Centroid,  $\alpha$ =dihedral angles between planes I & J,  $\beta$ =angle Cg(1)-Cg(J)

neighboring molecule exists in the unit cell. Also another intermolecular hydrogen bonding interaction between phenyl hydrogens and N(8) of nitrogen of the azide group is also present in the system. Thus  $\pi$ - $\pi$ , CH-- $\pi$ , ring-metal and hydrogen bonding interactions stabilize the unit cell packing and point out the possibility for metalloaromaticity [112].

### 3.3.4. Molecular and crystal structure of $[\text{CuL}^2(\text{SH})]_2 \cdot 2\text{H}_2\text{O}$

The asymmetric PLATON plot of the complex  $[\text{CuL}^2(\text{SH})]_2 \cdot \text{H}_2\text{O}$  is shown in Figure 3.7 illustrate the structural features of the compound for which selected bond lengths and bond angles are presented in Table 3.11. Crystal structure by X-ray diffraction reveals that the compound consists of a three-dimensional copper–thiosemicarbazone network. The structure consists of two units of  $[\text{CuL}^2]$ . Thus the three dimensional arrangement consists of two copper-thiosemicarbazone units, each with a distorted square pyramidal geometry where the apical position of the square pyramid is occupied by the pyridine N(2) nitrogen of the other sub unit. The structure contains two copper centers where each center is pentacoordinate with pyridyl nitrogen, azomethine nitrogen, thiolate sulfur of the thiosemicarbazone moiety, SH group and pyridyl nitrogen N(2) of second thiosemicarbazone moiety. Bond lengths of copper and other atoms are Cu(1)-S(1) (2.2624 Å), Cu(1)-S(2) (2.2866 Å), Cu(1)-N(1) (2.0267 Å), Cu(1)-N(3) (1.9768 Å), Cu(1)-N(2a) (2.3505 Å). The loss of a proton bound to N(4) in  $\text{HL}^2$  produces a negative charge, which is delocalised the N(3)-N(4)-C(12) system. This is indicated by the lengthening of the bond S(1)-C(12) (1.7279 Å) compared to that of the free ligand. The decrease in the bond length of C(12)-N(4) (1.3383 Å) from 1.377(2) Å of the thiosemicarbazone also supports thiolate formation. The bond angles are quite far from square pyramidal geometry with distortion of the basal square planes comprising of S(2), S(1), N(3) and N(1) atoms. The dihedral angle between the planes N(1)/C(5)/C(6)/N(3)/Cu(1) and S(1)/C(12)/N(4)/N(3)/Cu(1) is  $3.04^\circ$  also suggests that the newly formed metal chelate rings are coplanar. The dihedral

angle between the planes C(6)/N(3)/N(4)/C(12)/N(5) and N(1)/C(1)/C(2)/C(3)/C(4)/C(5) is  $5.90^\circ$  suggests the co-planarity of thiosemicarbazone moiety and the pyridyl ring. The Cu-N<sub>pyridyl</sub> bond length is 0.0999 Å higher than Cu-N<sub>imine</sub> bond length shows the strength of azomethine nitrogen coordination. The configuration of the thiosemicarbazone chain about C(6)-N(3) bond is *Z* which facilitate the coordination of thiolate sulphur to copper(II) in the complex. The C(6)-N(3) bond distance of 1.295(2) Å in the free ligand remain unaltered on complexation confirming the strength of azomethine nitrogen coordination to Cu(1). This indicates that there is no clear decrease in the double bond character of the C-N azomethine bond on chelation to the copper(II) ion. This can be attributed to the stabilization of the C-N azomethine bond in the copper(II) complexes due to the presence of an important metal-to-ligand  $\pi$ -back donation. The delocalisation of electron density in the thiosemicarbazone moiety gives rise to a reduction in the N(3)-N(4) (1.3547 Å) compared to the uncomplexed thiosemicarbazone in the complex.

The bond angles S(2)-Cu(1)-S(1) ( $95.30^\circ$ ), S(2)-Cu(1)-N(1) ( $96.57^\circ$ ), S(2)-Cu(1)-N(2) ( $97.40^\circ$ ), S(2)-Cu(1)-N(3) ( $143.74^\circ$ ), S(1)-Cu(1)-N(1) ( $163.62^\circ$ ), S(1)-Cu(1)-N(2) ( $100.55^\circ$ ), S(1)-Cu(1)-N(3) ( $83.70^\circ$ ), N(1)-Cu(1)-N(2) ( $89.09^\circ$ ), N(1)-Cu(1)-N(3) ( $80.23^\circ$ ), N(2)-Cu(1)-N(3) ( $114.54^\circ$ ), are quite far from square pyramidal geometry with distortion of the basal square plane comprising of Cu(1), S(2), S(1), N(3) and N(1) atoms. . If we use the  $\tau$  parameter where  $\tau = (\alpha - \beta)/60$ , (where  $\tau = 0$  for a square pyramidal geometry and  $\tau = 1$  for a trigonal bipyramidal geometry) defined by Addison *et al.* to quantify geometry [111]. Cu(1)-N(2) is selected as the axial position and N(1)-N(3)-S(1)-S(2) constitutes the base of the square pyramid. So  $\alpha = \text{S(1)-Cu(1)-N(1)} = 163.62^\circ$  and  $\beta = \text{S(2)-Cu(1)-N(3)} (143.74^\circ)$ , then  $\tau = 0.33$ . This means that coordination geometry of each copper(II) ion is distorted square pyramidal. The dihedral angle constituted by the planes N(1)/C(1)/C(2)/C(3)/C(4)/C(5) and N(1)/C(5)/C(6)/N(3)/Cu(1) is  $2.76^\circ$  shows that the pyridyl ring and newly

formed metal chelate rings are coplanar. Similarly the dihedral angle between the planes N(1)/C(5)/C(6)/N(3)/Cu(1) and S(1)/C(12)/N(4)/N(3)/Cu(1) is  $3.04^\circ$  also suggests the coplanarity of both metal chelate rings. The dihedral angle between the planes constituted by the thiosemicarbazone moiety C(6)/N(3)/N(4)/C(12)/N(5) and pyridyl ring N(1)/C(1)/C(2)/C(3)/C(4)/C(5) is  $5.90^\circ$  confirms that both metal chelate rings are almost coplanar.

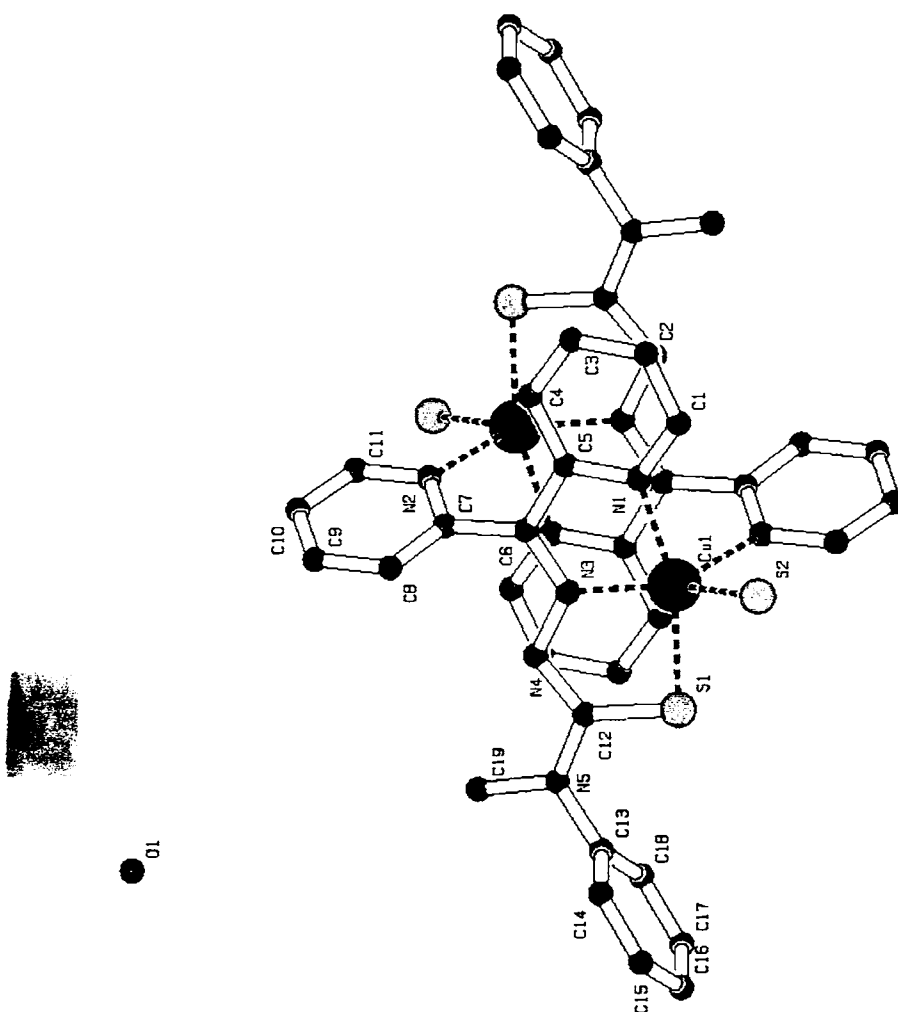


Figure 3.7. *PLATON* diagram of the compound  $[\text{CuL}^2(\text{SH})]_2 \cdot 2\text{H}_2\text{O}$  (13) with all hydrogen atoms excluded

**Table 3.11**Selected bond lengths (Å) and bond angles (°) of HL<sup>2</sup> and [Cu<sub>2</sub>L<sup>2</sup>(SH)]<sub>2</sub>·2H<sub>2</sub>O

	HL <sup>2</sup>	[Cu <sub>2</sub> L <sup>2</sup> (SH)] <sub>2</sub> ·H <sub>2</sub> O
S(1)-Cu(1)		2.2624
Cu(1)-S(2)		2.2866
Cu(1)-N(1)		2.0267
Cu(1)-N(3)		1.9768
Cu(1)-N(2)a		2.3505
S(1)-C(12)	1.6686(12)	1.7279
N(3)-N(4)	1.362(2)	1.3547
N(4)-C(12)	1.377(2)	1.3383
N(5)-C(12)	1.349(2)	1.3466
N(3)-C(6)	1.295(2)	1.3023
S(1)-Cu(1)-S(2)		95.30
S(1)-Cu(1)-N(1)		163.62
S(1)-Cu(1)-N(3)		83.70
S(1)-Cu(1)-N(2)a		100.55
S(2)-Cu(1)-N(1)		96.57
S(2)-Cu(1)-N(3)		143.74
S(2)-Cu(1)-N(2)a		97.40
N(1)-Cu(1)-N(3)		80.23
N(1)-Cu(1)-N(2)a		89.09
N(3)-Cu(1)-N(2)a		114.54
N(3)-N(4)-C(12)	118.67(16)	111.57
N(5)-C(12)-N(4)	113.73(16)	115.75
N(5)-C(12)-S(1)	123.48(14)	119.05
N(4)-C(12)-S(1)	122.79(14)	125.20

Fig 3.8 shows the unit cell-packing diagram of the viewed down the *c*-axis. There are 4 molecules in the unit cell. The molecules are arranged in such a manner two adjacent molecular units are geometrically opposite to each other. An interesting feature of the arrangement is that the unit cell as a whole is centrosymmetric. The assemblage of molecules in the unit cell is resulted by the diverse  $\pi$ - $\pi$  stacking, CH- $\pi$  and ring-metal and hydrogen bonding interactions are depicted in Tables 3.12. The metal chelate rings Cg(1) and Cg(2) are involved in  $\pi$  -  $\pi$  interactions with the pyridyl ring Cg(3) of the neighboring unit at distances of 3.6595 Å and 4.2894 Å respectively. The metal chelate ring Cg(1) is also involved in  $\pi$ - $\pi$  interaction with metal chelate ring of Cg(2) of the neighboring molecule at a distance of 4.0305 Å. These interactions are more related to a  $\pi$  deficient- $\pi$  deficient interaction that leads to a stable structure. The unit cell is further stabilized by two C-H-- $\pi$  interactions. The intramolecular hydrogen bonding interaction, C(11)-H(11)---S(2) and intermolecular hydrogen bonding interactions, C(9)-H(9)---S(2), and C(3)-H(3)--O(1) (where O(1) is the oxygen of water), in the unit cell also enhances its stability. Thus  $\pi$ - $\pi$  stacking, the CH- $\pi$  interactions between the pyridyl hydrogen and metal chelate rings in both compounds contribute to its stability. These interactions lead to the possibility for metalloaromaticity [112]. It is also observed that hydrogen bonding interactions co-exist with other interactions in the molecule.



Table 3.12

H-bonding,  $\pi$ --- $\pi$  and CH--- $\pi$  interaction parameters of the compound  
 $[\text{CuL}^2(\text{SH})]_2 \cdot 2\text{H}_2\text{O}$

<b>H-bonding</b>				
Donor---H...A	D-H (Å)	H---A (Å)	D---A (Å)	D-H---A (°)
C(3)---H(3)---O(1)	0.89	2.60	3.4578	161
C(9)---H(9)---S(2)	0.98	2.86	3.7787	156
C(11)---H(11)---S(2)	1.02	2.67	3.4016	129
<b><math>\pi</math>---<math>\pi</math> interactions</b>				
Cg(I)-Res(I)---Cg(J)	Cg-Cg(Å)	$\alpha$ (°)	$\beta$ (°)	
Cg(I)-(I)---Cg(2) <sup>a</sup>	4.0305	3.04	38.40	
Cg(1)-(I)---Cg(3) <sup>a</sup>	3.6595	5.79	24.28	
Cg(2)-(I)---Cg(1) <sup>a</sup>	4.0305	3.04	35.79	
Cg(2)-(I)---Cg(2) <sup>a</sup>	3.3700	0.00	17.96	
Cg(2)-(I)---Cg(3) <sup>a</sup>	4.2894	2.76	40.48	
Cg(3)-(I)---Cg(1) <sup>a</sup>	3.6595	5.79	25.36	
Cg(3)-(I)---Cg(2) <sup>a</sup>	4.2894	2.76	42.99	
Equivalent position codes		Cg(1)=Cu(1), S(1), C(12),N(4),N(3).		
a =2-x, 1-y, 1-z		Cg(2)= Cu(1), N(1), C(5),N(6),N(3).		
		Cg(3)=N(1), C(1), C(2), C(3),C(4),C(5)		
<b>CH---<math>\pi</math> interactions</b>				
X-H(I)---Cg(J)	H..Cg (Å)	X-H..Cg (°)	X-H..Cg (°)	
C(8)-H(8)(I)---Cg(1) <sup>b</sup>	3.0670	142.94	3.8310	
C(10)-H(10)-(1)---Cg(5) <sup>c</sup>	2.7520	153.41	3.6330	
Equivalent position codes		Cg(5)=C(13), C(14), C(15), (16),C(17),C(18)		
b=1-x, 1-y, 1-z				
c=1-x, 1/2+y, 1/2-z				

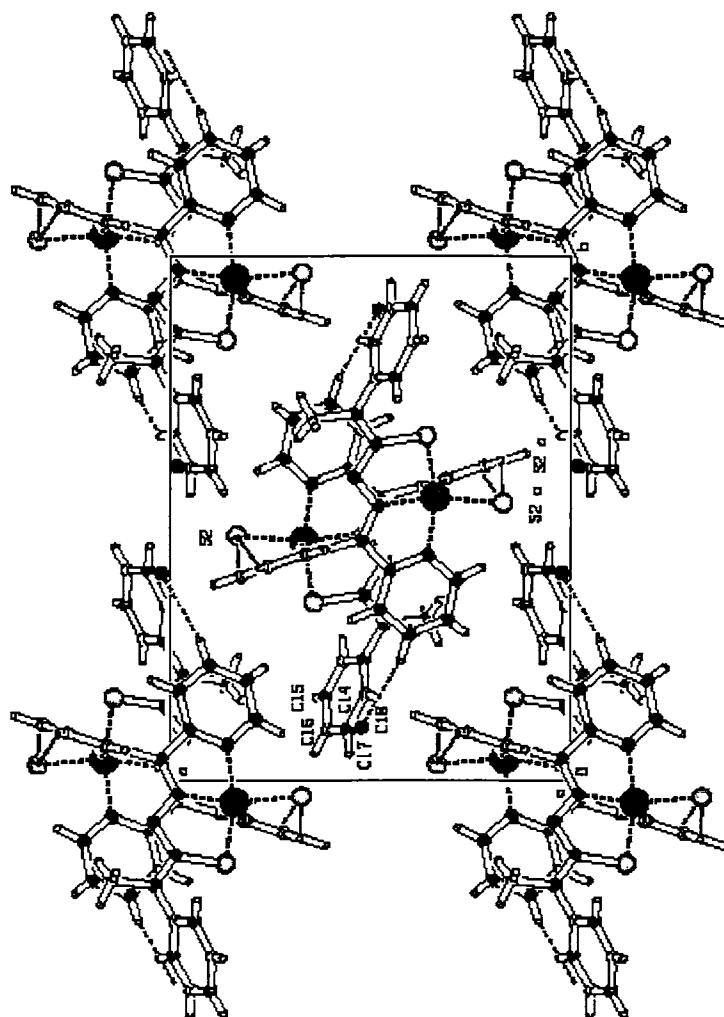


Figure 3.8. Unit cell packing diagram of the compound  $[\text{CuL}^2(\text{SH})]_2 \cdot 2\text{H}_2\text{O}$  viewed down the  $c$ -axis.

### 3.3.5. Magnetic susceptibility

Additional information on structure of complexes can be obtained from magnetic moment measurements. Because metals have a partially filled  $d$  or  $f$  orbitals, range of magnetic properties can be expected, depending on the oxidation state, electronic configuration and coordination number of the central metal. Magnetic moment of copper(II) complexes are measured at room

temperature and it was found that these complexes usually differ appreciably from spin only value (1.73 B.M). The reason for the departure from the spin only value lies partly in the existence of the second order Zeeman effect between the ground and higher ligand field terms. It lies mainly in the fact that, in the presence of spin orbit coupling, the quenching effect of the ligand cannot be complete. The spin- orbit coupling may be supposed to 'mix' in terms of different orbital degeneracy. It is also necessary to consider the effective reduction of orbital angular momentum of a metal ion consequent upon the delocalisation of electrons out of the  $t_{2g}$  orbital of the ion on to the ligand atoms. Such delocalisation takes place when the wave functions of the metal ion mix with those of ligand to form the molecular orbital of the complex. The effect of  $t_{2g}$  electron delocalisation is usually to bring the magnetic moment closer to the spin-only value, since it corresponds to an additional quenching of angular momentum [28].

Ray and Sen correlated color with magnetic moment and stereochemistry of the complex. They correlated red and yellow color with complexes of magnetic moments 1.7-1.9 B.M. and 1.9-2.2 B.M. to green and blue color of complexes. Octahedral copper(II) complexes show magnetic moments in the range 1.7-1.9 B.M.

The ground spectroscopic term of copper(II) ion ( $^2D$ ) splits into  $e_g$  and  $t_{2g}$  with energy of separation of  $10,000\text{ cm}^{-1}$  to  $20,000\text{ cm}^{-1}$ . Electronic transitions between the levels give rise to blue and green colors to complexes.

Orbital angular momentum about an axis is associated with the ability to rotate an orbital about an axis to give an identical degenerate orbital. Inspection shows that no rotation can turn the  $d_{z^2}$  orbital into  $d_{x^2-y^2}$  orbital as they differ in shape. There is no orbital angular momentum associated with the  $e_g$  set in cubic symmetry. Tetragonal distortion and complete removal of trans ligands from octahedral case leads to lower symmetries such as trigonal bipyramidal, square pyramidal, square planar etc. Orbital contribution to magnetic moment in

square planar complexes is very small, as orbital angular momentum amongst the  $d$  orbitals is quenched by the low symmetry. Some orbital angular momentum remains with the  $e_g$  orbital pair. In  $D_{4h}$  symmetry, rotation of  $d_{xz}$  orbital about the  $Z$ -axis by  $\pi/2$  yields the  $d_{yz}$  orbital. One difficulty in the interpretation of the magnetic behavior of square planar complexes is the lack of magnetic dilution. The absence of ligand groups above and below the plane of the complex may allow magnetic exchange between adjacent molecules. Magnetic moments measured at room temperature are also given in Table 3.1. The spin only magnetic moment for a multinuclear system is given by the expression,  $\mu_{eff}^2 = n(n+2)$  where  $n$  is the number of unpaired electrons in the cluster. Hence for copper(II),  $n = 1$  per copper atom, thus for a two copper system  $\mu_{eff}^2 = 2(2+2) = 8$ ,  $\mu_{eff}$  per copper atom is equal to 4 and hence magnetic moment was expected to be 2. In view of this, the magnetic moment of complexes **1**, **2**, **3**, **4**, **5**, **6** and **13**, are less than 1.74 B.M. indicating strong antiferromagnetic interaction of copper(II) ion with the neighboring copper center strongly supports the dimeric nature of the complexes. The magnetic moment of complexes **7**, **10** and **11** are greater than the spin only value for a dimeric system as suggested by the equation  $\mu_{eff}^2 = n(n+2)$  where  $n (= 2)$  is the number of unpaired electrons in the cluster. The magnetic moment values also indicates more than one copper center per molecule suggesting with spins of electrons are ordered parallel resulting in a high magnetic moment. Compounds **8** and **12** show magnetic moment values close to the spin only value per copper for a dimer suggesting that the distance between the copper centers is greater than the moderate distance needed for interaction. The compound **9** is diamagnetic strongly supports its existence as a dimer in the solid state [113]. Thus the magnetic moment values are agreeing with that of dimers having antiferro or ferromagnetic interactions and thus we have assigned tentatively dimeric structures to all the complexes.

### 3.3.6. Infrared spectra

Tables 3.13 and 3.14 lists the tentative assignments of main IR bands of copper(II) complexes for the ligands HL<sup>1</sup> and HL<sup>2</sup> and polyatomic anions in 4000-50 cm<sup>-1</sup> regions. The spectra of free ligands exhibit a medium band at *ca* 3050 cm<sup>-1</sup>, which is assigned to  $\nu(\text{NH})$  vibration. The absence of  $\nu(\text{NH})$  band in the spectra of complexes provide a strong evidence for the ligand coordination around copper(II) ion in its deprotonated form [114]. The spectra of complexes exhibit a systematic shift in the position of the bands in the region 1600-1350 cm<sup>-1</sup> due to  $\nu(\text{C}=\text{C})$  and  $\nu(\text{C}=\text{N})$  vibrational modes, and their mixing patterns are different from those present in the ligand spectrum. As a result of coordination, the band corresponding to azomethine nitrogen,  $\nu(\text{C}=\text{N})$  shifts to higher wavenumbers [106, 115-116] which may be due to the combination of  $\nu(\text{C}=\text{N})$  with newly formed N=C bond formed as a result of enolization followed by deprotonation. The coordination through azomethine nitrogen is also supported by new band at  $\sim 415$  cm<sup>-1</sup>. The enolisation is also supported by the positive shift in the  $\nu(\text{N}-\text{N})$  band by 10-50 cm<sup>-1</sup>. The downward shift of the bands at 1330 and 808 cm<sup>-1</sup> in HL<sup>1</sup>, and 1360 and 793 cm<sup>-1</sup> in HL<sup>2</sup> corresponding to  $\nu(\text{C}-\text{S})$  and  $\delta(\text{C}-\text{S})$  respectively to lower wavenumbers on complexation suggesting the change of bond order and strong electron delocalisation upon chelation [117]. The pyridine ring out-of-plane bending vibrations at 638 and 644 cm<sup>-1</sup> in HL<sup>1</sup> and HL<sup>2</sup> respectively shift to higher frequencies on complexation confirming the coordination of ligand to metal *via* pyridine nitrogen [118-120].

The sulfato complex (4) shows four fundamental vibrations. Of these four fundamentals, only  $\nu_3$  and  $\nu_4$  are infrared active. If the symmetry of the ion is lowered by complex formation, the degenerate vibration split and Raman-active modes appear in the infrared spectrum. The symmetry of sulfate ion is approximately  $T_d$ . On complexation the symmetry is lowered to  $C_{2v}$ . Thus  $\nu_1$  and  $\nu_2$  appear with medium intensity, and  $\nu_3$  and  $\nu_4$  each split into three bands. Bands at 970 cm<sup>-1</sup> due to  $\nu_1$ , medium band around 459 cm<sup>-1</sup> due to  $\nu_2$ , another

medium and weak split bands at 1240, and 1181 and 1112  $\text{cm}^{-1}$  corresponding to  $\nu_3$  and  $\nu_4$  does not appear in the spectra. Thus sulfato group in the complex is concluded to be a chelating bidentate ligand [34].

It is rather very difficult to differentiate the coordination modes of nitrate anion by IR spectroscopy. It was found that both nitrate complexes (**3** and **11**) exhibit three medium bands at  $\sim 1385$ ,  $\sim 1283$  and  $\sim 1013$   $\text{cm}^{-1}$  corresponding to  $\nu_4$ ,  $\nu_1$  and  $\nu_2$  of unidentate nitrate groups with a separation of 102  $\text{cm}^{-1}$  for  $\nu_4$  and  $\nu_2$  indicate the presence of terminally bonded monodentate nitrate groups [121]. A combination band  $\nu_1+\nu_4$  diagnostic for monocoordinate nitrate groups [122] around 1742  $\text{cm}^{-1}$  was found to be absent in the complex. The bands due to  $\nu_3$ ,  $\nu_5$  and  $\nu_6$  could not be assigned due to the richness of the spectra of the complexes. It was reported that for nitrate solids [34], unidentate and bidentate complexes exhibit two MO stretching bands in the region 350-250  $\text{cm}^{-1}$  and another medium band at 315  $\text{cm}^{-1}$  is identified for this mode.

Perchlorate anion (**6**) (Figure 3.9) coordinates to metal ions only when its complexes are prepared in non-aqueous solvents. The perchlorate complex (**6**) shows a broad unsplit band at 1090  $\text{cm}^{-1}$  [123] corresponding to  $\nu_3(\text{ClO}_4)$  and an unsplit strong band at 620  $\text{cm}^{-1}$  assignable to  $\nu_4(\text{ClO}_4)$ . This along with the absence of a band corresponding to  $\nu_1$  at  $\sim 920$   $\text{cm}^{-1}$  indicates the presence of an ionic perchlorate group [124].

The observed frequencies of azido complexes (**4** and **12**) in the spectra at 2042 (broad) and 1369  $\text{cm}^{-1}$  (strong) respectively can be attributed to  $\nu_a$  and  $\nu_s$  of the coordinated azido group. A medium band at  $\sim 650$   $\text{cm}^{-1}$  corresponds to  $\delta(\text{N-N-N})$  vibrations and another weak band at  $\sim 450$   $\text{cm}^{-1}$  is assignable to  $\nu(\text{Cu-N})$  of coordinating azide. This suggests that Cu-N-N-N bond is not linear. The bands due to  $\nu(\text{Cu-N}_{\text{azido}})$  appear weak which may be due to the bridging nature of azide to the copper centers. But it is not possible to determine the structures of these bridges from infrared spectra [34].

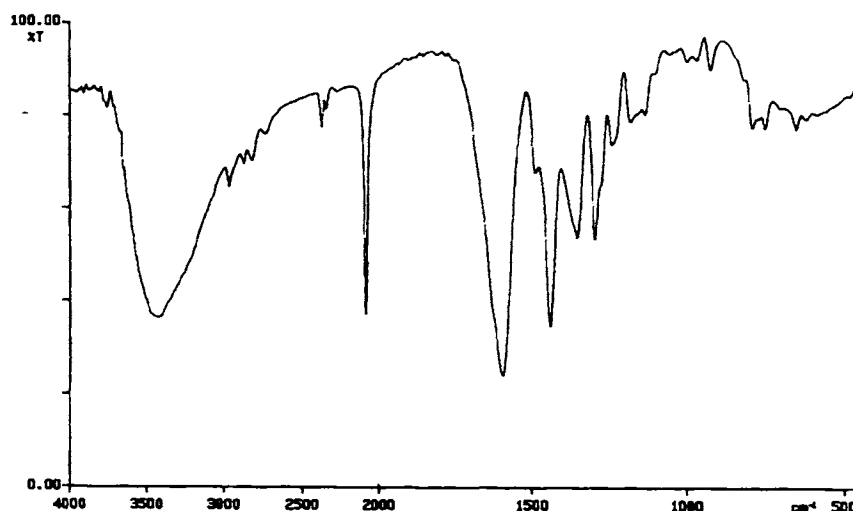
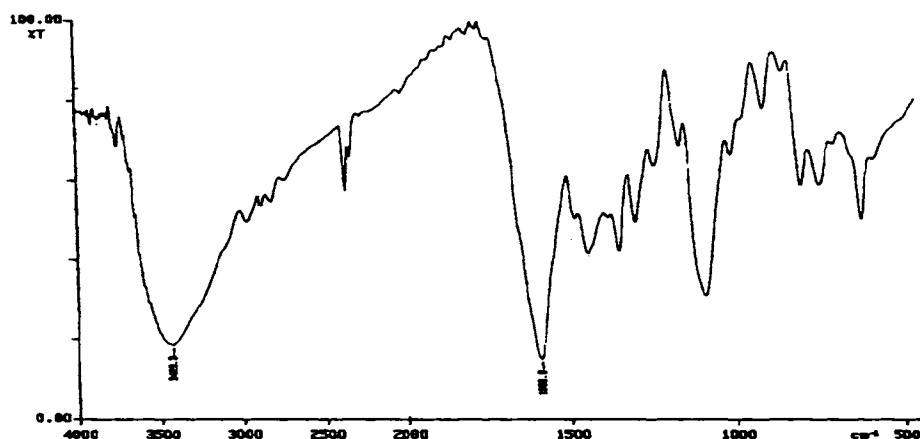
Compound 5 [CuL<sup>I</sup>(NCS)]Compound 6 [Cu<sub>2</sub>L<sup>I</sup><sub>2</sub>(OH)]ClO<sub>4</sub>·H<sub>2</sub>O

Figure 3.9. Infrared spectra of compounds 5 and 6

Thiocyanato complex (5) (Figure 3.9) exhibits a strong and sharp band at  $2081 \text{ cm}^{-1}$  [125], a weak band at  $787 \text{ cm}^{-1}$  and another weak band at  $480 \text{ cm}^{-1}$  which can be attributed to  $\nu(\text{CN})$ ,  $\nu(\text{CS})$  and  $\delta(\text{NCS})$  respectively. The CN stretching frequency indicates that the complex is N-bonded rather than S-bonded.

Table 3.13  
Selected IR bands ( $\text{cm}^{-1}$ ) with tentative assignments of copper(II) complexes with ligands HL<sup>1</sup> and HL<sup>2</sup>

Compound	$\nu(\text{C}=\text{N})^+$		$\delta(\text{C}=\text{S})$	$\delta(\text{o.p.})$	$\nu(\text{Cu}-\text{N})$	$\nu(\text{Cu}-\text{S})$	$\nu(\text{Cu}-\text{N})\text{py}$	$\nu(\text{Cu}-\text{X}^{\#})$
	$\nu(\text{N}-\text{H})$	$\nu(\text{N}=\text{C})$						
HL <sup>1</sup>	3049m	1582s	1330 s	808m	638 s	-----	-----	-----
[CuL <sup>1</sup> Cl] (1)	-----	1593s	1289 w	784 m	650 w	409 s	336 w	320 sh
[CuL <sup>1</sup> Br] (2)	-----	1594s	1285 m	780 w	650 w	412 s	325 m	250 w
[CuL <sup>1</sup> (NO <sub>3</sub> )] (3)	-----	1599 m	1278m	789m	632 w	411 s	328 m	310 m
[CuL <sup>1</sup> N <sub>3</sub> ] $\cdot\frac{1}{2}$ H <sub>2</sub> O (4)	-----	1592 s	1278w	784 w	651 w	410 m	334 w	445 sh
[CuL <sup>1</sup> (NCS)] (5)	-----	1593 s	1295m	787 w	650 w	419 m	325 m	318 sh
[Cu <sub>2</sub> L <sub>2</sub> (OH)]ClO <sub>4</sub> \cdot H <sub>2</sub> O (6)	-----	1590 s	1299 m	797 m	620 m	412 w	328 m	310 w
[Cu <sub>2</sub> L <sub>2</sub> Cl <sub>3</sub> ] (7)	-----	1599 m	1278m	789 m	632 w	411 s	328 m	310 m
[Cu <sub>2</sub> L <sub>2</sub> <sup>1</sup> SO <sub>4</sub> ] $\cdot\frac{1}{2}$ 6H <sub>2</sub> O (8)	-----	1593s	1296 m	784 w	650 w	406 s	332 w	303 m
HL <sup>2</sup>	3057	1580s	1360s	793m	644s	-----	-----	-----
[CuL <sup>2</sup> Cl] $\cdot\frac{1.5}{2}$ H <sub>2</sub> O (9)	-----	1592 m	1305 m	781 w	683 w	419 s	325 s	303 m
[CuL <sup>2</sup> Br] <sub>2</sub> (10)	-----	1590 w	1306 m	781 m	692 m	419 s	328 m	245 m
[CuL <sup>2</sup> (NO <sub>3</sub> )]\cdot H <sub>2</sub> O (11)	-----	1594 m	1310 sh	778 w	699 m	406 s	332 sh	315 m
[CuL <sup>2</sup> N <sub>3</sub> ] <sub>2</sub> (12)	-----	1592 w	1308 m	775 m	692 m	416 s	325 m	444 w
[CuL <sup>2</sup> (SH)] <sub>2</sub> \cdot 2H <sub>2</sub> O (13)	-----	1591 w	1315 m	789 m	696 m	412 s	330 w	320 w

s=strong, m= medium, w= weak, All values are reported in  $\text{cm}^{-1}$ , X<sup>#</sup>=Cl, Br, SO<sub>4</sub>, NO<sub>3</sub>, ClO<sub>4</sub>, NO<sub>3</sub>, N<sub>3</sub>, NCS, SH.



**Table. 3.14**  
**IR band assignments ( $\text{cm}^{-1}$ ) for the polyatomic anions in the copper(II) complexes of  $\text{HIL}^1$  and  $\text{HL}^2$**

Compound	Mode of coordination	$\nu_1$	$\nu_2$	$\nu_4$
<b>Nitrato complexes</b>				
$[\text{CuL}^1(\text{NO}_3)]$ (3)	unidentate	1013m	1285s	1384s
$[\text{CuL}^2[\text{NO}_3]] \text{H}_2\text{O}$ (11)	unidentate	1011m	1284s	1385s
<b>Azido complexes</b>				
$[\text{CuL}^1\text{N}_3] \frac{1}{2}\text{H}_2\text{O}$ (4)	unidentate	$\nu_s(\text{NNN})$	$\nu_s(\text{NNN})$	$\delta(\text{NNN})$
$[\text{CuL}^2\text{N}_3]_2$ (12)	unidentate	2042 s	1369 m	650 m
<b>Thiocyanato complex</b>				
$[\text{CuL}^1(\text{NCS})]$ (5)	unidentate	2041 s	1375 m	658 m
<b>Perchlorato complex</b>				
$\text{Cu}_2\text{L}^1_2(\text{OH})\text{ClO}_4 \cdot \text{H}_2\text{O}$ (6)	ionic	$\nu(\text{CN})$ ,	$\nu(\text{CS})$	$\delta(\text{NCS})$
<b>Sulfato complex</b>				
$[\text{Cu}_2\text{L}^2_2\text{SO}_4]_2 \cdot 6\text{H}_2\text{O}$ (8)	chelating bidentate	2081 s	787 m	480 w
		$\nu_1$	$\nu_3$	$\nu_4$
		-----	1090 s	620 m
		$\nu_1$	$\nu_2$	$\nu_3$
		970 w	459	1243 m, 1181 m, 1112 m
				----
				$\nu(\text{Cu-N})_{\text{thiocyanato}}$

It was further supported by the  $\nu(\text{CS})$  frequency at  $787\text{ cm}^{-1}$  and  $\delta(\text{NCS})$  at  $480\text{ cm}^{-1}$ . These values are typical for N-bonded thiocyanate complexes [34]. A medium band at  $325\text{ cm}^{-1}$  corresponds to  $\nu(\text{Cu-N})_{\text{thiocyanato}}$  vibrations which is in agreement with the reported values. [34].

Compounds **1**, **8** and **11** exhibits a sharp band at  $\sim 325\text{ cm}^{-1}$  indicating terminally bonded rather than bridging chlorine. Compounds **2** and **10** show sharp bands around  $\sim 248\text{ cm}^{-1}$  corresponding to  $\nu(\text{Cu-Br})$  vibrations suggestive for terminally bonded bromine [34]. The ratio of  $\nu(\text{Cu-Br})/\nu(\text{Cu-Cl})$  is 0.77 is consistent with the usual values obtained for transition metals.

### 3.3.7. Electronic spectra

The unique feature of first row of transition metals is their ability to form transition metal complexes in which octahedral, tetrahedral, square-coplanar and other stereochemistries predominate. The copper(II) ion is a typical transition metal ion which forms coordination complexes of different stereochemistries, but it is reluctant to take up regular octahedral or tetrahedral stereochemistries. The  $3d^9$  outer electronic configuration of copper(II) ion lacks cubic symmetry and hence it yields other distorted forms of the basic stereochemistries. The copper(II) ion form coordination complexes of the type in which coordination numbers four, five or six predominate. Due to large distortion in bond lengths, the splitting of electronic energy levels in copper(II) ions tends to be larger than other first row transition metals. Thus the electronic properties of copper(II) complexes are relatively sensitive to stereochemistry. Because of the general ease with which copper complexes can be made, there is an extraordinary amount of spectroscopic information available in the literature.

The magnetic and EPR properties are mainly determined by electronic configuration of copper(II) ion in the ground state. The electronic spectra are concerned with energy difference between ground and excited states. A precise knowledge of ground state and excited state is necessary to understand

electronic spectra. The measurement of EPR spectra gives most precise information on the electronic ground state. Hathaway and coworkers studied single crystal spectra of many copper(II) complexes of tetragonal symmetry and assigned numerous *d-d* bands and concluded that the energy order of the *d*-orbital for elongated octahedron and tetragonal pyramid is  $d_{x^2-y^2} > d_z^2 > d_{xy} > d_{xz}, d_{yz}$  [120].

The copper(II) complexes are characterized generally by intense blue or green colors. These colors probably arise from copper-ligand anion charge transfer bands. Solid-state electronic spectra of compounds **1** to **13** were determined in the region 200-900 nm. The electronic spectra of complexes **1**, **6** and **10** are shown in the Figure 3.10. The electronic spectral data are given in Table 3.15. The ligands (HL<sup>1</sup> and HL<sup>2</sup>) have absorption maxima at 36240 and 35100 cm<sup>-1</sup> respectively due to  $\pi^* \leftarrow \pi$  transition between the pyridyl ring and the imine function of thiosemicarbazone moiety. In the spectra of complexes,  $\pi^* \leftarrow \pi$  absorption maxima are observed at approximately same energy. The shift of the  $\pi^* \leftarrow \pi$  bands to the longer wavelength region in complexes is the result of the C=S bond being weakened and conjugation system being enhanced after the formation of the complex [31]. The bands at 29000 and 30864 cm<sup>-1</sup> for HL<sup>1</sup> and 26881 and 30000 cm<sup>-1</sup> for HL<sup>2</sup> corresponds to  $\pi^* \leftarrow n$  transition of the pyridyl nitrogen and these shift to higher energy on complexation. The intensity of  $\pi^* \leftarrow n$  band is diminished considerably in complexes compared to ligand suggesting coordination *via* pyridyl nitrogen.

Two metal-ligand charge transfer bands are found in complexes around 26315 and 23000 cm<sup>-1</sup> of both ligands. The bands in these ranges are in accordance with the previous studies of copper(II) complexes of similar type of ligands [126, 127]. The higher energy bands are assignable to Cu(II) $\leftarrow$ S transition is tailing to the visible region. The intense band in the lower energy region is due to a combination of Cu(II) $\leftarrow$ S and Cu(II) $\leftarrow$ N<sub>pyridyl</sub> LMCT transitions. The steric effect due to N(4) substituent of the thiosemicarbazone

moiety may cause absorption of this band to occur at lower wavelengths [128]. The charge transfer transition may occur from the  $p$  orbital of coordinated ketonic sulfur or nitrogen to the vacant  $d$  orbitals of copper(II).

In many recent books, the stereochemistry of the copper(II) ion is described as being dominated by the four coordinate square planar geometry involving four short in-plane bonds ( $R_s$ ) of *ca.* 2.0 Å. The presence of further ligands along the axial directions, at appreciably longer bond lengths,  $R_L$  (where  $R_L - R_s = 0.6$  Å) is recognized as elongated tetragonal octahedral (4+2 coordination) or square pyramidal (4+1 coordination). Square planar complexes of copper(II) are extensively studied by electronic spectra. For square planar complexes with  $d_{x^2-y^2}$  ground state [27], three transitions are possible  $d_z^2 \leftarrow d_{x^2-y^2}$ ,  $d_{xy} \leftarrow d_{x^2-y^2}$ ,  $d_{yz}$ ,  $d_{xz} \leftarrow d_{x^2-y^2}$  and ( ${}^2A_{1g} \leftarrow {}^2B_{1g}$ ,  ${}^2B_{2g} \leftarrow {}^2B_{1g}$ ,  ${}^2B_{2g} \leftarrow {}^2B_{1g}$ ). Since the four  $d$  orbitals lie very close together, each transition cannot be distinguished by their energy and hence it is very difficult to resolve the three bands into their components. The simplest way to resolve the band into components is by Gaussian analysis. The accuracy of this conventional method is convincing, except for the cases where distinct shoulders are obtained [33].

The  $d-d$  spectral transitions of tetragonal octahedral complexes show some evidence of an intense band at  $16000\text{ cm}^{-1}$ . The energy levels of square co-planar copper(II) complex would be expected to occur at higher energy than those of tetragonal octahedral complex. In  $D_{4h}$  symmetry, transitions at  $19200$  and  $17400\text{ cm}^{-1}$  corresponding to  $d_{xz}$ ,  $d_{yz} \leftarrow d_{x^2-y^2}$  and at  $18400$  and  $17400\text{ cm}^{-1}$  corresponding to  $d_z^2 \leftarrow d_{x^2-y^2}$  appears on the low frequency side. The diffuse reflectance spectrum of square based pyramidal complexes shows a relatively intense maximum at  $14000\text{ cm}^{-1}$ , appreciably lower in energy than bands of tetragonal octahedral complexes. The maximum at  $14000\text{ cm}^{-1}$  has been assigned to  $d_{xz}$ ,  $d_{yz} \leftarrow d_{x^2-y^2}$  transitions. In short, square planar and square pyramidal copper(II) complexes show  $d_{xz}$ ,  $d_{yz} \leftarrow d_{x^2-y^2}$  transition appear at energy greater or less than that for tetragonal octahedral complexes [129]

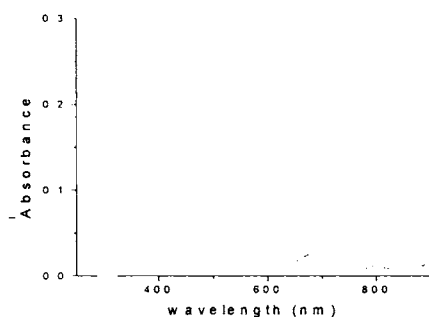
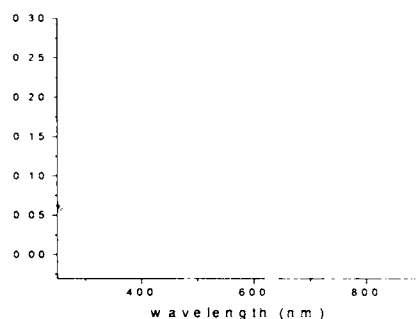
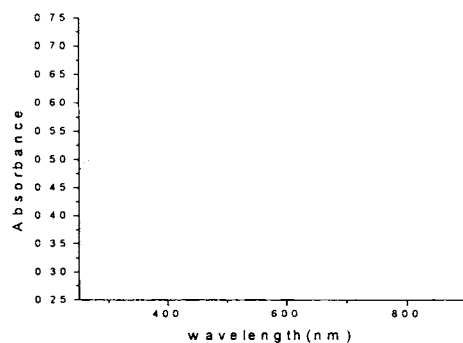
Compound 1 [CuL<sup>1</sup>Cl]Compound 6 [Cu<sub>2</sub>L<sup>1</sup><sub>2</sub>(OH)]ClO<sub>4</sub>·H<sub>2</sub>OCompound 10 [CuL<sup>2</sup>Br]<sub>2</sub>

Figure 3.10. Electronic spectrum of compounds 1, 6 and 10

Electronic spectral data of complexes are presented in Table 3.15. The complexes 5, 6 and 8 show d-d bands that appear as weak shoulders at 16000 cm<sup>-1</sup> corresponding to a square planar geometry [130]. Compounds 1, 2, 3, 4, 7, 9, 10, 11, 12, 13 show shoulders at ~14300 cm<sup>-1</sup> corresponding to  $d_{xz}$ ,  $d_{yz} \leftarrow d_{x^2-y^2}$

**Table 3.15**  
**Solid state electronic spectral data (cm<sup>-1</sup>) for copper(II) complexes with ligands HL<sup>1</sup> and HL<sup>2</sup>**

Compound	d-d	C T	$\pi^* \leftarrow \pi$	$\pi^* \leftarrow \pi$
HL <sup>1</sup>				
[CuL <sup>1</sup> Cl] (1)	17857, 13947.sh	27473, 23475sh, 22573sh,	30864, 29154sh	36231 sh, 35087 sh
[CuL <sup>1</sup> Br] (2)	17094w, 14534 sh	25445 sh, 23310 s,b	32154 s,	32679 sh
[CuL <sup>1</sup> (NO <sub>3</sub> )] (3)	17793, 13263sh	25445 sh, 23584 s.b	32573 s, 31152 sh	34634 sh
[CuL <sup>1</sup> N <sub>3</sub> ] $\cdot\frac{1}{2}$ H <sub>2</sub> O (4)	18050sh, 14471 sh	25641sh, 22883 s,b,	32467 s.b, 31446sh	262,m
[CuL <sup>1</sup> (NCS)] (5)	16000 sh	25380 sh, 23041 s,b,	32573 s.b	
[Cu <sub>2</sub> L <sup>1</sup> <sub>3</sub> (OH)]ClO <sub>4</sub> ·H <sub>2</sub> O (6)	15948,sh	25445 sh, 23584 s.b	31446 s,b	
[Cu <sub>2</sub> L <sup>1</sup> Cl <sub>3</sub> ] (7)	17730, 14347	26246 s, .22624 s,b	31152, 29411	33112 sh
[Cu <sub>2</sub> L <sup>1</sup> SO <sub>4</sub> ] <sub>2</sub> ·6H <sub>2</sub> O (8)	16025,sh	25125 sh,, 23809 s.b	31250 s,	
HL <sup>2</sup>				
[CuL <sup>2</sup> Cl] $\cdot\frac{1.5}{2}$ H <sub>2</sub> O (9)	17636, 14084sh	24814 sh, 23201 s	31645 sh, 31152 sh	37543,s, 32787,sh
[CuL <sup>2</sup> Br] <sub>2</sub> (10)	17699sh, 14556 sh	28169 sh, 23310 sh, 22831 s.b	26882s, 30030 sh	37313,s
[CuL <sup>2</sup> [NO <sub>3</sub> ]] H <sub>2</sub> O (11)	17007 sh, 14104 sh	23095 s,b, 16949	32154 s, 30395 b	37453,s
[CuL <sup>2</sup> N <sub>3</sub> ] <sub>2</sub> (12)	17211 sh, 144450,sh	26882sh, 22676 s,	32467 s, 31648 sh	38314 sh
[CuL <sup>2</sup> (SH)] <sub>2</sub> ·2H <sub>2</sub> O (13)	17482, 13869 sh	2667 sh,, 23202 s,	30487 s,b	

s=strong, b= broad, w= weak

transition suggesting a square pyramidal geometry. A broad band at  $14534\text{ cm}^{-1}$  can also be assigned for chloro and bromo complexes that corresponds to charge transfer spectra due to chloro and bromo ligand to copper(II) [131]. A shoulder at  $16950\text{ cm}^{-1}$  was found for nitrate complex which corresponds to charge transfer of nitrate group to Cu(II) [118]. (Figure 3.10).

From these observations we can come to the conclusion that (i) compounds **1, 2, 3, 4, 7, 9, 10, 11, 12, 13** contain more than one copper center suggesting a 5-coordinate geometry for each copper(II) ion and (ii) compounds **5, 6** and **8** contain copper centers having square-planar geometry with tetragonal distortion. [131].

### 3.3.8. EPR spectral investigations

EPR spectral studies on paramagnetic complexes are an effective tool for determining the stereochemistry of the ligand around the metal ion. Copper(II) complexes are extensively studied using EPR spectroscopy. The spectra of complexes in the powder state at 298 K, in DMF solution at 77 and 298 K were recorded in X- band spectra with 100-kHz field modulation. The  $g$  factors were quoted relative to the standard marker ( $g = 2.00277$ ). Since much information cannot be derived from the spectra recorded, this section is only an effort to study the stereochemistry of copper(II) in complexes in the dimeric or polymeric state. The EPR spectral parameters of complexes in the powder state at 298 K and in DMF solution at 77 K were presented in Table 3.16. The spin Hamiltonian parameters are presented in Table 3.17.

EPR spectral studies are used for predicting the geometrical arrangement of ligand around copper(II) ion. The relation between geometry of copper(II) ion in a complex and EPR spectra were extensively studied by Hathaway and co-workers [31].

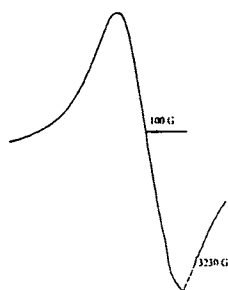
The copper(II) ion with a  $d^9$  configuration, has an effective spin of  $S=3/2$  and is associated with a spin angular momentum  $m_s = \pm 1/2$ , leading to a doubly degenerate spin state in the absence of a magnetic field. In a magnetic field this degeneracy is lifted and the energy difference between these states is given by  $E = h\nu = g\beta H$  where  $h$  is the plank's constant,  $\nu$  is the frequency,  $g$  is the Lande's splitting factor (equal to 2.0023 for a free electron),  $\beta$  is the Bohr magneton and  $H$  is the magnetic field. For a  $3d^9$  copper(II) ion the appropriate Spin Hamiltonian assuming a  $B_{1g}$  ground state is given by [118]

$$\hat{H} = \beta[g_{\parallel}H_zS_z + g_{\perp}(H_xS_x + H_yS_y)] + A_{\parallel}I_zS_z + A_{\perp}[I_xS_x + I_yS_y]$$

### Polycrystalline spectra

Compounds **7**, **11** and **13** give only one broad signal indicating only one  $g$  value ranging from 2.06 to 2.18. The isotropic spectrum is most common for a copper(II) complex containing grossly misaligned tetragonal axes and enhanced

**Compound 7** [ $\text{Cu}_2\text{L}^1\text{Cl}_3$ ]



**Compound 11** [ $\text{CuL}^2(\text{NO}_3)] \cdot \text{H}_2\text{O}$ ]

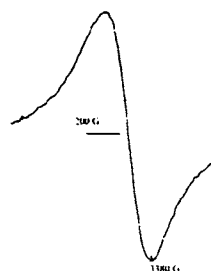


Fig 3.11. EPR spectra of compounds **7** and **12** in the polycrystalline state at 298 K

spin relaxation. This type of spectra gives no information on the electronic ground state of copper(II)ion [132]. (Figure 3.11)



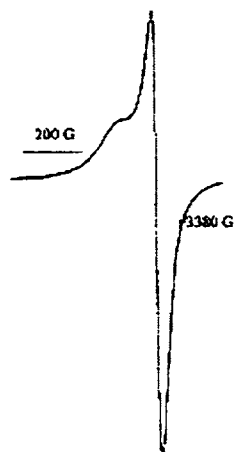
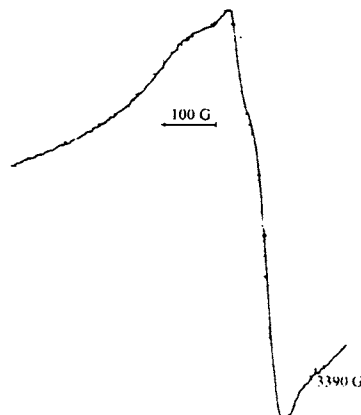
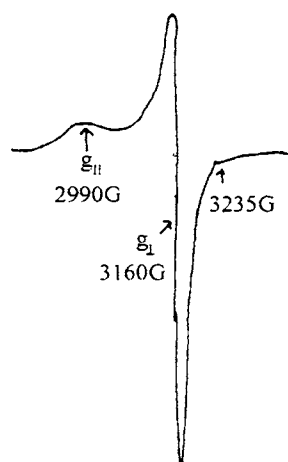
Compound 4  $[\text{CuL}^1\text{N}_3]\cdot\frac{1}{2}\text{H}_2\text{O}$ Compound 8  $[\text{Cu}_2\text{L}_2^1\text{SO}_4]_2\cdot 6\text{H}_2\text{O}$ Compound 9  $[\text{CuL}^2\text{Cl}]\cdot 1.5\text{H}_2\text{O}$ 

Figure 3.12. EPR spectra of compounds 4, 8 and 9 in the polycrystalline state at 298 K

The EPR spectra of the compounds 4, 6, 5, 8, 9, 10 and 12 in the polycrystalline state at 298 K show typical axial behavior with well-defined  $g_{\parallel}$  and  $g_{\perp}$  features (Figure 3.12). The variations in the  $g$  values indicate that the geometry of the compound which is affected by the nature of the coordinating ligands. The geometric parameter  $G$  that is calculated by the relation  $G = (g_{\parallel} - 2)/(g_{\perp} - 2)$  is a measure of the exchange interaction between copper centers in

the polycrystalline compound. If  $G > 4$ , the exchange interaction is negligible and if it is less than 4 exchange interaction is indicated in the complex. All complexes have values  $g_{\parallel} > g_{\perp} > 2$  and  $G$  values falling within this range 3 to 5 are consistent with a  $d_{x^2-y^2}$  ground state corresponding to square planar or square pyramidal geometry.

The spectra of compounds 1, 2 and 3 in the polycrystalline state at 298 K show rhombic features with three  $g$  values  $g_1$ ,  $g_2$  and  $g_3$ , which indicate rhombic distortions in their geometry. The  $g_1$  and  $g_2$  values are very close to each other for compounds 1 and 3, indicating a very small rhombic distortion. Such small distortions can be attributed to large spin lattice relaxation time and small value of spin orbit coupling (Figure 3.13).

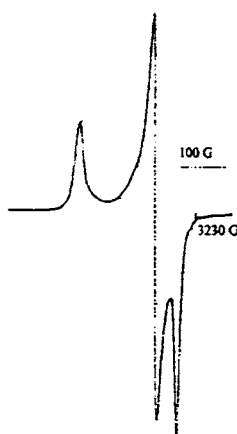


Figure 3.13. EPR spectrum of compound 1 in the polycrystalline state at 298 K

The geometric parameter  $G$  for rhombic systems is calculated by the relation  $G = (g_3 - 2)/(g_{\perp} - 2)$  and  $g_{\perp} = (g_1 + g_2)/2$ . The  $G$  values are found to fall in the range between 3 and 5. For compounds 1 and 3 the lowest  $g$  value ( $g_1$ ) is  $\sim 2.04$  and  $> 2.0448$  respectively indicating a rhombic, square coplanar or distorted square based pyramidal geometries. For the compound 2, the lowest  $g$  value ( $g_1$ ) is  $< 2.04$  indicating a compressed rhombic symmetry with all axes

aligned parallel and is consistent with distorted trigonal bipyramidal stereochemistry or a compressed axial symmetry or rhombic symmetry with slight misalignment of the axes [31]. In the spectra with  $g_1 < g_2 < g_3$ , rhombic spectral parameter  $R = (g_2 - g_1)/(g_3 - g_2)$  may be significant. If  $R > 1$ , a predominant  $d_z^2$  ground state is present and if  $R < 1$ , a predominant  $d_{x^2-y^2}$  ground state is present and when  $R = 1$ , then the ground state is an approximately equal mixture of  $d_z^2$  and  $d_{x^2-y^2}$ , the structure which is intermediate between square planar and trigonal bipyramidal. For the compounds 1, 2 and 3,  $R$  is less than 1 indicating a square planar or distorted square pyramidal geometry with  $d_{x^2-y^2}$  ground state. Absence of half field signals for the compounds reinforced the assumption of very weak super exchange interactions.

#### Solution spectra at 298 K

The solution spectra of all complexes in DMF at 298 K were recorded. All spectra are isotropic in nature with well-resolved hyperfine lines. It is due to the tumbling motion of the molecules in DMF. Spectra of compounds 3, 4, 6, 7, 8, 9, 12, and 13 showed clearly four hyperfine lines with well-resolved peaks ( $^{65}\text{Cu}$ ,  $I = 3/2$ ). This is due to the interaction of electron spin with copper nuclear spin. There are indications of nitrogen hyperfine splittings in the high field component in some spectra [133]. The  $A_0$  and  $g_0$  value shows variation in their values indicating dissimilarity in bonding in the above-mentioned complexes. (Figure 3.14)

#### Solution spectra at 77K

The solution spectra of some of the complexes in DMF at 77 K were presented in the Figure 3.16. However we are unable to get clearly resolved spectra in many cases due to poor glass formation. Some spectra show three well-resolved peaks in the low intensity region and unresolved peaks are obtained in the high field region.

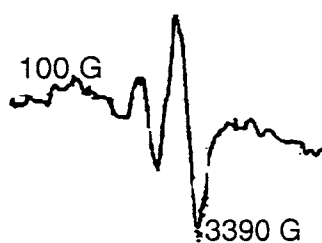
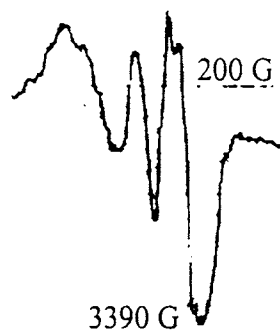
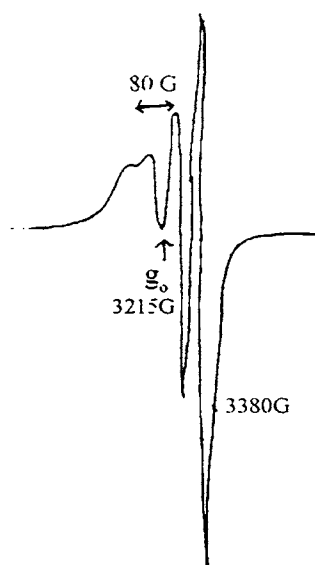
Compound 4  $[\text{CuL}^1\text{N}_3]\cdot\frac{1}{2}\text{H}_2\text{O}$ Compound 9  $[\text{CuL}^2\text{Cl}]\cdot 1.5 \text{H}_2\text{O}$ Compound 3  $[\text{CuL}^1(\text{NO}_3)]$ 

Figure 3.14. EPR spectra of 3, 4 and 9 in in DMF at 298 K

The  $g_{\parallel}$ ,  $g_{\perp}$ ,  $A_{\parallel}$ ,  $A_{\perp}$  values are calculated from the spectra and confirmed by the following equation:

$$g_{\perp} = (3g_0 - g_{\parallel})/2 \text{ and } A_{\perp} = (3A_0 - A_{\parallel})/2$$

In DMF solution the  $g$  values are altered indicating that partial substitution for the gegenions does occur, or that the solvent expands the coordination sphere as often happens with copper(II) complexes [15]. In the parallel region, three of the four hyperfine lines are moderately resolved while perpendicular features overlap with the fourth one. From the analysis of the parallel part of the spectra, the line width of the  $M_I = -3/2$ , component is small compared with the nitrogen coupling constants, leading to the appearance of nitrogen superhyperfine splitting pattern. The splitting in the perpendicular region of the spectra can be attributed to interaction of an unpaired electron spin with the copper nuclear spin and two  $^{14}\text{N}$  ( $I = 1$ ) donor nuclei. The smaller  $g_{\parallel}$  values for the complexes indicate delocalisation of the unpaired electron density away from the copper nucleus and may be interpreted in terms of increased covalency of the M-L bond.

EPR spectra of the complex **6**, and **8**, and **13** (Figure 3.15) show some axial behavior with four well-resolved hyperfine lines in the  $g_{\parallel}$  features ( $M_I = -3/2$  or  $M_I = 1/2$ ). The  $g_{\parallel} > g_{\perp}$  value suggests a distorted square pyramidal or tetragonal geometry (Figure 3.15). The superhyperfine lines are not clearly resolved. The similarity of  $g_{\parallel}$  values indicates that the bonding is dominated by the thiosemicarbazone moiety rather than the nature of the gegenion. Kivelson and Neiman [134] have reported that  $g_{\parallel}$  values less than 2.3 indicate considerable covalent character to M-L bonds and greater than 2.3 indicate ionic character. The  $g_{\parallel}$  values of the complexes are found to be less than 2.3, which indicate considerable covalent character to the M-L bonds. The relation calculates the geometric parameter  $G$  that is a measure of the exchange interaction between copper centers in the polycrystalline compound is  $G = (g_{\parallel} - 2.0032)/(g_{\perp} - 2.0032)$ . The  $G$  values are falling in the range 3 to 5 indicating a square planar or square pyramidal geometry.

The complexes **1**, **2**, **3**, **4**, **7**, **9**, **11**, and **12** in DMF at 77 K, show rhombic feature with three  $g$  values  $g_1$ ,  $g_2$ , and  $g_3$  where  $g_3 > g_2 > g_1$  (Figure 3.15).

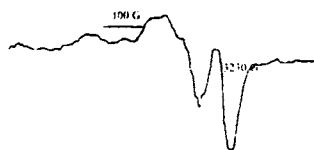
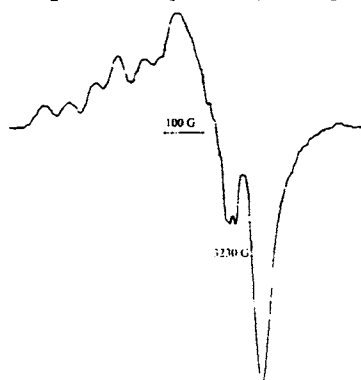
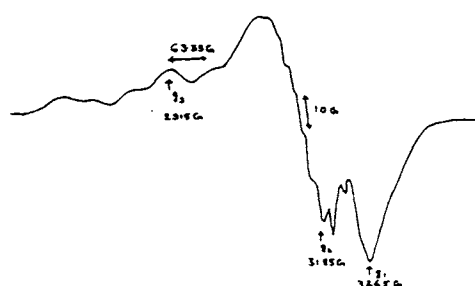
Compound 8  $[\text{Cu}_2\text{L}_2^1\text{SO}_4]_2 \cdot 6\text{H}_2\text{O}$ Compound 13  $[\text{CuL}^2(\text{SH})]_2 \cdot 2\text{H}_2\text{O}$ Compound 3  $[\text{CuL}^1(\text{NO}_3)]$ Compound 9  $[\text{CuL}^2\text{Cl}] \cdot 1.5 \text{H}_2\text{O}$ 

Figure 3.15. EPR spectra of compound 4, 8, 9 and 13 in DMF at 77

It is observed that the  $g$  values for complexes in the solid state at 298 K and in DMF at 77 K are not varying much from each other, hence the geometry around the copper(II) ion is unaffected on cooling the solution to liquid nitrogen temperature. For the compounds 2, 3, 4, 9, 11 and 12, the lowest  $g$  value ( $g_1$ ) is  $< 2.04$  indicating a compressed rhombic symmetry with all axes aligned parallel and is consistent with distorted trigonal bipyramidal stereochemistry or a compressed axial symmetry or rhombic symmetry with slight misalignment of the axes. In the spectra with  $g_1 < g_2 < g_3$ , rhombic spectral values  $R = (g_2 - g_1) / (g_3 - g_2)$  may be significant. If  $R > 1$ , a predominant  $d_{z^2}$  ground state is present. If  $R < 1$ , a predominant  $d_{x^2-y^2}$  ground state is present and when  $R = 1$ , then the ground state is an approximately equal mixture of  $d_{z^2}$  and  $d_{x^2-y^2}$ , the structure is

Table. 3.16.  
EPR spectral assignments (experimental) for the copper(II) complexes with ligands HL<sup>1</sup> and HL<sup>2</sup>

Compound	Solid (298 K)			DMF(298 K)			DMF (77 K)			
	$g_{\parallel}, g_{\perp}, g_3$	$g_{\perp}, g_{\parallel}, g_2$	$A_N$	$g_{\parallel}, g_{\perp}, g_3$	$A_0/gA_{iso}$	$A_N$	$g_{\parallel}, g_{\perp}, g_3$	$g_{av}$	$*A_{\parallel}$	$*A_{\perp}(N)$
[CuL <sup>1</sup> Cl] (1)	$g_{\parallel} 2.1817$ $g_2 2.0569$ $g_1 2.0375$	$g_{\perp} 2.06346$ $g_1 2.0311$	----	----	----	----	$g_{\parallel} 2.1817$ $g_3 2.1659$	2.0921	----	----
[CuL <sup>1</sup> Br] (2)	$g_{\parallel} 2.1638$	$g_2 2.0603$ $g_1 2.0280$	----	----	----	----	$g_2 2.0734$ $g_1 2.0279$	2.0890	-----	-----
[CuL <sup>1</sup> (NO <sub>3</sub> )] (3)	$g_{\parallel} 2.1825$	$g_2 2.0697$ $g_1 2.0448$	20	80	20	20	$g_2 2.0664$ $g_1 1.9869$	2.0991	65.83	16.66
[CuL <sup>1</sup> N <sub>3</sub> ] ½H <sub>2</sub> O (4)	$g_{\parallel} 2.1668$	$g_{\perp} 2.0503$	----	81.66	----	----	$g_2 2.0454$ $g_1 1.9717$	2.0680	75	----
[CuL <sup>1</sup> (NCS)] (5)	$g_{\parallel} 2.1688$	$g_{\perp} 2.0517$	----	----	----	----	2.1707	2.0926	183.33	15.83
[Cu <sub>2</sub> L <sup>1</sup> (OH)]ClO <sub>4</sub> ·H <sub>2</sub> O (6)	$g_{\parallel} 2.2976$	$g_{\perp} 2.0955$	25	91.66	25	25	2.1379	2.0765	136	----
Cu <sub>2</sub> L <sup>1</sup> Cl <sub>3</sub> (7)	$g_0 2.1871$	-----	---	53	---	---	$g_3 2.792$	2.0885	190	16.7
[Cu <sub>2</sub> L <sup>2</sup> SO <sub>4</sub> ] <sub>2</sub> ·6H <sub>2</sub> O (8)	$g_{\parallel} 2.1554$	$g_{\perp} 2.0636$	----	53.33	----	----	2.1817	2.0941	63.33	11.66
[CuL <sup>2</sup> Cl]·1.5 H <sub>2</sub> O (9)	$g_{\parallel} 2.1422$	$g_{\perp} 2.0576$	15	43.33	15	15	2.2224	2.1213	175	22
[CuL <sup>2</sup> Br] <sub>2</sub> (10)	$g_{\parallel} 2.1349$	$g_{\perp} 2.0602$	----	----	----	----	$g_{\parallel} 2.1349$	2.0851	----	----
[CuL <sup>2</sup> [NO <sub>3</sub> ]] H <sub>2</sub> O (11)	$g_0 2.0638$	-----	----	----	----	----	2.1961	2.0820	175	22
[CuL <sup>2</sup> N <sub>3</sub> ] <sub>2</sub> (12)	$g_{\parallel} 2.1484$	2.0384-	20	48.33	20	20	$g_3 2.1816$	2.0675	----	----
[CuL <sup>2</sup> (SH)] <sub>2</sub> ·2H <sub>2</sub> O (13)	$g_0 2.0858$	-----	17.5	60	17.5	17.5	2.1721	2.0714	178.33	20

\* A value  $\times 10^{-1} \text{ cm}^{-1}$

intermediate between square planar and trigonal bipyramidal geometries. For the complexes having values  $R < 1$  suggests a distorted square base pyramidal geometry with a  $d_{x^2-y^2}$  ground state. These observations are consistent with  $g$  values of the corresponding complexes in the polycrystalline state at 298 K further supports a distorted square pyramidal geometry for copper(II) ion in these complexes.

The EPR spectral parameters were obtained by computer simulation of the spectrum. As the experimental spectrum is not responding to EPR sensitively, we have made an effort to evaluate other magnetic parameters by computer simulation of the spectrum. Spectra of complexes were simulated to get accurate values of the magnetic parameters Figures (3.16-3.17). The EPR parameters  $g_{\parallel}$ ,  $g_{\perp}$ ,  $g_{av}$ ,  $A_{\parallel}(\text{Cu})$ ,  $A_{\perp}(\text{Cu})$  and energies of  $d-d$  transitions were used to evaluate the bonding parameters  $\alpha^2$ ,  $\beta^2$  and  $\gamma^2$  which may be regarded as a measure of covalency of the in-plane  $\sigma$  bonds, in-plane  $\pi$  bonds and out-of-plane  $\pi$  bonds respectively. The value of in-plane  $\sigma$  bonding parameter can be estimated from the expression [134, 135].

$$\alpha^2 = -(A_{\parallel}/0.036) + (g_{\parallel}-2.0023) + 3/7(g_{\perp}-2.0023) + 0.04$$

If  $\alpha^2 = 1$  the M-L in-plane  $\sigma$  bond is completely ionic and 0.5, it is completely covalent. For the complexes, 6, 7, 8, and 13 the  $\alpha^2$  values are less than 1 suggesting significant M-L covalent bond character. The in-plane  $\pi$  bonding parameter  $\beta^2$ , values ranges between 0.79 to 0.9 or close to unity and out of plane  $\pi$  bonding parameter  $\gamma^2$ , values ranges between 0.0.83 to 0.93, showing appreciable out-of-plane  $\pi$  bonding.

The orbital reduction factors  $K_{\parallel} = \alpha^2 \beta^2$  and  $K_{\perp} = \alpha^2 \gamma^2$  were calculated using the following expressions [32, 133]

$$K_{\parallel}^2 = (g_{\parallel} - 2.0023) \cdot \Delta E_{d-d} / 8\lambda_0$$

$$K_{\perp}^2 = (g_{\perp} - 2.0023) \cdot \Delta E_{d-d} / 2\lambda_0$$



where  $\lambda_0$  is the spin orbit coupling and is the value  $-828 \text{ cm}^{-1}$  for a copper(II)  $d^9$  system.

According to Hathaway [136] for pure  $\sigma$  bonding  $K_{\parallel} = K_{\perp} = 0.77$ , for in-plane bonding  $K_{\parallel} < K_{\perp}$ , while for out-of-plane bonding  $K_{\parallel} > K_{\perp}$ . It is seen that for complexes **3**, **9**, and **11**,  $K_{\parallel} > K_{\perp}$  indicating stronger out-of plane  $\pi$  bonding. For compounds **1**, **2**, **4**, **6**, **7**, **8** and **13**,  $K_{\parallel} < K_{\perp}$  suggesting a stronger in-plane  $\pi$  bonding

The tendency of  $A_{\parallel}$  to decrease with an increase of  $g_{\parallel}$  is an index of tetragonal distortion of coordination sphere of copper.[137]. The trend for  $A_{iso}$  is the same as that of  $A_{\parallel}$ . Moving from planar to a more distorted complex, a decrease of  $A_{iso}$  is apparent. The empirical factor  $f = g_{\parallel} / A_{\parallel}(\text{cm})$  is an index of tetragonal distortion. The value may vary from 105 to 135 for square planar complexes. In presence of tetragonally distorted structures the values can be much higher. It is seen that for compounds **1**, **2**, **3**, **4**, **7**, and **9** the  $f$  values are much higher which indicate distortion from planarity. Medium distortion is observed in complexes **6**, **8**, **11**, **13** where the  $f$  value is at *ca* 125.

The Fermi contact interaction term which is a measure of contribution of the  $s$  electrons to the hyperfine interaction, can be estimated from the following expression:

$$K_0 = A_{iso}/P\beta^2 + (g_{av} - 2.0023)/\beta^2$$

This is a dimensionless quantity and generally found to have a value 0.3. The values calculated are in the range 0.3 for all complexes (Table 3.16).

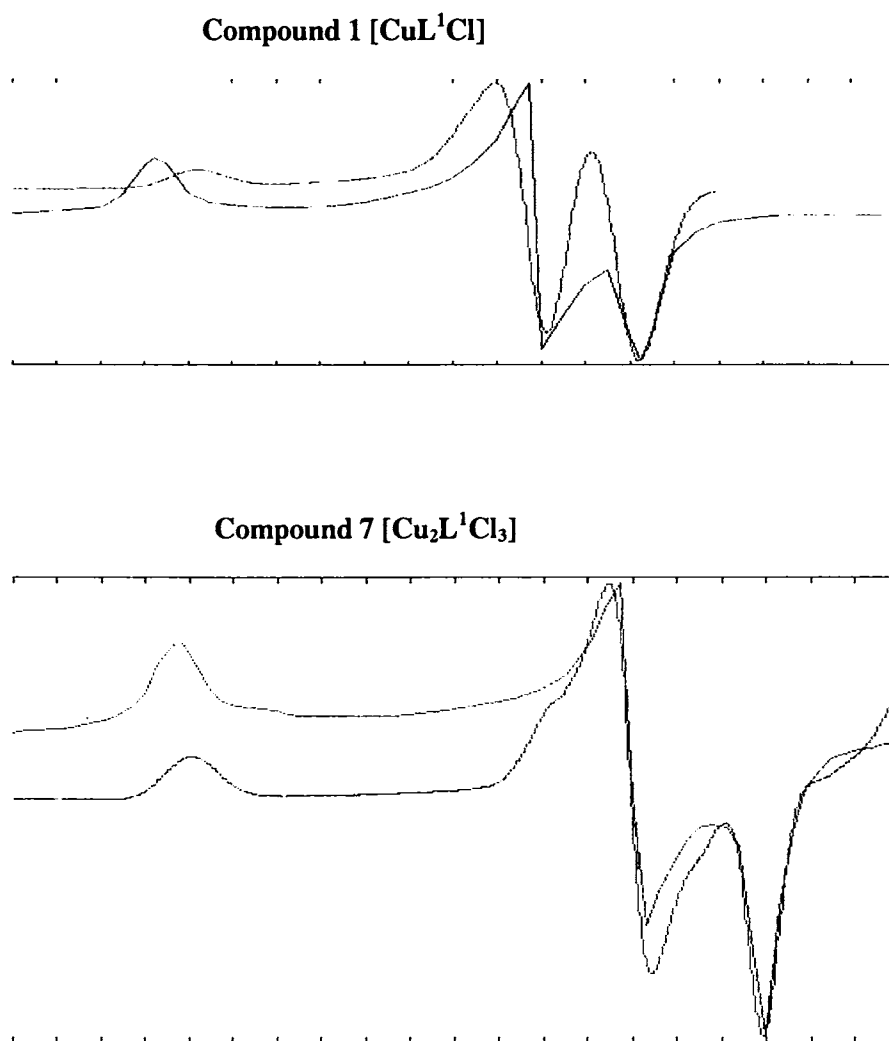


Figure 3.16. Experimental (green) and simulated( red) best fit pairs of the EPR spectrum of the compound 1 and 7 in DMF at 77 K.

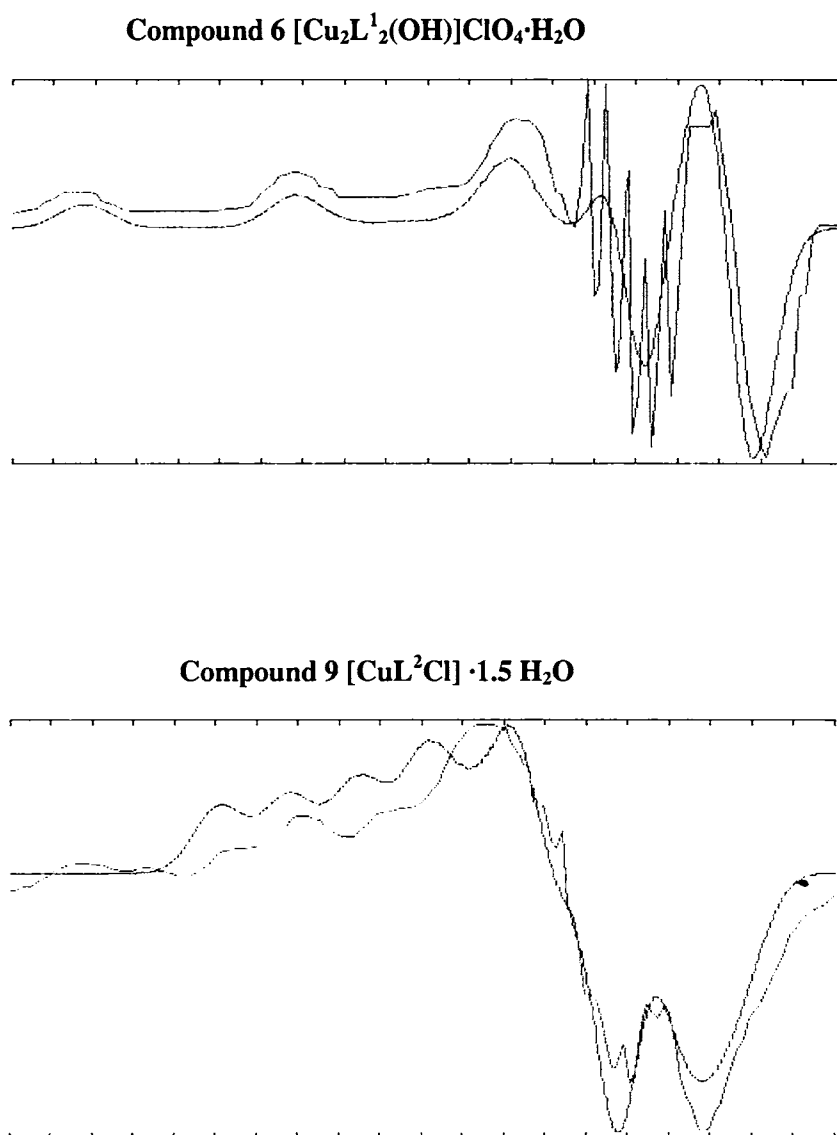


Figure 3.17. Experimental (green) and simulated (red) best fit pairs of the EPR spectrum of the compound **6** and **9** in DMF at 77 K.

The EPR spectra of compounds **5**, **10** and **12** are not fully resolved due to poor glass formation and hence we were not able to simulate spectra of the respective compounds. Also bonding parameters of compounds **1**, **2**, **3**, **4**, **7** and

Table 3.17. Spin Hamiltonian and orbital reduction parameters of copper(II) complexes with ligands HL<sup>1</sup> and HL<sup>2</sup>

Compound	1	2	3	4	6	7	8	9	11	13
$g_{\parallel}/g_{\perp}$ ( $g_3$ )	2.2200	2.2180	2.2180	2.1426	2.1563	2.1325	2.2002	2.2125	2.1920	2.1721
$g_{yy}$ ( $g_2$ )	2.0690	2.0812	2.0774	2.0558	2.0416	2.0775	2.0556	2.0525	2.0581	2.0475
$g_{xx}$ ( $g_1$ )	2.0680	2.0291	1.9973	1.9873	2.0416	2.0408	2.0556	1.9878	2.0450	2.0475
$g_{av}(77k)$	2.1190	2.1094	2.0976	2.0620	2.0798	2.0836	2.1038	2.0843	2.0984	2.0890
$g_{av}$ (solid)	2.0920	2.0855	2.0990	2.0891	2.1628	2.1871	2.0942	2.0858	2.0638	2.0858
$A_{\parallel}/A_{\perp}$ ( $a$ )	135.5	135.5-	70.83	120*	166.6	140.5	180	63.33-	178.90	178.33
$A_{yy}^a$	15	18	17.50	7	15.75	18	14	19.17	17.55	15
$A_{xx}^a$	18	35	10.85	12	15.75	15	14	17.98	16.33	15
$G$ (77K)	-----	-----	-----	-----	3.9	-----	3.7	-----	-----	3.62
$G$ (solid)	4.	3.85	3.27	3.4	3.16	-----	2.49	2.53	-----	-----
$R^c$	0.2736	0.381	0.570	0.7890	---	0.667	---	0.404	0.98	---
$\alpha^2$	---	---	---	---	0.6736	---	0.7609	---	---	0.7314
$\beta^2$	---	---	---	---	0.9039	---	0.9071	---	---	0.8152
$\gamma^2$	---	---	---	---	0.9133	---	0.9438	---	---	0.8411
$K_{\parallel}$	0.6770	0.6879	0.6660	0.5536	0.6089	0.5310	0.6902	0.6686	0.6357	0.5963
$K_{\perp}$	0.7495	0.89321	0.6178	0.6873	0.6152	0.8071	0.7182	0.6534	0.6030	0.6152
$K_0$	-----	-----	-----	-----	0.3330	-----	0.2531	-----	-----	0.2992
$f^b$ (cm)	158	157	301	177	128	152	119	338	119	120

<sup>a</sup> expressed in units of cm<sup>-1</sup> multiplied by a factor of 10<sup>-4</sup>, <sup>b</sup> parameter  $f = g_{\parallel}A_{\parallel}/g_{\perp}A_{\perp}$ , parameter  $R = (g_2 - g_1)/(g_3 - g_2)$

are not agreeing with usual values for square planar compounds indicating rhombic distortion.

### 3.4. Concluding remarks

The chapter deals with the syntheses and spectral characterization of copper(II) complexes of ligands HL<sup>1</sup> and HL<sup>2</sup>. All complexes were found to sparingly soluble in solvents like DMF, DMSO, chloroform, and acetone. The solubility relatively increases relatively in mixture of solvents. This indicates that complexes are not monomers. We isolated single crystals of complexes [Cu<sub>2</sub>L<sub>2</sub><sup>1</sup>(SO<sub>4</sub>)<sub>2</sub>·6H<sub>2</sub>O (**8**), [CuL<sup>2</sup>Br]<sub>2</sub> (**10**), [CuL<sup>2</sup>(N<sub>3</sub>)<sub>2</sub>] (**12**) and [CuL<sup>2</sup>(SH)]<sub>2</sub>·2H<sub>2</sub>O (**13**). X-ray analyses of the compounds **10** and **12** and **13** reveal that they are dimers with square pyramidal geometry around copper(II) ion. The compound **8** is tetrameric with square planar and square pyramidal geometries around the copper centers.. Magnetic susceptibility measurements show that complexes are paramagnetic except [CuL<sup>2</sup>Cl] which is diamagnetic reveals its dimeric nature. Electronic spectral studies also give some insight regarding the stereochemistry of complexes. Since the EPR spectra of complexes are not well resolved, we cannot explain fully the structure according to the reported studies of Hathaway and co-workers.

**SYNTHESES, STRUCTURAL AND SPECTRAL  
CHARACTERIZATION OF NICKEL(II) COMPLEXES OF  
DI-2-PYRIDYL KETONE 3-TETRAMETHYLENIMINYL  
THIOSEMICARBAZONE**

---

#### **4.1. Introduction**

Nickel is a moderately abundant element and is produced in large quantities. It is predominantly divalent and exists as nickel(II) in most of its complexes. Nickel(II) complexes are usually square planar in geometry. Complexes with octahedral geometry are also reported [138, 139]. Complexes of nickel(II) are generally diamagnetic and some paramagnetic compounds are also reported. [140]. The investigation of metal complexes with sulfur containing Schiff bases is a subject of current interest and it has been shown that many of them present anticancer activity [5]. Metal complexes with first row of transition metals containing thiosemicarbazone moieties as ligands have shown a wide range of biological properties [5-7]. It has been shown that NNS tridentate system is present in most of the thiosemicarbazones with carcinostatic potency [6].

This chapter deals with the syntheses, spectral and structural studies of nickel(II) complexes of a potential tetradentate ligand, di-2-pyridyl ketone 3-tetramethyleneiminyl thiosemicarbazone ( $HL^1$ ). An interesting aspect is that the ligand  $HL^1$ , though contains four potential donor atoms, it behaves in a tridentate manner in all of its nickel(II) complexes under study, since only one of the pyridyl nitrogens is coordinated to the metal.

## 4.2. Experimental

### 4.2.1. Materials and methods

Ligand HL<sup>1</sup> was synthesized by the methods as described in Chapter 2. Following materials and solvents were used. Nickel(II) chloride hexahydrate (Merck), nickel(II) acetate tetrahydrate (Merck), sodium azide, and potassium thiocyanate are used without any prior purification. The complexes were prepared in ethanol solvent. Solvent: Ethanol (99%) purified before use by reported methods.

### 4.2.2. Physical measurements

Details regarding physical measurements are presented in Chapter 3. <sup>1</sup>H NMR spectra of complexes were recorded in an AMX 400 MHz FT-NMR Spectrometer using CDCl<sub>3</sub> as solvent and TMS as the internal standard at Sophisticated Instruments Facility, Indian Institute of Science, Bangalore, India.

### 4.2.3. Syntheses of complexes

#### 4.2.3.1. Synthesis of [NiL<sup>1</sup>Cl]·½ H<sub>2</sub>O

A solution of the ligand HL<sup>1</sup> (0.311 g, 1 mmol) in 20 ml of hot ethanol was treated with an ethanolic solution of NiCl<sub>2</sub>·6H<sub>2</sub>O (0.237 g, 1 mmol). The solution was heated under reflux for 2 hours. The resulting solution was allowed to stand at room temperature and after slow evaporation, dark brown crystals of compound separated out [141], which were collected, washed with water, followed by ether and dried over P<sub>4</sub>O<sub>10</sub> *in vacuo*.

#### 4.2.3.2. Synthesis of [NiL<sup>1</sup>N<sub>3</sub>]·½ H<sub>2</sub>O

A solution of the ligand HL<sup>1</sup> (0.311 g, 1 mmol) in 20 ml of hot ethanol was treated with an ethanolic solution of Ni(OAc)<sub>2</sub>·4H<sub>2</sub>O (0.248 g, 1 mmol). The solution was heated under reflux and sodium azide (0.065 g, 1 mmol) was

added in portions to the solution and further refluxed for two hours. The resulting solution was allowed to stand at room temperature for few days and upon slow evaporation gave dark brown crystals of the compound [141]. The crystals separated out were collected, washed with water, followed by ether and dried over  $P_4O_{10}$  *in vacuo*.

#### 4.2.3.3. Synthesis of $[NiL^1(SCN)]$

A solution of the ligand  $HL^1$  (0.311 g, 1 mmol) in 20 ml of hot ethanol was treated with an ethanolic solution of  $Ni(OAc)_2 \cdot 4H_2O$  (0.248 g, 1 mmol). The solution was heated under reflux and an ethanolic solution of potassium thiocyanate (0.097 g, 1 mmol) was added to the mixture and further refluxed for 2 hours. The resulting solution was allowed to stand at room temperature. On slow evaporation at room temperature, dark brown crystals of the compound [141] separated out, which were collected, washed with water, followed by ether and dried over  $P_4O_{10}$  *in vacuo*.

Three nickel(II) complexes were prepared using  $HL^1$  and elemental analyses agrees with the proposed empirical formula  $[NiL^1X]$  where  $X = Cl$  (14),  $N_3$  (15),  $SCN$  (16)

#### 4.2.4. X-ray crystallography

Single crystals of compound  $[NiL^1Cl]$  (14) for X-ray analysis were grown by slow evaporation of the complex in methanol. Dark brown triclinic crystal of the compound having approximate dimensions 0.30 X 0.25 X 0.20  $mm^3$  was mounted on a glass fiber using epoxy cement. The X-ray diffraction data were measured in frames with increasing  $\omega$  (width of 0.3°/frame) at room temperature (293 K) using a Bruker SMART APEX CCD diffractometer, equipped with a fine focus sealed tube X-ray source. Selected crystal data and data collection parameters are given in Table 4.2. The intensity data were collected within the range of  $1.49^\circ < \theta < 27.88^\circ$  for  $hkl$  ( $-6 \leq h \leq 6$ ,  $-14 \leq k \leq 14$ ,



$-18 \leq l \leq 17$ ) in a triclinic system. About 3551 unique reflections were collected. The SMART software was used for data acquisition and the SAINT software for data extraction [70]. Empirical absorption corrections were made on the intensity data. The structure was solved by the heavy atom method and refined by full-matrix least squares using the SHELX system of programs [73] and the graphics tool was PLATON for windows [74]. All non-hydrogen atoms of the complex were refined anisotropically. Few hydrogen atoms were located from the difference Fourier map, and the rest were generated, assigned isotropic thermal parameters, and refined using a riding model. The hydrogen atoms were used for structure factor calculation only. The structure refinement gave goodness-of-fit (GOF) value of 1.114 with the maximum shift/esd value of 0.001. A dark brown crystal of the compound  $[\text{NiL}^1\text{N}_3]$  (**15**) was analyzed in a similar manner and the crystallographic data along with structural refinements are also given in Table 4.2.

### 4.3. Results and discussion

#### 4.3.1. Analytical data

Colors, partial elemental analyses and stoichiometries of ligand  $\text{HL}^1$  and its nickel(II) complexes are presented in Table 4.1. Partial elemental data (C, H, N) for all the complexes are consistent with the 1:1:1 molar ratio of the metal: thiosemicarbazone: gegenion. All complexes are brown, which is common to the complexes involving thiosemicarbazone coordination, resulting from the sulfur to metal charge transfer bands [108, 109]. Conductivity measurements in  $10^{-3}$  DMF solution indicate that all complexes are non-electrolytes in this solution [129]. The non-electrolytic nature of complexes indicates that the ligand, which behaves as a uninegative ion, coordinates to nickel(II) along with the chloro, azido and thiocyanato ions giving the formula  $[\text{NiLX}]$  (where X = Cl,  $\text{N}_3$  and NCS).

Table 4.1

Colors, partial elemental analyses and molar conductivities of Ni(II) complexes with ligand HL<sup>1</sup>

Compound	Empirical formula	Color	Composition% (Found/Calcd)			$\lambda_M^a$
			Carbon	Hydrogen	Nitrogen	
HL <sup>1</sup>	C <sub>16</sub> H <sub>17</sub> N <sub>5</sub> S	yellow	62.10 (61.71)	5.56 (5.50)	22.43 (22.49)	
[NiL <sup>1</sup> Cl] <sup>1</sup> ·½H <sub>2</sub> O ( <b>14</b> )	C <sub>16</sub> H <sub>17</sub> N <sub>5</sub> ClNiO <sub>0.5</sub> S	Brown	46.64 (46.47)	3.98 (4.14)	16.81 (16.93)	16
[NiL <sup>1</sup> N <sub>3</sub> ] <sup>1</sup> ·½H <sub>2</sub> O ( <b>15</b> )	C <sub>16</sub> H <sub>17</sub> N <sub>8</sub> NiO <sub>0.5</sub> S	Brown	45.81 (45.74)	3.98 (4.08)	26.29 (26.67)	8
[NiL <sup>1</sup> SCN] <sup>1</sup> ·½H <sub>2</sub> O ( <b>16</b> )	C <sub>17</sub> H <sub>16</sub> N <sub>6</sub> NiS <sub>2</sub>	Brown	46.75 (46.81)	3.72 (3.93)	19.00 (19.27)	13

<sup>a</sup> Molar conductivity, 10<sup>-3</sup> M DMF at 298 K

**Table 4.2****Crystal data and structure refinement for [NiL<sup>1</sup>Cl] and [NiL<sup>1</sup>N<sub>3</sub>]**

Parameters	[NiLCl]	[NiLN <sub>3</sub> ]
Empirical Formula	C <sub>16</sub> H <sub>16</sub> ClN <sub>5</sub> NiS	C <sub>16</sub> H <sub>16</sub> N <sub>8</sub> NiS
Formula weight (M)	404.56	411.14
Temperature (T) K	293(2)	293(2)
Wavelength (Mo K $\alpha$ ) (Å)	0.71073	0.71073
Crystal system	Triclinic	Orthorhombic
Space group	<i>P</i> $\bar{1}$	<i>Pbca</i>
Lattice constants <i>a</i> (Å)	5.3295(12)	14.483(3)
<i>b</i> (Å)	11.390(3)	11.962(2)
<i>c</i> (Å)	13.930(3)	20.344(4)
$\alpha$ (°)	99.721(4)	90
$\beta$ (°)	91.871(4)	90
$\gamma$ (°)	98.720(4)	90
Volume V (Å <sup>3</sup> )	822.3(3)	3524.5(12)
Z	2	8
Calculated density ( $\rho$ ) (Mg m <sup>-3</sup> )	1.634	1.550
Absorption coefficient ( $\mu$ ) (mm <sup>-1</sup> )	1.477	1.238
<i>F</i> (000)	416	1696
Crystal size (mm)	0.30 x 0.25 x 0.20	0.30 x 0.25 x 0.20
$\theta$ Range for data collection	1.49 - 27.88	2.00 - 26.04
Limiting Indices	-6 $\leq h \leq$ 6, -14 $\leq k \leq$ 14, -18 $\leq l \leq$ 17	-17 $\leq h \leq$ 17, -14 $\leq k \leq$ 14, -25 $\leq l \leq$ 25
Reflections collected	9069	2598
Unique Reflections	3551 [ <i>R</i> <sub>int</sub> = 0.0266]	3470 [ <i>R</i> <sub>int</sub> = 0.0227]
Completeness to $\theta$	27.88 (91.1 %)	26.04 (99.9 %)
Absorption correction	None	None
Max. and min. transmission	0.7566 and 0.6657	0.7899 and 0.7078
Refinement method	Full-matrix least-squares on <i>F</i> <sup>2</sup>	Full-matrix least-squares on <i>F</i> <sup>2</sup>
Data / restraints / parameters	3551/0/281	3470/0/299
Goodness-of-fit on <i>F</i> <sup>2</sup>	1.114	1.079
Final <i>R</i> indices [ <i>I</i> > 2 $\sigma$ ( <i>I</i> )]	<i>R</i> <sub>1</sub> = 0.0413, <i>wR</i> <sub>2</sub> = 0.0949	<i>R</i> <sub>1</sub> = 0.0258, <i>wR</i> <sub>2</sub> = 0.0657
<i>R</i> indices (all data)	<i>R</i> <sub>1</sub> = 0.0488, <i>wR</i> <sub>2</sub> = 0.0983	<i>R</i> <sub>1</sub> = 0.0310, <i>wR</i> <sub>2</sub> = 0.0688
Largest difference peak and hole (e Å <sup>-3</sup> )	0.455 and -0.189	0.276 and -0.166

### 4.3.2. Molecular and crystal structures of $[\text{NiL}^1\text{Cl}]$ and $[\text{NiL}^1\text{N}_3]$

The structures of  $[\text{NiL}^1\text{Cl}]$  (**14**) and  $[\text{NiL}^1\text{N}_3]$  (**15**) along with the atomic labeling are shown in Figures 4.1 and 4.2 respectively and selected bond lengths and bond angles are summarized in Table 4.3. The ligand is an NNS tridentate ligating system, coordinating *via* its pyridine nitrogen, azomethine nitrogen and the thiolate sulphur atom giving a distorted square planar geometry around nickel atom. The configuration of the thiosemicarbazone chain about C(6)-N(3) bond is *Z* which facilitate the coordination of thiolate sulphur to Ni(II) in both the complexes. The Ni(II) coordination is almost square planar in compound **14** with a maximum value for mean deviation for pyridine N(1), imino N(3), and thiolate S(1) and chloride Cl(1) atoms from their own plane of 0.0447 Å. Compared to this greater square planar deviation is observed in **15** as evident from the maximum mean deviation of 0.2042 Å for the plane constituted by N(1), N(3), S(1) and N(6). The bond angles, S(1)-Ni(1)-N(3) (87.32°) and Cl(1)-Ni(1)-N(1) (96.99°) of  $[\text{NiLCl}]$  (**14**) and N(3)-Ni(1)-N(2) (83.54°) and S(1)-Ni(1)-N(6) (95.40°) of  $[\text{NiL}(\text{N}_3)]$  (**15**) reveal the distortion of the square planes comprising of Ni(1), Cl(1), N(1), N(3) and S(1) atoms in compound **14** and Ni(1), N(2), N(3), N(6) and S(1) in compound **15** respectively. The bond angles Ni(1)-N(3)-C(6) (116.68°) and Ni(1)-N(1)-C(5) (112.16°) in compound **14** and Ni(1)-N(3)-C(6) (117.11°) and Ni(1)-N(2)-C(7) (112.97°) in compound **15** are almost identical. Similarly, the bond angles N(1)-Ni(1)-Cl(1) (96.99°); N(3)-Ni(1)-S(1) (87.00°) in compound **14** and N(2)-Ni(1)-N(6) (93.84°); N(3)-Ni(1)-S(1) (87.32°) in compound **15** are also analogous, as expected on the basis of the similar square planar nature for both complexes. The dihedral angles formed by the least square planes Cg(1) and Cg(2) are 2.29° and 42.14° respectively for **14** and **15**. This strongly supports distorted square planar confirmation of both molecules where greater distortion is observed for compound **15**. The C(6)-N(3) bond distance in the complexes are observed to be 1.293(3) and 1.308(2) Å in compounds **14** and **15** respectively and compared to the corresponding C(6)-N(3) (1.308(4) Å) bond in free ligand, and this bond

length is much shorter in **14**. This indicates that there is no clear decrease in the double bond character of the C-N azomethine bond on chelation to the Ni(II) ion. This can be attributed to the stabilization of the C-N azomethine bond in the nickel(II) complexes due to the presence of an important metal-to-ligand  $\pi$ -back donation.. The delocalisation of electron density in the thiosemicarbazone moiety gives rise to a reduction in the N(3)-N(4) bond length compared to uncomplexed thiosemicarbazone in both complexes. The loss of N(4)-H proton in HL<sup>1</sup> produces a negative charge, which is delocalised on the N(3)-N(4)-C(12) system, suggestive of the lengthening of the bond S(1)-C(12) in compounds **14** and **15** from the value of 1.671(4) Å in the free ligand. The decrease in the bond length of C(12)-N(4) to 1.331(3) Å in compound **14** and 1.329(2) Å in compound **15** from the value of 1.386(4) Å of the thiosemicarbazone also supports thiolate formation. Ring puckering analysis and least square plane calculations show that Cg(3) ring comprising of N(5), C(13), C(14), C(15) and C(16) adopts an envelope conformation on C(15) in both complexes **14** and **15**. These observations are consistent with the work on nickel(II) complexes of di 2-pyridyl ketone *N*(4)substituted thiosemicarbazones [141-142].

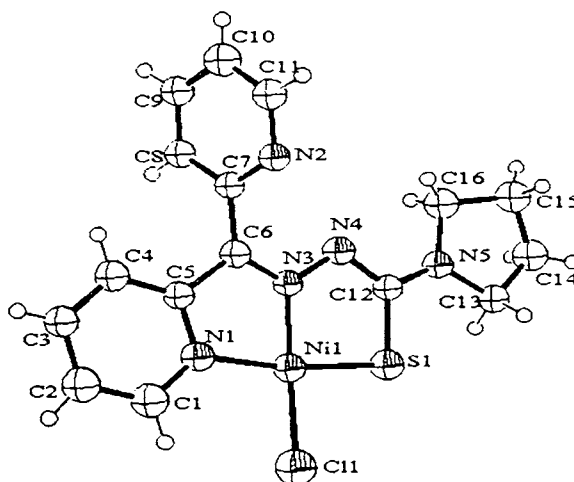


Figure 4.1. *ORTEP* diagram for compound [NiLCl](**14**). Displacement ellipsoids are drawn at 50% probability level and hydrogen atoms are shown as small spheres of arbitrary radii.

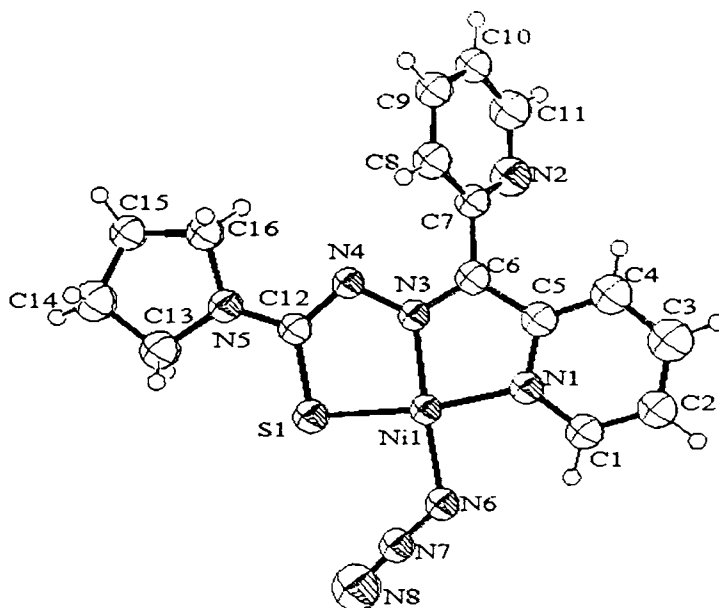


Figure 4.2. ORTEP diagram for compound  $[\text{NiL}^1\text{N}_3]$  (**15**). Displacement ellipsoids are drawn at 50% probability level and hydrogen atoms are shown as small spheres of arbitrary radii.

The arrangements of the molecules of  $[\text{NiL}^1\text{Cl}]$  in a face-to-face manner within a unit cell are shown in Figure 4.3. However, the molecules of  $[\text{NiL}^1(\text{N}_3)]$  (**15**) adopt a ‘zig-zag’ arrangement as is evident from the Figure 4.4. The unit cell is viewed down the  $a$ -axis and 2 and 8 molecules of compound **14** and **15** respectively are arranged in their unit cell. The assemblage of molecules in the respective manner in the unit cell is resulted by the diverse  $\pi$ - $\pi$  stacking; CH- $\pi$ , and ring-metal interactions depicted in Tables 4.4 and 4.5 respectively. The metal chelate rings Cg(1) and Cg(2) are involved in  $\pi$ - $\pi$  interaction between pyridyl rings of the neighboring unit at average distance of 3.787 and 3.773 Å in compounds **14** and **15** respectively. In addition to  $\pi$ - $\pi$  stacking, the CH- $\pi$  interaction between pyridyl hydrogen and metal chelate rings contribute to the stability of unit cell packing. Short ring-metal interactions at a distance of 3.586 Å from Ni center in compound **14** while they are perceived at 3.788 Å for Cg(5) from the metal in the packed molecule of compound **15**. The crystal structure of **14** is further stabilized by two CH- $\pi$  interactions *viz* C(3)-H(3)---

**Table 4.3****Comparison of selected bond lengths (Å) and bond angles (°) of HL<sup>1</sup>, [NiL<sup>1</sup>Cl] and [NiL<sup>1</sup>N<sub>3</sub>]**

	HL <sup>1</sup>	[NiL <sup>1</sup> Cl]	[NiL <sup>1</sup> N <sub>3</sub> ]
Ni(1)-N(3)		1.853(2)	1.8557(13)
Ni(1)-N(1)		1.922(2)	1.9145(14)
Ni(1)-S(1)		2.1374(8)	2.1419(5)
S(1)-C(12)	1.671(4)	1.741(3)	1.7422(16)
N(3)-C(6)	1.308(4)	1.293(3)	1.308(2)
N(3)-N(4)	1.371(4)	1.373(3)	1.3669(19)
N(4)-C(12)	1.386(4)	1.331(3)	1.329(2)
N(5)-C(12)	1.349(5)	1.334(3)	1.328(2)
Ni(1)-Cl(1)		2.1592(8)	
Ni(1)-N(6)			1.8723(15)
N(6)-N(7)			1.196(2)
N(7)-N(8)			1.146(2)
N(3)-Ni(1)-S(1)		87.07(7)	87.32(5)
N(3)-Ni(1)-N(1)		84.00(9)	83.54(6)
N(1)-Ni(1)-S(1)		170.96(6)	169.90(5)
C(12)-S(1)-Ni(1)		95.43(9)	94.93(6)
C(1)-N(1)-Ni(1)		129.50(19)	127.71(13)
C(5)-N(1)-Ni(1)		112.16(16)	112.97(11)
C(6)-N(3)-Ni(1)		116.68(17)	117.11(12)
N(4)-N(3)-Ni(1)		124.42(15)	123.62(10)
C(6)-N(3)-N(4)	118.6(3)	118.8(2)	119.25(14)
N(1)-Ni(1)-Cl(1)		96.99(6)	
N(1)-Ni(1)-N(6)			93.84(7)
N(3)-Ni(1)-Cl(1)		176.82(7)	
N(3)-Ni(1)-N(6)			176.95(6)
S(1)-Ni(1)-Cl(1)		92.01(3)	
N(6)-Ni(1)-S(1)			95.41(5)
N(7)-N(6)-Ni(1)			124.25(14)
N(8)-N(7)-N(6)			175.9(2)

Cg(5) and C(13)-H(132)---Cg(1) while stability is enhanced by C(2)-H(2)---Cg(1) and C(16)-H(162)---Cg(2) interactions in compound **15**. The  $\pi$ - $\pi$ , CH--- $\pi$  and ring-metal interactions point out the possibility for metalloaromaticity – a classic concept recently reviewed by Masui [112].

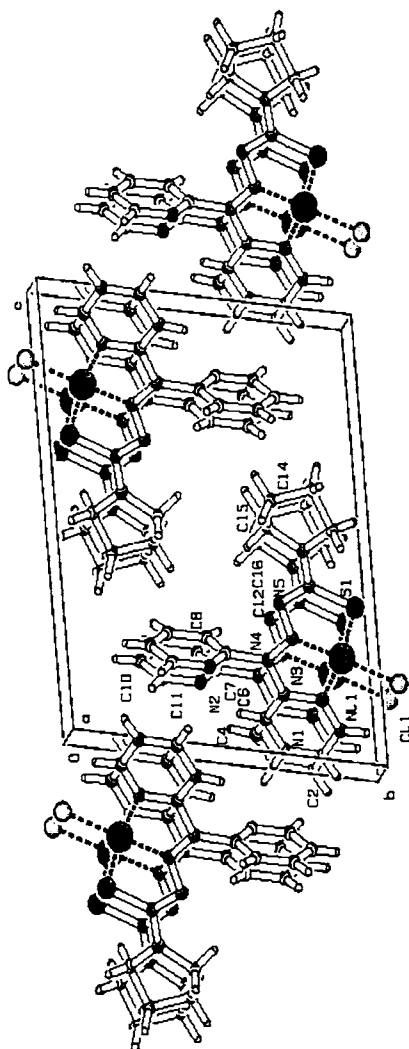


Figure 4.3. Unit cell packing diagram of  $[\text{NiL}^1\text{Cl}]$  viewed down  $a$ -axis



**Table 4.4****H-bonding,  $\pi$ --- $\pi$  interaction parameters of the compound [NiL<sup>1</sup>Cl]**

<b>H bonding</b>				
D-H---A	D-H (Å)	H---A (Å)	D---A(Å)	D- H---A(°)
C(1)-H(1)-Cl(1)(1)	0.93	2.66	2.2373	121
<b><math>\pi</math>---<math>\pi</math> interactions</b>				
Cg(I)-Res(1)---Cg(J)	Cg- Cg(Å)	$\alpha$ °	$\beta$ °	
Cg(1) [ 1 ] -> Cg(4) <sup>a</sup>	3.6176	2.29	24.97	
Cg(2) [ 1 ] -> Cg(4) <sup>a</sup>	3.9617	4.11	28.56	
Cg(4) [ 1 ] -> Cg(2) <sup>b</sup>	3.9617	4.11	32.55	
Equivalent position codes:		Cg(1)=N(1),S(1),C(12),N(4),N(3)		
a=1+x,y,z		Cg(2)=Ni(1),N(1),C(5),C(6),N(3)		
b=-1+x,y,z		Cg(4)=N(1),C(1),C(2),C(3),C(4),C(5)		
		Cg(5)=N(2),C(7),C(8),C(9),C(10),C(11)		
<b>CH---<math>\pi</math> interactions</b>				
XH(I)---Cg(J)	H..Cg(Å)	X-H..Cg (°)	X..Cg (Å)	
C(3)-H(3)[ 1 ] -> Cg(5) <sup>e</sup>	2.9502	134.61	3.6194	
C(13)-H(132) [ 1 ] ->Cg(1) <sup>f</sup>	2.8596	151.14	3.7287	
Equivalent position code;				
e = -1-x, 1-y, -z,				
f = 1+x, y, z				

(D=Donor. A=acceptor. Cg=Centroid,  $\alpha$ =dihedral angles between planes I & J.  $\beta$ = angle Cg(1)-Cg(J))

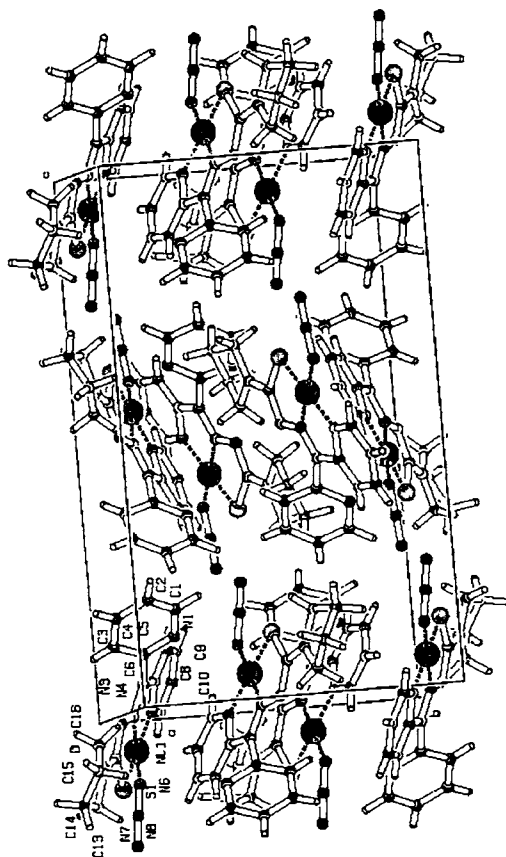


Figure 4. 4. Unit cell packing diagram of complex  $[\text{NiL}^1\text{N3}]$  viewed down a-axis

#### 4.3.3. Infrared spectra

Selected IR bands of the nickel(II) complexes and that of the polyatomic anions are listed in Tables 4.6 and 4.7 respectively. Infrared spectra of compounds **15** and **16** are shown in the Figure 4.5. The assignments of IR bands are observed to be in good agreement with the X-ray structural data. The spectrum of  $\text{HL}^1$  exhibits a medium band at  $3049\text{ cm}^{-1}$ , which is assigned to  $\nu(\text{NH})$  vibration. The absence of  $\nu(\text{NH})$  in the spectrum provides strong evidence for the ligand coordination around Ni(II) ion in its deprotonated form.

Table 4.5

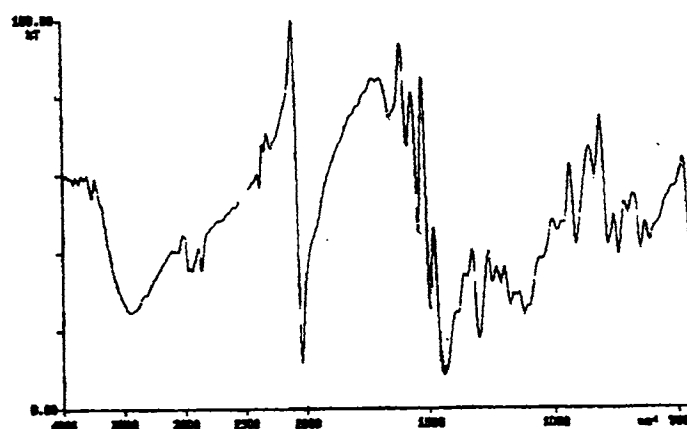
H-bonding,  $\pi$ --- $\pi$  interaction parameters of the compound [NiL<sup>1</sup>N<sub>3</sub>]

<b>H bonding</b>				
D-H---A	D-H (Å)	H---A(Å)	D---A(Å)	D- H---A(°)
C(8)-H(8)---N(1)	0.92	2.55	3.0813	117
C(11)-H(11)- N(6)	0.93	2.43	2.9710	118
<b><math>\pi</math>---<math>\pi</math> interactions</b>				
Cg(1)-Res(1)----Cg(J)		Cg-Cg(Å)	$\alpha$ °	$\beta$ °
Cg(1)-[ 1]----Cg(5) <sup>a</sup>		3.6650	7.99	18.30
Cg(2)-[ 1]----Cg(2) <sup>a</sup>		3.8815	0.02	31.20
Cg(5)-[ 1]----Cg(1) <sup>a</sup>		3.6650	7.99	26.21
Equivalent position codes:			Cg(1)=Ni(1), S(1), C(12), N(4), N(3)	
A = -x, -y, -z			Cg(2)=Ni(1), N(1), C(5), C(6), N(3)	
			Cg(5)=N(1), C(1), C(2), C(3), C(4), C(5)	
<b>CH---<math>\pi</math> interactions</b>				
X-H(I)----Cg(J)		H..Cg(Å)	X-H..Cg (°)	X..Cg(Å)
C(2)-H(2)----Cg(1) <sup>e</sup>		2.8692	153.22	3.7304
C(16)-H(162)-----Cg(2) <sup>f</sup>		3.0502	152.71	3.9291
Equivalent position code;				
e = -1/2+x, 1/2-y, -z				
f = 1/2-x, -1/2+y, z				

(D=Donor, A=acceptor, Cg=Centroid,  $\alpha$ =dihedral angles between planes I & J,  $\beta$ = angle Cg(1)-Cg(J))

The spectra of the complexes exhibit a systematic shift in the position of the bands in the region  $1600\text{-}1350\text{ cm}^{-1}$  due to  $\nu(\text{C}=\text{C})$  and  $\nu(\text{C}=\text{N})$  vibrational modes, and their mixing patterns are different from those present in the ligand spectrum.

Compound 15  $[\text{NiL}^1\text{N}_3]$



Compound 16  $[\text{NiL}^1(\text{SCN})]$

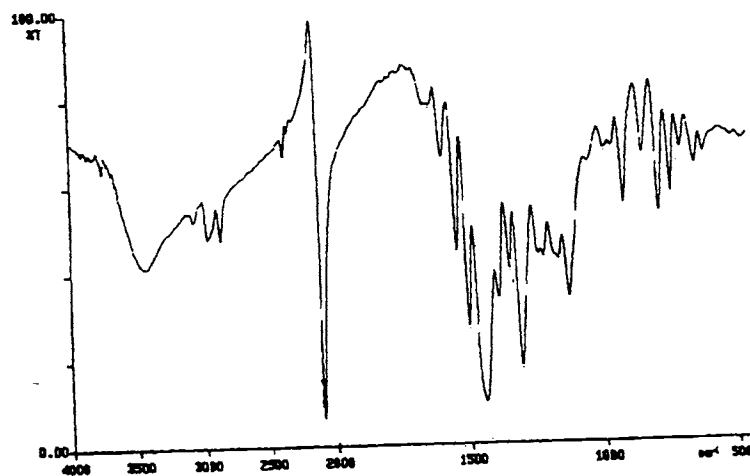


Figure 4.5. IR spectra of compounds 15 and 16

**Table 4.6**  
**Infrared spectral assignments (cm<sup>-1</sup>) for HL<sup>1</sup> and its Ni(II) complexes**

Compound	$\nu(\text{N-H})$	$\nu(\text{C=N})^+$ $\nu(\text{N=C})$	$\nu(\text{N-N})$	$\nu(\text{C=S})$	$\delta(\text{C=S})$	$\delta(\text{o.p})$	$\nu(\text{Ni-N})$	$\nu(\text{Ni-S})$	$\nu(\text{Ni-X}\#)$	$\nu(\text{Ni-N})\text{py}$
HL <sup>1</sup>	3049	1582s	1000m	1330 s	810m	638 s	-----	-----	-----	-----
[NiL <sup>1</sup> Cl] <sup>+</sup> (14)	----	1592s	1030w	1346 s	777 m	658 m	473 m	351m	304 m	281 m
[NiL <sup>1</sup> N <sub>3</sub> ] <sup>+</sup> (15)	----	1586s	1030	1340s	783m	649m	473 m	358 m	454	281 m
[NiL <sup>1</sup> SCN] <sup>+</sup> (16)	----	1591s	1025m	1345 w	787 m	650 m	465 m	354 m	345 m	

s=strong, m= medium, w= weak, All values are reported in cm<sup>-1</sup>, X<sup>#</sup> = Cl, N<sub>3</sub>, SCN. \*hydrate waters are omitted for convenience

**Table. 4.7**  
**IR band assignments (cm<sup>-1</sup>) for the polyatomic anions for the nickel(II) complexes with HL<sup>1</sup>**

Compound	Mode of coordination	$\nu_a(\text{N-N})$	$\nu_s(\text{N-N})$	$\delta(\text{N-N-N})$	$\nu(\text{Ni-N})$
[NiL <sup>1</sup> N <sub>3</sub> ] <sup>+</sup> (15)	unidentate	2037 s	1305 s	575 w	454 m
Thiocynato complex		$\nu(\text{CN})$ ,	$\nu(\text{CS})$	$\delta(\text{NCS})$	$\nu(\text{Ni-S})$
[NiL <sup>1</sup> SCN] <sup>+</sup> (16)	unidentate	2101s	702 w	420 w	345

s=strong, m = medium, = weak, sh= shoulder, \*hydrate waters are omitted for convenience

As a result of coordination, the band corresponding to azomethine nitrogen,  $\nu(\text{C}=\text{N})$  shifts to higher wavenumbers by *ca.* 5-10  $\text{cm}^{-1}$  in the complexes [106,110,115-116] which is due to the combination of  $\nu(\text{C}=\text{N})$  with newly formed  $\text{N}(4)=\text{C}(12)$  bond formed as a result of enolisation followed by deprotonation. The band at 810  $\text{cm}^{-1}$ , assigned to  $\nu(\text{C}=\text{S})$  in free ligand, shift to lower wavenumbers on complexation suggesting the change of bond order and strong electron-delocalisation upon chelation. A medium band around 470  $\text{cm}^{-1}$  corresponds to  $\nu(\text{Ni}-\text{N}_{\text{azomethine}})$  further supports azomethine nitrogen coordination. The far IR spectra of complexes exhibit bands at 355 corresponding to . The chloro complex has a band at 304  $\text{cm}^{-1}$  corresponding to  $\nu(\text{Ni}-\text{Cl})$ .

Azido complex (15) exhibits a strong band at 2037  $\text{cm}^{-1}$  corresponding to the  $\nu_a(\text{NNN})$  stretching vibration [34] of the coordinating azido group. The broad bands at 575 and 454  $\text{cm}^{-1}$ , assigned to  $\delta(\text{NNN})$  and  $\nu(\text{Ni}-\text{N})$  respectively [126] are not prominent, suggesting that Ni-N-N-N is not linear. Compound 3 shows a sharp band at 2101  $\text{cm}^{-1}$ , which is assigned to  $\nu(\text{C}-\text{N})$  of thiocyanato group, indicating the coordination through the thiocyanate sulfur [143]. A weak band at 700  $\text{cm}^{-1}$  and several bands near 420  $\text{cm}^{-1}$  further supports sulfur coordination of the thiocyanato anion with the nickel center [144-147].

#### 4.3.4. Electronic spectra

Solid-state electronic spectra of compounds 14, 15 and 16 were determined in the region 200-900 nm. Electronic spectra of compounds are shown in Figures 4.6 and the spectral data are listed in Table 4.8. The ligand HL<sup>1</sup> has an absorption maximum at 36240 and 35100  $\text{cm}^{-1}$  due to  $\pi^* \leftarrow \pi$  of the pyridyl ring and the imine function of thiosemicarbazone moiety respectively. There are two bands at 30880 and 29150  $\text{cm}^{-1}$  corresponding to  $\pi^* \leftarrow n$  transition of the pyridyl nitrogen and thioamide function respectively. These bands suffer marginal shift on complexation. The broad band at 31,150  $\text{cm}^{-1}$  in  $[\text{NiL}^1\text{Cl}]$  is assigned for both  $\pi^* \leftarrow n$  transitions and Ni(II)  $\leftarrow$  Cl charge transfer

transitions [148]. The shift of the  $\pi^* \leftarrow \pi$  bands to the longer wavelength region is the result of the C=S bond being weakened and conjugation system being enhanced after the formation of the complex [149]. The absence of bands below  $10,000 \text{ cm}^{-1}$  confirms the planar nature of complexes. The  $d-d$  spectral transitions can be assigned to  ${}^1E_g \leftarrow {}^1A_{1g}$ ,  ${}^1A_{2g} \leftarrow {}^1A_{1g}$  and  ${}^1B_{1g} \leftarrow {}^1A_{1g}$  in the order of decreasing energy [150]. The  $d-d$  bands appearing as weak shoulders centered around  $20000 \text{ cm}^{-1}$  region are typical of square planar monoligated Ni(II) complexes [114]. The presence of intense  $\pi^* \leftarrow \pi$  and  $\pi^* \leftarrow n$  transitions cause the lower energy  $d-d$  bands and LMCT bands to appear as weak shoulders, bringing about difficulty in the assignment of bands.

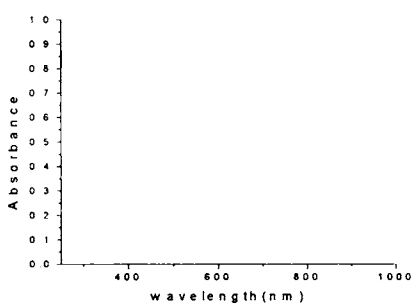
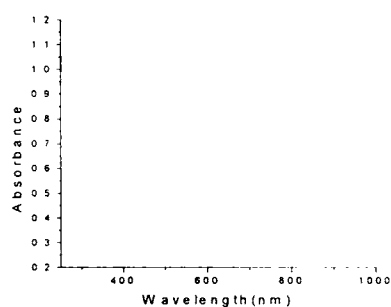
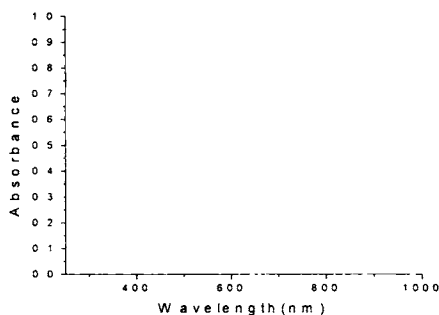
Compound 14 [NiL<sup>1</sup>Cl]Compound 15 [NiL<sup>1</sup>N<sub>3</sub>]Compound 16 [NiL<sup>1</sup>(SCN)]

Figure 4.6. Electronic spectra of compounds 14, 15 and 16

#### 4.3.5. $^1\text{H}$ NMR spectra

$^1\text{H}$  NMR spectral measurements are assigned as previously reported for di-2-pyridyl ketone *N*(4)-methyl and *N*(4)-dimethyl thiosemicarbazone and its metal complexes [16]. Table 4.9 shows that the *N*(4)H resonance is at  $\delta = 15.0$  ppm in HL<sup>1</sup>. The large downfield shift of this proton indicates its involvement in hydrogen bonding with the pyridyl nitrogen. This disappears in the spectra of complexes, which supports the enolization and coordination of sulfur to Ni(II) in the thiolate form after deprotonation. The signals corresponding to aromatic protons are shifted slightly upfield suggesting extensive delocalisation of electrons on complexation. This is due to the presence of an important metal-to-ligand  $\pi$ -back donation. The protons corresponding to the pyridyl rings of di-2-pyridyl ketone appear as separate signals in complexes, indicating its loss of equivalence due to imposition of a rigid geometry around the metal ion after complexation. This observation is consistent with the resonance of HL<sup>1</sup> protons with C(1)H and C(11)H at  $\delta=8.71$  and 8.57 ppm (2H, doublet), C(2)H and C(10)H at  $\delta = 7.34$  and 7.28 ppm (2H, triplet), C(4)H and C(8)H at  $\delta =8.07$  and 7.67 ppm (2H, doublet) ; C(3)H and C(9)H at  $\delta = 7.78$  ppm (2H, triplet), which on complexation resonate at different fields.(Figure 4.7).

#### 4.4. Concluding Remarks

The work presented in this chapter deals with the synthesis structural and spectral characterization of Ni(II) complexes. All complexes are brown and diamagnetic. These complexes are characterized by elemental analyses and spectral techniques such as IR,  $^1\text{H}$  NMR, and electronic spectra. We have isolated single crystals of two complexes  $[\text{NiL}^1\text{Cl}]$  and  $[\text{NiL}^1(\text{N}_3)]$ . But we failed to isolate the single crystal of  $[\text{NiL}^1(\text{NCS})]$ . The analytical and spectral studies reveal that coordination geometry around Ni(II) is square planar These observations are further supported by X-ray crystallographic studies



**Table 4.8**  
Electronic spectral assignments ( $\text{cm}^{-1}$ ) for HL<sup>1</sup> and its nickel(II) complexes

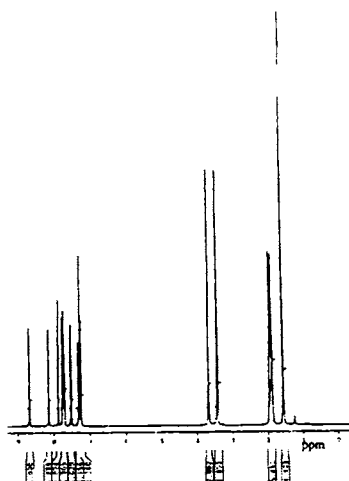
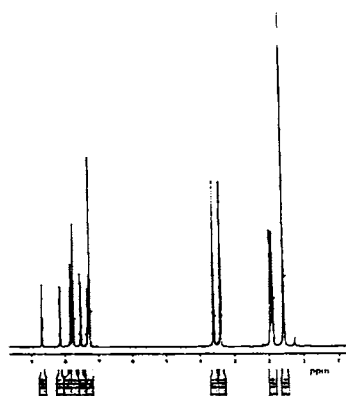
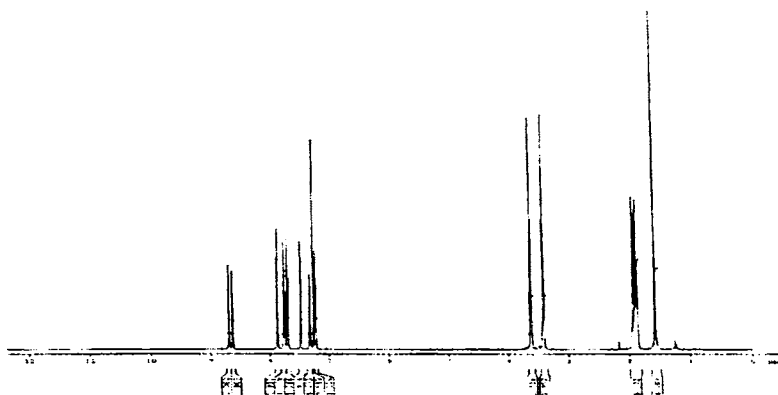
Compound	$\pi^* \leftarrow \pi$	$\pi^* \leftarrow n$	LMCT	d-d
HL <sup>1</sup>	36240, 35100	29150, 30880 sh		
[NiL <sup>1</sup> Cl] <sup>*</sup> (14)	32780 sh	31150	23640, 22880 sh	19340 sh, 18150 sh, 17210 sh
[NiL <sup>1</sup> N <sub>3</sub> ] <sup>*</sup> (15)	32360 sh	30490	23750, 22370 sh	19190 sh, 17510 sh, 16920 sh
[NiL <sup>1</sup> SCN] <sup>*</sup> (16)	32680	30670	23750	19450 sh, 17700 sh, 17030 sh

<sup>a</sup>hydrate waters are omitted for convenience, sh-shoulder

**Table 4.9**  
<sup>1</sup>H NMR assignments for HL<sup>1</sup> and its nickel(II) complexes<sup>a</sup>

Compound	solvent	N(4)H	C(1)H	C(2)H	C(3)H	C(4)H	C(8)H	C(9)H	C(10)H	C(11)H	C(14)H-C(17)H
HL <sup>1</sup>	CDCl <sub>3</sub>	14.89	8.71, 1H, d	7.34, 1H, t	7.78, 1H, t	8.07, 1H, d	7.67, 1H, d	7.78, 1H, t	7.28, 1H, d	8.57, 1H, d	3.87-2.05 (8H)
[NiL <sup>1</sup> Cl] <sup>*</sup> (14)	CDCl <sub>3</sub>	-	8.70, 1H, d	7.31, 1H, t	7.76, 1H, dt	7.87, 1H, d	7.47, 1H, d	7.70, 1H, dt	7.23, 1H, dt	8.63, 1H, d	3.6-1.9 (8H)
[NiL <sup>1</sup> N <sub>3</sub> ] <sup>*</sup> (15)	CDCl <sub>3</sub>	-	8.68, 1H, d	7.30, 1H, t	7.72, 1H, dq	7.87, 1H, d	7.50, 1H, d	7.72, 1H, dq	7.24, 1H, q	8.13, 1H, d	3.6-1.9 (8H)
[NiL <sup>1</sup> SCN] <sup>*</sup> (16)	CDCl <sub>3</sub>	-	8.68, 1H, d	7.32, 1H, t	7.76, 1H, t	7.87, 1H, d	7.53, 1H, d	7.76, 2H, t	7.27, 1H, t	8.13, 1H, d	1.9-3.6 (8H)

All chemical shift values are expressed in unit of ppm. <sup>a</sup> Numbering scheme of HL<sup>1</sup> is shown in Figure 2.1. Hydrate waters are omitted for convenience

Compound 15  $[\text{NiL}^1 \text{N}_3] \cdot \frac{1}{2} \text{H}_2\text{O}$ Compound 16  $[\text{NiL}^1 \text{SCN}] \cdot \frac{1}{2} \text{H}_2\text{O}$ Compound 14  $[\text{NiL}^1 \text{Cl}] \cdot \frac{1}{2} \text{H}_2\text{O}$ Figure. 4.7.  $^1\text{H}$  NMR spectra of compounds 14, 15, and 16

**SYNTHESIS, STRUCTURAL AND SPECTRAL  
CHARACTERIZATION OF MANGANESE(II) COMPLEXES  
OF DI-2-PYRIDYL KETONE 3-  
TETRAMETHYLENEIMINYLTHTIOSEMICARBAZONE  
AND DI-2-PYRIDYL KETONE *N*(4)-METHYL, *N*(4)-  
PHENYLTHIOSEMICARBAZONE**

---

### 5.1. Introduction

The  $\text{Mn}^{2+}$  is one of the stable derivatives of manganese atom. In the ground state all the five  $3d$  orbitals are occupied by one electron. The system has a spherical symmetry. In an octahedral field simple ligand field splitting occurs depressing the levels of  $t_{2g}$  orbitals and raising the level of the two  $e_g$  orbitals. For the same ligand, the energy separation is smaller for the  $\text{Mn}^{2+}$  ions. which supports the stability connected with  $d^5$  population of  ${}^6S$  ground state.  $\text{Mn}^{2+}$  forms many complexes which are octahedral and tetrahedral. The octahedral complexes are colored pink and the tetrahedral greenish yellow and the different effects of the octahedral and tetrahedral fields on the energy separation of the  $d$  orbital determine the difference. It is reported that +2 is most common among different oxidation states. Due to the absence of LFSE of  $d^5$  configuration the formation constants of manganese complexes are small and hence exist fewer number of manganese enzymes that contain manganese [151].

$\text{Mn}^{2+}$  is important in both animal and plant enzymes. In mammals, the enzyme *arginase* is produced in the liver. Manganese is an element essential for plants growth. It is also an essential element in a group of enzymes called *phosphotransferases* [152]. Also  $\text{Mn}^{2+}$  can replace  $\text{Mg}^{2+}$  in a large number of biological systems [153]. Few transition metal complexes of di-2-pyridyl

ketone thiosemicarbazones have yet been reported [19]. In this chapter we report the spectral and structural studies of manganese(II) complexes of NNNS quadridentate ligands HL<sup>1</sup> and HL<sup>2</sup> discussed in Chapter 2

## 5.2. Experimental

### 5.2.1. Materials and methods

Ligands HL<sup>1</sup> and HL<sup>2</sup> were synthesized by methods as described in Chapter 2. Following materials and solvents were used. Manganese acetate tetrahydrate (Merck) was used without any prior purification. The complexes were prepared in ethanol. Solvent: ethanol (99%) was purified before use by earlier reported methods.

### 5.2.2. Physical measurements

Details regarding physical measurements are discussed in Chapter 3.

### 5.2.3. Synthesis of complexes

Manganese(II) complexes of both ligands were prepared by the following general method of preparation.

A solution of the ligand (10 mmol) in 20 ml of hot ethanol was treated with an ethanolic solution of Mn(OAc)<sub>2</sub>·4H<sub>2</sub>O (5 mmol 0.12 g) in 2:1 molar ratio. The mixture was stirred for 5 hours using a magnetic stirrer. The resulting solution was allowed to stand at room temperature. On slow evaporation at room temperature, pink crystals of complexes separated out, which were collected by filtration, washed with water, followed by ether and dried over P<sub>4</sub>O<sub>10</sub> *in vacuo*.

Two manganese(II) complexes [ML<sup>1</sup><sub>2</sub>] (17) and [ML<sup>2</sup><sub>2</sub>] (18) are prepared and their elemental analyses values agree good with the proposed empirical formula [ML<sub>2</sub>].

#### 5.2.4. X-ray crystallography

Single crystals of the compound  $[\text{MnL}^1_2]$  (17) for X-ray analysis were grown by slow evaporation of the complex in 1:1:1 mixture of methanol, chloroform and acetone. Light pink crystal of approximate dimensions  $0.40 \times 0.19 \times 0.16 \text{ mm}^3$  was mounted on a glass fiber using epoxy cement. The X-ray diffraction data were measured in frames with increasing  $\omega$  (width of  $0.3^\circ/\text{frame}$ ) at room temperature using a Bruker SMART APEX CCD diffractometer, equipped a fine focus sealed tube X-ray source. Selected crystal data and refinement parameters are given in Table 5.2. The intensity data were collected within the range of  $1.72^\circ < \theta < 26.04^\circ$  for  $hkl$  ( $13 \leq h \leq 13$ ,  $-25 \leq k \leq 25$ ,  $-17 \leq l \leq 17$ ) in a monoclinic system. About 6257 unique reflections were collected. The SMART software was used for data acquisition and the SAINT software for data extraction [70]. Empirical absorption corrections were made on the intensity data. The structure was solved by the heavy atom method and refined by full-matrix least squares using the SHELXS system of programs [73] and the graphics tool was PLATON for windows [74]. All non-hydrogen atoms were refined anisotropically. Few hydrogen atoms were located from the difference Fourier map, and the rest were generated, assigned isotropic thermal parameters, and refined using a riding model. The hydrogen atoms were used for structure factor calculation only. The structure refinement gave goodness-of-fit (GOF) value of 1.094 with the maximum shift/esd value of 0.007.

#### 5.3. Results and discussion

Colors, partial elemental analyses (C, H, N) and stoichiometries of ligands ( $\text{HL}^1$  and  $\text{HL}^2$ ) and their manganese(II) complexes are presented in Table 5.1. Manganese(II) complexes are light pink. Partial elemental data of complexes are consistent with the 1:2 molar ratio of the metal: thiosemicarbazone. Conductivity measurements in  $10^{-3}$  DMF solution indicate

**Table 5.1**  
**Colors, partial elemental analyses, molar conductivities and magnetic moments of manganese(II) complexes of HL<sup>1</sup> and HL<sup>2</sup>**

Compound	Empirical formula	Color	Composition% (Found/Calcd)			$\lambda_{M}^a$	$\mu$ (B.M.) <sup>b</sup>
			Carbon	Hydrogen	Nitrogen		
HL <sup>1</sup>	C <sub>16</sub> H <sub>17</sub> N <sub>5</sub> S	Yellow	62.10 (62.70)	5.56 (5.46)	22.43(22.53)		
[MnL <sup>1</sup> ] <sub>2</sub> (17)	C <sub>32</sub> H <sub>32</sub> N <sub>10</sub> MnS <sub>2</sub>	pink	56.98 (56.89)	4.94 (4.74)	20.22 (20.74)	18	5.48
HL <sup>2</sup>	C <sub>19</sub> H <sub>17</sub> N <sub>5</sub> S	yellow	66.11 (65.70)	4.98 (4.89)	19.94 (20.17)		
[MnL <sup>2</sup> ] <sub>2</sub> (18)	C <sub>38</sub> H <sub>32</sub> N <sub>10</sub> MnS <sub>2</sub>	pink	61.53 (61.05),)	4.48 (4.28)	18.26 (18.74)	15	5.34

<sup>a</sup> Molar conductivity in 10<sup>-3</sup> DMF at 298 K

<sup>b</sup> Magnetic Susceptibility

**Table 5.2**  
**Crystal data and structure refinement for [MnL<sup>1</sup><sub>2</sub>]**

Empirical Formula	C <sub>32</sub> H <sub>32</sub> MnN <sub>10</sub> S <sub>2</sub>
Formula weight (M)	675.74
Temperature (T) K	293(2)
Wavelength (Mo K $\alpha$ ) (Å)	0.71073
Crystal system	Monoclinic
Space group	<i>P</i> 2 <sub>1</sub> / <i>c</i>
Lattice constants <i>a</i> (Å)	10.6814(14)
<i>b</i> (Å)	20.446(3)
<i>c</i> (Å)	14.5688(19)
$\alpha$ (°)	90(4)
$\beta$ (°)	93.331(2)
$\gamma$ (°)	90
Volume V (Å <sup>3</sup> )	3176(3)
<i>Z</i>	4
Calculated density ( $\rho$ ) (Mg m <sup>-3</sup> )	1.413
Absorption coefficient ( $\mu$ ) (mm <sup>-1</sup> )	0.588
<i>F</i> (000)	1404
Crystal size (mm)	0.40 x 0.19 x 0.16
$\theta$ Range for data collection	1.72-26.04
Limiting Indices	-13 $\leq h \leq$ 13, -25 $\leq k \leq$ 25, -17 $\leq l \leq$ 17
Reflections collected	24869
Unique Reflections	6257 [ <i>R</i> <sub>int</sub> = 0.0227]
Completeness to $\theta$	26.04 (99.8 %)
Absorption correction	None
Maximum and minimum transmission	0.9118 and 0.7989
Refinement method	Full-matrix least-squares on <i>F</i> <sup>2</sup>
Data / restraints / parameters	6257/0/534
Goodness-of-fit on <i>F</i> <sup>2</sup>	1.094
Final <i>R</i> indices [ <i>I</i> > 2 $\sigma$ ( <i>I</i> )]	<i>R</i> <sub>1</sub> = 0.0383, <i>wR</i> <sub>2</sub> = 0.0966
<i>R</i> indices (all data)	<i>R</i> <sub>1</sub> = 0.0446, <i>wR</i> <sub>2</sub> = 0.1007
Largest difference peak and hole (e Å <sup>-3</sup> )	0.333 and -0.183

that all complexes are essentially non-electrolytes [125] and this indicates that the ligand, which behaves as a uninegative ion, coordinates to manganese(II) giving the formula  $[\text{MnL}^1_2]$  and  $[\text{MnL}^2_2]$ . The octahedral geometry around manganese(II) in the complexes is evident from the electronic spectra, magnetic moment studies and X-ray crystal structure.

### 5.3.1. Magnetic susceptibility

Bivalent complexes of manganese are known in which manganese will be in the high spin (5/2) or low spin states (1/2). Manganese generally forms high spin complexes because of the additional stability of half filled orbital, which has an orbitally degenerate  $^6S$  ground state. For the  $^6A_{1g}$  ground term there is no temperature independent paramagnetic effect and no reduction of moment below the spin only value by spin orbit coupling with higher ligand field terms. The magnetic moments are found to 5.48 B.M and 5.34 for compounds **17** and **18** respectively [32]. These values are very close to the spin only value of 5.91 for manganese(II) indicating the presence of five unpaired electrons. Magnetic moments of complexes are presented in Table 5.1.

### 5.3.2. Molecular and crystal structure of $[\text{MnL}^1_2]$

The *PLATON* plot of  $[\text{MnL}^1_2]$  along with atomic labeling is shown in the Figure 5.1. Selected bond lengths and bond angles are summarized in Table 5.3. The structural analysis of the compound reveals that the Mn(II) ion is octahedrally bonded to N(1A), N(3A), S(1A) and N(1B), N(3B), S(1B) atoms belonging to the two units of the ligand HL<sup>1</sup>. The configuration of the thiosemicarbazone chain about C(6)-N(3) bond is *Z* which facilitate the coordination of thiolate sulphur to Mn(II) in the complex. The second pyridyl nitrogens N(2A) and N(2B) of the two ligand units are not coordinating with the metal. The octahedron of Mn(II) is formed by N(1A) and N(1B) of pyridyl nitrogens, S(1A) and S(1B) of thiolate sulfur, N(3A) and N(3B) nitrogens of the azomethine of both ligands units. The bond angles N(3A)-Mn(1)-N(3B)



(155.73(6)°), N(1A)-Mn(1)-N(1B) (92.38°), N(3A)-Mn(1)-S(1A) (76.68(4)°), S(1A)-Mn(1)-S(1B) (98.32(2)°), N(1B)-Mn(1)-S(1B) (147.79(4)°), N(1A)-Mn(1)-S(1B) (91.55(5)°), N(3A)-Mn(1)-N(1A) (71.68(6)°) and N(1A)-Mn(1)-N(1B) (92.38(6)°) are indicating significant distortion from octahedral geometry. There is no significant change in the C(6A)-N(3A) and C(6B)-N(3B) bond distances in the complex with that of uncomplexed thiosemicarbazone. There is no clear decrease in the double bond character of the C-N<sub>(azomethine)</sub> bond on chelation to the manganese(II) ion. This can be attributed to the stabilization of the (C-N<sub>azomethine</sub>) bond in the manganese(II) complex due to the presence of an important metal-to-ligand  $\pi$  back donation. Also, this implies that the double bond character for the bonds, C(6A)-N(3A) and C(6B)-N(3B) are not changed significantly on complexation [154, 155]. The delocalisation of electron density in the thiosemicarbazone moiety gives rise to a reduction in the N(3)-N(4) bond length compared to the uncomplexed thiosemicarbazone in the complex. The loss of N(4)-H proton in the ligand HL<sup>1</sup> produces a negative charge, which is delocalised on the N(3)-N(4)-C(12) system. The enolisation and deprotonation on complexation is also confirmed by the lengthening of bonds S(1A)-C(12A) and S(1B)-C(12B) from the value of 1.671(4) Å in the uncomplexed thiosemicarbazone. The decrease in the bond length of C(12A)-N(4A) and C(12B)-N(4B) from the value of 1.386(4) Å of the free ligand also supports thiolate formation. These observations are consistent with the work on manganese(II) complexes of N(4) substituted thiosemicarbazones prepared in our laboratory.[155]. The dihedral angle between the planes Cg(7) and Cg(3) is 3.84° suggesting that the pyridyl ring and newly formed metal chelate rings are coplanar.

A partial view of the unit cell of the compound shows the in-pairs packing of monomeric units, and the interaction between two monomers. As a result, the two molecular units arranged in a geometrically opposite manner within the unit cell as depicted in the Figure. 5.2. The unit cell is viewed along

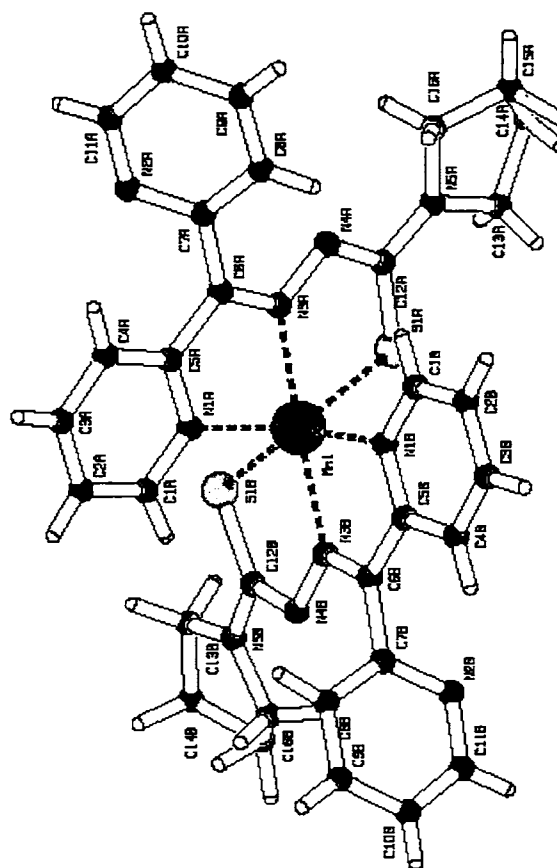


Figure 5.1. *PLATON* diagram of  $[\text{MnL}^{12}]$ .

the *a*-axis. There are 4 molecules in the unit cell and the assemblage of molecules in the respective manner in the unit cell is resulted by the diverse  $\pi$ - $\pi$  stacking, CH- $\pi$ , and ring-metal interactions depicted in Table 5.4. The metal chelate rings Cg(1) and Cg(3) are involved in  $\pi$ - $\pi$  interaction with metal chelate ring Cg(4) of the neighboring unit at distances of 3.4418 and 3.2145 Å in the compound. The pyridyl ring Cg(7) is also involved in  $\pi$ - $\pi$  interaction with Cg(7) of the neighboring unit at a distance of 3.6981 Å. The  $\pi$ - $\pi$  interaction between pyridyl rings and metal chelate rings adds to the stability of unit cell packing. In addition to  $\pi$ - $\pi$  stacking, the CH- $\pi$  interaction between pyridyl hydrogen and metal chelate rings contribute to the stability of unit cell. Intermolecular hydrogen bonding interactions between C(4A)-H(4A) and N(2A) of the second pyridyl ring also contribute to the stability of the unit cell.

**Table 5.3****Comparison of selected bond lengths (Å) and bond angles (°) of HL<sup>1</sup> and [MnL<sup>1</sup><sub>2</sub>]**

	HL <sup>1</sup>	MnL <sup>1</sup> <sub>2</sub>
Mn(1)-N(3)B		2.2378 (15)
Mn(1)-N(3A)		2.2499(16)
Mn(1)-N(1A)		2.2557(16)
Mn(1)-N(1B)		2.3114(17)
Mn(1)-S(1A)		2.4958(6)
Mn(1)-S(1B)		2.5397(7)
S(1A)-C(12A)	1.671(4)	1.730(2)
N(3A)-C(6A)	1.308(4)	1.303(2)
N(3A)-N(4A)	1.361(4)	1.357(2)
N(4A)-C(12A)	1.386(4)	1.3423
N(5A)-C(12A)	1.349(5)	1.340(2)
N(3B)-N(4B)	1.361(4)	1.360(2)
N(3B)-C(6B)	1.308(4)	1.297(2)
S(1B)-C(12B)	1.671(4)	1.7265(19)
N(4B)-C(12B)	1.386(4)	1.334(3)
N(5B)-C(12B)	1.349(5)	1.342(3)
N(3B)-Mn(1)-N(3A)		155.73(6)
N(3B)-Mn(1)-N(1A)		96.46(6)
N(3A)-Mn(1)-N(1A)		71.68(6)
N(3B)-Mn(1)-N(1B)		71.79(6)
N(3A)-Mn(1)-N(1B)		87.27(6)
N(1A)-Mn(1)-N(1B)		92.38(6)
N(3B)-Mn(1)-S(1A)		116.56(4)
N(3A)-Mn(1)-S(1A)		76.68(4)
N(1A)-Mn(1)-S(1A)		146.90(5)
N(1B)-Mn(1)-S(1A)		95.64(4)
N(3B)-Mn(1)-S(1B)		75.99(4)
N(3A)-Mn(1)-S(1B)		124.17(4)
N(1A)-Mn(1)-S(1B)		91.55(5)
N(1B)-Mn(1)-S(1B)		147.79(4)
S(1A)-Mn(1)-S(1B)		98.32(2)

The  $\pi$ - $\pi$ , C-H- $\pi$  and ring-metal interactions point out the possibility for metalloaromaticity [112].

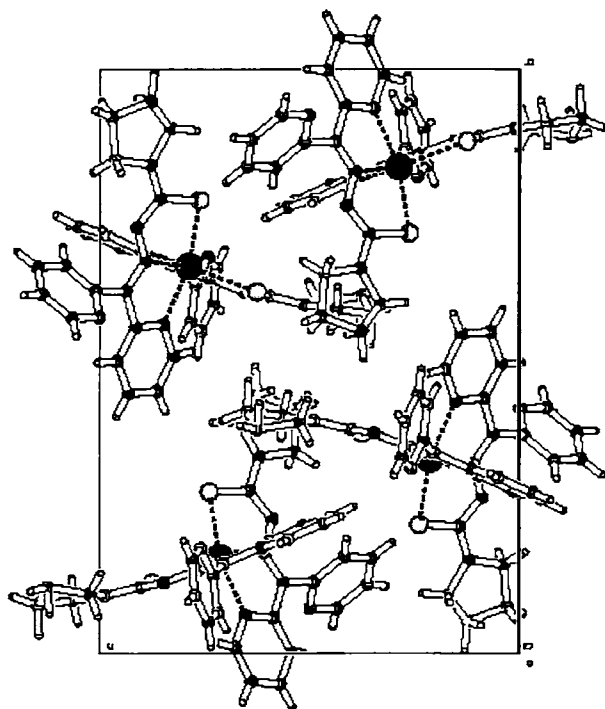


Figure 5.2. Unit cell packing of  $[\text{Mn}(\text{L}^1)_2]$  viewed down the a-axis

### 5.3.3. Infrared spectra

Infrared spectral assignments of significant bands of compounds **17** and **18** are presented in Table 5.5. Infrared spectrum of compound **18** is shown in the Figure 5.3. Two units of ligands coordinate to Mn(II) ion *via* pyridine nitrogen, azomethine nitrogen and thiolate sulfur. Infrared spectral studies give evidences for octahedral coordination geometry around manganese(II) ion which is consistent with X-ray crystallographic studies. The spectra of ligands exhibit a medium band at *ca*  $3050\text{ cm}^{-1}$ , which is assigned to  $\nu(\text{NH})$  vibration which is absent in complexes provide a strong evidence for the ligand coordination around Mn(II) ion in its deprotonated form. As a result of coordination, the band corresponding to azomethine nitrogen,  $\nu(\text{C}(6)\text{-N}(3))$  shifts to higher wavenumbers by  $\sim 7\text{ cm}^{-1}$  [106, 115-116], which is due to the

Table 5.4

H-bonding,  $\pi$ - $\pi$  and CH--- $\pi$  interaction parameters of the compound [MnL<sub>2</sub>]

<b>H-bonding</b>				
Donor---H---A	D-H (Å)	H---A (Å)	D---A (Å)	D-H---A (°)
C(4A)-H(4A)---N(2A)	0.93	2.44	2.9767	117
<b><math>\pi</math>-<math>\pi</math> interactions</b>				
Cg(I)-Res(1)---Cg(J)	Cg-Cg(Å)	$\alpha$ °	$\beta$ °	
Cg(1) [ 1 ] -> Cg(4) <sup>a</sup>	3.4418	83.88	59.71	
Cg(3) [ 1 ] -> Cg(4) <sup>a</sup>	3.2145	88.84	58.81	
Cg(7) [ 1 ] -> Cg(7) <sup>b</sup>	3.6981	0.00	22.24	
Equivalent position codes		Cg(1)=Mn(1),S(1A),C(12A),N(4A),N(3A)		
a=x, y, z		Cg(3)=Mn(1),N(1A),C(5A),C(6A),N(3A)		
b=-x,1-y,-z		Cg(4)= Mn(1),N(1B),C(5B),C(6B),N(3B)		
		Cg(7)=N(1A),C(1A),C(2A),C(3A),C(4A),C(5A)		
<b>CH---<math>\pi</math> interactions</b>				
X-H(I)---Cg(J)	H..Cg(Å)	XH---..Cg (°)	X..Cg (°)	
C(1A)-H(1A)[1] -> Cg(2) <sup>a</sup>	2.7519	122.76	3.3517	
C(1B)-H(1B) [1] -> Cg(1) <sup>a</sup>	2.7207	116.40	3.2420	
C(2B)-H(2B) [1] -> Cg(2) <sup>c</sup>	2.5932	140.01	3.3419	
C(3A)-H(3A) [1] -> Cg(8) <sup>b</sup>	2.7085	172.35	3.6282	
C(4B)-H(4B) [1] -> Cg(9) <sup>d</sup>	3.2290	118.36	3.7634	
C(10B)-H(10B) [1] -> Cg(3) <sup>d</sup>	3.0542	106.28	3.4073	
C(11B)-H(11B) [1]] -> Cg(1) <sup>d</sup>	3.0983	113.66	3.5487	
Equivalent position codes a=x, y, z		Cg(2)=Mn(1),S(1B),C(12B),N(4B),N(3B)		
b = -x, 1-y, -z		Cg(8)= N(1B),C(1B),C(2B),C(3B),C(4B),C(5B)		
c = x, 1/2+y, -1/2+z		Cg(9)=N(2A),C(7A),C(8A),C(9A),C(10A),C(11A)		
d = 1+x, y, z				

(D=Donor. A=acceptor. Cg=Centroid.  $\alpha$ =dihedral angles between planes I & J.  $\beta$ =angle Cg(1)-Cg(J))

combination of  $\nu(\text{C}=\text{N})$  with newly formed  $\text{N}(4)=\text{C}(12)$  bond formed as a result of enolization followed by deprotonation. The enolization is further supported by the increase in the  $\nu(\text{N}-\text{N})$  by  $25\text{-}50\text{ cm}^{-1}$ . A medium band at  $465\text{ cm}^{-1}$  for both complexes corresponding to  $\nu(\text{Mn}-\text{N})$  further supports azomethine nitrogen coordination to  $\text{Mn}(\text{II})$  ion. Coordination *via* thiolate sulfur is indicated by two bands,  $\sim 1300$  and  $\sim 800\text{ cm}^{-1}$  are assignable to  $\nu(\text{C}=\text{S})$  and  $\delta(\text{C}=\text{S})$  vibrations. These bands appear at lower values than that of the corresponding frequencies of free ligands. The downfield shift of these can be attributed to change of bond order and strong electron-delocalisation upon chelation [117]. The out-of-plane bending vibrations of the pyridine ring at  $600\text{ cm}^{-1}$  in uncomplexed ligand shifts to higher frequencies on complexation confirms the coordination of metal to ligand *via* pyridine nitrogen [119, 120, 138]. The low energy bands observed at  $\sim 407$  and  $\sim 305\text{ cm}^{-1}$  in both complexes are assigned to  $\nu(\text{Mn}-\text{S})$ , and  $\nu(\text{Mn}-\text{N})$  for pyridyl nitrogen.

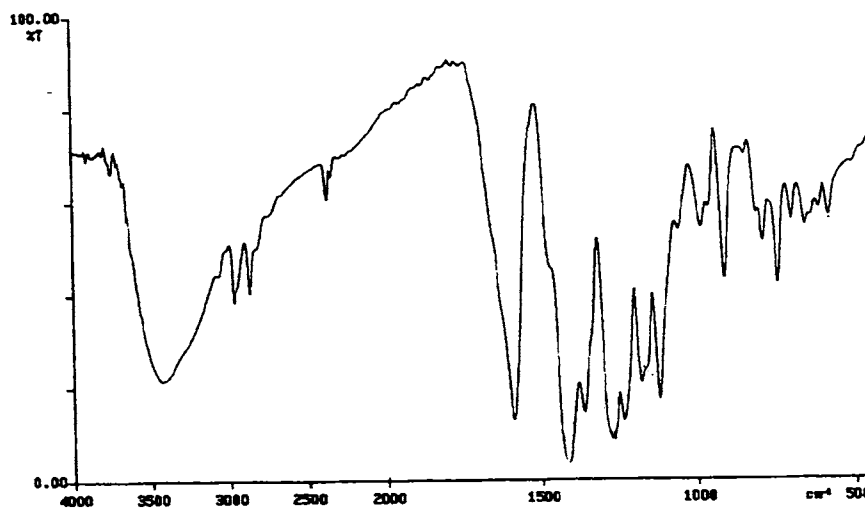


Figure 5.3. IR spectrum of  $[\text{MnL}^1_2]$  (17)

### 5.3.4. Electronic Spectra

Electronic (Diffuse reflectance) spectra of complexes are shown in the Figure 5.4 and electronic spectral data are presented in Table 5.6. Magnetic studies have shown that ground term of manganous ion is a sextet. The only sextet term in the ground state of the  $d^5$  configuration in octahedral geometry is  ${}^6A_{1g}$ . There can be no spin allowed transitions. These transitions are doubly forbidden and hence the transition intensities of octahedral manganese(II) complexes are very low [156-157]. The transitions are assigned from the  ${}^6A_{1g}$  ground state to quartet-excited terms. The electronic spectra of manganese(II) complexes have high intensity charge transfer bands. The observed  $d-d$  transitions of compound 17 and their energies in terms of Racah parameters are:

${}^6A_{1g} \rightarrow {}^4T_{1g} ({}^4G)$	$(10B+5C)$	$E = 1\ 8382\ \text{cm}^{-1}$
${}^6A_{1g} \rightarrow {}^4T_{2g}$	$(10B+5C)$	$E = 22936\ \text{cm}^{-1}$
${}^6A_{1g} \rightarrow {}^4E_g, {}^4A_{1g} ({}^4G)$	$(10B+4C)$	$E = 24272, 25252\ \text{cm}^{-1}$
${}^6A_{1g} \rightarrow {}^4E_g ({}^4D)$	$(17B+5C)$	
${}^6A_{1g} \rightarrow {}^4T_{1g} ({}^4P)$	$(7B+5C)$	$E = 3\ 0864\ \text{cm}^{-1}$



The broad band at  $22936\ \text{cm}^{-1}$  is typical of octahedral manganese(II) complexes arises due to charge transfer transitions. The unusual intense peaks in the visible region is attributed to the intensity stealing influence of sulfur containing ligands, where by the ligands steal the intensity of charge transfer bands into the visible region. The low energies of  $d-d$  transitions  ${}^4E_g \leftarrow {}^6A_{1g} ({}^4D)$  and  ${}^4E_g \leftarrow {}^6A_{1g}, {}^4A_{1g} ({}^4G)$  are independent of  $Dq$ , but depend only on the value of Racah parameters [33]. From the ratio of transition energies and Tanabe-Sugano diagram for a  $d^5$  system  $B$ ,  $C$  and  $Dq$  are evaluated [158].  $B$  is reduced to about 80% of the free ion value of  $\text{Mn}^{2+}$ . Transitions to the  ${}^4E_g(G)$  and  ${}^4A_{1g}$

are almost degenerate and are separated by about  $980\text{ cm}^{-1}$ . Vibronic coupling or spin orbit coupling does not broaden bands corresponding to these transitions since it does not raise the degeneracy of the terms concerned.

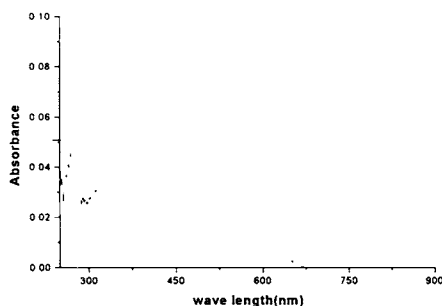
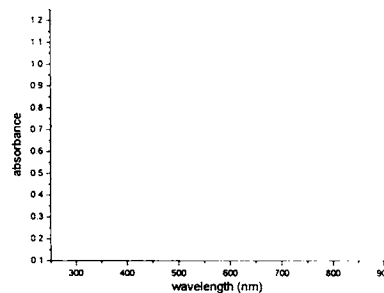
Compound 17 [ $\text{MnL}^1_2$ ]Compound 18 [ $\text{MnL}^2_2$ ]

Figure 5.4. Electronic spectra of compounds 17 and 18

### 5.3.5 Electron spin resonance spectra

Electron spin resonance spectra of coordination compounds of manganese(II) have been studied extensively, the majority of these were on diluted single crystal in which the metal ion geometry is slightly distorted from cubic geometry [159-161]. The high spin manganese(II) has an  ${}^6S_{5/2}$  ground state in the first order case. The combined action of electric field gradient and spin-spin interaction produces splitting of energy levels due to second order spin orbit coupling between  ${}^6A_1$  ground state and lowest level of the manifold  ${}^4A_{2g}$  state [162]. The axial field splitting parameter  $D$  in the case of an axially distorted octahedral field expects the magnitude of zero field splitting. The interpretation of ESR spectra for Mn(II) may be described by the spin Hamiltonian [163].

$$\hat{H} = g\beta H_S + D [S_z^2 - S(S+1)] + E(S_x^2 - S_y^2)$$



Table 5.5  
Tentative IR spectral assignments ( $\text{cm}^{-1}$ ) of Mn(II) complexes of HL<sup>1</sup> and HL<sup>2</sup>

Compound	$\nu(\text{C}=\text{N})+$		$\nu(\text{N}-\text{N})$	$\nu(\text{C}=\text{S})$	$\delta(\text{C}=\text{S})$	$\delta(\text{o.p.})$	$\nu(\text{Mn}-\text{N})$	$\nu(\text{Mn}-\text{S})$	$\nu(\text{Mn}-\text{N})\text{py}$
	$\nu(\text{N}-\text{H})$	$\nu(\text{N}=\text{C})$							
HL <sup>1</sup>	3049	1582s	1000m	1330 s	808m	638 s	-----	-----	-----
[MnL <sub>2</sub> ] <sup>1</sup> (17)	-----	1588s	1025w	1273 s	790 m	654 m	465 m	406 s	302 s
HL <sup>2</sup>	3057	1580s	998	1361s	793m	644m			
[MnL <sub>2</sub> ] <sup>2</sup> (18)	-----	1588s	1010m	1315 s	742 m	646 m	456 m	408 s	307 m

s=strong, m= medium, w= weak,

All values are reported in  $\text{cm}^{-1}$ .

Table 5.6  
Electronic (Diffuse reflectance) spectral data ( $\text{cm}^{-1}$ ) of Mn(II) complexes of HL<sup>1</sup> and HL<sup>2</sup>

compound	${}^1T_{1g} \leftarrow {}^6A_{1g}$	${}^1T_{2g} \leftarrow {}^6A_{1g}$	${}^1E_g \leftarrow {}^6A_{1g}$	${}^1E_g \leftarrow {}^6A_{1g}$	${}^1A_{1g} \leftarrow {}^6A_{1g}$	${}^1A_{1g}(P) \leftarrow {}^6A_{1g}$	$\pi^* \leftarrow n$	$\pi^* \leftarrow \pi$	B ( $\text{cm}^{-1}$ )	$\beta$ (B/B <sub>0</sub> )	10 Dq ( $\text{cm}^{-1}$ )	C ( $\text{cm}^{-1}$ )
HL <sup>1</sup>							29155, 30864	36232, 35088				
[MnL <sub>2</sub> ] <sup>1</sup> (17)	18382	22936	24272	25252	30864		30675	31175	766	0.80	8426	2144
HL <sup>2</sup>							27027, 29070	35971				
[MnL <sub>2</sub> ] <sup>2</sup> (18)	17794	22989	24272	26455sh	31546		31153	37879	741	0.78	8150	2077

where  $H$  is the magnetic field vector,  $g$  is the spectroscopic splitting factor,  $A$  is the manganese hyperfine splitting constant,  $D$  is the axial zero field splitting term,  $S$  is the electron spin vector,  $I$  is the nuclear spin vector  $S = 5/2$  and  $S_z$  is the diagonal spin operator. If  $S = 5/2$  and selection rule  $\Delta m_s = \pm 1$ , five e.s.r transitions would arise when field separations are dependent on  $\theta$ , the angle between the applied field and symmetry axis. The five transitions are

$$\Delta m_s = \pm 5/2 \leftrightarrow 3/2 \quad H = H_0 \pm 2D(3\cos^2\theta - 1)$$

$$\Delta m_s = \pm 3/2 \leftrightarrow 1/2 \quad H = H_0 \pm D(3\cos^2\theta - 1)$$

$$\Delta m_s = \pm 1/2 \leftrightarrow -1/2 \quad H = H_0$$

where  $H_0 = hv/g\beta$ . When the complex is octahedral only central  $\Delta m_s = -1/2 \leftrightarrow +1/2$  transition will be observed since it has only a second order dependence on  $D$ . The fine central line split into a sextet due to electron spin-nuclear spin hyperfine splitting. However if  $D$  is very large only transition between  $|+1/2\rangle \leftrightarrow |-1/2\rangle$  will be observed. Finally if  $D$  or  $E$  is very large, the doublets has an effective  $g$  value  $g_{\parallel} = 2$ ,  $g_{\perp} = 6$  for  $D \neq 0$  and  $E = 0$  but for  $D = 0$  and  $E \neq 0$ , middle Kramers doublet has an isotropic  $g$  value of 4.29.

### Polycrystalline state

In the polycrystalline state, the signals of the spectrum are broadened due to dipolar interactions and random orientation of the  $Mn^{2+}$  ions. The solid state EPR spectrum at 298 K of  $MnL^1_2$  was characterized by two  $g$  values  $g_2 = 2.7$  and  $g_3 = 6.3$  whereas the spectrum of  $MnL^2_2$  shows three  $g$  values  $g_1 = 1.88$ ,  $g_2 = 3.11$  and  $g_3 = 6.3$  (Figure 5.5, Table 5.7).

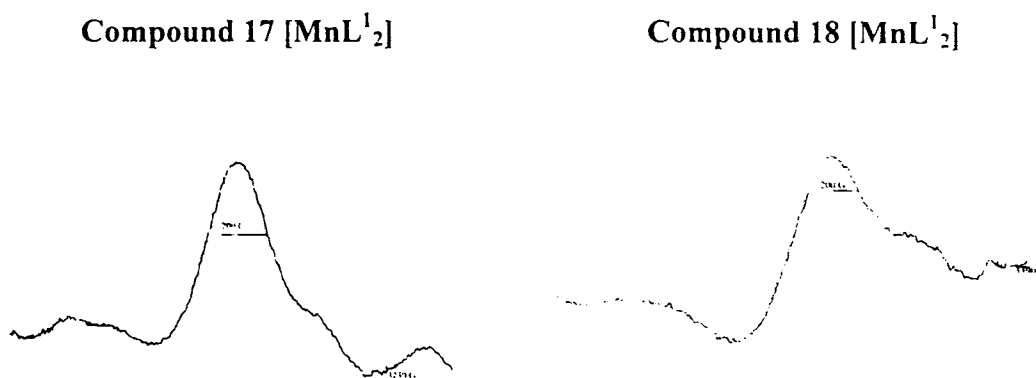


Figure 5.5. EPR spectra of compounds 17 and 18 in the polycrystalline state at 298 K

#### Solution spectra at 298 K

Only few manganese compounds give solution spectra at room temperature. The hyperfine splitting is controlled by axial zero field splitting parameters  $D$  and  $E$ . In manganese complexes with distorted cubic symmetry, this is significant. Magnitude of zero field splitting in such complexes depend on the relative orientation of molecular axis and magnetic field direction.

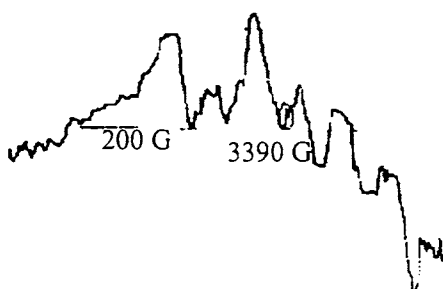


Figure 5.6. EPR spectrum of  $MnL_2^2$  in DMF at 298 K

Molecular tumbling motion will modulate this interaction and hence line broadening is so large so that EPR signals often go undetected. [164]. Of the compounds, compound **17** does not give any spectrum in DMF where as the compound **18** (Figure 5.6) give an isotropic spectrum with six hyperfine splitting.

### Solution spectra at 77 K

For both complexes, a hyperfine sextet is observed with  $g$  values centered on 2.0089 and  $A_0$  at 96 G. The hyperfine spectrum comprising of six lines is due to electron spin nuclear spin coupling. The six hyperfine lines corresponds to  $m_I = +5/2, +3/2, +1/2, \dots, -1/2$  ( $\Delta m_s = \pm 1, \Delta m_I = 0$ ).

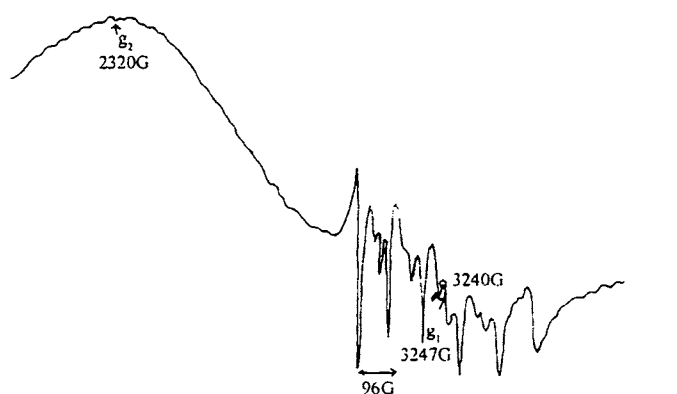


Figure 5.7. EPR spectrum of  $[\text{MnL}_2^1]$  (**18**) in DMF at 77 K.

The observed  $g$  values are very close to free electron spin value suggestive of the absence of spin orbit coupling in the ground state. The  $A_{iso}$  values are consistent with octahedral coordination; since  $A_{iso}$  in tetrahedral sites is 20-25% lower than octahedral sites. The  $A_{iso}$  values are somewhat lower than pure ionic compounds thus reflect the covalent nature of metal ligand

**Table 5.7**  
**EPR spectral parameters of Mn(II) complexes of HL<sup>1</sup> and HL<sup>2</sup>**

Compound	Polycrystalline at 298 K			DMF at 298 K		DMF at 77 K	
	$g_1$	$g_2$	$g_3$	$g_0$	$A_0 \times 10^{-4}$	$g_{\text{iso}}$	$A_{\text{iso}}$
MnL <sup>1</sup> <sub>2</sub> (17)	---	2.7	6.3			2.0089	96 G
MnL <sup>2</sup> <sub>2</sub> (18)	1.88	3.11	6.3	1.98	96	2.0089	96 G

A values are expressed in cm<sup>-1</sup>

bond in complexes. In addition to this axial field spectrum a pair of low intensity forbidden lines lying between each of the two main hyperfine lines with an average spacing of 24 G is observed in the solution spectra of complexes in DMF. These forbidden lines corresponds to  $\Delta m_I = \pm 1$ , due to the mixing of hyperfine lines by zero-field splitting Hamiltonian (Figure 5.7).

#### 5.4 Concluding remarks

We have prepared two manganese complexes of ligands, di-2-pyridyl ketone 3-tetramethyleneiminylthiosemicarbazone (HL<sup>1</sup>) and di-2-pyridyl ketone *N*(4)-methyl *N*(4)-phenylthiosemicarbazone (HL<sup>2</sup>). These complexes are characterized by different physico-chemical methods. The stated quantities of manganese(II) acetate with ligand HL<sup>1</sup> in ethanol and HL<sup>2</sup> in methanol gave products with empirical formula [MnL<sub>2</sub>]. Molar conductivity measurements in 10<sup>-3</sup> M DMF suggest that both complexes are essentially non-electrolytes. The complexes are paramagnetic at room temperature, confirming that manganese is in the +2 oxidation state and hence corresponds to a *d*<sup>5</sup> ion in a strong field. Infrared spectral data suggest that the ligands coordinate to the manganese(II) ion through pyridyl nitrogen, azomethine nitrogen and thiolate sulfur. Electronic spectra of manganese(II) complexes exhibit five low intensity *d-d* bands corresponding to the transitions. These observations are consistent with an octahedral geometry around manganese(II) ion in complexes. Single crystal X-ray diffraction studies of compound **17** reveal that the complex has a distorted octahedral geometry around manganese(II). For compound **18**, IR, electronic, and magnetic susceptibility measurements are similar to that of compound **17**. Compound **18** is assigned octahedral geometry on the basis of physico-chemical studies.

**SYNTHESIS, STRUCTURAL AND IR SPECTRAL  
CHARACTERIZATION OF VANADATE(V) COMPLEX OF  
DI-2-PYRIDYL KETONE 3-  
TETRAMETHYLENEIMINYLTHTIOSEMICARBAZONE**

---

### 6.1. Introduction

The coordination chemistry of vanadium has been of great interest due to the presence of vanadium in enzymatic systems and ability of vanadium complexes to elicit the effects of insulin in diabetic mammals [165, 166]. Much of the biochemistry of vanadium is centered on the ability of vanadate to adopt a four coordinate, tetrahedral geometry and trigonal bipyramidal geometry. The coordination chemistry of vanadium received considerable attention since the discovery of vanadium in enzymes like *bromoperoxidases* and *azobactervinelandii* [167]. Recent investigation on biological properties revealed that vanadium is involved in biological system in more than one way [168]. Some vanadium dependent *bromoperoxidases* enzymes were isolated from marine algae [169] and terrestrial lichen [170]. Vanadium bromoperoxidase catalyses peroxide dependent halogenations of organic compounds in the presence of halide ions. Thus vanadium catalyses both oxidative and reductive processes in biological systems. A few vanadium compounds seem to have therapeutic effects [171]. Some vanadium compounds appear to possess insulin-mimetic properties [172]. Recently reported vanadium compounds are some of the best-known insulin mimetics. They also display anticancer effects. These compounds are competitive inhibitors of protein tyrosine phosphates [173]. Vanadium is commercially important and often used as a catalyst. The maximum oxidation state of vanadium is (+V). For example.

vanadium (+II) and (+III) states are reducing. (+IV) state is stable, and (+V) state is the most stable. Most of vanadium compounds contain  $\text{VO}^{2+}$  unit. This unit is known as vanadyl group. Vanadyl systems usually form square planar complexes with axial oxo ligands [174]. Vanadate(V) is diamagnetic and EPR silent due to its  $d^0$  electronic configuration whereas vanadium(IV) ion is paramagnetic and EPR active ( $d^1$  configuration). In this chapter, we report the synthesis and structural aspects of vanadate(V) complex of di-2-pyridyl ketone 3-tetramethyleneiminylthiosemicarbazone ( $\text{HL}^1$ ).

## 6.2. Experimental

### 6.2.1. Materials and methods

Vanadium acetylacetonate (Merck) was used as received. The complex was prepared in ethanol solvent. The solvents were purified by standard procedures. The preparation of ligand  $\text{HL}^1$  was described in Chapter 2.

### 6.2.2. Physical measurements

Elemental analyses were carried out using a Heraeus Elemental Analyzer at Regional Sophisticated Instrumentation Center, Central Drug Research Institute, Lucknow, India. Molar conductance measurements of the complex was carried out in DMF solvent at  $28 \pm 2$  °C on a Century CC-601 digital conductivity meter with dip type cell and platinum electrode. An approximately  $10^{-3}$  M solution was used. Infrared spectra were recorded on a Shimadzu DR 8001 series FTIR instrument as KBr pellets for spectra run from 4000 to  $400\text{ cm}^{-1}$ . Crystal data was measured at room temperature (293 K) using a Bruker SMART APEX CCD diffractometer at IISc Bangalore.

### 6.2.3. Synthesis of the complex $[\text{VO}_2\text{L}^1]$

A solution of the ligand ( $\text{HL}^1$ ) (5 mmol) dissolved in 20 ml dichloromethane was mixed with an equimolar amount of vanadyl(IV)



acetylacetonate (5 mmol) in 10 ml dissolved in the same solvent.. The mixture was stirred for 24 hours using a magnetic stirrer. The solution turned wine red in color. The resulting solution was allowed to stand at room temperature and after slow evaporation, orange red crystals of the complex separated out, which were collected by filtration, washed with ether and dried over  $P_4O_{10}$  *in vacuo*. Elemental data: Found (%);  $C_{16}H_{16}N_5O_2SV$ : carbon, 48.9; hydrogen, 4.16, nitrogen 17.77: Calcd (%): carbon, 48.7, hydrogen, 4.31, nitrogen, 17.76.

One vanadium(V) complex was prepared using HL<sup>1</sup> and its partial elemental analysis (C,H, N) agrees with the empirical formula  $[VL^1O_2]$  (19)

#### 6.2.4. X-ray crystallography

Single crystals of compound  $[VO_2L^1]$  (19) for X-ray analysis were grown by slow evaporation of the complex dissolved in a 1:1 mixture of methanol and dichloromethane. Orange red rectangular crystal of approximate dimensions  $0.40 \times 0.25 \times 0.22 \text{ mm}^3$  was mounted on a glass fiber using epoxy cement. The X-ray diffraction data were measured in frames with increasing  $\omega$  (width of  $0.3^\circ/\text{frame}$ ) at room temperature (293 K) using a Bruker SMART APEX CCD diffractometer, equipped a fine focus sealed tube X-ray source. Selected crystal data and structure refinement parameters are given in Table 6.1. The intensity data were collected within the range of  $2.40^\circ < \theta < 28.06^\circ$  for  $hkl$  ( $-15 \leq h \leq 14$ ,  $-14 \leq k \leq 14$ ,  $-17 \leq l \leq 18$ ) in a monoclinic system. About 4134 unique reflections were collected. The SMART software was used for data acquisition and the SAINT software for data extraction [70]. Empirical absorption corrections were made on the intensity data. The structure was solved by the heavy atom method and refined by full-matrix least squares using the SHELXS-97 system of programs [73] and the graphics tool was PLATON for windows [74]. All non-hydrogen atoms of the complex cations were refined anisotropically. Few hydrogen atoms were located from the difference Fourier map, and the rest were generated, assigned isotropic thermal parameters, and refined using a riding model. The hydrogen atoms were used for structure

**Table 6.1**  
**Crystal data, and structure refinement data for [VO<sub>2</sub>L<sup>1</sup>]**

Parameters	[VO <sub>2</sub> L <sup>1</sup> ]
Empirical Formula	C <sub>16</sub> H <sub>16</sub> N <sub>5</sub> O <sub>2</sub> S V
Formula weight (M)	393.34
Temperature (T) K	293(2)
Wavelength (Mo K $\alpha$ ) (Å)	0.71073
Crystal system	Monoclinic
Space group	<i>P</i> 2 <sub>1</sub> / <i>c</i>
Lattice constants: <i>a</i> (Å)	11.718(5)
<i>b</i> (Å)	10.794(5)
<i>c</i> (Å)	13.868(6)
$\alpha$ (°)	90
$\beta$ (°)	99.727(8)
$\gamma$ (°)	90
Volume V (Å <sup>3</sup> )	1728.9(14)
Z. Calculated density ( $\rho$ ) (Mg m <sup>-3</sup> )	4, 1.511
Absorption coefficient ( $\mu$ ) (mm <sup>-1</sup> )	0.715
<i>F</i> (000)	808
Crystal size (mm)	0.40 x 0.25 x 0.22
$\theta$ Range for data collection	2.40 to 28.46
Limiting Indices	-15 $\leq h \leq$ 14, -14 $\leq k \leq$ 14, -17 $\leq l \leq$ 18
Reflections collected	15040
Unique Reflections	4134 [ <i>R</i> <sub>int</sub> = 0.0211]
Completeness to $\theta$	28.06 (98.7 %)
Absorption correction	None
Maximum. and minimum transmission	0.8586 and 0.7631
Refinement method	Full-matrix least-squares on <i>F</i> <sup>2</sup>
Data / restraints / parameters	4134/0/290
Goodness-of-fit on <i>F</i> <sup>2</sup>	1.024
Final <i>R</i> indices [ <i>I</i> > 2 $\sigma$ ( <i>I</i> )]	<i>R</i> <sub><i>I</i></sub> = 0.0387, <i>wR</i> <sub>2</sub> = 0.1003
<i>R</i> indices (all data)	<i>R</i> <sub><i>I</i></sub> = 0.0535, <i>wR</i> <sub>2</sub> = 0.1089
Largest difference peak and hole (e Å <sup>-3</sup> )	0.354 and -0.203

factor calculation only. The structure refinement gave goodness-of-fit (GOF) value of 1.024 with the maximum shift/esd value of 0.001.

### 6.3 Results and discussion

Dioxovanadium(V) complex isolated is of the general formula  $\text{VO}_2\text{L}^1$ . The complex is orange red in color characteristic of vanadate(V) complexes with thiosemicarbazone coordination resulting from the sulfur to metal charge transfer bands [108, 109]. The complex is highly soluble in dichloromethane, chloroform, DMF and DMSO. Partial elemental (C,H,N) analysis data for the complex is consistent with the empirical formula  $[\text{VO}_2\text{L}^1]$ . Conductivity measurements ( $10^{-3}$  DMF solution) indicate that the complex behave as a non-electrolyte. The non-electrolytic nature of the complex confirms that the ligand, which behaves as a uninegative ion, coordinates to vanadium(V) giving the empirical formula  $\text{VO}_2\text{L}^1$  where  $\text{L}^1$  is the uninegative ion of ligand  $\text{HL}^1$  and confirms the absence of gegenion outside the coordination sphere.

#### 6.3.1. Molecular and crystal structure

Figure 6.1 illustrates the structural features of the complex  $[\text{VO}_2\text{L}^1]$  for which selected bond lengths and bond angles are listed in Table 6.2. The structure contains a vanadium(V) center pentacoordinate to pyridyl nitrogen N(1), azomethine nitrogen N(3), thiol sulfur S(1) of the thiosemicarbazone moiety and two oxygen atoms O(1) and O(2). The bond length and bond angle values suggest a distorted square pyramidal geometry. Each vanadium atom is coordinated by five bond distances V(1)-O(1) (1.6072 Å), V(1)-O(2) (1.6177(16) Å), V(1)-N(1) (2.0788 Å), V(1)-N(3) (2.1768 Å), V(1)-S(1) (2.3612 Å). The V(1)-O(2) bond is 0.0105 Å greater than V(1)-O(1) bonds suggesting a distorted square pyramidal geometry. The V(1)-N(1) bond length is 0.08 Å larger than V(1)-N(3) bond length that determines the strength of azomethine nitrogen coordination. The pyridine nitrogen N(1), the imino nitrogen N(3) and the thiol sulfur S(1) together with O(2) of the dioxovanadium

constitutes the basal plane around vanadium(V). The configuration of the thiosemicarbazone chain about C(6)-N(3) bond changes to *Z* to facilitate the coordination of thiolate sulphur to vanadium in the complex. The C(6)-N(3) bond lengths do not show any significant shift from that of the ligand on complexation due to electron delocalisation on to the central metal ion [174]. The delocalization of electron density from the coordinating nitrogens on to the central metal ion gives rise to a reduction in the N(3)-N(4) bond length compared to the uncomplexed thiosemicarbazone in the complex. This is indicated by the lengthening of the bond S(1)-C(12) (1.7333 Å) compared to the value of 1.671 Å in the free ligand indicates that the bond order is decreased. The decrease in the bond length of C(12)-N(4) (1.329 Å) from the value of 1.386 Å of the thiosemicarbazone also supports thiolate formation. Thus the basal positions are occupied by S(1), N(1) and N(3) of the thiosemicarbazone moiety and one of the oxygen atoms O(2). The axial site is occupied by the second oxygen atom O(1). The V(1)-O(1) bond distance is shorter than V(1)-O(2) indicating that O(1) is in the compressed state. The *trans* angles O(2)-V(1)-N(3) (133.72(8)°) and N(1)-V(1)-S(1) (150.45(5)°) indicate a compressed geometry. Two oxygen atoms are *cis* to each other with the vanadium center as indicated by the bond angle O(1)-V(1)-O(2) (109.09(9)°). One of the oxygen atom O(1) is involved in hydrogen bonding [175]. The dihedral angles formed by the least square planes Cg(1) and Cg(2) is 6.48° strongly supports that both newly formed metal chelate rings are coplanar. The dihedral angle between the planes constituted by Cg(1) with S(1)/V(1)/O(2) and O1/V1/N1 are 44.44° and 64.51° respectively also confirms a distorted geometry. The dihedral angle between the planes S(1)/V(1)/O(2) and O(1)/ V(1)/ N(1) is 74.62° shows that both newly formed metal chelate rings are not coplanar.

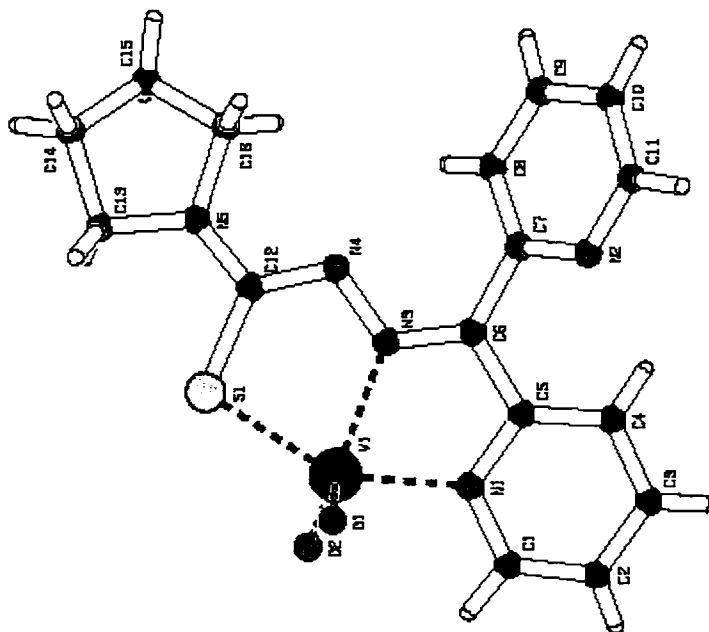


Figure 6.1. *PLATON* diagram of the compound  $[\text{VO}_2\text{L}^1]$  (**19**)

Figure 6.2 shows the unit cell-packing diagram of the compound **19** viewed along the *b*-axis. The unit cell contains 4 molecules arranged in layers where two molecular units in one layer are placed geometrically opposite. The molecular layers are linked through hydrogen bonding. Thus assemblage of molecules in the respective manner in the unit cell is resulted by the diverse  $\pi$ - $\pi$  stacking, CH- $\pi$ , and ring-metal and hydrogen bonding interactions as depicted in Table 6.3 respectively. The metal chelate rings Cg(1) and Cg(2) are involved in  $\pi$ - $\pi$  interactions with the pyridyl ring of the neighboring unit. The crystal structure is further stabilized by five CH--- $\pi$  interactions. The weak  $\pi$ - $\pi$  interaction between pyridyl rings and metal chelate rings makes the unit cell packing more stable. CH--- $\pi$  interactions between the pyridyl hydrogen and the metal chelate rings also adds to the stability of the unit cell packing. Weak hydrogen bonding interactions are also found to exist. The  $\pi$ - $\pi$ , C-H--- $\pi$  interactions point out the possibility for metalloaromaticity [112]. . Weak hydrogen bonding interactions between are also found to exist adds to the

**Table 6. 2****Comparison of selected bond lengths (Å) and bond angles (°) of HL<sup>1</sup> and [VO<sub>2</sub>L<sup>1</sup>]**

	HL <sup>1</sup>	[VO <sub>2</sub> L <sup>1</sup> ]
V(1)-O(1)		1.6072(17)
V(1)-O(2)		1.6177(16)
V(1)-N(1)		2.0788(17)
V(1)-N(3)		2.1768(16)
V(1)-S(1)		2.3612(9)
S(1)-C(12)	1.671(4)	1.7333(19)
N(3)-C(6)	1.308(4)	1.311(2)
N(3)-N(4)	1.371(4)	1.359(2)
N(4)-C(12)	1.386(4)	1.329(2)
O(1)-V(1)-O(2)		109.09(9)
O(1)-V(1)-N(1)		97.36(8)
O(2)-V(1)-N(1)		95.80(8)
O(1)-V(1)-N(3)		116.85(8)
O(2)-V(1)-N(3)		133.72(8)
N(1)-V(1)-N(3)		73.72(6)
O(1)-V(1)-S(1)		103.43(7)
O(2)-V(1)-S(1)		96.97(7)
N(1)-V(1)-S(1)		150.45(5)
N(3)-V(1)-S(1)		78.20(5)
C(12)-S(1)-V(1)		99.22(7)
C(1)-N(1)-V(1)		120.89(13)
C(6)-N(3)-N(4)	118.6(3)	118.27(14)
C(6)-N(3)-V(1)		117.18(12)
N(4)-N(3)-V(1)		123.73(11)
C(12)-N(4)-N(3)	119.8	112.62(14)

stability of unit cell packing. The  $\pi$ - $\pi$ , and C-H $\cdots$  $\pi$  interactions coexist with the hydrogen-bonding network.

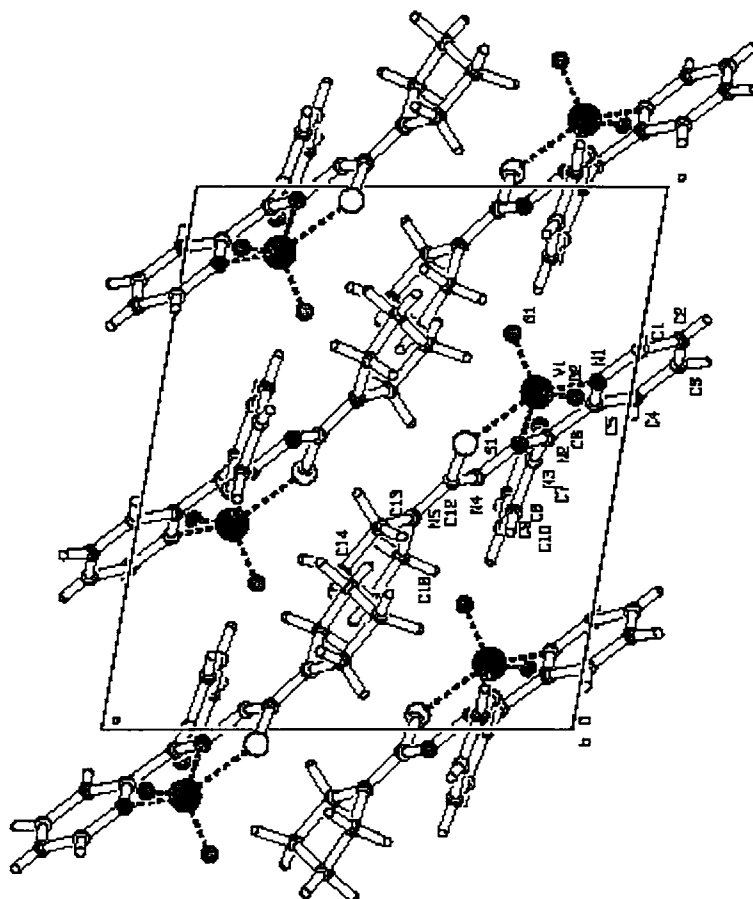


Figure 6.2. Unit cell packing of  $[\text{VO}_2\text{L}^1]$  (19) viewed down the b axis

### 6.3.2. Infrared Spectra.

Selected IR bands are listed in Table 6.4 and the spectrum is shown in the Figure 6.3. The assignments of infrared bands are found to be in good agreement with the X-ray structural data. A medium band at  $3049\text{ cm}^{-1}$ , which is assigned to  $\nu(\text{NH})$  vibration in the free ligand is absent in the spectrum of complex is consistent with ligand coordination around vanadium(V) ion in its

Table 6.3

H-bonding,  $\pi$ - $\pi$  interaction parameters of the compound [VO<sub>2</sub>L<sup>1</sup>]

<b>H-bonding</b>				
Donor---H....acceptor	D-H (Å)	H---A (Å)	D---A (Å)	D-H---A (°)
C(4)-H(4)---N(2)	0.91	2.49	2.9497	112
C(8)-H(8)---N(4)	0.87	2.47	2.8574	108
C(13)-H(132)---O(1)	0.92	2.58	3.4138	150
<b><math>\pi</math>-<math>\pi</math> interactions</b>				
Cg(I)-Res(I)----Cg(J)	Cg-Cg(Å)	$\alpha$ (°)	$\beta$ (°)	
Cg(1) [1] -> Cg(4) <sup>a</sup>	3.7065	9.43	19.85	
Cg(2) [1] -> Cg(2) <sup>a</sup>	3.8568	0.00	21.59	
Cg(2) [1] -> Cg(4) <sup>a</sup>	3.6672	3.23	17.28	
Cg(4) [1] -> Cg(1) <sup>a</sup>	3.7065	9.43	26.36	
Cg(4) [1] -> Cg(2) <sup>a</sup>	3.6672	3.23	14.05	
Equivalent position codes: a= -x, 1-y, 1-z		Cg(1)=V(1),S(1),C(12),N(4),N(3) Cg(2)=V(1),N(1),C(5),C(6),N(3) Cg(4)=N(1),C(1),C(2),C(3), C(4),C(5)		
<b>CH--<math>\pi</math> interaction</b>				
X-H(I)----Cg(J)	H--Cg(Å)	X-H--Cg (°)	X---Cg (Å)	
C(3)-H(3)[ 1] -> Cg(1) <sup>a</sup>	3.2903	84.42	3.3256	
C(9)-H(9) [ 1] ->Cg(2) <sup>c</sup>	3.2490	150.92	4.0472	
C(9)-H(9) [ 1] ->Cg(4) <sup>c</sup>	3.2574	110.97	3.6695	
C(13)-H(131) [ 1] ->Cg(5) <sup>b</sup>	3.3891	149.47	4.3005	
C(14)-H(141) [ 1] ->Cg(2) <sup>b</sup>	2.9279	168.30	4.0102	
C(16)-H(161) [ 1] ->Cg(2) <sup>b</sup>	3.0339	139.34	3.8377	
Equivalent position codes:		Cg(1)= V(1),S(1),C(12),N(4),N(3) Cg(2)= V(1),N(1),C(5),C(6),N(3) Cg(4)=N(1),C(1),C(2),C(3), C(4),C(5) Cg(5)=N(2),C(7),C(8),C(9),C(10),C(11)		
a= -x, 1-y, 1-z				
b = 1-x, 1-y, 1-z				
c= x, 1/2-y, -1/2+z				

(D=Donor. A=acceptor. Cg=Centroid.  $\alpha$ =dihedral angles between planes I & J.  $\beta$ =angle Cg(1)-Cg(J))



deprotonated form. The spectrum of the complex exhibits a systematic shift in the position of the bands in the region  $1600\text{-}1350\text{ cm}^{-1}$  due to  $\nu(\text{C}=\text{C})$  and  $\nu(\text{C}=\text{N})$  vibrational modes, and their mixing patterns are different from those present in the ligand spectrum. As a result of coordination, the band corresponding to azomethine nitrogen,  $\nu(\text{C}=\text{N})$  shifts to higher wavenumbers from that of free ligand by  $8\text{ cm}^{-1}$  in the complex [106, 115-116]. A medium band at  $465\text{ cm}^{-1}$  further supports azomethine nitrogen coordination. The band due to azomethine nitrogen on complexation shift to higher wavenumbers can also be attributed to the combination of  $\nu(\text{C}=\text{N})_{\text{azomethine}}$  and the newly formed  $(\text{C}12=\text{N}(4))$  bond, hence implies that the sulfur is in thiolate form.. The enolization is further supported by the increase in the  $\nu(\text{N}-\text{N})$  from that of free ligand by  $50\text{ cm}^{-1}$ .

Coordination *via* thiolate sulfur is indicated by shift in the two bands,  $1298\text{ cm}^{-1}$  and  $791\text{ cm}^{-1}$  assignable to  $\nu(\text{C}=\text{S})$  and  $\delta(\text{C}=\text{S})$  vibrations. These bands appear at lower values than the corresponding frequencies of free ligand. The downfield shift of bands in complexes corresponding to  $\nu(\text{C}=\text{S})$  and  $\delta(\text{C}=\text{S})$  in free ligands can be attributed to change of bond order and strong electron-delocalisation upon chelation [117]. The pyridine ring out of plane bending vibrations of the free ligand at  $638\text{ cm}^{-1}$  shifts to higher frequencies on complexation further confirms the coordination of ligand to metal *via* pyridine nitrogen.[119, 120].

A strong band at  $939\text{ cm}^{-1}$  corresponds to  $\nu(\text{V}=\text{O})$  stretching vibration indicates the occupation of coordination sites of vanadium ion by oxygen and the two  $\text{V}=\text{O}$  groups are found to be indistinguishable [176].

Table 6.4  
IR spectral assignments ( $\text{cm}^{-1}$ ) of vanadate complex with ligand HL<sup>1</sup>

Compound	$\nu(\text{N-H})$	$\nu(\text{C}=\text{N})^+$ $\nu(\text{N}=\text{C})$	$\nu(\text{N-N})$	$\nu(\text{C}=\text{S})$	$\delta(\text{C}=\text{S})$	$\delta(\text{o.p})$	$\delta(\text{V}=\text{O})$	$\nu(\text{V-N})$	$\nu(\text{V-S})$	$\nu(\text{V-N})\text{py}$
HL <sup>1</sup>	3049	1582s	1000m	1330 s	808m	638 s	-----	-----	-----	-----
[VOL <sub>2</sub> ] <sup>1</sup> (19)	-----	1590s	1050w	1298 s	792 m	646 m	939 s	465 m	406 s	307 s

s = strong, m = medium, w = weak,  
All values are reported in  $\text{cm}^{-1}$ .

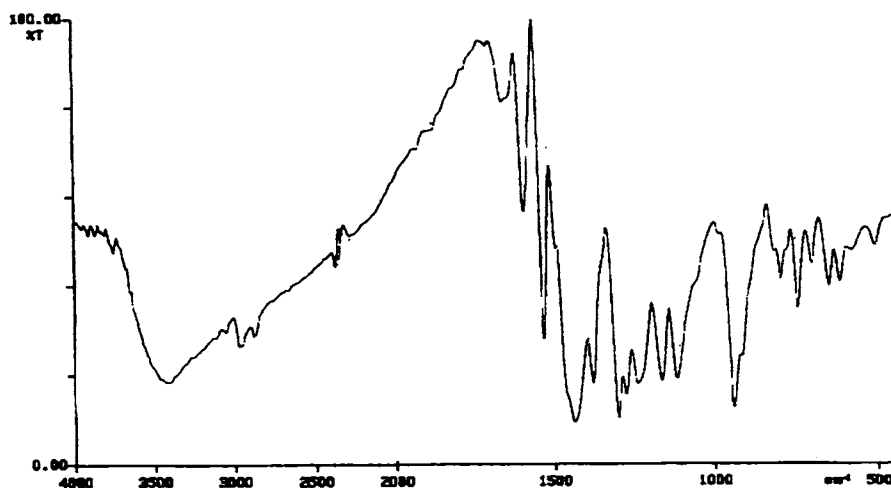


Figure. 6.3. Infrared spectrum of the compound  $[\text{VO}_2\text{L}^1]$

#### 6.4. Concluding Remarks

Under normal refluxing conditions vanadium is susceptible to oxidation. It usually oxidizes to the +5 state. The complex is wine red characteristic of dioxovanadium complexes of NNS donors. The compound is characterized by elemental and IR spectral studies. Slow evaporation of the stirred solution yielded monoclinic single crystals of the complex. X-ray crystallographic studies revealed a distorted square pyramidal geometry around  $\text{V}^{+5}$  ion with one of the oxygen atom at the apical position of the square pyramid. The unit cell packing is stabilized by hydrogen bonding,  $\pi$ - $\pi$ , C-H--- $\pi$  and ring-metal interactions between molecules. X-ray diffraction study further confirms the structural characterization by IR spectral data.

**SYNTHESIS, STRUCTURAL AND SPECTRAL  
CHARACTERIZATION OF COBALT(III) COMPLEXES OF  
DI-2-PYRIDYL KETONE 3-  
TETRAMETHYLENEIMINYLTHTIOSEMICARBAZONE**

---

### 7.1. Introduction

Thiosemicarbazones and their complexes are extensively studied during recent years owing to their pharmaceutical properties [115]. The most common oxidation state of cobalt is +3 and its complexes are produced easily. Many complexes of cobalt in +2 and +3 oxidation states have been prepared and investigated, with emphasis on the reactivity of the metal ions in the transmethylation reaction and reversible absorption of molecular oxygen [177, 178]. Cobalt(III) generally forms cationic, anionic and neutral complexes. All complexes of cobalt(III) are generally octahedral. The metal has a  $d^6$  configuration and most of the ligands are strong enough to cause spin pairing giving the electronic arrangement  $(t_{2g})^6 (e_g)^0$ . This arrangement has very large crystal field stabilization energy. Such complexes are diamagnetic. Complexes with nitrogen donor ligands are most common. Cobalt(III) complexes are usually prepared by oxidation of a solution containing cobalt(II) in air. Recently some interesting reports of cobalt(III) complexes of thiosemicarbazones have appeared [97, 126]. In addition, studies on mixed ligand complexes of cobalt(III) have also been reported [179].

Cobalt(III) complexes derived from Schiff bases are reported to be biologically active. Vitamin B<sub>12</sub> is an important cobalt(III) complex. Vitamin B<sub>12</sub> was isolated from liver. Injection of vitamin B<sub>12</sub> is an effective treatment of

pernicious anemia. Vitamin B<sub>12</sub> is a coenzyme, and serves as a prosthetic group, which is tightly bound to several enzymes in the body. Cobalt is biologically important in some enzymes. *Glutamic mutase* is involved in the metabolism of amino acids and ribonucleotide reductase in the biosynthesis of DNA. Traces of cobalt are essential in the diet of animals. Some sheep raised in Australia, New Zeland suffered from a deficiency disease, which was traced to them, grazing on cobalt deficient soil. This can be remedied either by treating the soil periodically or by forcing the animals to swallow pellets of cobalt [152].

This chapter describes the synthesis, and spectral characterization of cobalt(III) complexes of the ligand di-2-pyridyl ketone 3-tetramethyleneiminylthiosemicarbazone (HL<sup>1</sup>).

## 7.2. Experimental

### 7.2.1. Materials and methods

Thiosemicarbazone ligand (HL<sup>1</sup>) is prepared as described in Chapter 3. Cobalt(II) chloride, cobalt(II) nitrate of A.R grade (Merck) were used without any prior purification. The complexes were prepared in ethanol solvent. The solvents were purified by standard procedures.

### 7.2.2. Physical measurements

Details regarding physical measurements are described in Chapter 3. <sup>1</sup>H NMR spectra of the complexes were recorded in an AMX 400 MHz FT-NMR Spectrometer using CDCl<sub>3</sub> as a solvent and TMS as an internal standard at Sophisticated Instruments Facility, Indian Institute of Science, Bangalore, India.

### 7.2.3. Synthesis of the complexes

#### 7.2.3.1. Synthesis of $[\text{CoL}^1_2]\text{Cl}\cdot 2\frac{1}{2}\text{H}_2\text{O}$

A solution of the thiosemicarbazone ( $\text{HL}^1$ ) (10 mmol) dissolved in 20 ml methanol was mixed with a solution of cobalt(II) chloride (5 mmol) in 10 ml dissolved in the same solvent and refluxed for 2 hours. The resulting solution was allowed to stand at room temperature. On slow evaporation, brown crystals of the complex separated out, which were collected by filtration, washed with ether and dried over  $\text{P}_4\text{O}_{10}$  *in vacuo*.

#### 7.2.3.2. Preparation of $[\text{CoL}^1_2]\text{NO}_3\cdot 2\frac{1}{2}\text{H}_2\text{O}$

A solution of the thiosemicarbazone ( $\text{HL}^1$ ) (10 mmol) dissolved in 20 ml methanol was mixed with a solution of cobalt(II) nitrate (5 mmol) dissolved in 10 ml of the same solvent and refluxed for 2 hours. The resulting solution was allowed to stand at room temperature. On slow evaporation brown crystals of complex separated out, which were collected by filtration, washed with ether and dried over  $\text{P}_4\text{O}_{10}$  *in vacuo*.

Two cobalt(III) complexes were prepared using  $\text{HL}^1$  and elemental analyses data agrees with the proposed empirical formula  $[\text{CoL}^1_2]\text{X}$  where  $\text{X} = \text{Cl}$  (20) and  $\text{NO}_3$  (21)

### 7.3. Results and discussion

Cobalt(II) ion undergoes oxidation in the presence of methanol and chloroform. Cobalt(III) complexes are of the general formula  $[\text{CoL}^1_2]\text{X}$  where  $\text{X} = \text{Cl}$  or  $\text{NO}_3$ . The refluxed mixture on slow evaporation in air at room temperature yielded microcrystals of complexes. Colors, partial elemental analyses and stoichiometries of ligands ( $\text{HL}^1$ ) and cobalt(III) complexes are presented in Table 7.1 is consistent with a 1:2:1 metal: thiosemicarbazone: gegenion. All complexes are stable in air, highly soluble in dichloromethane,

**Table 7.1**  
**Colors, partial elemental analyses and molar conductivities of cobalt(III) complexes with ligand HL<sup>1</sup>**

Compound	Empirical formula	Color	Composition% (Found/Calcd)			$\lambda_M^a$
			Carbon	Hydrogen	Nitrogen	
HL <sup>1</sup>	C <sub>16</sub> H <sub>17</sub> N <sub>5</sub> S	Yellow	62.10 (62.70)	5.56 (5.46)	22.43(22.53)	
[CoL <sup>1</sup> <sub>3</sub> ]Cl·2½H <sub>2</sub> O ( <b>20</b> )	C <sub>32</sub> H <sub>37</sub> N <sub>10</sub> ClCoO <sub>2.5</sub> S <sub>2</sub>	Pink	50.21 (50.50)	4.75 (4.87)	17.96 (18.41)	48
[CoL <sup>1</sup> <sub>3</sub> ]NO <sub>3</sub> ·2½H <sub>2</sub> O ( <b>21</b> )	C <sub>32</sub> H <sub>37</sub> N <sub>11</sub> CoO <sub>5.5</sub> S <sub>2</sub>	Pink	49.10 (48.85)	4.53 (4.70)	19.40 (19.59)	52

<sup>a</sup> Molar conductivity, 10<sup>-3</sup> (M) DMF at 298

chloroform, DMF and DMSO. The stated quantities of cobalt(II) chloride, cobalt(II) nitrate with ligand HL<sup>1</sup> in methanol gave products of composition [CoL<sup>1</sup><sub>2</sub>]Cl·2½H<sub>2</sub>O and [CoL<sup>1</sup><sub>2</sub>]NO<sub>3</sub>·2H<sub>2</sub>O. Both complexes are reported to be diamagnetic at room temperature, confirming that cobalt is in the +3 oxidation state and hence corresponds to a d<sup>6</sup> ion in a strong field. Molar conductivity measurements in 10<sup>-3</sup> DMF solution reveal that gegenions are outside the coordination sphere.

### 7.3.1. Infrared spectra

Selected IR bands are listed in Table 7.2. The characteristic IR bands (50-4000 cm<sup>-1</sup>) for the free ligand (HL<sup>1</sup>) from those of its complexes **20** and **21** provide significant indications regarding the bonding sites of the ligand. A medium band at 3049 cm<sup>-1</sup> in the free ligand is due to ν(NH) vibration disappears in the spectra of complexes providing a strong evidence for the ligand coordination around cobalt(III) ion in its deprotonated form. Bands ranging from 1600-1350 cm<sup>-1</sup> suffers a significant shift in the spectra of complexes can be attributed to ν(C=C) and ν(C=N) vibrational modes, and their mixing patterns are different from those present in the ligand spectrum. The positive shift of band corresponding to ν(C=N) at 1582 cm<sup>-1</sup> in free ligand in complexes is consistent with of azomethine nitrogen coordination to the central cobalt(III) ion [106,115, 116]. A medium band at *ca.* 430 cm<sup>-1</sup> corresponding to ν(Co-N) further supports azomethine nitrogen coordination [34, 180]. The enolisation of the ligand is supported by the increase in the ν(N=N) by 25 cm<sup>-1</sup>. The bands at 1330 and 808 cm<sup>-1</sup> due to ν(C=S) and δ(C=S) in the free ligand has been found to shift to at lower values by 30 and 20 cm<sup>-1</sup> indicative of coordination of thiolate sulfur to cobalt(III) ion. The downfield shift of bands in complexes corresponding to ν(C=S) and δ(C=S) in free ligands can be attributed to change of bond order and strong electron-delocalisation upon chelation [117]. Another medium band at *ca.* 360 cm<sup>-1</sup> is assignable to ν(Co-S). A positive shift corresponding to out-of-plane bending vibrations of pyridine ring in the free



**Table 7.2**  
**IR spectral assignments ( $\text{cm}^{-1}$ ) of cobalt(III) complexes of HL<sup>1</sup>**

Compound	$\nu(\text{C}=\text{N})^+$		$\nu(\text{N}-\text{N})$	$\nu(\text{C}=\text{S})$	$\delta(\text{C}=\text{S})$	$\delta(\text{o.p})$	$\nu(\text{Co}-\text{N})$	$\nu(\text{Co}-\text{S})$	$\nu(\text{Co}-\text{N})\text{py}$
	$\nu(\text{N}-\text{H})$	$\nu(\text{N}=\text{C})$							
HL <sup>1</sup>	3049m	1582s	1000m	1330 s	808m	638 s	-----	-----	-----
$[\text{CoL}_2]\text{Cl}\cdot 2\frac{1}{2}\text{H}_2\text{O}$ ( <b>20</b> )		1587s	1025 sh	1299s	787 m	660 m	440 m	361 m	282 m
$[\text{CoL}_2]\text{NO}_3\cdot 2\frac{1}{2}\text{H}_2\text{O}$ ( <b>21</b> )	-----	1590s	1025 sh	1300m	785m	660m	457	352	281 s

s=strong, m= medium, w= weak, sh= shoulder  
 All values are reported in  $\text{cm}^{-1}$ .

ligand ( $638\text{ cm}^{-1}$ ) to higher frequencies in complexes is confirmative of pyridine nitrogen coordination to cobalt(III) ion [118-120]. A weak band at *ca.*  $270\text{ cm}^{-1}$  corresponding to  $\nu(\text{Co-N}_{\text{pyridyl}})$  is pointing to the coordination of pyridyl nitrogen to the cobalt(III) ion [15]. The bands at 1500, 1300, 992,  $230\text{ cm}^{-1}$  corresponds to different NO stretching frequencies of the nitrate group (Figure 7.1).

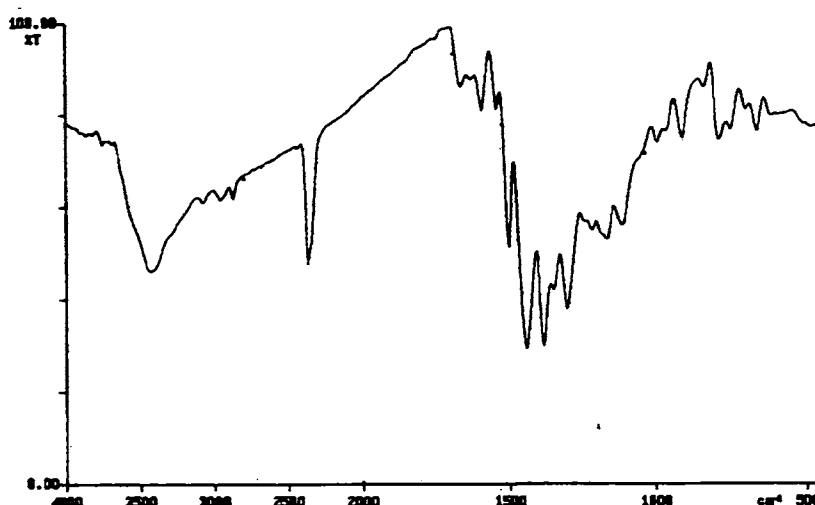


Figure. 7.1. Infrared spectrum of  $[\text{CoL}^1_2]\text{NO}_3 \cdot 2\frac{1}{2}\text{H}_2\text{O}$  (21)

### 7.3.2. Electronic spectra

Electronic spectral data of complexes **20** and **21** are presented in Table 7.3. The spectra of spin paired trivalent cobalt complexes are much more certainly interpreted. Complexes of approximate  $O_h$  symmetry have the following assignments of  $d \leftarrow d$  bands:  $\nu_1: {}^1T_{1g} \leftarrow {}^1A_{1g}$ ;  $\nu_2: {}^1T_{2g} \leftarrow {}^1A_{1g}$ ;  $\nu_3: {}^3T_{1g} \leftarrow {}^1A_{1g}$ ;  $\nu_4: {}^3T_{2g} \leftarrow {}^1A_{1g}$  [126]. The bands are assigned values:  $\nu_1 \sim 22000\text{ cm}^{-1}$ ,  $\nu_2 \sim 25400\text{ cm}^{-1}$ . The band due to  $\nu_3 \sim 6700\text{ cm}^{-1}$  is neglected. There are two broad bands, near  $21978$  and  $25575\text{ cm}^{-1}$  corresponding to charge transfer transitions. The bands assigned are spin allowed transitions. Bands at  $\sim 22000$  and  $\sim 25400\text{ cm}^{-1}$  corresponding to  ${}^1T_{1g} \leftarrow {}^1A_{1g}$  and  ${}^1T_{2g} \leftarrow {}^1A_{1g}$  transitions are masked by intraligand and charge transfer bands. The broad band at  $\sim 25400\text{ cm}^{-1}$  can be

assigned as tail of charge transfer band, mask the higher energy band due to  ${}^1T_{2g} \leftarrow {}^1A_{1g}$ . A very weak band at  $\sim 18000 \text{ cm}^{-1}$  corresponds to spin forbidden  ${}^3T_{2g} \leftarrow {}^1A_{1g}$  transition.. The band at  $\sim 6750 \text{ cm}^{-1}$  corresponding to  ${}^3T_{1g} \leftarrow {}^1A_{1g}$  is weak and difficult to assign because it is spin forbidden. Assignment of the two higher energy bands is complicated by overlap with the more intense intraligand and charge transfer bands. From the spectra it can be concluded that two well separated high energy bands corresponding to spin allowed singlet  $\rightarrow$  singlet transitions have been observed with occasional presence of low energy spin forbidden bands. Many peaks and shoulders in the spectra are indicative of more than one type of cobalt center. The B value is reduced to 66% of the free ion value and  $Dq = 2336 \text{ cm}^{-1}$  indicates that the ligand  $\text{HL}^1$  provides a strong ligand field and bonds are more covalent [32] (Figure 7.2).

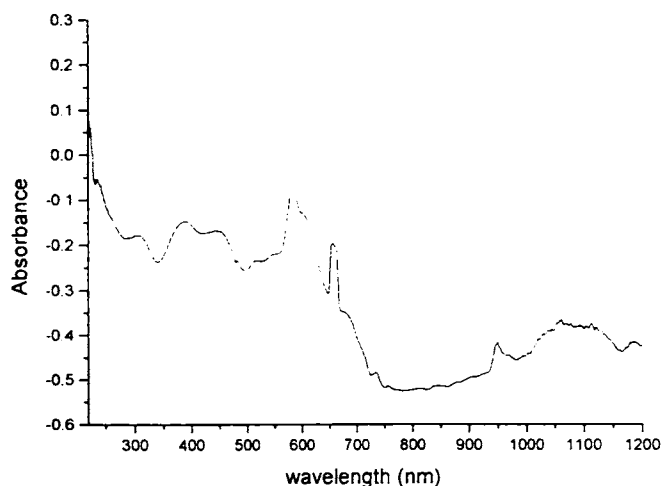


Figure 7.2. Electronic spectrum of  $[\text{CoL}^1_2]\text{Cl}\cdot 2\frac{1}{2} \text{H}_2\text{O}$  (20)

### 7.3.3 ${}^1\text{H}$ NMR spectra

Table 7.4 gives selected  ${}^1\text{H}$  NMR assignments for the ligand and cobalt(III) complexes in order to compare the coordinated, anionic ligand species in the

complex with free ligand molecule.  $^1\text{H}$  NMR spectral measurements are assigned as previously reported for di-2-pyridyl ketone *N*(4)-methyl and *N*(4), *N*(4)-dimethylthiosemicarbazone and its metal complexes [15]. The  $^1\text{H}$  NMR spectra of complexes when compared to that of free ligand point out that (i) *N*(4)H resonance is obtained at 15.00 ppm in free ligand disappears in the spectra of complexes suggesting deprotonation on complexation which supports the enolization and coordination through thiolate sulfur (ii) the deshielding of aromatic protons signals by 0.2 to 0.4 ppm on complexation. This is due to the electron withdrawal from the aromatic ring during the coordination of pyridyl nitrogen with the metal. The maximum downfield shift occurs with C(1)H from  $\delta \sim 8.71$  ppm in free ligand to  $\delta \sim 8.82$  ppm in complexes due to the coordination of pyridyl nitrogen to the cobalt(III) ion. (iii) The protons corresponding to the pyridyl rings of di-2-pyridyl ketone appear as separate signals in complexes, indicating its loss of equivalence due to imposition of a rigid geometry around the metal ion after complexation. This observation is consistent with the resonance of HL<sup>1</sup> protons with C(1)H and C(11)H at  $\delta = 8.71$  and 8.57 ppm (2H, doublet), C(2)H and C(10)H at  $\delta = 7.34$  and 7.28 ppm (2H, triplet), C(4)H and C(8)H at  $\delta = 8.07$  and 7.67 ppm (2H, doublet); C(3)H and C(9)H at  $\delta = 7.78$  ppm (2H, triplet), which on complexation resonate at different fields.. Due to the hydrogen bonding and CH--- $\pi$  interactions, the resonance absorptions of protons of the pyridyl ring are shifted further downfield. (Figure 7.3)

**Table 7.3**  
**Electronic (Diffuse reflectance) spectral data (cm<sup>-1</sup>) of cobalt(III) complexes of HL<sup>1</sup>**

Compound	<sup>1</sup> T <sub>1g</sub> ← <sup>1</sup> A <sub>1g</sub>	<sup>1</sup> T <sub>2g</sub> ← <sup>1</sup> A <sub>1g</sub>	<sup>3</sup> T <sub>1g</sub> ← <sup>1</sup> A <sub>1g</sub>	<sup>3</sup> T <sub>2g</sub> ← <sup>1</sup> A <sub>1g</sub>	$\pi^* \leftarrow \pi$	B(cm <sup>-1</sup> )	$\beta(B/B_0)$	Dq (cm <sup>-1</sup> )
HL <sup>1</sup>					36232, 35088			
[CoL <sub>2</sub> ]Cl (20) <sup>a</sup>	21929 w	25575 w	6729 w	18149 w	29155, 30864	731	0.66	2336
[CoL <sub>2</sub> ]NO <sub>3</sub> (21) <sup>a</sup>	22123 w	25316 w	6887 w	18018 w	30488s	737	0.67	2358

s= strong, m= medium, w = weak <sup>a</sup> hydrate waters are omitted for convenience, sh-shoulder

**Table 7.4** <sup>1</sup>H NMR spectral assignments ( $\delta$  ppm) of cobalt(III) complexes of HL<sup>1 a</sup>

Compound	N(4)H	C(1)H	C(2)H	C(3)H	C(4)H	C(8)H	C(9)H	C(10)H	C(11)H
HL <sup>1</sup>	14.89, 1H, s	8.71, 1H, d	7.34, 1H, t	7.78, 1H, t	8.07, 1H, d	7.67, 1H, d	7.78, 1H, t	7.28, 1H, q	8.57, 1H, d
[CoL <sub>2</sub> ]Cl (20) <sup>b</sup>	-----	8.82, 1H, d	7.55, 1H, t	7.87, 1H, t	8.06, 1H, d	7.79, 1H, d	8.02, 1H, t	7.48, 1H, t	8.28, 1H, d
[CoL <sub>2</sub> ]NO <sub>3</sub> (21) <sup>b</sup>	-----	8.82, 1H, d	7.46, 1H, q	7.80, 1H, q	8.06, 1H, d	7.80, 1H, q	8.02, 1H, t	7.46, 1H, q	8.28, 1H, d

All chemical shift values are expressed in unit of ppm.:<sup>a</sup> The numbering scheme is shown in Figure 2.1.<sup>b</sup> hydrate waters are omitted for convenience

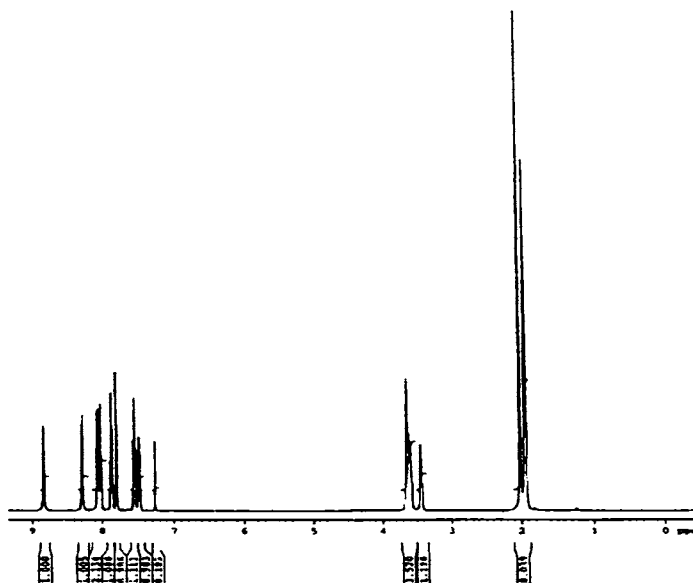


Figure 7.3.  $^1\text{H}$  NMR spectrum of the compound  $[\text{CoL}_2]\text{Cl}\cdot 2\frac{1}{2}\text{H}_2\text{O}$  (**20**)

The numbering scheme and tentative structure assigned to  $[\text{CoL}^1_2]\text{Cl}\cdot 2\frac{1}{2}\text{H}_2\text{O}$  (**20**) is shown in the Figure. 7.4

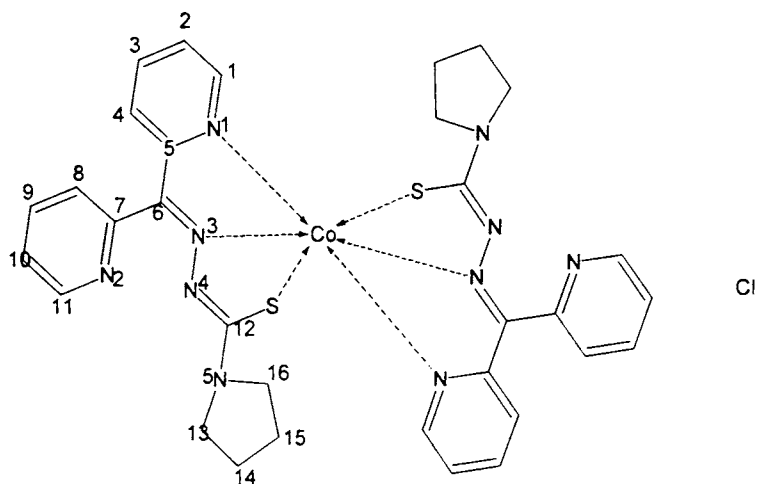


Figure 7.4. Structure of  $[\text{CoL}^1_2]\text{Cl}\cdot 2\frac{1}{2}\text{H}_2\text{O}$

#### 7.4. Concluding remarks

Cobalt(III) complexes of the ligand di-2-pyridyl ketone 3-tetramethyleneiminyl thiosemicarbazone ( $HL^1$ ) have been prepared with chloride and nitrate as counter ions. These complexes were analyzed by different physico-chemical methods. The stated quantities of cobalt(II) chloride, cobalt(II) nitrate with ligand  $HL^1$  in methanol gave products of composition  $[CoL_2]Cl \cdot 2\frac{1}{2}H_2O$  and  $[CoL_2]NO_3 \cdot 2\frac{1}{2}H_2O$ . Molar conductivity measurements in  $10^{-3}M$  DMF solution suggest that the gegenions are outside the coordination sphere. Both complexes are found to be diamagnetic at room temperature, confirming that cobalt is in the +3 oxidation state and hence corresponds to a  $d^6$  ion in a strong field. IR spectral data suggest that the ligand coordinates to the cobalt(III) ion through pyridyl nitrogen, azomethine nitrogen and thiolate sulfur.  $^1H$  NMR spectral data also supports the enolization of the ligand on complexation. Diffuse reflectance spectra of cobalt(III) complexes exhibit four d-d bands are consistent with an octahedral geometry. Hence it may be concluded that the potentially quadridentate ligand  $HL^1$  behaves as a tridentate one coordinating to cobalt(III) ion through pyridyl nitrogen, azomethine nitrogen and thiolate sulfur and the tentative structure proposed for complexes is octahedral.

**SYNTHESIS AND SPECTRAL CHARACTERIZATION OF  
ZINC(II) AND CADMIUM(II) COMPLEXES OF DI-2-  
PYRIDYL KETONE.3-  
TETRAMETHYLENEIMINYLTIOSEMICARBAZONE**

---

### 8.1. Introduction

The elements, zinc and cadmium have a  $d^{10}s^2$  electronic arrangement and typically form  $Zn^{2+}$  and  $Cd^{2+}$  ions. Because these ions have a complete  $d$  shell, they do not behave as transition elements. Both metal ions form complexes with O donor ligands and also with N and S donor ligands and with halide ions.  $Zn^{2+}$  and  $Cd^{2+}$  occur largely in four coordination spheres as tetrahedral complexes. Zinc and cadmium also form several octahedral complexes. The octahedral complexes of zinc are not very stable. But cadmium forms octahedral complexes readily and they are more stable than zinc complexes because of its larger size [181]. There are reports of zinc(II) and cadmium(II) complexes of 2-formylpyrrole thiosemicarbazone where metal atoms are tetracoordinated, ligands are neutral and sulfur monodentate [182]. Non-linear optical properties of zinc(II) complexes are also reported [183]. Non-linear optical materials exhibiting efficient second harmonic generation (SHG) at short wavelength are needed in the fields of high optical density recording, laser printing and optical measurement systems.

Heterocyclic thiosemicarbazones and salicylaldehyde and 2-hydroxyacetophenone thiosemicarbazone have been extensively studied because of their strong ability to form metal complexes [184] as tridentate ligands and their wide spectrum of biological applications [9]. Heterocyclic



thiosemicarbazones are important because of their greater versatility as ligands, with several donor atoms, their flexibility and ability to coordinate in either neutral or deprotonated forms. It was suggested that zinc fingers may be a very common feature in many protein- (DNA-RNA) interactions. Further researches in this field revealed that efficient modeling of metal sites in enzymes requires designing of polydentate ligands having nitrogen and sulfur donors are the donor units for the protein environment. This is specifically so for zinc enzymes [185-187]. The NNS donor ligand uses all these monodentate functions and encapsulates the zinc ion. In this Chapter we report the syntheses, and spectral characterization of zinc(II) and cadmium(II) complexes of the ligand, di-2-pyridyl ketone 3- tetramethyleneiminylthiosemicarbazone (HL<sup>1</sup>).

## 8.2. Experimental

### 8.2.1. *Materials and methods*

Thiosemicarbazone (HL<sup>1</sup>) is prepared as described in Chapter 2. Zinc(II) chloride, zinc(II) nitrate, zinc(II) acetate, sodium azide, potassium thiocyanate of A.R grade (Merck) were used without any prior purification. Zinc complexes are prepared in methanol and cadmium complex in ethanol medium. The solvents were purified by standard procedures.

### 8.2.2. *Physical measurements*

Details regarding physical measurements are presented in Chapter 3. <sup>1</sup>H NMR spectra were recorded in an AMX 400 MHz FT-NMR Spectrometer using CDCl<sub>3</sub> as a solvent and TMS as an internal standard at Sophisticated Instruments Facility, Indian Institute of Science, Bangalore, India.

### 8.2.3. *Synthesis of complexes*

#### 8.2.3. *Synthesis of zinc(II) complexes*

Zinc(II) complexes were prepared by refluxing an equimolar solution of the ligand (HL<sup>1</sup>) (0.5 mmol, 0.174 g) in 20 ml of hot methanol and the

corresponding zinc(II) salt (0.5 mmol) in methanol for two hours. Azido and thiocyanato complexes were prepared by refluxing an equimolar mixture of ligand and zinc(II) acetate in hot methanol and to the refluxing solution, sodium azide or potassium thiocyanate was added in portions in the same molar ratio. On slow evaporation at room temperature, yellow crystals of complexes were separated out, which were collected, washed with water, followed by ether and dried over  $P_4O_{10}$  *in vacuo*.

#### 8.2.3.2. Synthesis of cadmium(II) complex

A solution of the thiosemicarbazone  $HL^1$  (10 mmol) dissolved in 20 ml methanol was mixed with a solution of cadmium(II) acetate (5mmol) dissolved in the same solvent. The solution was heated under reflux for 2 hours. The resulting solution was allowed to stand at room temperature. On slow evaporation pink crystals of complex separated out, which were collected by filtration, washed with water followed by ether and dried over  $P_4O_{10}$  *in vacuo*.

We have synthesized five zinc complexes, with empirical formula  $[ML^1X]$  where  $X = Cl$  (**22**),  $NO_3$  (**23**),  $OAc$  (**24**),  $N_3$  (**25**),  $SCN$  (**26**) and one cadmium(II) complex  $[Cd(HL^1)(L^1)] OAc$  (**27**)

### 8.3. Results and discussion

All zinc(II) complexes are yellow and the cadmium complex is pink, soluble in solvents like dichloromethane, chloroform, DMF and DMSO. Partial elemental analyses data of zinc(II) complexes are consistent with the 1:1:1 ratio of the metal:thiosemicarbazone:gegenion and that of cadmium(II) complex agrees good with the 1:2 molar ratio of metal: thiosemicarbazone (Table 8.1). The analyses values indicate that all zinc complexes are four coordinate and the cadmium complex is six coordinate in geometry. In zinc(II) complexes the fourth coordination site is occupied by mono or polyatomic anion. Molar conductivity measurements in  $10^{-3}$  (M) DMF solution reveal that gengenions are in the coordination sphere

Table 8.1

Colors, partial elemental analysis, and molar conductivities of zinc (II) and cadmium(II) complexes with HL<sup>1</sup>.

Compound	Empirical formula	Color	Composition% (Found/Calcd)			$\lambda_M^a$
			Carbon	Hydrogen	Nitrogen	
HL <sup>1</sup>	C <sub>16</sub> H <sub>17</sub> N <sub>3</sub> S	Yellow	62.10 (62.70)	5.56 (5.46)	22.43 (22.53)	16
[ZnL <sup>1</sup> Cl]·2H <sub>2</sub> O (22)	C <sub>16</sub> H <sub>20</sub> ZnN <sub>5</sub> ClO <sub>2</sub> S	Yellow	42.95 (42.96)	3.88(4.48)	15.27 (15.66)	25
[ZnL <sup>1</sup> NO <sub>3</sub> ] (23)	C <sub>16</sub> H <sub>16</sub> ZnN <sub>6</sub> O <sub>3</sub> S	Yellow	44.03 (43.89)	3.75 (3.65)	18.94 (19.20)	10
[ZnL <sup>1</sup> (OAc)]·½H <sub>2</sub> O (24)	C <sub>18</sub> H <sub>20</sub> ZnN <sub>5</sub> O <sub>2.5</sub> S	Yellow	48.74(48.71)	4.55(4.51)	15.05(15.78)	22
[ZnL <sup>1</sup> N <sub>3</sub> ]·½H <sub>2</sub> O (25)	C <sub>16</sub> H <sub>17</sub> ZnN <sub>8</sub> O <sub>0.5</sub> S	Yellow	45.76(45.03)	3.92(3.98)	25.69(26.26)	18
[ZnL <sup>1</sup> SCN]·½H <sub>2</sub> O (26)	C <sub>17</sub> H <sub>17</sub> ZnN <sub>6</sub> O <sub>0.5</sub> S <sub>2</sub>	Yellow	46.65(47.11)	3.80(3.84)	18.91(18.99)	22
[Cd(HL <sup>1</sup> )(L <sup>1</sup> )]OAc (27)	C <sub>34</sub> H <sub>36</sub> CdN <sub>10</sub> O <sub>2</sub> S <sub>2</sub>	Pink	51.47(51.49)	4.28(4.54)	17.69(17.67)	

<sup>a</sup> Molar conductivity, 10<sup>-3</sup> at 298 K

### 8.3.1. Infrared spectra.

Selected IR bands are listed in Table 8.2 and 8.3. The spectra of compounds **23**, **25**, **26**, and **27** are shown in Figures 8.1 and 8.2. The broad band at  $3428\text{ cm}^{-1}$ , probably arise from the O-H stretching mode of uncoordinated water molecules. A medium band at  $3049\text{ cm}^{-1}$ , which is assigned to  $\nu(\text{N-H})$  vibration in the ligand is found absent in zinc(II) complexes, which is consistent with the deprotonation of the ligand on complexation. In the cadmium complex, a shoulder at  $3049\text{ cm}^{-1}$  due to  $\nu(\text{N-H})$  suggests that the ligand exists in the thione form. Bands ranging from  $1600\text{-}1350\text{ cm}^{-1}$  suffers a significant shift in the spectra of complexes can be attributed to  $\nu(\text{C}=\text{C})$  and  $\nu(\text{C}=\text{N})$  vibrational modes, and their mixing patterns are different from those present in the ligand spectrum. The band corresponding to azomethine nitrogen,  $\nu(\text{C}=\text{N})$  in the free ligand at  $1582\text{ cm}^{-1}$  shifts to higher wavenumbers by  $\sim 10\text{-}20\text{ cm}^{-1}$  on complexation is indicative of azomethine nitrogen coordination [106, 115, 116]. The positive shift in  $\nu(\text{C}=\text{N})$  can be attributed to the combination of  $\nu(\text{C}=\text{N})$  and newly formed  $\text{N}=\text{C}$  frequencies suggesting that sulfur is in the thiolate form. The enolization is further supported by an increase in the  $\nu(\text{N}-\text{N})$  frequency by  $10\text{-}12\text{ cm}^{-1}$ .

Weak bands at  $1290$  and  $785\text{ cm}^{-1}$  are due to  $\nu(\text{C}=\text{S})$  and  $\delta(\text{C}=\text{S})$  vibrations in the complexes. These bands are found at lower values than that of the corresponding frequencies of free ligand. The downfield shift of bands in complexes corresponding to  $\nu(\text{C}=\text{S})$  and  $\delta(\text{C}=\text{S})$  in free ligands can be attributed to change of bond order and strong electron-delocalization upon chelation [117]. A medium band  $\sim 390\text{ cm}^{-1}$  corresponds to  $\nu(\text{Zn-N})$  stretching vibration in all compounds indicates the coordination of azomethine nitrogen to the metal ion [34]. A weak band at  $\sim 340\text{ cm}^{-1}$  is indicative of  $\nu(\text{Zn-N}_{\text{pyridyl}})$  vibration in all complexes.

The metal-chlorine frequency in the chloro complex (**22**) appears at  $320\text{ cm}^{-1}$ . For the compound **23**, bands at  $1500$ ,  $1300$ ,  $992$ , and  $230\text{ cm}^{-1}$  corresponds

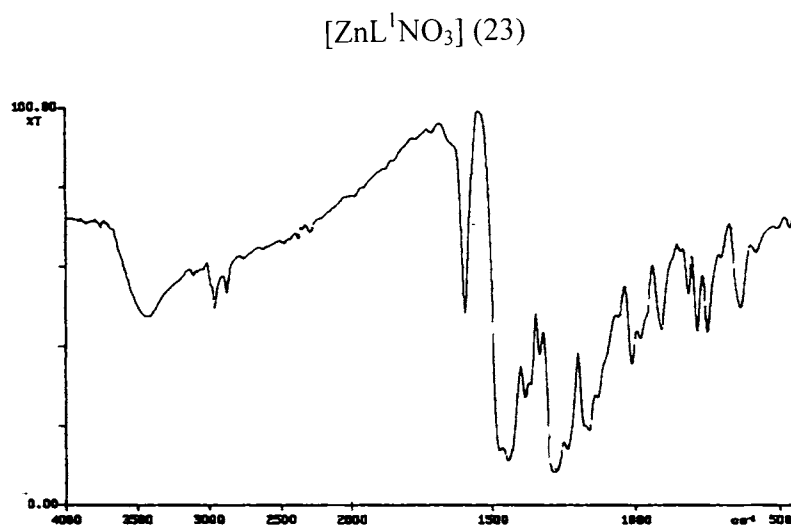
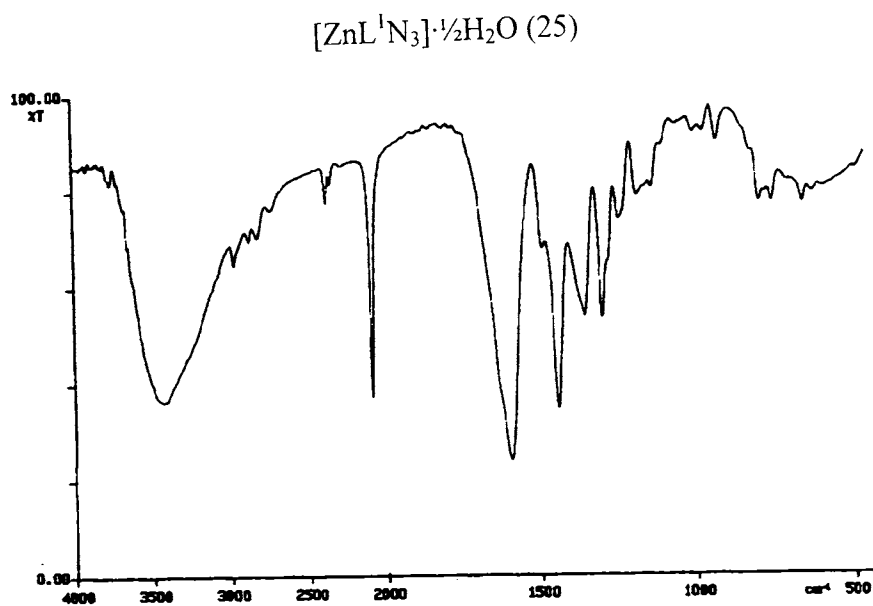


Figure 8.1. Infrared spectrum of compounds 23 and 25

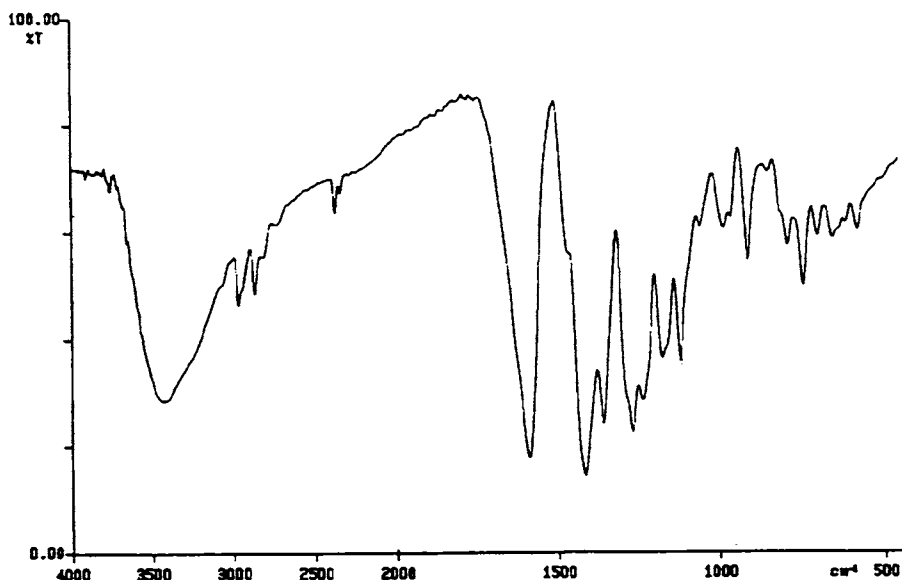


Figure 8.2. IR spectrum of  $[\text{Cd}(\text{HL}^1)(\text{L}^1)] \text{OAc } 27$

to different NO stretching frequencies of the coordinated nitrate group. Azido complex (**25**) exhibits a strong band at  $2054 \text{ cm}^{-1}$  corresponding to the  $\nu_a(\text{NNN})$  stretching vibration [34] of the coordinating azido group. The broad bands at  $636$  and  $353 \text{ cm}^{-1}$ , assigned to  $\delta(\text{NNN})$  and  $\nu(\text{Zn-N})$  respectively [34], suggesting that  $\text{Zn-N-N-N}$  is not linear. The thiocyanato complex (**26**) shows a sharp band at  $2067 \text{ cm}^{-1}$ , which is assigned to  $\nu(\text{C-N})$  of the thiocyanato group, indicating coordination through the nitrogen of the thiocyanato group [125]. A single sharp band near  $480 \text{ cm}^{-1}$  corresponding to  $\delta(\text{NCS})$  of the thiocyanato group further supports nitrogen coordination of the thiocyanato anion with the zinc center [34]. For the compound **24**, the band at  $1600$  and  $1439 \text{ cm}^{-1}$  correspond to symmetric and asymmetric stretching vibrations of the acetato group are consistent with the presence of a monodentate acetato group [106]. The band at  $1600 \text{ cm}^{-1}$  is very intense, is a combination of  $\nu(\text{C=N})$  and

**Table 8.2**  
**IR spectral assignments ( $\text{cm}^{-1}$ ) of zinc(II) and cadmium(II) complexes with HL<sup>1</sup>**

Compound	$\nu(\text{C}=\text{N})^+$									
	$\nu(\text{N}-\text{H})$	$\nu(\text{N}=\text{C})$	$\nu(\text{N}-\text{N})$	$\nu(\text{C}=\text{S})$	$\delta(\text{C}=\text{S})$	$\delta(\text{o.p.})$	$\nu(\text{M}-\text{N})$	$\nu(\text{M}-\text{S})$	$\nu(\text{M}-\text{N})\text{py}$	$\nu(\text{M}-\text{X})^a$
HL <sup>1</sup>	3049m	1582s	1000m	1330 s	808m	638 s	-----	-----	-----	-----
[ZnL <sup>1</sup> Cl]·2H <sub>2</sub> O (22)	-----	1595s	1050 m	1292 w	800 m	623 m	385 sh	298 s	340w	3200 w
[ZnL <sup>1</sup> NO <sub>3</sub> ] (23)	-----	1594 s	1014 m	1283 w	783m	634 m	390 sh	279 m	345 w	305 m
[ZnL <sup>1</sup> (OAc)]·½H <sub>2</sub> O(24)	-----	1600 s	1014 w	1291 w	786 m	631 m	380 w.	290 m	344 ws	353 w
[ZnL <sup>1</sup> N <sub>3</sub> ]·½H <sub>2</sub> O (25)	-----	1597 s	1020 w	1291 w	786 w	636 m	395 w	281 m	347w	-----
[ZnL <sup>1</sup> SCN]·½H <sub>2</sub> O(26)	-----	1597 s	1020 w	1276 w	784 w	640 m	380 w	270 m	350 w	---
[Cd(HL <sup>1</sup> )(L <sup>1</sup> )] OAc (27)	3050 sh	1589 s	981 w	1270 m	788 m	651 w	397 m	290 m	376 m	352 m

s=strong, m= medium, w= weak. All values are reported in  $\text{cm}^{-1}$ . X<sup>a</sup>=Cl, NO<sub>3</sub>, CH<sub>3</sub>COO, N<sub>3</sub>, NCS.

**Table 8.3**  
**IR spectral assignments for the polyatomic anions in the zinc(II) complexes and cadmium complex with HL<sup>1</sup>**

Compound	Mode of coordination		$\nu_1$	$\nu_2$	$\nu_3$
<b>Nitrato complexes</b>					
[ZnL <sup>1</sup> NO <sub>3</sub> ] (23)	unidentate		992m	1300s	1500s
<b>Azido complexes</b>					
[ZnL <sup>1</sup> N <sub>3</sub> ] (25)	unidentate		$\nu_a(\text{NNN})$ 2054 s	$\nu_s(\text{NNN})$ 1370 m	$\delta(\text{NNN})$ 636 m
<b>Thiocynato complex</b>					
ZnL <sup>1</sup> SCN](26)	unidentate		$\nu(\text{CN})$ , 2067s	$\nu(\text{CS})$ 784 m	$\delta(\text{NCS})$ 480 w
<b>Acetato complex</b>					
[ZnL <sup>1</sup> (OAc)] (24)	unidentate		$\nu_a(\text{CH}_3\text{COO})$ 1600,s	$\nu_s(\text{CH}_3\text{COO})$ 1329 m	$\nu(\text{Cu}-\text{N})_{\text{thiocyanato}}$

s=strong, m= medium, w= weak, All values are reported in  $\text{cm}^{-1}$ . \* hydrate waters are omitted for convenience

**Table 8.4**  
Electronic spectral assignments ( $\text{cm}^{-1}$ ) of  $\text{HL}^1$  and its zinc(II) and the cadmium(II) complex

Compound	$\pi^* \leftarrow \pi$	$\pi^* \leftarrow n$	LMCT
$\text{HL}^1$	36232, 35088	29155, 30864	
$[\text{ZnL}^1\text{Cl}]\cdot 2\text{H}_2\text{O}$ (22)	36765m	31153s,b	27933 sh, 23641 s
$[\text{ZnL}^1\text{NO}_3]$ (23)	31348 s	31348 s,b	23585 s
$[\text{ZnL}^1(\text{OAc})]\cdot \frac{1}{2}\text{H}_2\text{O}$ (24)	35461 m	31949 s	25641 sh, 23810 s
$[\text{ZnL}^1\text{N}_3]\cdot \frac{1}{2}\text{H}_2\text{O}$ (25)	31646 s	316 s,b	23641 s
$[\text{ZnL}^1\text{SCN}]\cdot \frac{1}{2}\text{H}_2\text{O}$ (26)	31847 s	31847 s	23641 s,b
$[\text{Cd}(\text{HL}^1)(\text{L}^1)]\text{OAc}$ (27)	35335 m	31056 s	23641 s

**Table 8.5**  
 $^1\text{H}$  NMR spectral assignments of zinc(II) complexes and cadmium(II) complex with  $\text{HL}^1$

Compound	Solvent	N(4)H	C(1)H	C(2)H	C(3)H	C(4)H	C(8)H	C(9)H	C(10)H	C(11)H	C(13H)- C(16)H
$\text{HL}^1$	$\text{CDCl}_3$	14.89, 1H,s	8.71, 1H,d	7.34, 1H,t	7.78, 1H,t	8.07, 1H,d	7.67, 1H,d	7.78, 1H,t	7.28, 1H,q	8.57, 1H,d	3.87-2.05
$[\text{ZnL}^1\text{Cl}]$ (22)	$\text{CDCl}_3$	-----	9.48, 1H,d	7.65, 1H,t	7.95, 1H,t	8.11, 1H,t	7.88, 1H,d	7.95, 1H,t	7.65, 1H,t	8.89, 1H,d	3.95-2.05
$[\text{ZnL}^1\text{NO}_3]$ (23)	$\text{CDCl}_3$	-----	9.22, 1H,d	6.96, 1H,t	7.66, 1H,t	8.43, 1H,t	8.43, 1H,t	7.33, 1H,t	6.74, 1H,d	7.50, 1H,d	3.75-2.75
$[\text{ZnL}^1(\text{OAc})]$ (24)	$\text{CDCl}_3$	-----	9.63, 1H,d	6.87, 1H,t	7.53, 1H,p	7.97, 1H,t	7.30, 1H,p	7.53, 1H,p	6.87, 1H,d	8.19, 1H,t	3.05-2.05
$[\text{ZnL}^1\text{N}_3]$ (25)	$\text{CDCl}_3$	-----	9.38, 1H,s	7.33, 1H,t	7.67, 1H,t	8.05, 1H,d	8.05, 1H,d	7.45, 1H,t	6.91, 1H,t	8.05, 1H,d	3.6-2.7
$[\text{Cd}(\text{HL}^1)(\text{L}^1)]\text{OAc}$ (27)	$\text{CDCl}_3$	-----	8.75, 1H,d	7.09, 1H,sep	7.84, 1H,p	7.51, 1H,d	7.30, 1H,se	7.84, 1H,p	7.09, 1H,sep	8.27, 1H,d	3.45-3.93

All chemical shift values are expressed in ppm  
\* hydrate waters are omitted for convenience



$\nu_a(\text{CH}_3\text{COO})$  stretching vibrations. These observations are consistent with the work on zinc(II) complexes of di-2-pyridyl ketone thiosemicarbazone prepared in our laboratory [175].

### 8.3.2. *Electronic spectra*

Solid-state electronic spectra of compounds were determined in the region 200-900 nm. The data are listed in Table 8.4. The ligand ( $\text{HL}^1$ ) has absorption maximum at 36232 and 35088  $\text{cm}^{-1}$  due to  $\pi^* \leftarrow \pi$  of the pyridyl ring and the imine function of thiosemicarbazone moiety respectively. There are two bands at 29155 and 30864  $\text{cm}^{-1}$  corresponding to  $\pi^* \leftarrow n$  transition of the pyridyl nitrogen and thioamide function respectively. These bands suffer marginal shifts on complexation. The shift of the  $\pi^* \leftarrow \pi$  bands to the longer wavelength region is the result of the C=S bond being weakened and conjugation system being enhanced after the formation of the complex

### 8.3.3. *$^1\text{H}$ NMR spectra*

$^1\text{H}$  NMR spectral measurements are assigned as previously reported on di-2-pyridyl ketone N(4)-methyl and N(4)-dimethyl thiosemicarbazone and its metal complexes [141]. The signal due to N(4)H resonance is obtained downfield at 15.0 ppm in the free ligand as depicted in Table 8.5. The large downfield shift of this proton indicates its involvement in hydrogen bonding with the pyridyl nitrogen. The non-appearance of N(4)H signal in the spectra of zinc(II) complexes shows that the ligand is deprotonated on complexation which supports the enolization and coordination of sulfur to zinc(II). The non appearance of the N(4)H signal in cadmium complex shows that the ligand deprotonated in  $\text{CDCl}_3$  solution. The signals corresponding to aromatic protons are shifted downfield by 0.2 to 0.4 ppm on complexation. This is due to the electron withdrawal from the aromatic ring during the coordination of pyridyl nitrogen with the metal. The protons corresponding to the pyridyl rings of di-2-pyridyl ketone appear as separate signals in complexes, indicating its loss of equivalence due to imposition of a rigid geometry around the metal ion after

complexation. This observation is consistent with the resonance of HL<sup>1</sup> protons with C(1)H and C(11)H at  $\delta = 8.71$  and  $8.57$  ppm (2H, doublet), C(2)H and C(10)H at  $\delta = 7.34$  and  $7.28$  ppm (2H, triplet), C(4)H and C(8)H at  $\delta = 8.07$  and  $7.67$  ppm (2H, doublet); C(3)H and C(9)H at  $\delta = 7.78$  ppm (2H, triplet), which on complexation resonate at different fields. There is significant downfield shift of the proton alpha to pyridyl nitrogen. It is also observed that some protons in the pyridyl ring of both zinc and cadmium complexes suffer an upfield shift from that of free ligand, which is due to the electron transfer from filled metal  $3d$ -orbitals to the vacant  $\pi^*$  antibonding orbital of the ligand or due to the loss of hydrogen bonding. <sup>1</sup>H NMR spectrum of compound **23** is shown in Figure 8.3. and the tentative structures of the compounds **22** and **27** are given in Figure 8. 4.

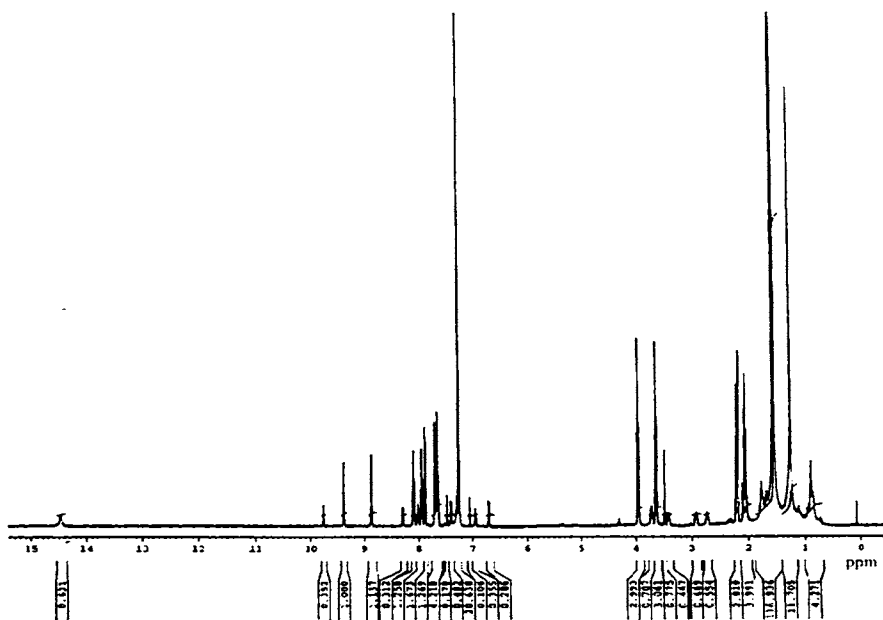


Figure 8.3. <sup>1</sup>H NMR spectrum of  $[ZnL'Cl]$  (**22**)

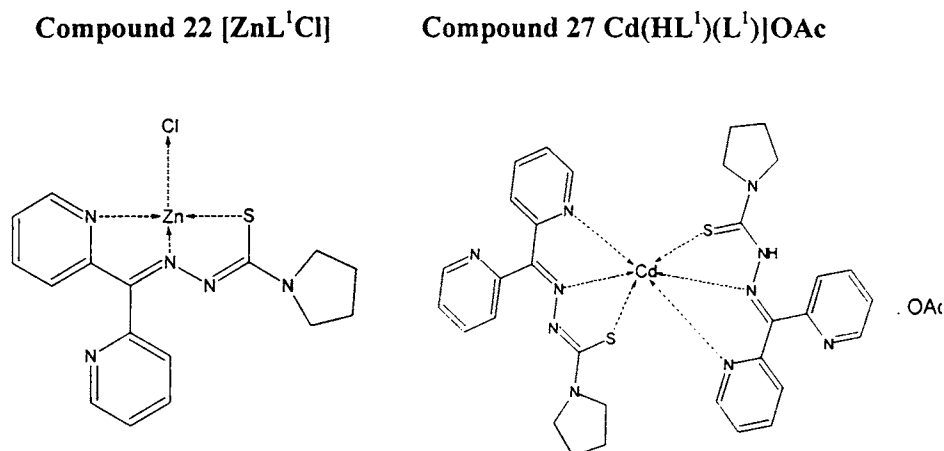


Figure. 8.4. Tentative structures of **22** and **27**

#### 8.4. Concluding remarks

The physico-chemical measurements suggest that the ligand is tridentate in nature. Conductivity measurements show that complexes are non-electrolytes in DMF except **27** (which is a 1:1 electrolyte) indicating that the gegenions are in the coordination sphere. Infra red spectral data further supports the tridentating nature of the ligand, coordinating to the metal ion through pyridyl nitrogen, azomethine nitrogen and thiolate sulfur. As per the elemental data, conductivity measurements, electronic and <sup>1</sup>H NMR spectra, a square planar structure is suggested for zinc(II) and an octahedral structure for cadmium(II) complexes. The tentative structures of the zinc(II) complex (**22**) and the cadmium(II) complex (**27**) (Figure 8.4) are shown below.

## REFERENCES

- [1] F. Baslo, R. G. Pearson, Mechanism of Inorganic Reactions, Wiley Eastern Company Ltd, New Delhi (1973).
- [2] F.,A. Cotton, R. G. Wilkinson, Advanced Inorganic Chemistry., 5<sup>th</sup> Ed, Wiley Eastern Company Ltd, New Delhi (1973).
- [3] M. A. Ali, S. E. Livingstone, Coord. Chem. Rev.13 (1974) 101.
- [4] S. E. Livingstone, Quart. Rev. Chem. Soc. 19 (1965) 386.
- [5] D. L. Klayman, J. F. Bartosevich, T. S. Griffin, C. J. Mason, J. P. Scovill, J. Med. Chem. 22 (1979) 855 and references therein.
- [6] E. J. Blanz Jr, F.A. French, Cancer Res. (1968).
- [7] A. S. Dobek, D. L. Klayman, E. J. Dickson Jr, J. P. Scovill, E. C. Tramont, Antimicrob. Agents. Chemoether. 18 (1980) 27 and references therein.
- [8] S. P. Mittal, S. K. Sharma. R. V. Singh, J. P Tandon, Curr Sci. 50 (1981) 483 and references therein.
- [9] S. Padhye, G. B. Kauffman, Coord. Chem. Rev. 63 (1985) 127.
- [10] D. X. West, H. Gebremedhin, R. J. Butcher, J. P. Jasinski, A. E. Liberta, Polyhedron. 12 (1993) 2489 and references therein.
- [11] P. Domino, G. G. Fava, M. Nardelli, P. Sagarabotto, Acta Crystallogr. 25B (1969) 343; G. D. Andreetti, G. G. Fava, M. Nardelli, P. Sagarabotto, Acta Crystallogr 26B (1970) 1005.
- [12] V. I. Gerasimov, M. D. Revenko, V. M. Golyshu, N. V. Gerbeleri, N. V. Belov, Kristallografiya. 21 (1976) 399.
- [13] F. Tui, K.E. Turta, N. V.Gerbeleri, Russ. J. Inorg. Chem. 2 (1977) 1497.
- [14] A. V. Ablov, N. I. Belichuk, Russ. J. Inorg. Chem.8 (1963) 38.
- [15] B. S. Garg, M. R. P. Kurup. S. K. Jain, Y. K. Bhoon, Transition. Met. Chem. 16 (1991) 111.

## References

- [16] J. K. Swearingen, D. X. West, *Transition. Met. Chem.* 26(3) (2001) 252.
- [17] U. N. Shetti, V. K. Revankar, V. B. Mahale, *Proc. Indian. Acad .Sci (Chem.Sci).* 109 (1977) 7.
- [18] D. X. West, J. S. Ives, G. A. Bain, A. E. Liberta, J. Valdies- Martinez-Ortega, *Polyhedron* 19 (1997) 1895.
- [19] C. Y. Duan, B. Wu, T. C. Mak, *J. Chem. Soc., Dalton Trans.* (1996) 3485.
- [20] M. Mohan, P. Sharma, N. K. Jha, *Inorg. Chim. Acta* 9 (1980) 125.
- [21] I. Cogi, A. M. M. Lanfredi, A. Tiripicchipo, *J.Chem.Soc.,Perkin Trans. 2* (1976) 1808.
- [22] V. N. Byushkin, Y. M. Chumakov, N. M. Samus, I. O. Baka, *Z. Strukt Khim.* 28 (1987) 140.
- [23] D. X. West, G. A. Bain, R. J. Butcher, J. P. Jasinski, Y. Li, R. Y. Pozdникav, J. Valdies-Martinez, R. A. Toscano, S. Hernandez-Ortega, *Polyhedron* 15 (1996) 665.
- [24] B. S. Garg, M. R. P. Kurup, S. K. Jain, Y. K. Bhoon, *Transition Met. Chem.* 13 (1988) 247.
- [25] B. S. Garg, M. R. P. Kurup, S. K. Jain, Y. K. Bhoon, *Transition Met. Chem.* 13 (1988) 92.
- [26] A. Sreekanth. M. R.P. Kurup, *Polyhedron* 23 (2004), 969.
- [27] R. P. John, A. Sreekanth, M. R. P. Kurup, A. Usman, A. R. Ibrahim, H. K. Fun, *Spectrochim. Acta Part A* 59 (2003) 1349.
- [28] M. E. Hossain, M. N. Alam, J. Begum, M. A. Ali, M. Nazimuddin, F. E. Smith, R.C. Hynes, *Inorg. Chim. Acta* 249 (1996) 217.
- [29] R. Raina, T. S. Srivastava, *Indian. J. Chem.* 22A (1983) 701.
- [30] N. K. Jain, B. S. Garg, *Transition.Met.Chem.* 11 (1986) 89.
- [31] B. J. Hathaway, D. E. Billing, *Coordin. Chem. Rev.* 5 (1970) 143.
- [32] B. N. Figgis, *Introduction To Ligand Field*, Interscience, New York (1966).

## References

- [33] A. B. P. Lever, *Inorganic Electronic Spectroscopy*, 2<sup>nd</sup> Ed, Elsevier, New York (1984).
- [34] K. Nakamoto, *Infrared and Raman Spectra of Coordination Compounds*, 3<sup>rd</sup> Ed., John Wiley and Sons, New York (1978).
- [35] B. Dogmak, R. Behnisch, F. Mietzsch, H. Schmidt, *Naturwissenschaften*. 33 (1946) 315.
- [36] J. C. Logan, M. P. Fox, J. H. Morgan, A. M. Makhon, C. J. Pfau, *J. Gen. Virol.* 28 (1975) 271.
- [37] S. J. Lippard., I. Bertini, H. B. Grany, J. S. Lippard, *Bioinorganic Chemistry: Metals in Medicine*, University Science Books, 1 (1994) 207.
- [38] R. W. Brockman, J. R. Thomson, M. J. Bell, H. E. Skipper, *Cancer Res.* 16 (1956) 167.
- [39] E. J. Blanz Jr, F. A. French, J. R. DoAmral D. A. French, *J. Med. Chem.* 13 (1970) 1124.
- [40] D. X. West, C. E. Ooms, J. S. Saleda, H. Gebremedhin, A.E Liberta, *Transition .Met. Chem.* 19 (1994) 553.
- [41] A. E.Liberta, D. X. West, *Biometals.* 5 (1992) 121.
- [42] D. X. West, J. S. Ives, J. Krejici, M. M. Salberg, T. L. Zumbahlen, G. A. Bain, A. E. Liberta, J. Valdes-Martinez, S. Hernandez-Ortega, R. A Toscano, *Polyhedron* 14 (1995) 2189 and references therein.
- [43] S.Sivakumar, Ph.D. thesis, Cochin University of Science & Technology, 2003.
- [44] J. G. Cory, A. E. Fleischer, *Cancer. Res.* 39 (1979) 4600.
- [45] A. C Satorelli, K. C. Agrawal, A. S. Tsftsoglou and E.C. Moore, *Advances in enzyme regulation.* 15 (1977) 117.
- [46] M. Caron, W. F. Bendict, *Science.* 178 (1972) 62.
- [47] D. X. West, A. C. Whyte, F. D. Sharif, H. Gebremedhin A.E. Liberta, *Transition Met. Chem.* 18 (1993) 238.
- [48] K. R. Koch, *J. Coord. Chem.* 22 (1991) 289.

## References

- [49] D. X. West, M. K. Lockwood, A. E. Liberta, Xin Chen, R. D. Robert, *Transition Met Chem.* 18 (1993) 221.
- [50] L. A. Saryan, E. Ankel, C. Krishnamurthi, D. H. Petering, H. Elford. *J. Med Chem.* 22 (1979) 1218.
- [51] R. W. Brockman, J. R. Thomson, M. J. Bell, H. E. Skipper, *Cancer Res.* 21 (1956) 349.
- [52] F. A. French, E. J. Blanz Jr, *Cancer Res.* 26 (1966) 1638.
- [53] F. A. French, E. J. Blanz Jr. *J. Med. Chem.* 9 (1966) 385.
- [54] K. C Agrawal, A. C Sartorelli, G. P. In Ellis, G. B. West (Eds), *Progress in Medicinal Chemistry*, Elsevier 15 (1978) 321.
- [55] D. H. Petering, H. In Sigel (ed), *Metal ions in Biological systems*, Marcel Dekker 11 (1973) 198.
- [56] D. Hamre, K. Brownlee, R. Donovanick, *J. Immunol.* 67 (1950) 305.
- [57] D. Hamre, J. Bernstein, R. Donovanick, *Proc Soc Exp Biol Med.* 73 (1950) 275.
- [58] D. Bauer, *Br Jexp Pathol.* 36 (1955) 105.
- [59] D. Bauer, P. Sadler, *Nature (London).* 190 (1961) 1167.
- [60] D. Bauer, K. Dumbell, P. Fox-Hulme, P. Sadler, *Bull WHO* 26 (1962) 772.
- [61] D. Bauer, P. Sadler, *Lancet* 1 (1960) 1110.
- [62] D. Bauer, L. St. Vincent, C. Kempe, A. Downie, *Lancet* 2 (1963) 494.
- [63] D. Bauer, W. Levinson, W. A Corter, *Ion Selective Inhibitors of Viral Infections* (Ed), CRS press 213 (1972).
- [64] C. Shipman Jr, S. H Smith, J .C. Drach, D.L Klayman, *Antimicrob Agents Chemother.* 19 (1981) 682.
- [65] B. Christenson, J. R. Rodriguez, H.F. Gorbea, C.H. Ramirez-Ronda. *Antimicrob. Agent Chemother.* 27 (1985) 570.
- [66] C. E. Emery, F. A. Stancato, R. E. Brown, D. A. Prichard, A. D. Wolf. *Life Sci* 33 (1983) 1285.
- [67] D. L. Klayman, A. J. Lin, *Org. Prep. Proc. Int.* 16 (1981) 79.

## References

- [68] J. P.Scovill, Phosphrous Sulfur Silicon. 60 (1991) 25.
- [69] A. Usman, I. A. Razak, S. Chantrapomma, H. K. Fun, V. Philip. A. Sreekanth, M. R. P. Kurup, Acta Crystallogr.C 58 (2002) 0652.
- [70] Siemens, SMART and SAINT, Area Detector Control and Integration Software., Siemens Analytical X-ray Instruments Inc., Madison, Wisconsin, USA (1996).
- [71] G. M. Sheldrick, SADABS, Program for Empirical absorption correction of Area, Detector Data, University of Göttingen, Göttingen, Germany (1997).
- [72] G. M. Sheldrick, Acta Crystallogr. A 46 (1990) 467.
- [73] G. M. Sheldrick, SHELXS-97, Program for the Solution of Crystal Structures, University of Göttingen: Göttingen, Germany (1997).
- [74] A. L. Speck, PLATON, A Multipurpose Crystallographic Tool, Utrecht University, Utrecht, The Netherlands (1999).
- [75] R. H. Blessing, Acta. Crystallogr. A (1995) 33.
- [76] F. H. Allen, O. Kennard, D. G. Watson, L. Brammer, A. G. Orpen, R. Taylor, J. Chem. Soc., Perkin.Trans. 2 (1987) S1-19.
- [77] G. J. Palenik, D. F. Rendle, W. S Carter, Acta. Crystallogr. B 30 (1974) 2390.
- [78] R. Restivo, G. J. Palenik, Acta Crystallogr.Section B 26 (1970) 1397.
- [79] E. J. Gabe, M. R Taylor, J. P. Glusker, J. A. Minkin, A. L. Patterson, Acta Crystallogr. Section B 25 (1969) 1620.
- [80] L. E. Sutton, Tables of Interatomic Distances on Configuration in Molecules and Ions, Supplement, The Chemical Society, London (1965).
- [81] S. K. Jain, B. S Garg, Y. K.Bhoon, D. L. Klayman, J. P Scovill, Spectrochim. Acta 41A (1985) 407
- [82] M. R. P. Kurup, Marthakutty Joseph, Unpublished Results.
- [83] M. R. P. Kurup. P. F. Raphel, Unpublished Results.
- [84] D. X. West, J. K. Swearingen, A. K. El-Swaf, Transition Met. Chem. 25 (2000) 87.



## References

- [85] D. X. West, C. S. Carlson, K. J. Bouck, A.E Liberta, *Transition Met. Chem.* 16 (1996) 271.
- [86] D. X. West, B.L Mokijewski, H. Gebremedin, T. J Romak, *Transition Met. Chem.* 17 (1992) 384.
- [87] D. X. West, A. M. Stark, G. A Bain and A. E Liberta, *Transition Met. Chem.* 21 (1996) 289.
- [88] D. X. West, I. S. Billeh, G. A. Bain, J. Valdes-Martinez, K. H. Ebert, S. Hernandez-Ortega, *Transition Met. Chem* 21 (1996) 572.
- [89] E. Lukevics, D. Jansone, K. Rubina, E. Abele, S. Germane, L. Leite, M. Shymanska, J. Popelis, *Eur. J. Med. Chem.* 30 (1995) 983.
- [90] L. A Saryan, E. Ankel, C. Krishnamurthi, W. Antholine, D.H .Petering, *Biochem. Pharmacol.* 30 (1981) 595.
- [91] D. X. West, A. E. Liberta, K. G Rajendran, I. H. Hall, *Anticancer Drugs* 4 (1993) 241.
- [92] S. Padhye, R. Chikate, A. Kumbhar, J. M. Shallon, M. P. Chitnis, *Biometals.* 5 (1992) 67.
- [93] G. Nocentini, F. Federici, P. Franchetti, A. Barzi, *Cancer Res.* 53 (1993) 19.
- [94] J. N. Brown K. C Aggrawal, *Ac (Engl Transl).* 28 (1987) 119.
- [95] A. G. Bingham, H. Bogge, A. Muller, E. W. Ainscough, A. M. Brodie, *J. Chem. Soc., Dalton Trans.* (1987) 493.
- [96] C. F. Bell, Ch. R. Theocharis, *Acta Crystallogr. Sect. C.* 43 (1987) 26.
- [97] J. N. Brown, K. C. Aggrawal, *Acta Crystallogr. Sect. B* 33 (1977) 980.
- [98] J. N. Brown, K.C Aggrawal, *Acta Crystallogr. Sect. B.* 34 (1978) 2038.
- [99] M. B Ferrari, G. G. Fava, P. Tarasconi, C. Pelizzi, *J. Chem Soc., Dalton Trans.* (1989) 361.
- [100] M. B. Ferrari, G. G. Fava, E. Leporati, C. Pelizzi, P. Tarasconi, *J. Chem .Soc., Dalton Trans.* (1986) 2455.
- [101] M. B. Ferrari, G. G. Fava, E. Leporati, and C. Pelizzi, P Tarasconi, G. Tosi, *J. Chem .Soc Dalton Trans.* (1987) 227.

## References

- [102] P. I. Bopondos, K. S. Murray, P. Robson, J. Wilson, G.A. Williams. J. Chem. Soc., Dalton Trans. (1987) 1585.
- [103] M. B. Ferrari, G. G. Fava, E. Leporati, C. Pelizzi and P. Tarasconi. J. Chem. Soc., Dalton Trans. (1992) 2153.
- [104] M. C. Rodriguez-Arguelles, L. P. Battaglia, M.F. Bellicche, G. F. Gasparri, C. Pelizzi, G. Pelosi. J. Chem. Soc., Dalton Trans. (1995) 2297.
- [105] P. Ray, D. N. Sen, J. Indian Chem. Soc. 25 (1948) 473.
- [106] B S. Garg, M. R. P. Kurup, S. K. Jain, Y.K. Bhoon, Transition Met. Chem. 13 (1988) 309.
- [107] K. D. Karlin, and J. Zubieta (Eds), (a) 'Copper Coordination Chemistry 'Biological and Inorganic Perspectives'. Adenine Press, NY (1983); (b) 'Biological and Inorganic Copper Chemistry', Adenine Press, NY (1986).
- [108] H. Beraldo, L. P. Boyd, D. X West, Transition. Met. Chem. 23 (1998) 67.
- [109] H. Beraldo, S. B Kaisner, J. D. Turner, I. S. Billeh, J. S. Ives and D. X West, Transition Met. Chem. 22 (1997) 459.
- [110] A. Sreekanth, M. R. P. Kurup, Polyhedron 22 (2003) 3321.
- [111] W. Addison, T. N. Rao, J. Reedijk, J. Chem Soc, Dalton Trans. (1984) 1349.
- [112] H. Mausi, Coord. Chem. Rev. 957 (2001) 219.
- [113] G. Maddock, A. Sharpe, R. L. Martin, Proc. Roy. Austral. Chem. Inst. 38 (1971) 33.
- [114] M. R. P. Kurup, Marthakutty Joseph, Synth. React. Inorg. Met.-Org. Chem. 33 (2003) 1275.
- [115] M. R. P. Kurup, Ph.D Thesis., University of Delhi, Delhi (1988).
- [116] M. J. M. Campbell, Coord. Chem. Rev. 17 (1975) 279.
- [117] P. Bera, R. J. Butcher, S. Chaudhuri, N. Saha, Polyhedron. 21 (2002) 1.
- [118] M. A. Ali, M. T. H. Tarafdar, J. Inorg .Nucl .Chem., 39 (1977) 1785.

## References

- [119] E. Bayer, C. G Witte, *J. Coord. Chem.* 7 (1977) 13.
- [120] D. F. Little, C. J. Long, *Inorg. Chem.* 7 (1968) 3401.
- [121] A. B. P. Lever, *Inorg. Chem.* 4 (1964) 1042.
- [122] A. B. P. Lever, E. Mantovani, B.S. Ramaswamy, *Can. J. Chem.* 49 (1971) 1957.
- [123] A. M. Bond, R. L. Martin, *Coord. Chem. Rev.* 54 (1984) 23.
- [124] R. Osterberg, *Coord. Chem. Rev.* 12 (1974) 309.
- [125] E. W. Ainscough, A. M. Brodie, J. D. Ranford, J. M. Waters, *Dalton Trans.* 23 1991 2125.
- [126] R. P. John, A. Sreekanth, M. R. P. Kurup, S. M. Mobin, *Polyhedron.* 21 (2002) 2515.
- [127] M. A. Ali, D. A. Chowdhary, M. Nazimuddin, *Polyhedron.* 3 (1984) 595.
- [128] Y. K. Bhoon, *Indian J. Chem.* 22A (1983) 430.
- [129] W. J. Geary, *Coord. Chem. Rev.* 7 (1971) 81.
- [130] P. Bindu, M. R. P. Kurup, *Transition Met. Chem.* 22 (1997) 578.
- [131] B. J. Hathaway, A. A.G. Tomlinson, *Coord. Chem. Rev.* 5 (1970) 24.
- [132] E. Mabbs, Some aspects of the Electron Paramagnetic Resonance Spectroscopy of d-Transition Metal Compounds., Chemistry Department, University of Manchester, Manchester, M 13 (1991) 9.
- [133] P. Bindu, M. R. P. Kurup, T. R. Satyakeerthy, *Polyhedron.* 18 (1999) 321.
- [134] D. Kivelson, R. Nieman, *J. Chem. Phys.* 35 (1961) 149.
- [135] A. H. Maki, B. R. McGarvey, *J. Chem. Phys.* 29 (1958) 35.
- [136] B. J. Hathaway, G. Wilkinson, R. D. Gillard, J. A. McCleverty (Eds), *Comprehensive Coordination Chemistry* 5 (1987) Pergamon, Oxford, m1987.
- [137] U. Sakaguchi, A. W. Addison, *J. Chem. Soc., Dalton Trans.* (1979). 600 ; A. Diaz, R. Pogni, R. Cao, R. Basosi, *Inorg. Chim. Acta* 275-276 (1998) 552.

## References

- [138] M. Canadas, E. Lopez-Torres, A. Martinez-Arias, M. Antonia Mendiola M. Tera Sevilla, *Polyhedron* 12 (2000) 2060.
- [139] M.A. Ali, A. H. Mirza, M. Nazimuddin, H. Rahman, R. J. Butcher, *Polyhedron* (2001) 2431.
- [140] M. Mathew, G. J. Palenik, G. R. Clark, *J. Inorg. Chem.* 12 (1973) 346.
- [141] V. Philip, V. Suni, M. R. P. Kurup, M. Nethaji, *Polyhedron* 23 (2004) 1225.
- [142] J. K. Swearingen, W. Kaminsky, D. X. West, *Transition. Met. Chem.* 27 (2002) 7.
- [143] R. A. Bailey, S. L. Kozak, T. W. Michelsen, W. N. Mills, *Coord. Chem. Rev.* 6 (1971) 407.
- [144] C. H. Mitchel, R. J. P. Williams, *J. Chem. Soc.* (1960) 1912.
- [145] A. Turco, C. Pecile, *Nature* 191 (1961) 66.
- [146] J. Lewis, R. S. Nyholm, P. W. Smith, *J. Chem. Soc.* (1960) 1912.
- [147] A. Sabatini, I. Bertini, *Inorg. Chem.* 4 (1965) 959.
- [148] M. Suzuki, H. Kanatomi, H. Koyama, I. Murase, *Bull. Chem. Soc. Japan* 53 (1980) 1961.
- [149] Q. Li, H. Tang, Y. Li, M. Wang, L. Wang, C. Xia, *J. Inorg. Biochem.* 78 (2000) 167.
- [150] L. D. Dave, P. Frances, *Indian. J. Chem.*, 22A (1983) 422.
- [151] F. Basuli. Peng, S. Bhattacharya, *Inorg. Chem.* 36 (1997) 5645 and references therein.
- [152] J. D. Lee, *Concise Inorganic Chemistry*, 5<sup>th</sup> Ed, Blackwell Science Inc, Malden, USA (1996).
- [153] M. D. Deuton, A. Ginsberg, *Biochemistry* 8 (1969) 1714.
- [154] N. Gokhale, S. Padhye, D. Rathbone, D. Billington, P. Lowe, C. Schwalbe, C. Newton, *Inorganic Chemistry Communications* 4 (2000) 26.

## References

- [155] A. Usman, I. A. Razak, S. Chantrapromma, H. K. Fun, A. Sreekanth, S. Sivakumar, M. R. P. Kurup, *Acta Cryst. C Cryst. Struct. Commun.* **58** (2002) m461
- [156] W. Linert, F. Renz, R. Boca, *J. Coord. Chem.* **40** (1996) 293.
- [157] S. Purohit, A. P. Koley, L. S. Prasad, P. T. Manoharan, S. Ghosh, *Inorg. Chem.* **28** (1989) 375.
- [158] S. Olari, B. C. Harry, *Inorg. Chem.* **13** (1974) 1185.
- [159] R. D. Dowsing, J. F. Gibson, *J. Chem. Phys.* **50** (1969) 294.
- [160] R. D. Dowsing, B. Nieuwenhuijse, J. Reedijk, *Inorg. Chim. Acta.* **5** (1971) 301.
- [161] C. J. O. Connor, R. L. Carlin, *Inorg. Chem.* **14** (1975) 291.
- [162] A. S. Chakravorthy, *J. Chem. Phys.* **39** (1963) 1004.
- [163] J. E. Wertz, J. R. Bolton, *Electron Spin Resonance Elemental Theory and Practical Applications*, Chapman and Hall Ltd. W47 (1986) 335.
- [164] S. I. Chan, B. M. Fung, H. Lutje, *J. Chem. Phys.* **47** (1967) 2121.
- [165] N. D. Chasteen, *Vanadium in Biological Sciences*, Ed Kluwer Academic Publishers, Dordrecht, The Netherlands (1990).
- [166] H. Sigel, A. Sigel, *Vanadium and its role in life.*, Eds; Marcel Dekker: New York 31 (1995).
- [167] C. J. Carrano, C. M. Nunn, R. Quan, J. A. Bonadies, V. L. Pecoraro, *Inorg. Chem.* **20** (1990) 941.
- [168] R. P. Ferrai, E. Laurenti, S. Poli, Casella, *J. Inorg. Biochem.* **45** (1992) 21.
- [169] H. S. Soejak, A. Butler, *Inorg. Chem.* **29** (1990) 5015.
- [170] H. Plat, B. E. Krenn, R. Wever, *J. Biochem.* **248** (1987) 277.
- [171] D. Rehder, *Met. Ions. Biol. Syst.* **31** (1995) 1.
- [172] C. Orvig, K. H. Thompson, M. Battel, J. H. McNeill, *Met. Ions. Biol. Syst.* **31** (1995) 575.
- [173] H. S. Anderson, J. F. Iversen, C. B. Jeppesen, N. P. Moller, *J. Biol. Chem.* **275** (2000) 7101.

## References

- [174] M. Balasubramanyam, V. Mohan. *J. Biol. Chem.* 135 (1989) 5106.
- [175] A. Sreekanth, S. Sivakumar, M. R. P. Kurup. *J. Mol. Struct.* 655/1 (2003) 47.
- [176] C. W. Hahn, P. G. Rasmussen, J. C. Bayon, *Inorg. Chem.* 31 (1992) 1963.
- [177] J. P. Costes, G. Cros, M. H. Darbieu, J. P. Laurent, *Inorg. Chim. Acta.* 60 (1982) 111.
- [178] A. Bottcher, T. Takeuchi, K. I. Hardcastle, T. J. Meade, H. B. Gray, D. C. Wickel, M. Kapon, Z. Dori, *Inorg. Chem.* 36 (1997) 2498.
- [179] N. Mondal, D. K. Dey, S. Mitra, K. M. Abdul Malik, *Polyhedron* 19 (2000) 2707.
- [180] A. Sreekanth, U. L. Kala, C. R. Nayar, M. R. P. Kurup. *Polyhedron*, 23/1 (2004) 41.
- [181] J. E. Huheey, E. A. Keiter, R. A. Keiter, *Inorganic Chemistry*., 4<sup>th</sup> Ed, Harper Collin College Publishers, New York (1993).
- [182] A. Castineiras, R. Carballo, T. Perez, *Polyhedron* 20 (2001) 441.
- [183] Y. P. Tian, Wen-T Yu, Cun-Yuan Zhao, Min-Hua Jiang. Zhi-Gang. Cai, H.K. Fun, *Polyhedron* 21 (2002) 1217.
- [184] D. X. West, S. B. Padhye, P. S. Sonawane, *Struct. Bond* 76 (1991), 1 and references therein.
- [185] T. G. Spiro, *Zinc Enzymes*, Wiley, NY, 1983; I. Bertini, C. Luchinat, W. Maret and M. Zeppezauer, *Zinc Enzymes*., Birkhauser, Boston (1986).
- [186] H. Eklund, B. Nordstrom, E. Zeppezauer, G. Soderlund, I. Ohlsson, T. Bowie, B. O. Soderberg, O. Tapia, C. I. Branden, *J. Mol. Biol.* 102 (1976) 27.
- [187] M. H. Bracey, J. Christiansen, P. Towar, S. P. Cramer, S. G. Bartlet, *Biochemistry* 33 (1994) 13126.

## ***ABBREVIATIONS***

HL <sup>1</sup>	Di-2-pyridyl ketone tetramethyleneiminylthiosemicarbazone
HL <sup>2</sup>	Di-2-pyridyl ketone <i>N</i> (4)-methyl, <i>N</i> (4)-phenylthiosemicarbazone
BM	Bohr Magneton
shf	superhyperfine (EPR)
m	medium (IR spectra)
s	strong (IR spectra)
sh	shoulder (electronic spectra)
tbp	trigonal bipyramidal
sp	square pyramidal
δ	chemical shift
CT	charge transfer
L	ligand
M	metal
α <sup>2</sup>	in-plane sigma bonding parameter
β <sup>2</sup>	in-plane pi bonding parameter

G9064

### Publications

- 1 Di-2-pyridyl ketone  $N^R, N^R$ -(butane-1,4-diyl) thiosemicarbazone, A.Usman, I.A. Razak, S.Chantrapomma, H.K.Fun, V.Philip, A.Sreekanth and M.R.P.Kurup, *Acta.Cryst. C Cryst. Struct. Commun.* **58**, o652, 2002.
- 2 Structural and spectral studies of Ni(II) complexes of di-2-pyridyl ketone  $N_4, N_4$ -(butane-1,4-diyl) thiosemicarbazone, V.Philip, V.Suni, M.R.P.Kurup, M.Nethaji, *Polyhedron*, 23 (2004) 1225-1233.

### **Papers Presented**

- 1 Synthesis and spectral studies of Co(II) and Mn(II) complexes of a substituted di-2-pyridyl ketonethiosemicarbazone, Varugese Philip, M.R.Prathapachandra Kurup, 10<sup>th</sup> Symposium on Modern Trends in inorganic chemistry, December 15-17, 2003, Indian Institute of Technology, Bombay, India.
- 2 Synthesis and Structural Studies of Dioxovanadium(V) Complexes of a Substituted di-2- pyridyl ketone thiosemicarbazone, Varughese Philip and M.R. Prathapachandra Kurup, National Symposium on Current Trends in Inorganic Chemistry, March 15-17" 2004, Cochin University of Science and Technology, Kochi.

